Burning Behaviour of Liquid Pool Fires in Corridors and Thermal Characteristics of Resulting Externally Venting Flames

Konstantinos Chotzoglou (BSc, MEng)

Faculty of Computing, Engineering and the Built Environment of Ulster University

Thesis submitted for the degree of Doctor of Philosophy

October 2018

(I confirm that the word count of this thesis is less than 100,000 words)

TABLE OF CONTENTS

LIST OF FIGURES

LIST OF TABLES

ACKNOWLEDGMENTS

I am really grateful I had the opportunity of implementing my research in FireSERT lab, supported by talented and amazing people who have helped me to go through this long process. It is noted that the present research was part of The Energy Efficient Lightweight-Sustainable-Safe-Steel Construction (ELISSA) project, financially supported by the EU under Grant No 609086. I would like to express my gratitude to the following people for taking part in my research and being part of my life.

Firstly, I would like to express my sincere gratitude to Prof. Michael Delichatsios, an expert on the field of fire dynamics, who accepted me as a PhD student and was my main supervisor for the first years of my research. His motivation, his patience and his immense knowledge were great guidance for me through this challenging project. It was truly a pleasure to be supervised by him and I will always be thankful for his continuous support through the past years.

My sincere thanks also goes to Dr. Jianping Zhang. Initially, although he was my second supervisor, he was always closely involved in my experimental work, providing me with his advice and recommendations. But more importantly, I would like to thank him for becoming my main supervisor almost two years after the start of my project. Although this change was challenging for both, I strongly believe that his role was crucial to finally submit a thesis towards the award of PhD and to disseminate the results of this research. It was always a pleasure discussing with him, accommodating any difficulties arised during my work, always guided by his insightful knowledge. Thank you so much.

I must also recognize that my experimental work would not be successfully completed without the guidance and assistance of the ‘main men’ of the laboratory: Mr. Maurice McKee and Mr. Billy Veighey. In more details, Maurice introduced me to most of the laboratory equipment, providing me with details and useful information on how-to-use, based on his years of experience. Technical assistance of Billy was critical on refurbishing (more than once to be accurate) the experimental rig used in my project and designing any new parts of it needed for the experiments. They were always there, helping me to deal with any technical difficulties, but most importantly to cheer me up and not lose my motivation during the period performing

the experimental work. I must finally say that I consider them as true friends. Additionally, is worth mentioning technical assistance of Mr. William Allison and Mr. Kris Kowalski, who mainly helped me in my experimental work during my first years of my research.

I would also like to mention Dr. Eleni Asimakopoulou, close friend and excellent researcher, who was the one responsible for coming in contact with the fire engineering field (thanks for that Eleni). It's always been a pleasure working with her. Special thanks goes to Dr. Talal Fateh, for his many suggestions on my experimental work and his great support through the years of my research study. I continuously learn a lot from him, especially on some practical aspects of fire engineering. I would also like to thank Dr. Choi, who accepted to become my second supervisor during this project. Of course, not to forget all the researchers working in the laboratory, with whom I have spent most of the days of the past years.

It is also very important to thank all my friends who supported me throughout this challenging path. Although I am not going to mention any of them (I would feel so sad if I forget anyone), their support and help was daily (even if they haven't even noticed) and it made me thankful for having all these beautiful people around me. Thanks to all my closest friends in Greece and of course all the new people I have met abroad and especially in Belfast. I feel so much appreciation for every moment I have spent with all of you so far. The person in which I would also like to express my gratitude is Maria, who has been supporting me every day for the last two years. Thank you for the time we spend together and all the (exciting) moments we share.

Last but not least, my family for their tremendous support and love they have shown me, as they have always been on my side. It is really impossible to put in words my feelings for you, but I want you to know that I will always be on your side as well, no matter what. A great thanks to my grandparents for the time they have spent telling us stories and fairy tales, but especially my parents, Evangelos and Glykeria, who have raised three amazing people by being always there for us. Special thanks to my brothers -and my best friends- Dimitris and Alexandros for supporting each other and for the time we spend just chatting every day.

ABSTRACT

Recent major fire events clearly demonstrate the urgency of understanding fundamental physics and mechanisms of fire development in enclosures and those of resulting externally venting flames (EVF). Even though great effort has been devoted for addressing fire development inside cubic-like enclosures, limited data exist in corridor-like enclosures. This work investigates experimentally the burning behaviour of liquid pool fires in a corridor enclosure having an opening and a façade extending above. A parametric study was performed to examine the influence of the size and location of the pool fire, the opening size and the fuel type on the fire development inside the corridor and thermal characteristics of resulting EVF on the facade. Experimental results indicate that fire development of liquid fuels is considerably different from that of gaseous fuels, because its burning rate depends on the heat feedback from the flame and hot gases whereas it is predefined for gaseous fuels. Three distinct regions were observed for burning behaviour and subsequent EVF depending primarily on the fire size and ventilation factor. Under ventilation-controlled conditions, the fuel burning rate and the air inflow rate were found less than in cubic enclosures due to non-uniform temperature distribution inside the corridor. A power dependence of EVF height in relation to excess heat release rate was deduced. The heat flux along the centreline of the façade shows similar trends to those observed for gaseous fuels, except for the cases with large opening widths in which the maximum heat flux on the façade was located off the centreline and EVF emerge from the opening as two separate flames. In practical, the correlations developed in this research can be applied to predict fire development inside a corridor and heat exposure of the façade and the data obtained are useful for validation of computational fluid dynamics (CFD) models.

NOMENCLATURE

Symbol	Quantity	Units
A_f	Fuel surface area	m^2
A_o	Opening area	m^2
A_W	Total wall cross sectional area	m^2
C	Ventilation coefficient	-
C_p	Specific heat of air at ambient conditions	1005 J/kgK
D	Diameter of the pool	m
ε	Emissivity	-
F	Configuration factor	-
g	Gravitational acceleration	9.81 m/s^2
h_c	Convective heat transfer coefficient	kW/m^2K
H_o	Opening height	m
I	Intermittency	-
k	Extinction coefficient	m^{-1}
k_c	Thermal conductivity of the pan's material	W/mK
L_V	Heat of evaporation	kJ/kg
l_1, l_2, l_3	Length scales	-
$\dot{m}_f$	Fuel mass rate	kg/s
$\dot{m}_a$	Mass flow rate of incoming air to the	kg/s
$\dot{m}''$	Burning rate per unit area	kg/m^2s
$\dot{m}''_\infty$	Mass loss rate of an infinite diameter pool	kg/m^2s
$\dot{m}_T$	Burning rate of fuel	kg/s
$\dot{Q}$	Heat Release Rate	kW
$\dot{Q}_{fire}$	Heat Release Rate of fire	kW
$\dot{Q}_{fuel}$	Heat Release Rate from evaporation of fuel	kW
$\dot{Q}_{cond}$	Heat Release Rate through conduction	kW
$\dot{Q}_{conv}$	Heat Release Rate through convection	kW
$\dot{Q}_{rad}$	Heat Release Rate through radiation	kW
$\dot{Q}_{loss}$	Heat losses	kW
$\dot{Q}_C$	Convective heat losses of gas flow	kW
$\dot{Q}_R$	Rate of heat radiated through the opening	kW

$\dot{Q}_W$	Rate of heat transferred to the walls of the enclosure	kW
$\dot{Q}_G$	Heat stored in gas volume	kW
$\dot{Q}_{act}$	Actual heat release rate measured in hood	kW
$\dot{Q}_{ex}$	Excess Heat Release Rate	kW
$\dot{Q}^*_{ex}$	Dimensionless excess heat release rate	-
$\dot{Q}_{th}$	Theoretical heat release rate	kW
$\dot{Q}_{st,in}$	Maximum heat released inside the enclosure	kW
$\dot{q}$	Heat flux	kW/m^2
RH	Ambient relative humidity	%
r_o	Equivalent radius of the opening	-
S	Stoichiometric fuel's ratio	-
t_{dur}	Duration of test	s
T	Temperature	^oC
T_g	Upper gas layer temperature	^oC
T_∞	Ambient temperature	15.25^oC
T_f	"Effective" flame temperature	K
T_s	Temperature of the fuel's surface	K
u_w	Wind Velocity	m/s
W_o	Opening width	m
$Y_{O2,air}$	Oxygen mass fraction in ambient air	0.23
Z	Height from Neutral plane	m
Z_f	Mean height of flame	m
Z_n	Height of the compartment neutral plane	m
β	Mean beam length corrector	-
ΔH_{air}	Heat of combustion of air	3000 kJ/kg
ΔT_z	Plume centerline temperature rise above ambient	K
ΔH_c	Effective heat of combustion	kJ/kg
η	Combustion efficiency	-
ρ_z	Density of the hot combustion products	kg/m^3
ρ_∞	Air density at ambient conditions	$1.204\ kg/m^3$
σ	Stefan Boltzmann constant	5.67×10^{-8} $kgs^{-3}K^{-4}$
φ	Equivalence ratio	-

Abbreviations

CO	Carbon monoxide
EVF	Externally Venting Flames
GER	Global Equivalence Ratio
HRR	Heat Release Rate
MLR	Mass loss rate
N.P	Neutral plane

CHAPTER 1

INTRODUCTION

1.1 Introduction

Over last decades there is an increasing need on designing larger and more complex infrastructure used as living and working places, transportation means etc. by billions of people daily. This pattern undoubtedly arises a great deal of concern over safety in such infrastructure and more particularly fire safety (Karlsson and Quintiere, 2000; Quintiere, 2006). Fire development within an enclosure and possible vertical or horizontal spread to adjacent infrastructure is of great importance when a fire starts, thus understanding of the physics and mechanisms of fire development in enclosures and flames emerging through openings is fundamental to ensure effective fire prevention.

When a fire starts in an enclosure such as a compartment, the initial fire growth is usually very slow and characterised by localised burning, after which the fire can either self-extinguish (or burn in a very slow rate) or increase in size and eventually progress to involve all combustibles in the compartment. Self-extinguishment of the fire can either occur if the initial fire source is in an isolated position or there is very limited ventilation into the compartment to sustain burning (Drysdale, 2011). In the case when the fire involves all the combustible surfaces, a major hazard of fire spread is the external flames which may appear through the openings (such as broken windows) of the original fire room. External flames can cause spread of fire to adjacent buildings by radiation, or, especially in high-rise buildings, vertical fire spread to upper floors, as the flames appearing on the external façade of the building tend to attach to the façade surface and ignite either the façade (if it is made of combustible materials) or any combustible materials close to the windows on the upper floors (Delichatsios, 2014). Several recent fire incidents in high-rise buildings (see Fig.1.1 and Table 1) have attracted the interests of numerous fire engineers and regulators, highlighting the importance of studying façade fires initially generated in burning enclosures. Consequences of flames emerging through openings and spread to adjacent floors or buildings include loss of life and injuries, health impact through smoke exposure, property and infrastructure loss, business interruption, ecosystem degradation and huge firefighting costs (White and Delichatsios, 2014).

Table 1 Recent high-rise building fires involving upward fire spread.

Building	Location	Year	External fire spread	Details
Marina Torch Tower	Dubai, UAE	2017	√	Fire started from a cigarette falling on to balcony plants and setting them alight, no injuries or deaths.
Grenfell Tower	London, UK	2017	√	Fire started by a faulty refrigerator, fast upward spread due to combustible façade/cladding materials, 71 deaths, 74 injuries.
Ajman One residential cluster	Ajman, UAE	2016	√	The fire erupted at a building in the Ajman One residential cluster of 12 towers and spread to at least one other tower, 1 injuries.
Address Hotel	Dubai, UAE	2016	√	Fire started on the 20th floor of the building and only affected the exterior of the structure, 16 injuries.
Docklands Apartment Tower	Melbourne, Australia	2015	√	Fire started from an unextinguished cigarette on the sixth-floor balcony, no deaths or injuries.
Marina Torch Tower	Dubai, UAE	2015	√	Fire started in the middle of the tower before spreading downwards, no deaths or injuries.
Residential Building	Grosny, Russia	2013	√	Fire started from a short circuit in an air-condition, no deaths or injuries.
Polat Tower	Istanbul, Turkey	2012	√	Fire burned through the building's external insulation, no deaths or injuries.
Mermoz Tower	Roubaix, France	2012	√	Fire initiated at the second floor and spread rapidly upwards, 1 fatality, 10 injuries.
Residential Building	Dijon, France	2010	√	Fire started at the basis of the building from waste containers, 7 deaths.
Residential Building	Shanghai, China	2010	√	Fire started during renovation for installing exterior wall insulations, 58 deaths, 71 injuries.

Figure 1.1 Grenfell tower fire (2017) in London, UK (left) and Beijing TV Cultural Centre fire (2009) in Beijing, China (right).

As façade fires are usually resulted from fires occurring inside the enclosures, it is therefore crucial to firstly address fire growth and development inside different types of enclosures before investigating fires appear outside the enclosures. It has been demonstrated (Karlsson and Quintiere, 2000; Drysdale, 2011) that the internal fire spread in enclosure is influenced by a number of factors, such as the geometry of the enclosure, the size and location of the opening(s), the size and location of the fire, thermal material properties of the enclosure walls and environmental conditions, as shown in Fig. 1.2.

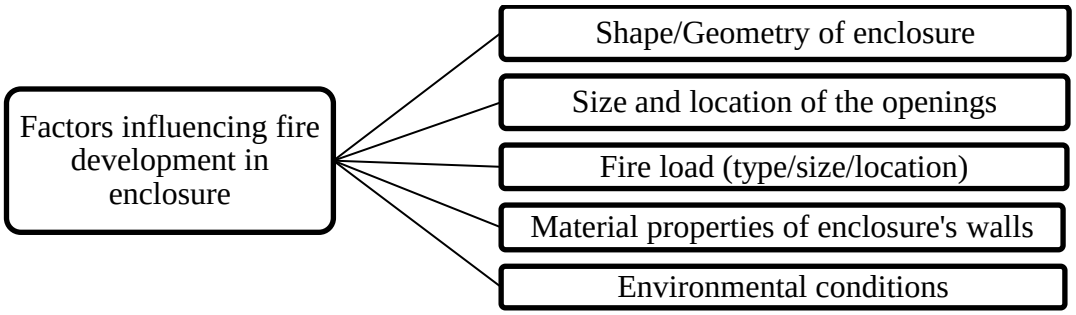

Figure 1.2 Factors affecting fire development in enclosures.

However, as pointed out by Karlsson and Quintiere (2000), 'the interactions between the flame, its fuel and the surroundings can be strongly nonlinear, and quantitative estimation of the processes involved is often complex'. These interactions are still to be identified as many of them have been of limited investigation.

Some of these parameters have been investigated by a number of researchers using cubic-like compartment fires (Kawagoe, 1958; Thomas et. al., 1967; Steckler et. al., 1982; Yii, 2002; Parkes, 2009). For example, the effects of the size of the opening, thus the ventilation factor, on the burning behaviour of compartment fires has been extensively studied in (Kawagoe, 1958; Thomas et. al., 1967; Steckler et. al., 1982; Fleischmann and Parkes, 1997). The fuel type was also found to significantly influence the burning behaviour of fires within rectangular enclosures (Delichatsios and Silcock, 2002), as well as the location of the fire source (Parkes, 2009).

The geometry of the enclosure (rectangular- or corridor-like enclosure) was also found to influence the burning behaviour of enclosure fires (Miyazaki and Watanabe, 1998; Delichatsios et. al., 2004), (Lee, 2006), (Delichatsios, 2014). Whilst there is a significant amount of data in cubic-like enclosures (Kawagoe, 1958; Steckler et. al., 1982; Delichatsios and Silcock, 2002, Parkes, 2006; Lee et al., 2007), there is still limited data from experiments in non-cubic-like enclosures (Audouin et. al., 1997; Thomas and Bennetts, 1999; Beji et. al., 2012; Ukleja, 2012). As mentioned by Delichatsios et. al. (2004) owing to limited data in corridor enclosure fires, '*this does not allow development of analysis similar to this has been achieved in compartment configurations*'. Years after, Yuan et. al. (2015) also identified lack of experimental studies regarding tunnel fires under natural ventilation conditions.

For the few studies in corridor-like enclosures (Beji et. al., 2012; Ukleja, 2012), mainly gaseous fuels were used. But as the mass flow rate (thus heat release rate) of gaseous fuels must be pre-defined, it does not consider the interaction between the flame, hot gas layer and the pyrolysis rate of the fuel, which is of fundamental importance in growth and development of real fires.

For façade fires, recent work (Ohmiya et. al., 1998; Lee et. al., 2007; Yii et. al., 2007; Delichatsios, 2014) has shown that the mass inflow rate of fresh air entering the enclosure is affected by the geometry of the enclosure, which in turn has a significant influence on the behaviours of the external flames. Heat exposure on the façade was also studied in terms of the mass inflow rate of air and heat flux correlations for façade fires in cubic-like enclosures (Lee et. al., 2007; Lee et. al., 2009). The validity of these correlations in long enclosures like corridors and tunnels

was examined using gaseous fuels in a corridor-like enclosure (Beji, 2009; Ukleja, 2012). These studied showed clear differences in the burning behaviours between the two configurations, which highlight the importance to further examine the burning behaviours in long corridor configuration, as limited data exist for such configurations especially for liquid fuels. Subsequently, further investigation need to be performed using different types of fuels with unknown burning rate, such as pool fires.

As the heat release rate is primary factor regarding the fire development in corridor fires (Babrauskas and Peacock, 1992; Delichatsios and Silcock, 2002), this work examines the steady-state heat release rate period that occurs after the development of the fire. This parametric study aims to extend previous works regarding the influence of the ventilation geometry, the pool size and pool location to the burning behaviour of corridor fires. As new façade design concepts and construction materials continuously challenge the established fire safety solutions and applications, façade fires generated by liquid pool fires are also studied in the current work to incorporate the influence of these parameters into findings regarding heat exposure of the façade in terms of flame heights and heat fluxes.

1.2 Aim and Objectives

1.2.1 Aim

This fundamental research work seeks to add some more insight in fire dynamics of fires developed within corridor-like enclosures and their either horizontal or vertical spread. The aim of this work is to investigate the fire dynamics and burning behaviours of liquid pool fires in a corridor-like enclosure and the burning characteristics of the resulting façade fires. The study of the liquid pool fires in the enclosure is assessed in terms of mass burning rate and heat release rate of the fire, gas temperature and heat flux on the enclosure floor, whereas façade fires in terms of the height of external flames and heat flux of the façade.

1.2.2 Objectives

The objectives of this PhD study are:

- To perform experiments in a reduced-scale corridor-like enclosure using liquid pool fires of constant fuel surface level as the fire source.

- To gain more insights into the fire dynamics in corridor-like enclosure fires and investigate the effects of opening geometry, location and size of the pool fire on the burning rate, the heat release rate and the mass inflow rate through the opening.

- To investigate experimentally the heat exposure of a façade after flames ejected through the opening of the corridor-like enclosure in terms of flame height and heat fluxes.

- To develop and propose appropriate engineering correlations for the mass burning rate/heat release rate and the mass inflow rate for fires in corridor-like enclosures and the flame height and the heat flux on the exposed façade due to the emerging flame.

1.3 Research Methodology

The methodology of the present work consists of experimental investigation of corridor-like enclosure and façade fires and development of correlations, as well as comparison with available data of previous works.

In order to investigate the fire dynamics in modern practical configurations such as tunnels, long offices, transportation means (airplanes, trains, etc) and high-rise constructions, a reduced scale 3-m corridor-like enclosure with an adjusted façade above the opening was constructed. A parametric study was performed using different opening sizes, pool sizes and pool locations to examine their effects on the burning behaviour of enclosure fires and façade fires under steady-state conditions. Liquid pool fires were chosen as the fire source in comparison to gaseous fuels with prescribed mass fuel loss that have been previously used in (Lee, 2006; Beji, 2009; Ukleja, 2012). The use of liquid pool fires simulates a more realistic fire scenario, as

it takes into consideration the interaction of the heat feedback from the hot gas layer and compartment walls and the burning rate of the fuel. Steady-state burning of liquid pool fires within the enclosure were achieved by using pool fires with a constant level of fuel surface. Moreover, comparison with available literature data using gaseous fuels also performed to highlight differences between the two fuels related to the burning behaviour, the heat release rate and the external flame characteristics. An extensive set of measurement equipment within and outside the enclosure is used to properly investigate such enclosure pool fires, consisting of thermocouples, heat flux meters, camera, gas analyser and balance.

1.4 Structure of the thesis

The thesis is structured in the following way.

Chapter 2: This chapter presents the literature review of enclosure and façade fires. Main focus is in fires starting within long enclosures like corridors and tunnels and ejected flames through the openings and their impact on the façade.

Chapter 3: A detailed presentation of the experimental set-up is presented in this chapter, accompanied with the description of the experimental equipment and an uncertainty analysis of various measurements. In addition, a summary of the experimental conditions for all the cases investigated in this work is presented.

Chapter 4: This chapter presents the experimental findings and discussion of the results for the cases when the pool fire source is located at the front of the corridor-like enclosure (close to the opening). The effects of the opening size and the size of the pan are investigated.

Chapter 5: The experimental results and related discussion is presented for the cases when the pool fire was placed closer to the closed end of the corridor-like enclosure. Findings for different opening sizes and pool size are compared.

Chapter 6: In this chapter the effect of pool location is investigated, comparing cases using the pool fire either close to the opening of the corridor or close to the closed end of the corridor. In addition, fuel type effect is studied, as pool fire experiments investigated in the present work are compared with experiments performed in the same enclosure geometry using different fuel type (gaseous fuel).

Chapter 7: The main conclusions of this work are presented in this chapter, followed by recommendations for future work.

Additional information regarding the tests performed (such as list of tests, measurement probe locations etc.) in the present work is provided in appendices.

CHAPTER 2

LITERATURE REVIEW

2.1 Introduction

Façade fires have been found to be the main hazard in buildings (Sun et. al., 2013; White and Delichatsios, 2014; Delichatsios, 2014), as the upward flame spread from floor to floor or to adjacent buildings can lead to catastrophic loss of life and property. Since the late nineteen-fifties fire safety of high rise buildings has attracted many fire researchers who addressed the hazard of façade fires to the flames emerging through openings from burning enclosures. This connection motivated researchers to seek the complete understanding of the physics of fire development inside an enclosure which is associated with façade fires by conducting small and large-scale experiments and performing computer simulations. In order to assess and evaluate likely fire development in enclosures and its contribution to façade fires, different fire sources have been used in fire research literature, such as real furniture (Klopovic and Turan, 2001), liquid pool fires (Yokoi, 1960, Asimakopoulou, Chotzoglou et. al., 2016) and gaseous fuels (Oleszkiewicz, 1989; Ohmiya et. al., 1998; Lee et. al., 2007). Liquid pool fires are a more complex fuel configuration than gaseous burners, as gaseous burners can provide constant and prescribed burning rate. However, this is far from real enclosure fires where many and different materials can influence the burning rate (Drysdale, 2011), so configurations without having the ability of controlling the burning rate need to be investigated. Another reason for studying liquid pool fires is that thermoplastic pool fires which are of great interest in an enclosure can also be treated by the same techniques as liquid pool fires (Babrauskas, 1986). Subsequently, a fire scenario like this can be simulated using a pool fire in an enclosure. Therefore, pool fires were chosen to be used in the present experimental study, this chapter provides firstly a general background behind the pool fires in open conditions. Existing experimental correlations and theoretical calculations are presented for heat release rate, burning rate and flame height of pool fires as well as the factors influence them. Subsequently, enclosure and facade fires are reviewed. The development of a fire inside an enclosure and the interactions between the fire and the enclosure boundaries are presented and supported by significant findings of many earlier research works in terms of general burning behaviour, including heat release rate and burning rate. Studies of flames emerging from an enclosure and their interaction with

the burning enclosure are also presented. Finally, the summary identifies research knowledge gaps and relates them with the research plan of this thesis.

2.2 Liquid Pool Fires in Open (free-burn) Conditions

The term ‘liquid pool fire’ is used to describe a liquid of a free surface burning within any confining configuration such as a tray, an open tank etc. (Drysdale, 2011). As pool fires combine combustion, fluid dynamics and heat and mass transfer, they are characterised as complex systems and therefore it is useful to identify firstly the heat transfer mechanisms in a pool fire. Based on the heat transfer mechanism which dominates under different conditions (e.g. pool fire size, pool material), discussions in relation to heat release rate and burning rate are followed.

2.2.1 Heat Transfer Mechanisms in Liquid Pool Fires

This subsection presents a brief summary of the heat transfer mechanisms in a pool fire, which are fundamental to assess the burning rate and heat release rate of pool fires, the main measurements investigated in the present research. A detailed analysis of the heat transfer in pool fires can be found in (Hottel, 1959; Hamins et. al., 1999; Quintiere, 2006; Drysdale, 2011; Vali, 2014).

In a pool fire, heat is transferred from the flame to the fuel surface (heat feedback to the fuel surface) through conduction ($\dot{Q}_{cond}$), convection ($\dot{Q}_{conv}$), and radiation ($\dot{Q}_{rad}$), and these terms are balanced by primarily the heat losses ($\dot{Q}_{loss}$) on the fuel surface and the energy which is required for the evaporation of the fuel ($\dot{Q}_{fuel}$),, as shown in Fig. 2.1.

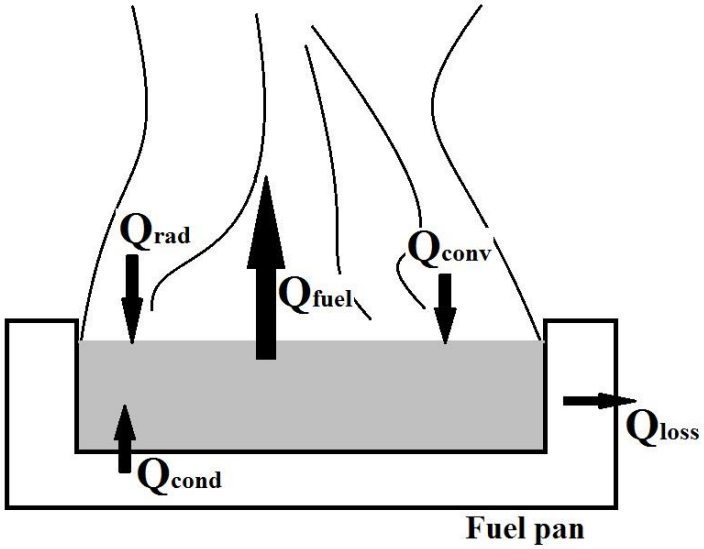

Figure 2.1 Heat transfer mechanisms of a free-burn liquid pool fire

The conduction term refers to heat transfer from the flame to the fuel surface through the walls of the pan and is influenced by the pan's material, the depth of the fuel inside the pan and the fuel properties. Conduction is given by the following equation (Hamins et. al., 1999):

$$\dot{Q}_{cond} = k_c A_W \frac{dT}{dz} \tag{2.1}$$

where:

k_c is the thermal conductivity of the pan's material (W/mK)
dT/dz is the thermal gradient in the wall (K/m)
A_w is the wall cross sectional area (m^2)

Convection is calculated by the following equation:

$$\dot{Q}_{conv} = h_c A_f (T_f - T_s) \tag{2.2}$$

where:

h_c is the convective heat transfer coefficient (kW/m^2K)

A_f is the fuel surface area (m^2)
T_f and T_s are the flame and surface temperature (K) respectively

Finally, radiation in a pool fire is calculated:

$$\dot{Q}_{rad} = \sigma F \varepsilon \left(T_f^4 - T_s^4\right) \quad (2.3)$$

where:

σ is the Stefan-Boltzmann constant (5.67×10^{-11} kW/m^2K^4)
F is the configuration factor (see (Drysdale, 2011))
ε is the emissivity

Emissivity is a measure of the efficiency of the surface as a radiator. The perfect emitter is the 'black body' which has emissivity of unity.
Radiation depends on the flame shape and height, the pool diameter and the temperature distribution in the flame.

2.2.2 Heat Release Rate

As noted by Babrauskas and Peacock (1992), the most important single parameter in order to characterize a fire is the rate at which the energy is released. Theoretically, the heat release rate (HRR), ($\dot{Q}_{fire}$), is expressed in terms of the mass burning rate per unit area, ($\dot{m}''$), thus:

$$\dot{Q}_{fire} = \eta \dot{m}'' \Delta H_c A_f \quad (2.4)$$

where:

ΔH_c is the effective heat of combustion of the fuel volatiles (kJ/kg)
η is the combustion efficiency

Equation 2.4 provides the maximum theoretical heat release rate (HRR) for a given pool fire. In real situations, HRR can be determined experimentally by using the

oxygen consumption calorimetry method. This method is based on a theory which was originally proposed by Thornton (1917), who showed that for a large number of organic liquids and gases, the heat generated per unit mass of oxygen consumed for complete combustion appears to be constant. Years later, Huggett (1980) found this value to be 13100 kJ/kg with +/- 5% accuracy. Using this method, the HRR can be calculated by measuring the amount of oxygen consumed in combustion (Babrauskas and Grayson, 1992 and Babrauskas, 2002).

2.2.3 Mass Burning Rate and Burning Behaviour

The burning rate of a pool fire in steady-state conditions is:

$$\dot{m}'' = \frac{\dot{q}'' - \dot{Q}''_{loss}}{L_V} \text{ (kg/m}^2\text{s)} \qquad (2.5)$$

where:

$\dot{q}''$ is the heat flux from the flame (kW/m^2)

$\dot{Q}''_{loss}$ is the heat losses through the fuel surface (kW/m^2)

L_V is the latent heat of evaporation (kJ/kg)

Therefore, the burning rate depends on the mechanisms of which heat is transferred from the flame to the fuel surface (sum of conduction, convection and radiation).

Blinov and Khudiakov (1957) were the first researchers who identified the dependence between the burning rate of small pool fires and the heat transfer mechanism, associating the burning rate with the diameter of the pool. They investigated the burning rate of small hydrocarbon pool fires in terms of the regression rate. The regression rate is equivalent to the volumetric loss of liquid fuel per unit surface area of the pool in unit of time and is measured in mm/min. They observed that for very small pool diameters, i.e., less than 0.03 m, the flame is laminar and conduction is the mechanism which dominates the heat transferred. In this region, the regression rate was found to decrease with an increase of the pool fire. For pool diameters between 0.03 – 1 m a transitional behaviour was observed between laminar and turbulent flames. In this region, conduction is not important anymore and both convection and radiation become more important. For smaller

diameters in this region convection is the main mechanism by which heat is transferred to the fuel surface, but as the diameter of the pool increases the radiation becomes dominant. Eventually, for large pool fires of a diameter larger than 1 m radiation is the principle mechanism of heat transfer and flame becomes fully turbulent. The three regimes described are shown clearly in Fig. 2.2. The same three regimes were also identified by Hottel (1959).

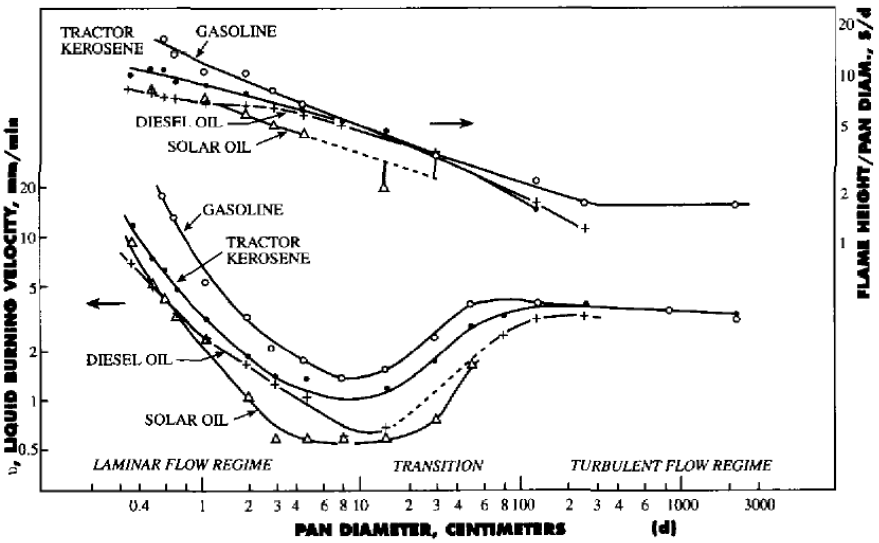

Figure 2.2 Regression rate of liquid pool fires over the pan diameter (Blinov and Khudiakov, 1957).

Babrauskas (1983) examined pool fires with diameters ranging from 0.5 m to more than 1 m, classifying them to four regimes as given in Table 2. He stated that the transition from laminar (convection dominates) to turbulent (radiation dominates) occurs at a pool diameter of 0.2 m. In addition, he concluded that flame could be either optically thin or optically thick in the radiative regime. He finally noted the importance of studying pool fires in which radiation is the dominant mechanism of heat transfer; diameter larger than 0.2 m.

Table 2 Regimes of heat transfer in pool fires (Babrauskas, 1983)

Pool Diameter (m)	Heat transfer regime
<0.05	convective, laminar
0.05-0.2	convective, turbulent
0.2-1	radiative, optically thin
>1	radiative, optically thick

In order to estimate the burning rate of liquid pool fires having a diameter larger than 0.2 m (radiation dominant), a correlation was proposed by Zabetakis and Burgess (1962):

$$\dot{m}'' = \dot{m}''_{\infty}(1 - \exp(-k\beta D)) \quad (\text{kg/m}^2\text{s}) \tag{2.6}$$

where

$\dot{m}''_{\infty}$ is the mass loss rate of an infinite diameter pool

k is an extinction coefficient (m^{-1})

β is mean beam length corrector

D is the diameter of the pool

The $\dot{m}''_{\infty}$, k, β are empirical constants which characterize each fuel. For some common fuels these empirical constants can be found in (Babrauskas, 1983 and Drysdale, 2011).

In case of alcohols, like ethanol and methanol, the correlation proposed in (Zabetakis and Burgess, 1962) is modified to:

$$\dot{m}'' = \dot{m}''_{\infty} \tag{2.7}$$

For ethanol, the empirical constants are given in Table 2.2. According to Table 3 and Eq. 2.7, the burning rate of an ethanol pool fire is 0.015 kg/m^{2}s regardless the pool diameter for diameters > 0.2.

Table 3 Empirical constants for estimating the burning rate of pool fires (Babrauskas, 1983).

Liquid	$\dot{m}''_{\infty}$ **(kg/m^{2}s)**	**kβ (m^{-1})**
Ethanol	0.015	-

Another correlation was developed by Ditch et. al. (2013) based on the heat of gasification and the smoke point height. This correlation was based on free-burn pool fire experiments performed using different fuels and was validated with experimental data of Modak and Groce (1977) showing good agreement.

The equations presented are used for predicting the burning rate under ideal circumstances but in many situations there are additional parameters which could influence the heat transfer to the fuel surface, resulting in changes on the burning rate, e.g., pool dimensions, pool's wall material and lip height. The most common of these parameters are listed in (deRis, 1979; Babrauskas, 1983; Steinhaus et. al., 2007) and investigated by many researchers over the last 50 years. A summary for some of the most important parameters affecting the burning rate of pool fires are described in the following subsections.

2.2.3.1 Lip Height Effect

The distance between the fuel level inside the pan and the pan's lip is known as lip height which is identified as a very important parameter influencing the burning of liquid pool fires. Lip height can cause edge effects, such as shorter flame height (Hall, 1972), higher convective heat transfer to the fuel surface due to greater turbulence at the base of the flame (Orloff, 1981; Babrauskas, 1983), and higher gas emissivity (Babrauskas, 1983) which is responsible for altering the burning behaviour of the pool fire.

Two different test conditions are applied in all works related to burning rate of pool fires. The fuel surface can be either kept on a constant height inside the pool (steady) or can decrease during burning (unsteady), both of which are of practical importance. Although in this work burning rate under steady conditions is examined, much research (Koseski and Yumoto, 1988; Hayasaka, 1997) has been conducted in unsteady conditions providing experimental data for such cases. A list of selected works in free-burn pool fires is shown in Table 4 with information regarding the fuel level conditions provided also. A short review of both conditions is followed for better understanding of the lip height effect.

Table 4 Summary of selected works of free-burn pool fires.

Reference	Test condition	Fuel	Geometry	Dimension (m)
(Rasbach et. al., 1956)	Steady	Methanol Kerosene	Circular	0.3
(Blinov and Khudiakov, 1957)	Steady	Gasoline Kerosene Diesel Oil Solar Oil	Circular	0.004-30
(Akita and Yumoto, 1965)	Steady	Methanol	Circular	0.01-0.06
(Byram et. al., 1966)	Steady	Ethanol	Square	0.06-0.33
(Corlett and Fu, 1966)	Steady	Ethanol Methanol	Circular	0.25-0.38
(Koseski and Yumoto, 1988)	Unsteady	Heptane	Circular	0.3-6
(Klassen and Gore, 1992)	Steady	Ethanol Methanol Heptane Toluene	Circular	0.046-1
(Hamins et. al., 1994)	Steady	Methanol Heptane MMA Toluene	Circular	0.075-0.3
(Hayasaka, 1997)	Unsteady	Heptane Methanol Kerosene	Circular	0.05
(Chatris et. al., 2001)	Steady	Diesel Oil Gasoline	Circular	1.5-4
(Tewarson and Marlair, 2004)	NA	Ethanol	Circular	5
(Ditch et. al., 2013)	Steady	Ethanol Methanol Heptane Toluene	Circular	0.25-1
(Hu et. al., 2013)	Steady	Ethanol Heptane	Square	0.11-0.28

Further work by Blinov and Khudiakov (1961) showed that the burning rate of liquid pool fires is a function of the fuel level inside the pan. The burning rate is strongly affected by the level of fuel, which decreases during burning. For small diameter pool fires, it was found that the flame stays at the top of the burner independent of the lip height. With an increase in the pool diameter, the flame was observed to enter the pan with larger lip heights. This phenomenon affects the surface temperature which has an important impact on the heat balance of pool fire. A monotonic decrease of the burning rate was observed with an increase of the lip height, which is in correspondence with the finding by Magnus (1961). A contradictive observation was made by Orloff (1981), who found that the burning rate of a pool fire increases due to hotter temperatures near the surface of the fuel.

Hayasaka (1997) carried out experiments using small pool fires with a decreasing fuel level. He found that when fuel and tank temperatures increase, the burning rate of hydrocarbons (heptane and kerosene) increases, due to a change in the heat losses. An interesting finding related to methanol, in correspondence with previous results for alcohol's burning rates (Drysdale, 2011), was that the burning rate was almost constant during burning. This was justified by the fact that the evaporation heat of methanol is almost 4-5 times bigger than that of heptane and kerosene. Different trends of burning rate have been observed during burning when fuel level is not constant throughout the experiment. Shinotake et. al. (1985) observed large variation of burning rate throughout the experiment, which is in contrast to experimental work by Hamins et. al. (1994) who observed a linear mass burning rate throughout the experiment.

As Babrauskas (1983) stated, there was a large variation for this phenomenon and more data were expected in order to completely understand this effect. But even almost 35 years after Babrauskas statement, there is still a large gap to be filled in this research area (Steinhaus et. al., 2007).

2.2.3.2 Effect of Pan Material

The heat balance in any pool fire could be expected to show changes if the pan materials differ. Due to different material conductivities, the conduction losses are expected to differ, thus the materials used to construct the pan can influence the burning rate of pool fires. Blinov and Khudiakov (1961) investigated this impact on small pool fires using ethanol, butanol and acetone as fuels, showing that different type of materials of the pan can affect the conduction losses. This phenomenon was also investigated experimentally by Vali and his co-workers (2013), confirming the theory of (Blinov and Khudiakov, 1961). In their experimental work they tried to identify the influence of different pan materials to the burning rate and flame height of methanol pool fires. They showed that during steady-state burning, the burning rate was increased with an increase in the temperature of the pan base due to different materials used.

2.2.3.3 Wind Effect

The effects of wind or other applied ventilation on a pool fire are complex. Lots of studies have investigated how burning rates of pool fires are influenced by wind conditions. Although many studies have been conducted, no concrete conclusions were made, and it has been reported that wind effects both increase (Lam et. al., 2004; Jiang and Lu, 2013) and decrease (Hu et. al., 2009) the burning rate.

Most of the data uisng hydrocarbon fuels (diesel, kerosene, gasoline, JP4, JP8) of circular pool fires (diameter 15-50cm) show that burning rate increases monotonically with an increase of wind speed. In the experimental work of Lam and co-workers (2004), using fuels (JP4 and JP8) of 20cm circular pool fire, it was shown that the burning rate was increased as the wind velocity increases.

Hu et al. (2009) conducted experiments in a wind tunnel using methanol (alcohol) and gasoline (hydrocarbon) as fuels. In case of gasoline, increasing air flow speed resulted in a monotonously increase of burning rate. On the other hand, for methanol fires, the burning rate firstly decreased until a wind speed of 1-1.5 m/s and then increased. According to Tao et. al. (2013), a similar behaviour (Hu et al., 2009) for alcohols was also observed. In their 4-10 cm square pool fire experiments the same behaviour was observed for ethanol, altering wind speed between 0-3 m/s. They also found that burning rates are sensitive to wind impingement angle, but in a non-monotonic relationship. In another experimental work by Hu et. al. (2013), no significant increase of burning rate found in case of large wind velocities.

Some other effects also affect burning rate in case of a pool fire subjected to wind. The size of pool fire is one of them. In large pool diameters (1.5-4 m) the influence of wind speed to burning rates was negligible for up to 2m/s according to (Chatris et. al., 2001). A certain effect was observed for gasoline and diesel oil pool fires only with larger values than 2 m/s of wind velocities. In the work of Jiang and Lu (2013) using hydrocarbon fuel (aviation fuel) under the same cross air flow velocity, for 0.3-0.6 m diameter pool fires, the burning rate of pool fires increase with an increase in the fuel pan diameters.

Another significant observation was made by Hu et al. (2013) who showed that orientation of pools also plays a crucial role, as pool fires with longer rim parallel to the longitudinal air flow had faster increase of burning rate.

The temperature of wall's pan was also found to influence the burning intensity of a pool fire in different wind speeds (Tao et. al., 2013). According to this work, pan's rim temperature is a good indicator of burning intensity, as under quiescent conditions is close to boiling point, while in case of increasing wind speed the temperature increases due to directly heat by the flame. In this case the flame wrapped around the pan, increasing the burning rate.

2.2.4 Flame Height

Flame height is a very important parameter for predicting how flame interacts with the surroundings, and the ignition of combustible items close to the fire source. The difficulty in calculating flame height arises from the fluctuations of the intermitted region of the flame during burning (see Fig. 2.3). Due to those fluctuations, flame height is defined as the height at which the flame is observed at least 50% of the time (Audouin et al., 1995; Zukoski, 1995; Iqbal and Sulley, 2003).

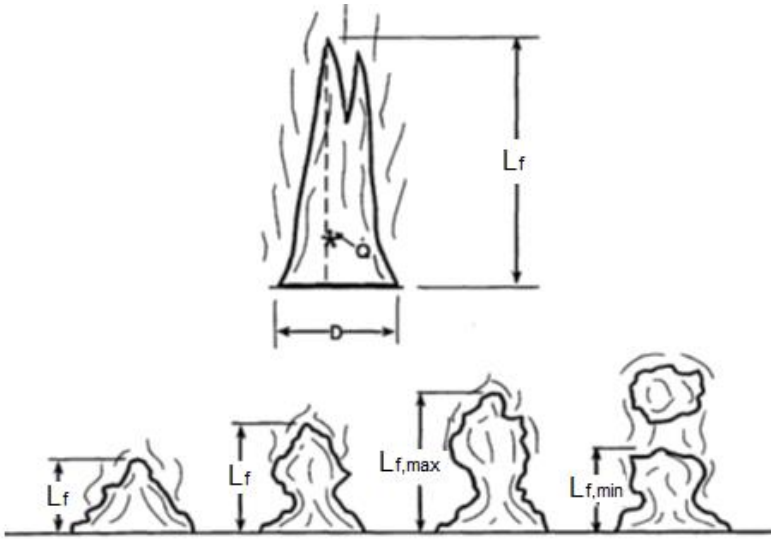

Figure 2.3 Flame height calculation (Iqbal and Sulley, 2003).

Using Froude number, the flow rate of fuel and velocity, a non-dimensional expression (Quintiere, 2006) for heat release rate can be written (see also section 6.4.5.3) as:

$$\Pi_2 = \dot{Q}^* = \frac{\dot{Q}}{\rho_\infty c_p T_\infty \sqrt{gD} D^2} \tag{2.8}$$

Then, a relationship is established between non-dimensional HRR and mean flame height, $\frac{Z_f}{D}$, as given by:

$$\frac{Z_f}{D} = f(\dot{Q}^*) \tag{2.9}$$

Many researchers have developed correlations using Froude number scaling in order to investigate flame height. Two commonly used correlations were developed by Thomas (1962) and Heskestad (1983).

Thomas (1962) conducted experiments using mainly wood cribs as the fire source and developed the following correlation for calculating flame height:

$$Z_f = 42D \left(\frac{\dot{m}''}{\rho_\infty \sqrt{gD}}\right)^{0.61} \quad \text{(m)} \tag{2.10}$$

Heskestad (1983), collecting data from a variety of fire sources, proposed a correlation for flame height which is based on heat release rate ($\dot{Q}$) and diameter (D) of the pool fire:

$$Z_f = 0.23\dot{Q}^{2/5} - 1.02D \quad \text{(m)} \tag{2.11}$$

As the main scope of this work is to study pool fires in corridor-like enclosures, only the basic characteristics of pool fires burning in free-burn conditions are presented in this section. Interested reader can find more details in relevant publications. In the following subsections, more insights into the enclosure effects are given.

2.3 Enclosure Fires

When a pool fire is placed in an enclosure, the burning behaviour of the pool fire is significantly influenced by enclosure boundaries. Although some theories and formulas from open-burn conditions may still apply in such cases, it is widely

recognised that an enclosure fire is a completely different fire scenario. For example, Bullen and Thomas (1979) investigated the burning rate of free-burn and enclosure fires and found that the burning rate of a liquid pool fire within an enclosure can be up to seven times than that of a free burning fire.

Burning of a fire in an enclosure over time is characterized by the four stages (Quintiere, 2006), (Drysdale, 2011) as shown in Fig. 2.4:

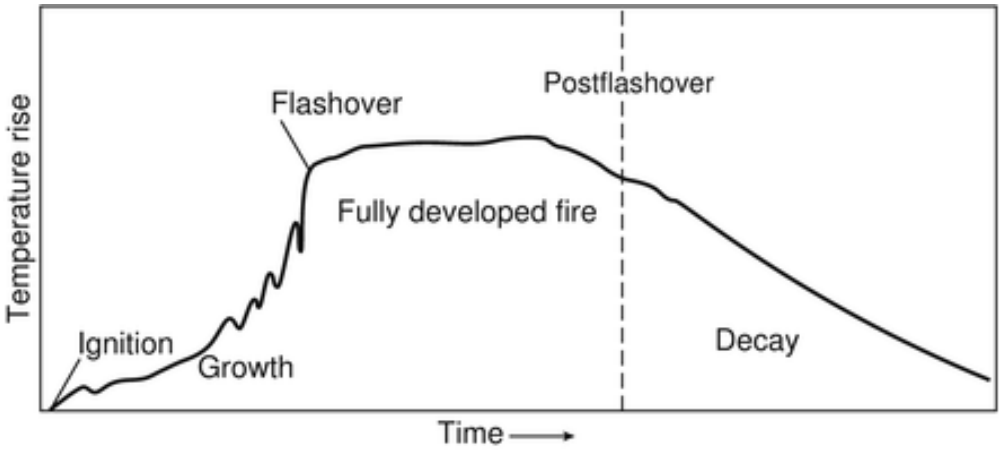

Figure 2.4 Stages of an enclosure fire.

During the growth stage (pre-flashover) fire grows slowly over time, as gas temperatures begin to rise and heat is released inside the enclosure. The growth rate is usually unpredictable, as it is affected by many factors, such as air mass inflow rate (ventilation of the enclosure) and fuel type (size, configuration). This stage is also characterised as fuel-controlled or over-ventilated. During this stage the temperatures continue to rise until the occurrence of flashover. When flashover occurs, the rate of temperature increase will change significantly and the fire will become fully developed.

The fully developed stage (post-flashover) is characterized by the peak values of HRR and gas temperatures inside the enclosure and the burning rate is usually controlled by the rate of inflowing air. This stage is also called ventilation-controlled or under-ventilated. A fire controlled by ventilation (under-ventilated condition) is the worst scenario for enclosure and façade fires, as the mass of the fuel pyrolysed may not completely burned inside the enclosure due to restrictions on the oxygen

availability. As a result, external fire spread can occur easily through ejected flames from openings. This is a major issue in high-rise buildings (Delichatsios, 2014). During the fully developed stage for under-ventilated conditions, temperatures inside the enclosure can reach 1200^{o}C, but its distribution could be affected by the geometry of the enclosure. In cubic-like enclosures temperature distribution inside the enclosure is nearly uniform (Ohmiya et. al., 2000), whereas in corridor-like enclosures non-uniform (Miyazaki and Watanabe, 1998), (Delichatsios and Silcock, 2002).

The decay stage is characterised by a decrease in HRR as the majority of the fuels have been consumed. The temperatures inside an enclosure may increase for a while initially, but they will eventually drop as heat release also does. There are two main danger issues arise in this stage though. First, the existence of non-flaming combustibles which can result in starting a new fire and secondly, the occurrence of backdraft (Drysdale, 2011) by the re-entrainment of oxygen to a volatile enclosure.

Many researchers have studied the burning rate, the heat release rate and possible external flame in enclosure fires in terms of parameters, such as the geometry of the enclosure (rectangular- or corridor-like enclosure) (Delichatsios et. al., 2004), (Lee, 2006), (Delichatsios, 2014), the opening dimensions of the enclosure (Kawagoe, 1958), (Thomas et. al., 1967), (Steckler et. al., 1982), (Yii, 2002), (Utiskul et. al., 2005), the size of the burner (Utiskul et. al., 2005), the location of the burner (Steckler et. al., 1982), (Delichatsios and Silcock, 2002), (Parkes, 2009), (Huang et. al., 2009), and the type of fuel used as fire source (Delichatsios and Silcock, 2002). In the next subsections, some relevant works to the present study are presented and discussed.

2.3.1 Heat Transfer Mechanisms in Enclosure Fires

When a fire occurs inside an enclosure, convection, conduction to the boundaries and radiation are the main mechanisms of heat transfer. As shown in Fig. 2.5, assuming the whole enclosure as a single control volume, the following equilibrium is established during quasi-steady burning on a post-flashover fire compartment:

$$\dot{Q}_{fire} = \dot{Q}_C + \dot{Q}_R + \dot{Q}_W + \dot{Q}_G \tag{2.12}$$

Where: $\dot{Q}_{fire}$ is the heat released by fire

$\dot{Q}_C$ are the convective heat losses of gas flow

$\dot{Q}_R$ is rate of heat radiated through the opening

$\dot{Q}_W$ is rate of heat transferred to the walls of the enclosure

$\dot{Q}_G$ is the heat stored in gas volume

It is interesting to mention that Kawagoe (1958) proposed that for a steady post-flashover fire the last term of the right-hand side of Eq. 2.12 can be neglected due to its small contribution comparing to other terms. Similar finding was found in (Hamins et. al., 2008).

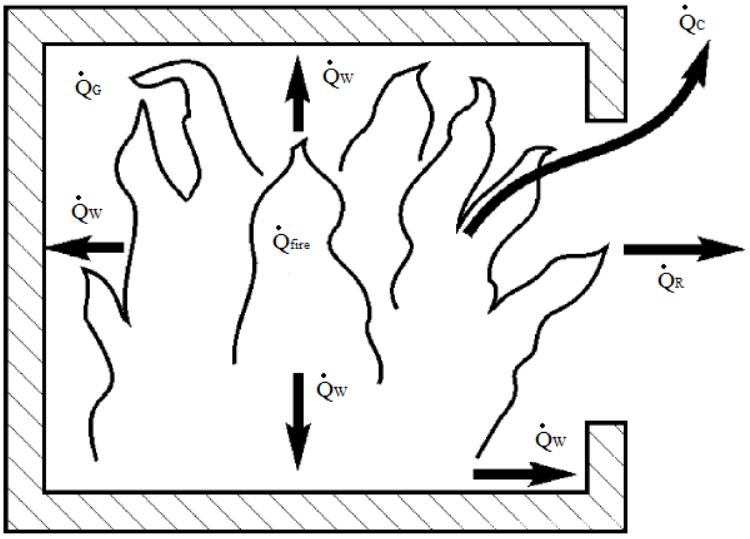

Figure 2.5 Heat transfer mechanisms in a post-flashover fire compartment.

2.3.2 Summary of Previous Research in Enclosure Fires

One of the first and most important studies was conducted by Kawagoe (1958) who carried out experiments in a small-scale room (0.4 m x 0.4 m x 0.2 m) using timber as fuel and allowed it to burn to extinction. He found that the temperature inside the room could be considered uniform and that the mass flow of air entrained the room through the opening was proportional to $A_o H_o^{1/2}$, with A_o being the area of the opening and H_o the height of the opening.

In a following work, Kawagoe and Sekine (1963), produced an energy balance and found that the burning rate of wood cribs in a cubic (0.3 m) enclosure was strongly dependent on the size and the height of the opening. They finally correlated the burning rate of fuel, $\dot{m}_T$ (kg/s), with the ventilation factor, $A_oH_o^{1/2}$

$$\dot{m}_T = 0.1 A_o H_o^{1/2} \tag{2.13}$$

Apart from the significant findings of their work, the very important contribution in fire research field was the introduction of the ventilation factor in order to describe the ventilation conditions which has been used since then in many correlations. The correlation proposed by Kawagoe was also validated in the work of Thomas et. al. (1967).

Bullen and Thomas (1979) conducted experiments in a 2 m x 1 m x 1 m enclosure using ethanol pool fires. Using two different pool fire sizes and three ventilation openings they evaluated differences in the burning rate of the pool fire within the enclosure and in free-burn conditions. They found that the pool fires within the enclosure during the growth stage were burning like in free-burn conditions. The difference was noted during the fully-developed stage, where the burning rate of the ethanol pool fires inside the enclosure was found increased by almost six times than the free-burn burning rate.

Steckler et. al. (1982) investigated the effect of the opening geometry, the fire power and the location of the fire source on the mass flow rate of air entering an enclosure, using a methane gaseous burner. In their work, they used ten different door- and window-like openings, eight burner locations and four fire powers in a full-scale room (2.8 m x 2.8 m x 2.18 m). They concluded that the air flow rate was higher when the burner is located close to the opening and reduced when the burner is moved towards the rear end of the enclosure along its centreline. They also found that using fixed opening and burner location, the mass flow of air entraining through the opening increased with an increase of fire power. Finally, they correlated the mass inflow rate, $\dot{m}_a$ (kg/s), with the ventilation factor

$$\dot{m}_a = 0.52 A_o H_o^{1/2} \tag{2.14}$$

The correlation of air inflow rate was later re-examined by Delichatsios et. al. (2004), who proposed a correction using non-dimensional relations of mass and energy balance.

$$\dot{m}_a = 0.5 A_o H_o^{1/2} - 0.5 \dot{m}_T \quad \text{(kg/s)} \tag{2.15}$$

The effect of the enclosure geometry was investigated by Thomas and Bennetts (1999) in their experimental work using a 1.5 m x 0.6 m x 0.3 m long enclosure with varying opening geometries. In their work, a liquid (96% ethanol-4% methanol) pool fire was used as the fire source. They found that in addition to the ventilation geometry, mass loss rate is also affected by the geometry of the enclosure, as long enclosures had lower mass loss rate than wide enclosures. Furthermore, they concluded that the width of the opening influenced the mass loss rate as the change of the width resulted in different flow behaviours inside the enclosure.

Delichatsios and Silcock (2002) found that the air inflow rate depends not only on the ventilation geometry but also on the geometry of the enclosure. Using data from experiments in cubic and corridor enclosures they developed the following correlation:

$$\dot{m}_T = 0.22 \dot{m}_a \quad \text{(kg/s)} \tag{2.16}$$

Another important contribution of this work was the expected behaviour of the steady-state enclosure burning rate over the ventilation factor. They stated that in any enclosure the mass pyrolysis rate increases first as the ventilation factor increases until it reaches a maximum value corresponding to the stoichiometric combustion conditions. After that point, the mass pyrolysis rate decreases with a further increase of the ventilation until the ventilation factor become infinite large corresponding to free-burn burning conditions. For very large ventilation factor the mass pyrolysis rate becomes constant. This behaviour is shown in Fig. 2.6

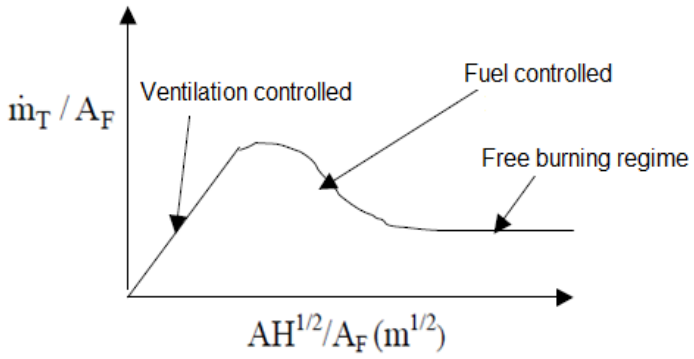

Figure 2.6 Pyrolysis rate, $\dot{m}_T$, in enclosure fires versus the ventilation factor, $AH^{1/2}$, both normalised by the area of the fuel, A_f.

Fully involved enclosure fires in terms of the mass pyrolysis rate, air inflow mass rate and excess pyrolysate were investigated by Delichatsios et. al. (2004). Many interesting conclusions were made as summarised below:

- They described the physics of the mass pyrolysis rate and the air inflow rates based on the data attained from cubic and corridor-like enclosure fire experiments. For cubic-like (rectangular) enclosures, they developed correlations for calculating the mass pyrolysis rate in both under- and well-ventilated conditions. The slope of 0.1 which Kawagoe (1963) proposed was validated for different fuels as Fig. 2.7 shows.
- The mass pyrolysis rate is affected by the mass inflow rate and flame heat fluxes during the under- and well-ventilated fire conditions respectively.
- Close to stoichiometric and well-ventilated conditions, the mass pyrolysis rate is affected by both the mass inflow rate and the air to fuel ratio by mass.
- They proposed that all the incoming air is consumed in under-ventilated fires.
- The mass inflow rate depends on the opening size, the fuel area and the enclosure geometry.

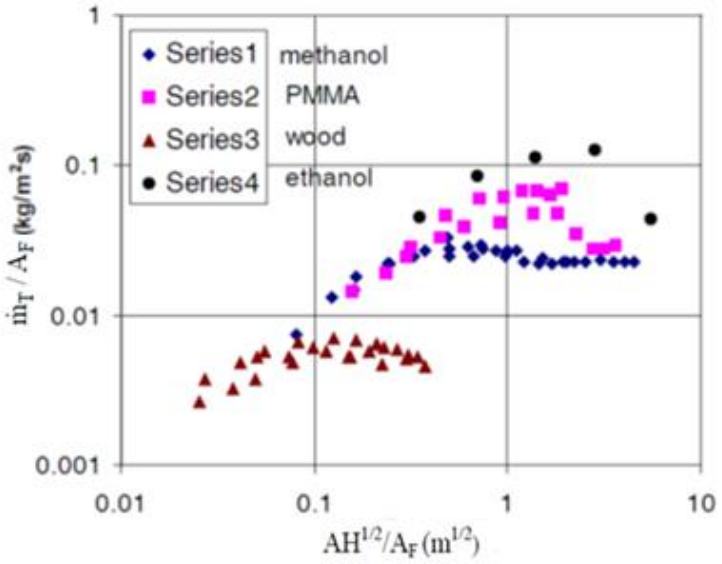

Figure 2.7 Data of mass pyrolysis rate, $\dot{m}_T$, of different fuels versus the ventilation factor, $AH^{1/2}$, both normalised by the area of the fuel, A_f, for experiments in cubic-like enclosures (Delichatsios et. al., 2004).

In the same work, some interesting findings were made for fires in corridor-like enclosures, based on the experimental work by Miyazaki and Watanabe (1998), who used heptane pool fires inside a corridor having both ends open, as shown in Fig. 2.8. Correlating the data for mass pyrolysis rate of heptane pool fires, Delichatsios et. al. (2004) concluded that the mass pyrolysis rate in a corridor-like enclosure is less than the mass pyrolysis rate in cubic-like enclosures. Thus, the slope in the under-ventilated (ventilation-controlled) regime is less than 0.1 and specifically it was found to be 0.025 as depicted in Fig. 2.9. This difference was attributed to the gas temperature profile distribution, as it changes from uniform in cubic enclosures to layered in corridor enclosures. They finally pointed out the need of further investigation to more precisely correlate the mass pyrolysis rate in corridor-like enclosures, as there is lack of experimental data in such enclosures.

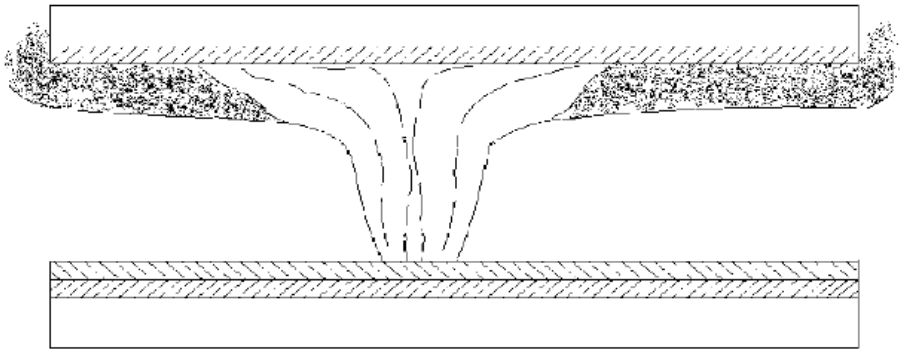

Figure 2.8 Sketch of experiments in a corridor geometry enclosure (Miyazaki and Watanabe, 1998).

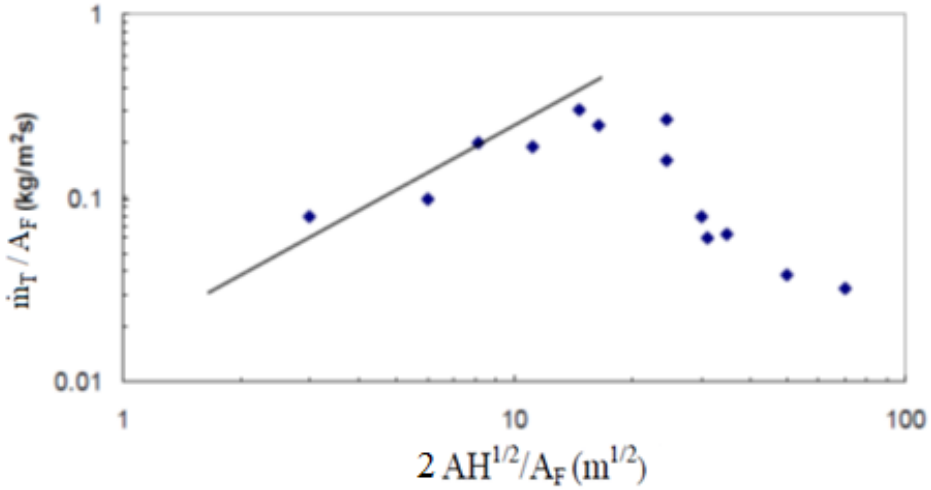

Figure 2.9 Correlation of mass pyrolysis rate versus the ventilation factor for experiments in corridor-like enclosure.

In another work in deep enclosures, Thomas et. al. (2005) investigated the fire behaviour in an 8 m long x 2 m wide x 0.6 m high enclosure with different ventilation openings. They used sixteen pans of ethanol-water mixture as the fire source, which was placed along the enclosure. Confirming some previous experiments in deep enclosures (Thomas and Bennetts, 1999), they showed that the ventilation geometry strongly affects the mass loss rate of the fires. The fires were also found to be non-uniform through the length of the enclosure, as temperatures near the ceiling were found more severe closer to the opening than closer to the closed end of the enclosure.

Thomas et. al. (2007) studied the influence of the fuel location in an ISO 9705 room (ISO 9705, 1993) by using liquid pool fires as the fire source. They used three different locations (front, centre and back) inside the enclosure in order to study the

fuel location effect and found that when the pan was placed in the centre of the enclosure, the HRR is the lowest, as the distance from the walls was larger than in the other cases, thus the radiation feedback from the walls was small. For the case when the pool fire is located at the front, closer to the opening, the burning rate is highest due to the increased radiation feedback from the enclosure and also the enhanced availability of oxygen compared to the other cases.

2.3.2.1 Experimental Studies Using Constant Level Liquid Pool Fires

As discussed in the previous section, lip height influences the burning rate of a liquid pool fire, thus many researchers have tried to minimise this effect. By minimising the lip effect of a pool fire in an enclosure fire experiment, steady conditions can be established within the enclosure, thus researchers can study fire behaviour and characteristics during steady-state.

In order to investigate steady-state conditions, researchers use systems (usually using header tanks outside the enclosure) to continuously fill the pool with fuel during burning and avoid the level of fuel to decrease. For example, Fleischmann and Parkes (1997) investigated the influence of the ventilation factor on the mass loss rate in a small rectangular enclosure. The enclosure was 1 m x 1.5 m x 1 m, with ventilation factors ranging from 0.0039 to 0.071. They used heptane in a 0.2 m diameter pan with the level of fuel inside the pan kept constant. This was achieved by a header tank connected with the pan which was constantly fed by a tank during the experiment. They found that the mass loss rate when the pool fire was placed within the enclosure was almost seven times higher compared to the mass loss rate of free-burn pool fires, showing a large enhancement due to radiation feedback.

In another work, Parkes and Fleischmann (2005) studied the effects of pool fire location and the ventilation size on the mass loss rate in a large-scale enclosure. The enclosure was of dimensions 2.4 m wide x 3.6 m long x 2.4 m height and heptane pool fires were used as fire source. The level of the fuel within the pan (20 cm diameter) during the experiments was kept constant and three locations were studied, front, centre and rear. Three different ventilation openings were used to investigate the ventilation influence on the mass loss rate. They found that the location of the pool fire has a pronounced effect on the steady-state mass loss rate. As the pan was

moved towards the back of the enclosure, the mass loss rate was higher. At the front location, closer to the opening, the mass loss rate was found slightly smaller than the free-burn case which was due to the incoming ventilation velocity through the opening. The velocity of the incoming air was found to push over the flame, so the flame was in contact with the floor, reducing the heat release rate.

Yii (2002) performed a series of compartment fire experiments in a reduced-scale room using heptane pool fires as fire source, studying the compartment ventilation and the burning behaviour of fuel in post-flashover fires. The objective of the experimental work was to obtain flow rate data from a compartment which had dimensions 1.5 m length x 1 m width x 1 m height and various wall and roof openings. He used a header tank outside the compartment for keeping the level of fuel constant inside the fuel pan during the experiments. The header tank set up for maintaining the fuel's level is shown in Fig. 2.10. He described the vent flows using extended formulas by including the roof vent and showed that the area of the roof vent and the distance between the ceiling and the soffit of the wall opening are important parameters for calculating the air inflow rate in such cases.

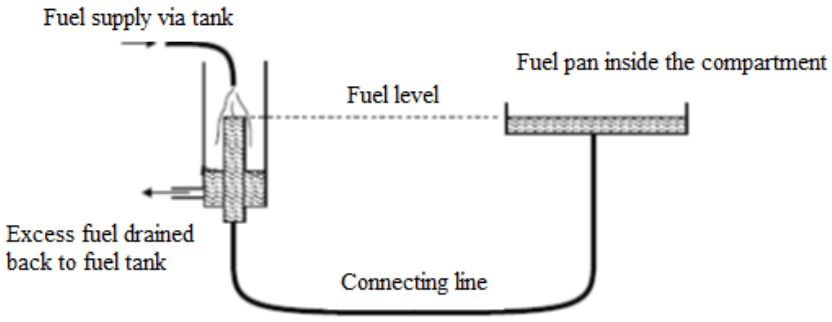

Figure 2.10 Fuel supply system of Yii (2002).

A similar header tank set up was also used in compartment fire experiments performed by Parkes (2009). He conducted heptane pool fire experiments in a 3.6 m long x 2.4 wide x 1.2 m high room with various opening geometries and three different fuel locations. Some of the findings of his work were described earlier (Parkes and Fleischmann, 2005). The header-tank set up is shown in Fig. 2.11.

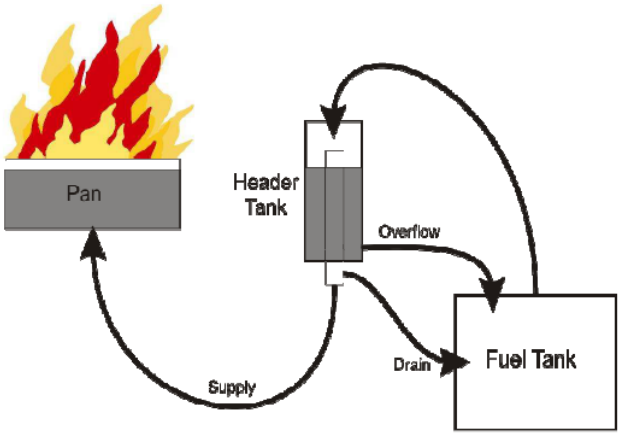

Figure 2.11 Fuel supply system of Parkes and Fleischmann (2005) and Parkes (2009).

2.3.2.2 Experimental Studies in Rectangular- and Corridor-like Enclosures

The corridor-like enclosure used in the present work has been used by the author's research group in some work. The main difference with past works is that a gaseous burner issuing propane or methane was used as the fire source instead of liquid pool fires.

Lee (2006) studied the burning behaviour of methane and propane gaseous fuels in a rectangular enclosure as well as façade fires generated by those gaseous fuels at under-ventilated conditions. He performed experiments in a rectangular enclosure having a 0.5 m cross section and length ranging from 0.5 to 1.5 m. He studied the effects of enclosure and opening geometry on the burning behaviour and the fuel supply rate and the fuel location inside the enclosure on the mass air inflow rate. In addition, he studied the influence of the mass inflow rate and mass loss rate on the flames ejected through the opening and the heat exposure on the façade of the assembly. Some significant findings regarding the burning behaviour of gaseous fuels were:

- Gas temperatures inside the enclosure were found uniform for door-like openings and enclosure geometries having length to width ratio up to three to one.
- The maximum HRR inside the enclosure was $1500A_oH_o^{1/2}$, verifying previous works. This formula was verified for propane and methane fuels.

- He verified that the mass inflow rate through the opening is 0.5 $A_oH_o^{1/2}$ due to the uniform gas temperatures.
- A new correlation for the gas temperatures inside the enclosure was developed, by incorporating the adiabatic gas temperature.

Findings of this work regarding the façade fires are given in the next section.

Beji (2009) modified the length of the corridor to 3 m, performing experiments using a propane gaseous burner as fire source. In these experiments, he studied the burning behaviour of gaseous fires with respect to the ventilation factor by using four different door-like openings and the distance between the opening and the fire source. He confirmed that the maximum ventilation-controlled HRR (Lee, 2016) is still valid for this configuration. When the fire source was located at the rear end of the enclosure, the ventilation-controlled stage was identified by a plateau HRR reached at the value of the maximum ventilation-controlled HRR. The flames detached from the burner travelling towards the opening of the enclosure and when flames were ejected from the opening the HRR increased suddenly to the theoretical value calculated by the mass flow rate and the effective heat of combustion. An example of this behaviour is shown in Fig. 2.12 (left). In over-ventilated fire experiments no flames were ejected through the opening. The location of the fire source was also a factor influencing the fire burning behaviour, as in cases that fire source was located close to the opening, flames were ejected quickly through the opening. An example of HRR history for a case with fire source located in the front box, closer to the opening, is given in Fig. 2.12 (right).

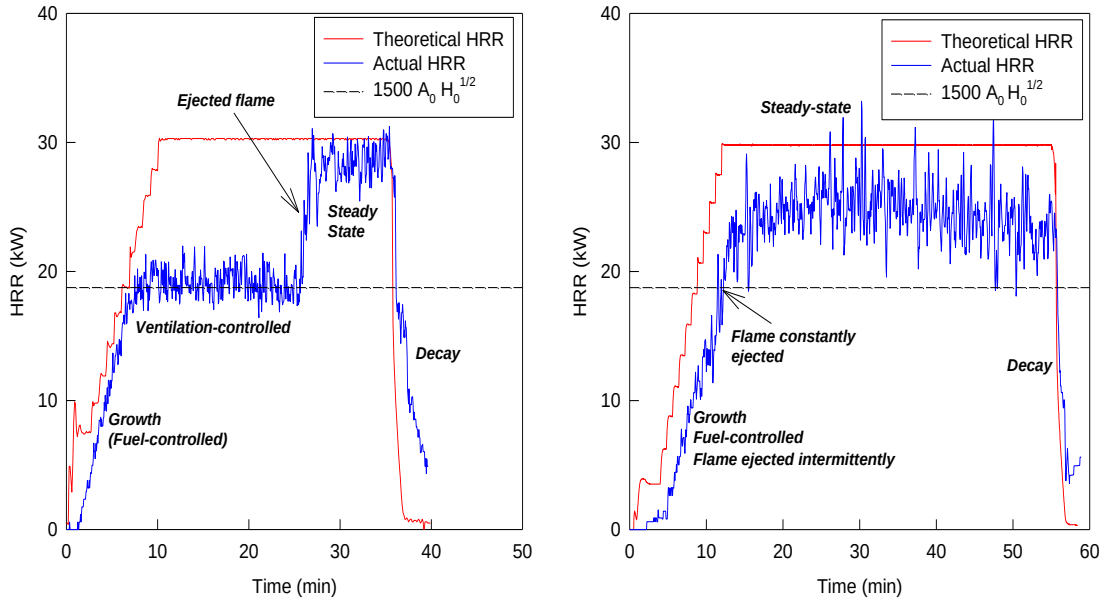

Figure 2.12 HRR profiles for two test cases using the same opening but different location of the burner, far from the opening (left) and close to the opening (right).

Ukleja (2012) used the same corridor-like enclosure to investigate the factors affecting the smoke and CO production in such enclosures. He conducted experiments using a propane gaseous burner located at the rear end of the corridor and four different opening geometries. Measurements of smoke and CO concentration were performed in different locations inside the enclosure and outside by collecting the combustion products in the hood. He found that in under-ventilated fire experiments the gas temperatures inside the enclosure has an influence on the smoke production as well as on the fuel and global equivalence ratio (GER). In addition, the smoke concentration inside the enclosure was increasing during the ventilation-controlled regime, which was attributed to the reverse flows noticed behind the flame as it was moving towards the opening. He also verified the previous findings (Lee, 2006), (Beji, 2009) regarding the HRR and burning behaviour of gaseous fuels located close to the rear end of the corridor.

2.4 Façade Fires

During the fully developed stage of an enclosure fire, flames may be ejected through the openings, which can be a major and disastrous hazard for the construction itself and the people around. Especially in high rise buildings, which are so popular in today's construction design, this significantly increases the risk of upward fire

spread. Subsequently, external flames can cause catastrophic results on the façade itself and the whole construction of the building. For this reason, this has been an attractive area of research for the last 60 years. Numerous experimental works in medium- and large-scale compartments have been carried out to investigate flames ejecting from burning enclosures, supplemented often with numerical work. Pioneering work was conducted by Yokoi (1960), who focused on the identification and characterization of external flames and the geometric parameters of the enclosure affecting them. He also proposed a correlation for flame height. Webster et al (1961) and Seigel (1969) also worked on the influence of the enclosure geometric characteristics on the flames ejecting through the opening and the characteristics of external flames. Thomas and Law (1974) improved previous correlations by re-examining previous works of Yokoi (1960), Webster et al. (1961) and Seigel (1969). More recently, Lee et al. (2007) and Lee et. al. (2012) revised Yokoi's work and proposed a correlation for flame height and heat fluxes by introducing two new length scales describing flame characteristics in both under- and over-ventilated fires. Considerable work on external flames from a burning enclosure has also been conducted by research group of Ohmiya in (Ohmiya et. al., 1998; Ohmiya et. al., 2000; Ohmiya et. al., 2003). Many studies have also investigated the thermal exposure of facades (Law, 1978), (Oleszkiewicz, 1989), (Klopovic and Turan, 2001), (Lee et al., 2007), (Empis, 2010) and (Lee et al., 2009). Law (1978) and Oleszkiewicz (1989; 1990) did a significant work towards the investigation of heat exposure of facades by identifying the parameters influencing the thermal exposure. Lee et al. (2007) and Empis (2010) proposed heat flux correlations for façade fires and in another work of Lee et al. (2009), heat flux correlation was proposed for an opposite building façade studying the presence of flames from a burning enclosure. Some research also investigated different ventilation conditions and presence of wind (Himoto et al., 2009), (Huang et al., 2009) and the presence of an opening soffit (Ohmiya et al., 2001). Some of the research related to external flames is described in detail next.

2.4.1 Fundamentals of External Flames

Façade fires can occur from a burning enclosure after flames are ejected through the openings and spread on the façade of the construction. In such case, fire is visible outside the compartment and vertical spread (on the façade) is of major risk.

External flames can occur in two different ways:

I. During the growth stage of a fire in an enclosure all combustion takes place inside the fire enclosure. As fire grows, even when a fire is fuel-controlled, flames can be long enough to reach the opening location and eject through the opening. This case is illustrated in Fig. 2.13.

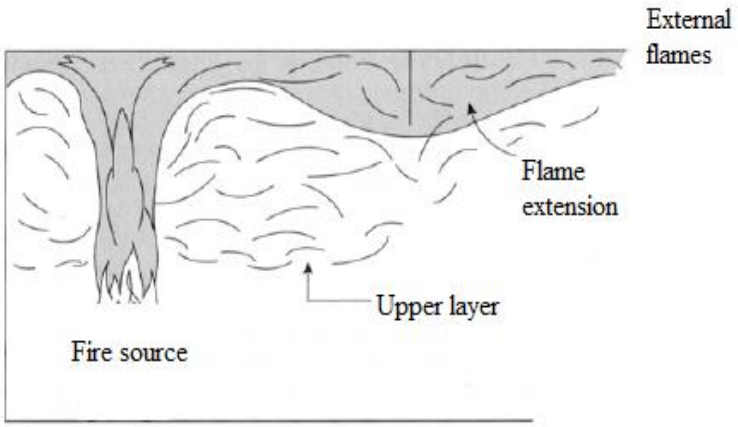

Figure 2.13 Long flames reaching the opening and ejecting through it.

II. In ventilation-controlled fires, unburnt fuel may escape from the enclosure through the opening. When they mix with the oxygen outside the enclosure combustion will occur. In this case, flames will appear outside the enclosure, as illustrated in Fig. 2.14.

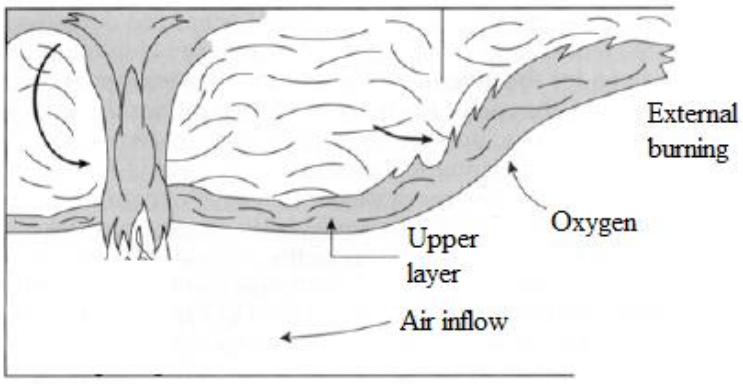

Figure 2.14 Mixing of unburnt fuel with air outside the compartment in ventilation-controlled fires.

As noted by Delichatsios (2014), fire spread on the façade of a high-rise building, illustrated in Fig. 2.15, occurs in three different mechanisms:

I. Flames ejected through a window can break the window of the upper floor resulting ignition.
II. Failure to stop the fire between the floor slab and the exterior wall.
III. Heat exposure of the inner façade allowing flames through.

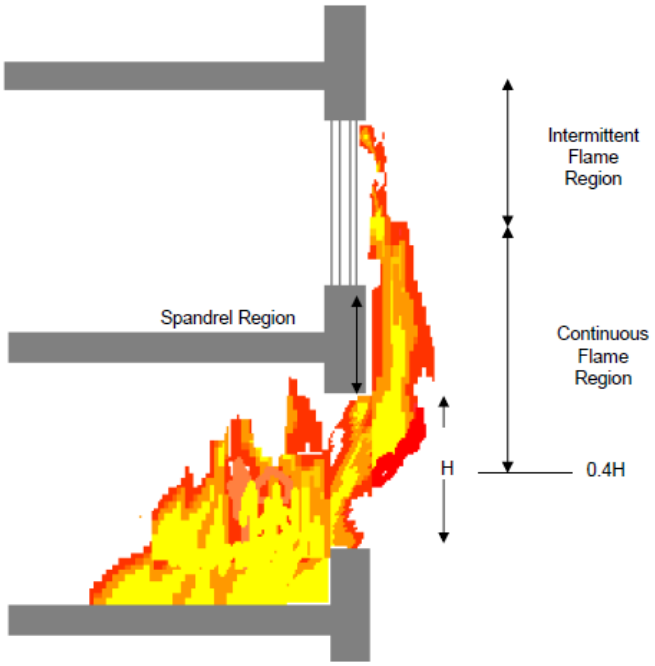

Figure 2.15 Enclosure fire and upward fire spread (Delichatsios, 2014).

In order to prevent the fire from spreading from floor to floor, it is essential to be able to determine initially the size of the fire in the enclosure and subsequently the external flame characteristics, such as the flame height and heat flux.

2.4.2 Flame Height of External Flames

Yokoi (1960) was the first researcher who studied flames emerging through openings from a burning enclosure. He conducted experiments using alcohol fuels in an enclosure of dimensions 0.4 m x 0.4 m x 0.2 m (high) and varied the dimensions of the opening. He investigated the temperature distribution of the flame emerging through the opening for well-ventilated cases in which all the combustion occurred inside the enclosure. He found that the geometry of the opening and especially the

width, had a significant effect on the flame trajectory of the fire plume, as in cases with a wide opening the fire plume projects close to the façade, whereas it projects far from the façade in cases of a narrow opening. He also introduced a length scale to represent the outflow of hot gas at the opening region. He assumed that the dimension of the upper half of the opening corresponds to the area of the horizontal rectangular heat source and used the radius, r_o, of Eq. 2.17 to correlate the temperature distribution, Θ, to the distance along the trajectory, z/ r_o, of the hot gas emerging through the opening as Fig. 2.16 shows.

$$r_o = \sqrt{\frac{HW}{2\pi}} \tag{2.17}$$

$$\Theta = \frac{\Delta T_z r_o^{5/3}}{\sqrt[3]{\frac{\dot{Q}^2 T_\infty}{c_p^2 \rho_z^2 g}}} \tag{2.18}$$

Where:

ΔT_z is the mean temperature rise at location z from the window surface along the axis of the outflow (K)

T_∞ is the ambient temperature (K)

$\dot{Q}$ is the convective heat flow rate at the opening (kW)

ρ_z is the local density of the hot gases outflow (kg/m^3)

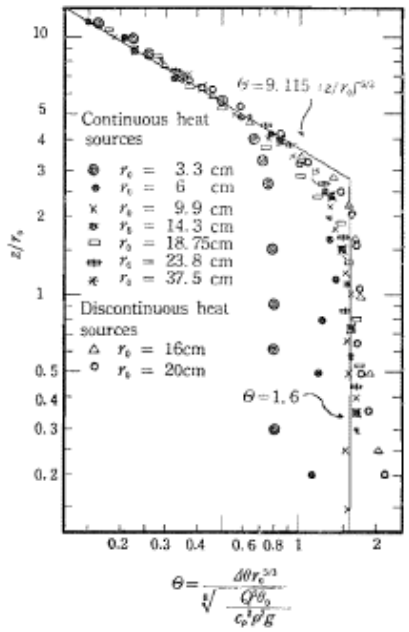

Figure 2.16 Correlation of Yokoi (1960).

Later, a correlation was derived by Thomas and Law (1974) for calculating the flame length above the window of a burning building. In their work, using data from (Yokoi, 1960), (Webster et al. 1961) and (Seigel, 1969), and applying dimensional analysis of the buoyant plume, they deduced the following equations:

With natural draught:

$$Z + H_o = 12.8\left(\frac{\dot{m}}{W_o}\right)^{2/3} \tag{2.19}$$

With forced draught:

$$Z + H_o = 16.9\left(\frac{1}{u_w}\right)^{0.43}\left(\frac{\dot{m}}{A_o^{1/2}}\right) \tag{2.20}$$

where:

z is the height of flame tip above the window (m)

H_o is the height of the window (m)

W_o is the width of the window (m)

A_o is the area of the window (m^2)

$\dot{m}$ is the burning rate (kg/s)
u_w is the wind velocity (m/s)

Ohmiya et. al. (1998) developed a room fire model for estimating the heat release rate due to combustion of excess fuel in external flames, $\dot{Q}_{ext}$, in the fully developed stage of enclosure fires. The model predicts the burning rate, $\dot{m}_T$, according to the equation:

$$\dot{Q}_{ex} = \Delta H_c \dot{m}_T - \Delta H_{air} \dot{m}_a \tag{2.21}$$

They compared their predictions with data from experiments in (Ohmiya et al., 1995) and found that the model predictions agree reasonably well with the experimental data.

Recently, Yamaguchi and Tanaka (2005) applied the neutral plane concept and modified Yokoi's model and deduced the same heat release rate in under-ventilated conditions in an enclosure as that by Kawagoe (1958).

$$\dot{Q}_{st,in} = \dot{m}_a \Delta H_{air} = 3000 \times 0.5 A_o \sqrt{H_o} = 1500 A_o \sqrt{H_o} \tag{2.22}$$

Significant work in flames ejecting a burning enclosure was also carried out by Lee, Delichatsios and their co-workers (Lee, 2006; Lee et. al., 2007). Using a small-scale 0.5 m cubic compartment and propane gaseous burner as fire source, Lee et. al. (2007) deduced three characteristic length scales associated with the flow at the exit of the enclosure as:

$$l_1 = \left(A_o \sqrt{H_o}\right)^{2/5} \tag{2.23a}$$

$$l_2 = \left(A_o {H_o}^2\right)^{1/4} \tag{2.23b}$$

$$l_3 \propto \left(A_o {H_o}^{4/3}\right)^{3/10} \tag{2.23c}$$

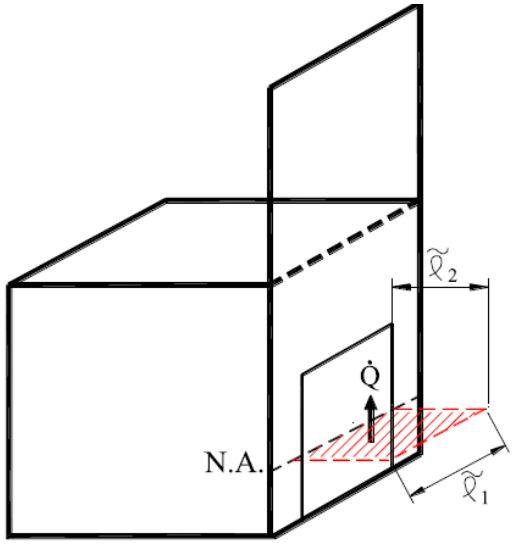

Figure 2.17 Physical meaning of length scales l_1 and l_2 (Lee et. al., 2012).

According to Fig. 2.17, the first length scale is related to the size of the opening required to accommodate the convective flow and the other two length scales express the horizontal extension of the flow with or without flames outside the enclosure owing to the competition of horizontal momentum with the buoyancy. The flame height, using length scale, l_1, and the excess HRR, $\dot{Q}_{ex}$, is given by the expression:

$$\frac{Z_f - Z_n}{l_1} = f\left(\frac{\dot{Q}_{ex}}{\rho_\infty c_p T_\infty \sqrt{g} {l_1}^{5/2}}\right) \tag{2.24}$$

where:

Z_f is the mean flame height (m)

Z_n is the location of the neutral plane (m)

As explained in (Lee et. al., 2007), (Lee, 2006), (Delichatsios, 2014), burning occurs inside the enclosure of HRR (=$1500A_oH_o^{1/2}$). In under-ventilated enclosure fires, when HRR becomes larger than this value, external burning may occur.

Based on the length scales proposed in (Lee et. al., 2007), correlations for flame height have been proposed in façade fires of enclosures with openings having

sidewalls (Lu et. al., 2013) and in cases of façade fires of enclosures having two openings of same geometry on the façade wall (Lu et al., 2015).

2.4.3 Heat Flux on the Facade

The heat flux is measured on the façade, usually by Gardon gauge meters, to investigate how flames ejecting through the openings can impact on the façade of a burning enclosure. Oleszkiewicz (1989) performed large-scale experiments using gaseous propane burners, to study the impact of the opening area and the HRR on the exterior wall. His facility was consisted of a 10.3 m high three-storey burn facility having a fire compartment at the ground floor and a concrete block front wall covered by 13mm thick non-combustible boards. The total heat flux on the external wall was measured using Gardon gauge meters. He used five different opening geometries and four HRR values and found that an increase of HRR resulted in increase of heat exposure on the external structure. He also concluded that a wider window caused large heat flux on the façade.

Klopovic and Turan (2001) performed tests in a large-scale facility of a three-storey building having a burning room of dimensions 5.31 m x 3.6 m x 2.4 m (high) in the first floor. The façade was consisted of 9 mm thickness compressed cement sheeting. The burning room had a 2.4 m x 1.5 m window on the south wall (where the façade was located) and a 0.82 m x 2.04 m on the opposite side (north wall). By opening or closing the openings, both forced and non-forced draught ventilation and wind conditions were investigated. Real furniture was used as the fuel source. On the façade, six Gardon gauge meters were used. In every experiment, the glass of the upper storey compartment was breached even though its distance from the lower window was three times larger than that recommended (Yokoi, 1960) for preventing vertical fire spread, showing an underestimation of potential vertical fire spread risk in real fire scenarios. High heat fluxes to the façade were attributed to the fuel used (real furniture instead of wood cribs used in previous experimental works) and its distribution throughout the burning compartment. Their measurements indicated that further investigation is essential for proposing heat flux correlations and used in design.

Ohmiya et al. (2003) performed experiments in a small-scale compartment of various opening geometries, using methane gas fuel of various supply rates as the fire source. They found that flames ejected through the opening not only in under-ventilated enclosure fires but in over-ventilated (Delichatsios, 2014). They proposed a correlation for heat flux on the façade of the enclosure, $\dot{q}''$, based on the width, W_o, and height, H_o, of the opening, the flame height, Z_f, and the outside heat release rate of the plume, $\dot{Q}_{conv}$:

$$\frac{\dot{q}''Z_f}{(\dot{Q}_{conv}/W_o)} = f\left(\frac{Z}{Z_f}, \frac{W_o}{H_o}\right) \tag{2.25}$$

assuming that:

$$\dot{Q}_{conv,} = max\{[(\dot{m}_f + 0.5A_o{H_o}^{1/2})c_p(T_g - T_{oo})], [(\dot{m}_f + 0.5A_oH_o^{1/2})c_p(T_g - T_{oo}) + \dot{Q}_{ex}]\}$$

A significant work related to heat exposure on the façade performed by Lee et. al. (2007). Using an enclosure of 1.5 m x 0.5 m x 0.5 m (high) and a façade above the opening, they correlated the flame height based on the length scales described in Eq. 2.23. Regarding heat exposure of the façade, they measured the total heat flux on the façade using steel plate heat flux meters (Zhang and Delichatsios, 2009) and proposed a correlation for the heat flux in the centre of the façade as shown in Fig. 2.18. For the correlation proposed, they used the length scale l_1, and the correlation was reasonably applied in experiments of different openings, enclosure geometry (length ranging from 0.5 – 1.5 m) and gas supply rate. Three regions were also identified, showing the continuous and the intermittent flame and the purely convective flow.

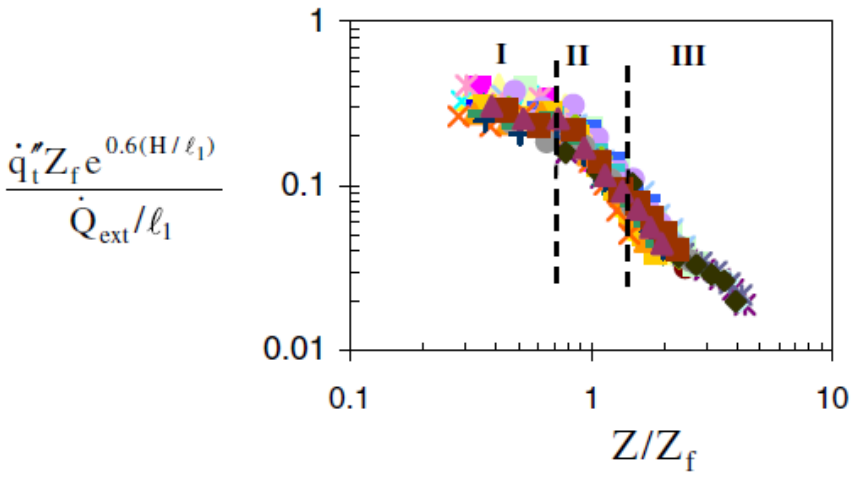

Figure 2.18 Correlation for the heat flux on the façade (Lee et. al., 2007).

Lee et. al. (2009) also investigated the heat flux of an opposite wall facing the burning enclosure. They used the same enclosure as (Lee et. al., 2007) and investigated the impact of various opening geometries, fire supply rate and distance between the enclosure and the opposing façade to the heat exposure of both facades. They proposed a correlation for heat fluxes on the façade using length scales l_1 and l_3.

Finally, Empis (2010) conducted full-scale experiments (Dalmarnock fire test) to investigate the internal structural behaviour and the heat exposure of a non-combustible façade from externally venting flames in a real high-rise building. The main aim of the experiments was to collect a comprehensive set of data from a realistic fire scenario during post-flashover stage and use it to evaluate analytical fire models. In this work, a simplified model for predicting heat fluxes on the façade was formed and validated. In addition, it was clearly noted that further investigation should be performed using realistic fire scenarios for characterising external flames and heat exposure of facades.

2.5 Conclusions and Design of Research Plan

In this chapter literature review was conducted. Firstly, free-burn burning of liquid pool fires was reviewed, focusing on factors influencing the burning behaviour (burning rate-HRR) and their characteristics (flame height). The main part of this chapter was focused in enclosure fires, reviewing the experimental work which has been carried out in burning enclosures. Burning behaviour of fires within an

enclosure is investigated, focusing on the burning rate of different fuels and the parameters which impact on the fire development inside different types of enclosures. Finally, the characteristics of façade fires were studied, as flames ejecting from burning enclosures is one of the most significant hazards in case of a fire.

The literature review conducted in this chapter resulted in the following conclusions which act as a guide to the design of the current research program.

1. As Delichatsios (2014) pointed out, it is essential to investigate the development of an enclosure fire before attempting to study its spread to adjacent buildings or spread from floor to floor in high-rise buildings. Thus, this work mainly focuses on enclosure fires and the characteristics of flames possible emerging from a burning enclosure.
2. In most of the previous work, rectangular or cubic-like enclosures were used. Although Thomas and Bennetts (1999) concluded that the geometry of an enclosure affects the burning rate of liquid pool fires and fire development, there is a lack of experimental data in other types of enclosures with large aspect ratios. As a result, there is an urgent need of more experimental data from experiments in such enclosures to evaluate correlations related with burning rate, HRR and flame height, as noted by Delichatsios et. al. (2004) and Delichatsios (2014). Considering that the modern constructions differ from the typical cubic-like enclosures (see tunnels, large offices etc.), there is a strong need to assess and further investigate the burning behaviour in non-typical enclosures. These are the key reasons why a corridor-like enclosure is used in this work as a burning enclosure.
3. In terms of the fire source, liquid pool fires of constant fuel level inside the pool during burning were chosen to be used in this work. Most previous work in a corridor-like enclosure was performed using gaseous fuels (Lee, 2006; Beji, 2009; Ukleja, 2012). Using a gaseous burner, the mass flow rate and thus the HRR is prescribed. On the contrary, the burning rate of a liquid pool fire is influenced by many factors, such as the geometry of the enclosure, the location and size of the pan and the size of the opening. Liquid pool fires represent a more ‘realistic’ fire source, as its burning rate and fire development is more difficult to be controlled or predicted.

4. The study of fundamental fire phenomena within a burning enclosure is achieved by establishing steady-state conditions inside the enclosure. Choosing to keep the level of the fuel constant inside the pool during burning helps towards this direction as data during steady-state conditions can be collected. A fuel delivery system was constructed for that reason, like those described in (Yii, 2002) and (Parkes, 2009).
5. There are many parameters influencing the fire development (Quintiere, 2006; Drysdale, 2011) within an enclosure and some of them have been extensively studied in cubic-like enclosures (Kawagoe, 1958; Bullen and Thomas, 1979; Steckler et. al. 1982; Delichatsios et. al., 2004; Parkes, 2009; etc.). In this study three parameters finally were chosen to be studied, namely the opening dimensions, the fire size and the fire source location.
6. The use of liquid pool fires is also important with respect to façade fires. In the majority of research work relevant to façade fires, gaseous burners providing steady-state conditions have been used (Oleszkiewicz, 1989; Ohmiya et. al., 2003; Lee et. al., 2007; Lu et. al., 2013; Delichatsios, 2014). Only a few studies (Klopovic and Turan, 2001, Empis, 2010, Asimakopoulou, Chotzoglou et. al., 2016) have been performed using liquid pool fires as fire source, thus more results from experiments with such fire source need to be evaluated with existing correlations regarding flame height and heat exposure of the façade.

CHAPTER 3

EXPERIMENTAL METHODOLOGY

3.1 Introduction

This chapter describes the experimental methodology and setup used in the present work. It starts with a detailed description of the experimental enclosure, including the size and construction of the corridor-like enclosure, along with the ventilation geometries. Details on the pool fire source are given, such as the size, the location and the delivery system used in the corridor experiments. Subsequently, the measuring devices are presented. Measurements of fuel's mass loss, heat release rate, gas temperatures, heat fluxes, flame height were taken during the experiments using appropriate techniques. Location of the measuring equipment, uncertainties of measurements and calibration process are also given in detail. Then, a short description of the procedure followed in the experiments and a matrix with all the experiments conducted, including the factors altered during this experimental work, are given. Finally, a summary of the experimental methodology presented in this chapter is given in the conclusions' section.

3.2 Corridor-like Enclosure and External Façade Rig

A corridor-like enclosure was used in the present study, having dimensions of 3 m long x 0.5 m wide x 0.5 m high. The enclosure was constructed using six cubic boxes, as shown in Figs. 3.1 and 3.2. All boxes are placed on a steel frame.

Each box is a 0.5 m cubic box made of two different wall lining materials. High temperature resistant boards of 40mm thickness (Unifrax LD) and of high emissivity (close to unity) are used as inner insulation walls, whereas the outer walls are constructed using 12mm MDF layer boards. All the connections and attachments of the walls were made in such a way that no parts of the steel frame were exposed to fire.

A facade is extended over the corridor-like enclosure, on the side where the opening is, in order to study external flames coming out of the enclosure. The façade is 1.15 m high by 1 m wide and is constructed using a 40 mm thick insulation board. The unexposed surface of the insulation board is attached to a 12 mm MDF layer board (see Fig. 3.3).

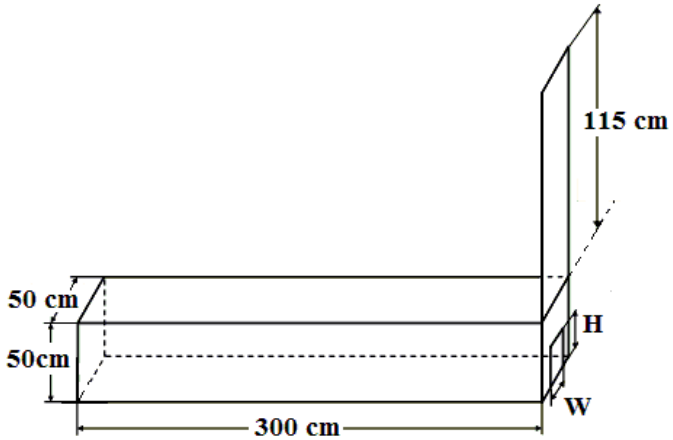

Figure 3.1 A 3-D sketch of the corridor-like enclosure along with the façade.

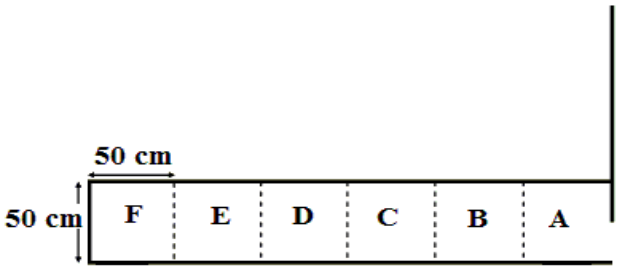

Figure 3.2 The side view of the corridor-like enclosure.

Figure 3.3 Photos of the corridor-like enclosure experimental rig. a) the corridor made by putting together 6 cubic boxes b) the back box (Box F) separated, made by MDF board and the inner thermal insulation boards and c) inner walls of the corridor enclosure.

Investigating how the ventilation factor affects the burning behaviour of the pool fire, eight different door-like opening geometries were used in the present work. A full list of the openings' dimensions and their ventilation factors are summarised in Table

5. The openings were created by modifying 40mm thick Unifrax LD insulation boards and always located in the front box (Box A).

Table 5 Opening dimensions, ventilation factors and maximum HRR inside the enclosure of the openings studied in the present work.

Width (W_o) x Height (H_o) (cm)	**Ventilation Factor ($A_oH_o^{1/2}$)**	**$Q_{st,in}$ (=1500 $A_oH_o^{1/2}$)**
10 x 10	0.0032	4.8
15 x 15	0.0087	13.1
10 x 25	0.0125	18.8
20 x 20	0.0179	26.7
25 x 25	0.0313	46.5
30 x 30	0.0493	73.5
50 x 25	0.0625	93.8
50 x 50	0.1767	265.1

3.3 Pool Fire Source

Liquid pool fires were used as the fire source in this work. Although a significant amount of work has been previously carried out using gaseous burners (Lee, 2006), (Beji, 2009), (Ukleja, 2012) in corridor enclosures and façade fires, limited work is done using liquid fuel pool fires. In the present work, ethanol of 98% purity was used. Ethanol is a common commercial liquid fuel used in many previous experimental works especially in quiescent conditions (Hu et al., 2013), (Ditch et al., 2013), (Klassen and Gore, 1992), (Tewarson and Marlair, 2004) but limited studies (Bullen and Thomas, 1978) have been conducted using ethanol in enclosure fires to the best knowledge of the author. This work seeks to fill this knowledge gap by providing experimental data in long enclosures. Basic characteristics of ethanol are given in the Table 6 (Drysdale, 2011).

Table 6 Characteristics of Ethanol used as fuel in this work.

Chemical Formula	C_2H_6O
Boiling Point	78 ^oC
Density	789 kg/m^3
Effective Heat of Combustion	26780 KJ/kg

3.3.1 Pool Fire Size and Location

Two different pan sizes and locations inside the corridor were studied in this project. Both pans used were circular, made of stainless steel, having a 3 mm thick wall and a 5mm thick base. The height of the pans was 60 mm having dimensions of 0.2 and 0.3 m in diameter. The 30 cm diameter pan is shown in Fig. 3.4. According to the literature (Hottel, 1959), (Zabetakis and Burgess, 1961), the controlling mechanism of heat transfer in a pool fire is convection when the diameter is less than 0.2 m, but as diameter increases the radiation becomes dominant. As it was noted by Babrauskas (Babrauskas, 1986), pool fires of less than 0.2 m diameter are not of interest in enclosure fires, as burning rates are not sufficiently high. Therefore, it was decided to investigate a 0.2 m diameter pan and a 0.3 m diameter pan which can be considered as a large pool fire scenario dominated by radiation.

Figure 3.4 The 30 cm diameter pan, placed inside the corridor.

The pans were wrapped by a water-cooled circuit as shown in Fig. 3.5. The water flowing inside the 6 mm diameter copper pipe was able to cool down the wall of the pans during burning. Small pebbles were placed inside the pan (see Fig. 3.4) in order to minimise boiling of the surface of the fuel due to heat feedback.

The locations of a pool fire examined in this research were based on the distance from the opening of the corridor. In particular, the pan was placed on the floor at the centre of the front box (Box A), being close to the opening or at the centre of the rear box (Box F), being furthest from the opening.

Figure 3.5 The 20 cm pan with the water-cooling circuit wrapped around the walls during its construction.

3.3.2 Fuel Delivery and Level Maintenance System

The fuel level inside the pan was kept constant during burning using a newly designed fuel delivery and level maintenance system, consisting of three tanks. The fuel level was kept at around 10mm from the pan's rim during burning for minimising the lip effect (see Literature review of Chapter 2). Fuel is driven by gravity from the upper tank to the header tank. Applying the communicating vessels principle, a copper tube connects the header tank and the bottom of the pan, with excess fuel in the header tank flushed to the lower tank as shown in Fig. 3.6. The whole fuel supply was placed on a balance with a maximum load of 36 kg and 0.2 g accuracy. Mass was recorded every 3 s. All tanks were placed next to the corridor minimising the length of the tube connecting the tanks and the pan. For safety reasons, manually handled valves were hooked on different spots of the tubes of the system for cutting immediately the fuel supply in case of emergency. Similar systems have been used in cubic-like enclosures (Parkes, 2009), (Yii, 2002) as well as in open conditions (Hu et al., 2013).

The level of the fuel inside the header tank was monitored by visual observations during each experiment, as the header tank was made of a transparent material. In addition, two K-type thermocouples of 1 mm bare bead diameter were placed inside the pan, 2 mm above and 2 mm under the surface of the fuel respectively. The thermocouple placed under the fuel surface was not exposed to fire, so the temperature was always under the boiling point of the fuel. Any rapid change observed on the temperature measured under the surface would indicate that surface of the fuel was lowering, thus was not kept constant. On the other hand, the thermocouple above the surface was exposed to fire, so the temperatures monitored

were higher. Because both ways of monitoring the level were found to be accurate, after a few experiments conducted it was decided to remove the thermocouples from the pan.

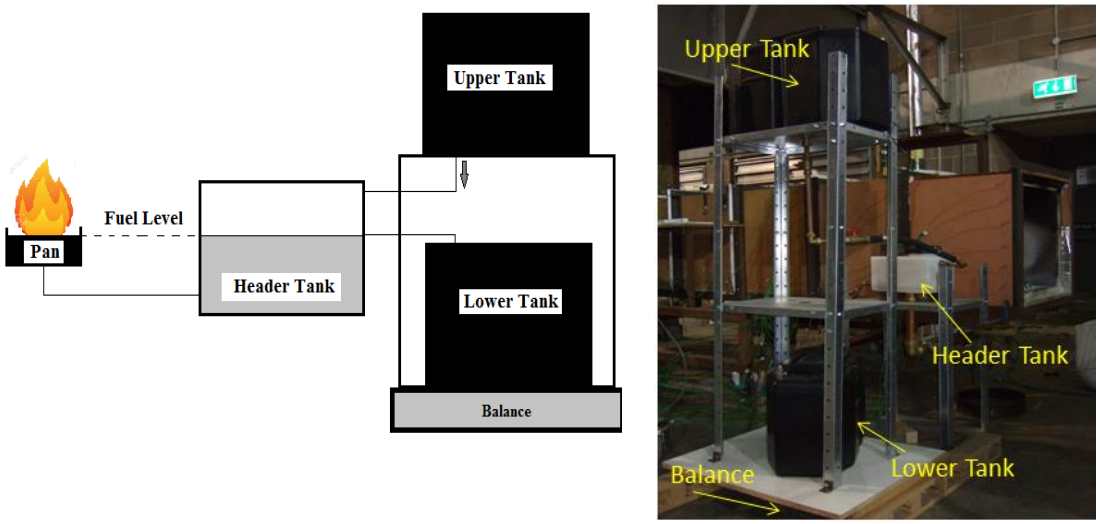

Figure 3.6 A sketch of the fuel supply and level maintenance system (left) and a picture of it (right).

3.4 Measurements Performed

This section provides a detailed description of the measurement techniques applied in the present research, along with the locations of the instrumentation (thermocouples, steel plate heat flux sensors, Gardon gauges, CCD camera, hood). The experimental uncertainties and calibration details are also provided.

3.4.1 Heat Release Rate

The assembly was placed under a 3 m x 3 m oxygen depletion system exhaust hood for measuring the actual heat release rate. The whole assembly is shown in Fig. 3.7. Hence, CO, CO_2, O_2 and smoke produced during the combustion were collected in the hood. Data were collected every 3 s. The oxygen consumption method (Janssens and Parker, 1992) was applied on the data of CO, CO_2, and O_2 collected, in order to calculate HRR. Furthermore, in order to corroborate the results of actual heat release rate, calculations were also performed by using data of CO and CO_2 only (Tewarson, 1995), (Tewarson, 2008). The calorimeter analyser was developed by Dark Star Ltd (UK).

The measured heat release rate was then compared with the theoretical maximum heat release rate, which was calculated by multiplying the measured mass loss rate by the digital balance and the effective heat of combustion of ethanol.

$$\dot{Q}_{th} = \dot{m}_f \times \Delta H_c \quad (3.1)$$

where

$\dot{Q}_{th}$ is theoretical heat release rate (kW)

$\dot{m}_f$ is the mass loss rate calculated from the mass loss data (kg)

ΔH_c is the effective heat of combustion of ethanol which is 26780 kJ/kg

Figure 3.7 The assembly placed under the 3 x 3 m hood.

3.4.1.1 Drift of Oxygen Analyser

As mentioned by Ukleja (2012), the oxygen analyser tends to drift over time. In preliminary experiments conducted in this research, this drift was particularly large when there was not sufficient time for calibrating the HRR before each test. Thereafter, it was decided to run the calibration for more than an hour before each experiment conducted for limiting drifting.

3.4.1.2 Calibration of HRR

Calibration of the hood was carried out before each experiment using a small 0.2 x 0.1 m gas burner. The gas burner was placed in front of the corridor's opening as shown in Fig. 3.8 during calibration and removed after calibration was completed. Propane gas was used and each calibration run was consisted of a few steps in different HRR levels by controlling the gas supply, thus the theoretical HRR. An example of a calibration run in different HRR levels is illustrated in Fig. 3.9. Heat release rate calculated by both the oxygen depletion method and only CO/CO_2 measurement are also plotted. Good agreement is observed between the theoretical and actual heat release rates calculated using both methods.

Figure 3.8 The propane gas burner placed in front of the opening for calibrating the hood.

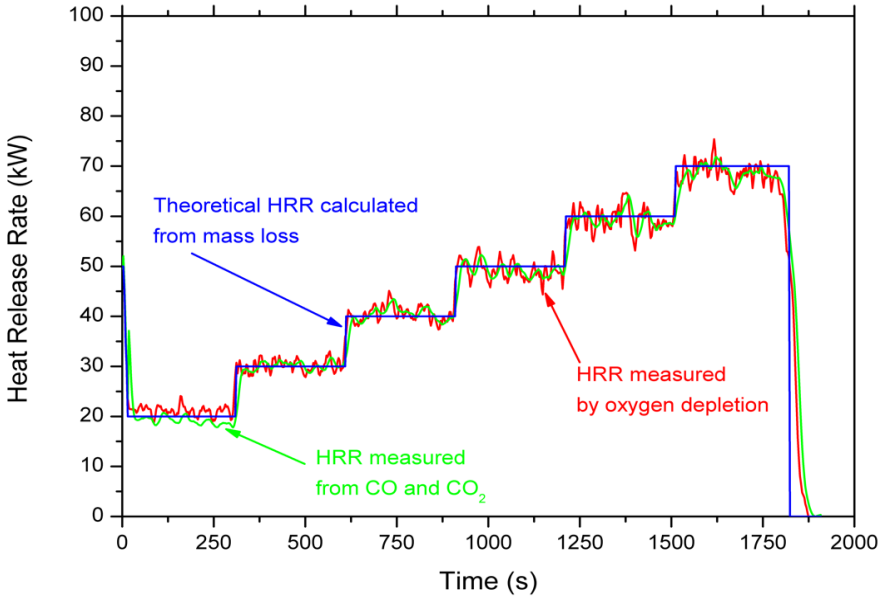

Figure 3.9 Heat release rate calibration run, showing HRR measured a) by oxygen depletion (red), b) from CO and CO_2 (green) and c) the theoretical HRR calculated from mass loss (blue).

3.4.2 Mass Loss of Fuel

In order to measure the mass loss rate of fuel during burning, the upper and lower tanks of the fuel supply and level maintenance system (Fig. 3.6) were placed on a balance. The mass of the remaining fuel inside those tanks was recorded during the experiment. The balance has a maximum load of 36 kg with 0.2 g accuracy. The mass was logged and recorded every 3 s.

Before experiments were conducted in the corridor-like enclosure, free-burn ethanol pool fire experiments were conducted for comparison reasons and to ensure that the fuel delivery and level maintenance system works properly (see Fig. 3.10). Each test run lasted for about 15-20 minutes to ensure steady-state conditions are established. The pans' walls were kept cooled using the water-cooling circuit which was wrapped around the walls and the fuel surface was kept at constant height of about 1 cm from pan's rim inside the pan during burning. Before the start of the experiment, the gas analyser of the hood was calibrated. Ignition was achieved using a lighter in the centre of the fuel surface.

Figure 3.10 Burning of the 30 cm diameter ethanol pool fire in free-burn conditions.

3.4.2.1 Repeatability of free-burn pool fire experiments

To ensure repeatable results and examine the measuring capability of the fuel supply and delivery system, three experiments were conducted for each pan. Figure 3.11 shows a comparison of the MLR history from the three repeatability tests using the

30 cm diameter pan. It is observed that the burning rates of the pool fires are close under the same free-burn conditions indicating good repeatability of the experiments.

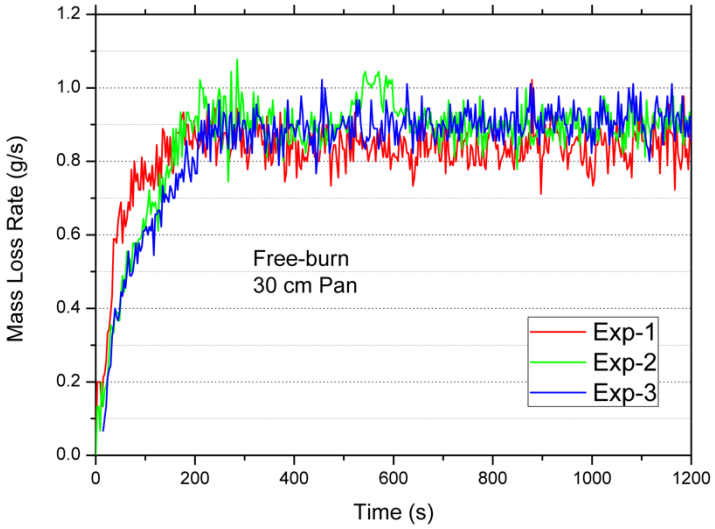

Figure 3.11 Experimental results of MLR histories over time for three repeating experiments of the 30 cm diameter pool fire in free-burn burning showing good repeatability of MLR measurements.

3.4.2.2 MLR and HRR measurements of the free-burn pool fires

The burning rate (g/s) histories for the two diameter pans (FB20 and FB30 cases) used in this work in free-burn conditions are shown in Fig. 3.9. In both cases, after the ignition, the fire spreads to the whole surface of the pool before steady burning is achieved for the rest of the experiment. These periods are distinguished in Fig. 3.12.

- An initial growth period, corresponding to the development of the fire. In both cases this growth period lasted about 240 s and, as will be discussed next, this duration is affected by fuel properties and suppression of convective motion. The burning rate in this period progressively increases over time and the fire spreads over the surface of the fuel inside the pan accompanied by an increase of the flame size.
- A steady burning period, starting at the time when the burning rate becomes steady. In this period steady-state conditions are established. This period is taken into account for calculating the average free-burn burning rates for cases FB20 and FB30.

Same regime periods have been found in literature (Rasbach et al., 1956), (Chatris et al., 2001), (Ditch et al., 2013) regarding burning of pool fires in free-burn conditions. It should be noted that in these studies a decay period was observed following the steady burning, in which burning rate decreases due to the decrease of the fuel amount inside the pan. However, this is considered beyond the scope of this study, as the fuel level was kept constant in this study.

After the growth period, steady-state conditions were established, and MLR and HRR became steady. During the steady-burning period, the average burning rate of the 20 cm diameter pan was calculated as 0.34 g/s and for the 30 cm diameter pan 0.92 g/s respectively. The theoretical maximum HRR for each case is calculated by multiplying the burning rate of the steady-state period by the heat of combustion of ethanol (ΔH_c=26.78 MJ/kg). Subsequently, the theoretical HRR for FB20 and FB30 cases are calculated as 9.1 kW and 24.6 kW respectively.

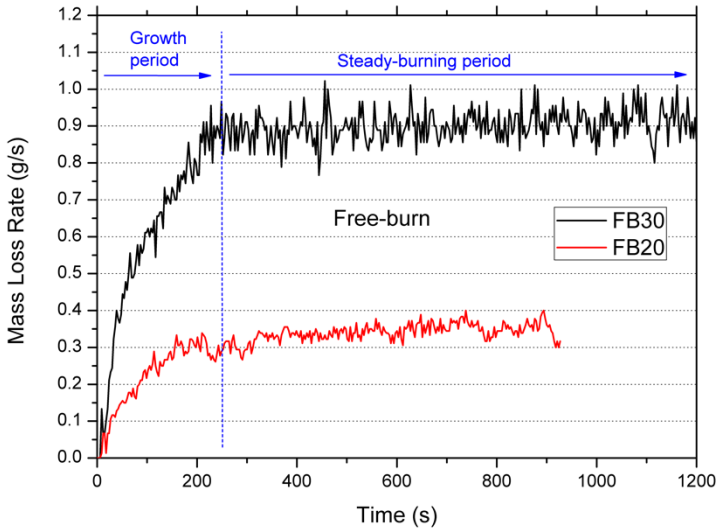

Figure 3.12 Burning rate histories for the FB20 and FB30 cases (20 cm and 30 cm pans in free-burn).

Figure 3.13 shows a comparison of the theoretical and measured HRR profiles for the FB30 case. Very good agreement of the two measurements during steady-state period is observed. The main difference was observed during the growth period, which is possibly due to the time needed initially for transporting fuel to the pan from the tank. The growth period was found to last about 240 s as shown in Fig. 3.12 for both cases. After ignition, the fire keeps increasing while it spreads quickly over the surface of the fuel. A measure for suppressing convective motion in the liquid

during the burning period was taken, by filling the pan with small pebbles as is shown in Fig. 3.14. It is suggested in (Hu et. al, 2013) that such a method could be used for suppressing large convective motion in pool fires, but this finding still requires further validation. As noted by Luketa (2010) in his study using hydrocarbon fuels, it is unclear how this method affects the mass burning rate. Whilst it can reduce convective motion, it may also enhance the reflectivity of the surface, thus influences the radiation feedback from the flames back to the pool.

A reason for the initial long growth period could be the low temperature of the water flowing inside the water-cooling circuit. As tap water was used, temperature of the water flowing around the pans' walls was measured 15-20^{o}C during burning. The walls of the pans were kept cooled and the liquid fuel in depth was not heated fast.
Ditch and his co-workers (Ditch et al., 2013) noted that fuel properties are also responsible for the time that it takes for the burning rate of pool fires to become steady. They observed that burning of less sooty fuels (alcohols) has a longer growth period than the sootier fuels, such as hydrocarbon fuels.

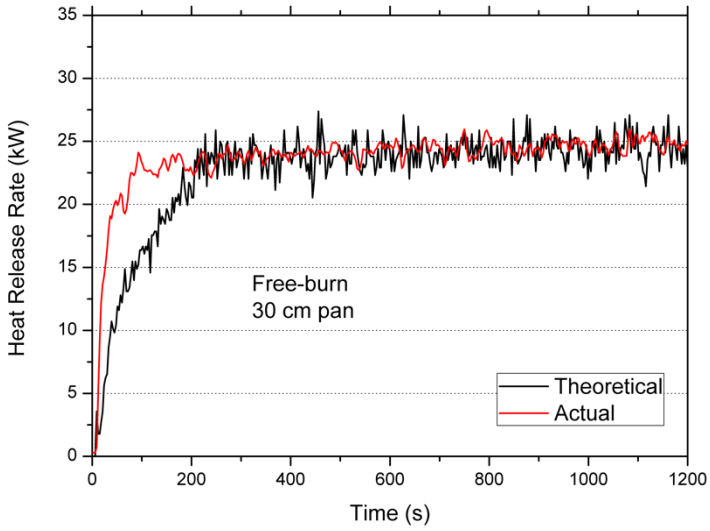

Figure 3.13 Actual and theoretical HRR profiles over time for the free-burn case of the 30 cm pan.

Figure 3.14 Use of small pebbles inside the pan.

The average combustion efficiency during the steady-state period, which was calculated by dividing the measured actual HRR using oxygen calorimetry by the theoretical HRR, was found to be 0.97 for both pan sizes.

Because flame height calculations using video images were not made for the open burning cases (i.e., FB20 and FB30), an estimation of the flame height was made based on Heskestad's correlation, i.e., Eq. 2.11 (Heskestad, 1983). The mean flame height during steady-state burning for the FB20 case is calculated to be 0.35 m and for FB30 case 0.53 m. A summary of all the results found in free-burn conditions can be found in Table 7.

Table 7 Summary of results of free-burn cases.

Test case	Burning rate (g/s)	$\dot{Q}_{th}$ (kW)	$\dot{Q}_{act}$ (kW)	Combustion Efficiency	Flame Height (m) (Heskestad, 1983)
FB20	0.34	9.1	8.8	0.97	0.35
FB30	0.92	24.6	23.8	0.97	0.53

3.4.2.3 Comparison with Literature Data

Since 1950 many works (Byram et al., 1966; Hayasaka, 1997, Ditch et al., 2013) have been devoted to investigating the burning rate of liquid pool fires and a wide range of pool sizes, pool configurations and fuel types were examined. One of the most widely used alcohol fuels is ethanol and Table 8 presents some literature studies in which ethanol was used in free-burn conditions, accompanied with information regarding the level of the fuel surface and the pool size. As discussed in Chapter 2, many different parameters can influence the burning rate of pool fires (lip height, wind effect etc.), so it is essential to know the exact test conditions of each test before comparing results from different studies.

Table 8 Summary of ethanol free-burn pool fire studies.

Reference	Constant level	Pool diameter or Equivalent pool diameter (m)
(Byram et. al., 1966)	No	0.33
(Corlett and Fu, 1966)	Yes	0.25-0.38
(Klassen and Gore, 1992)	Yes	0.046 and 0.071
(Tewarson and Marlair, 2004)	Not determined	5
(Ditch et. al., 2013)	Yes	0.25-1
(Hu et. al., 2013)	Yes	0.11-0.28

Figure 3.15 shows the burning rate per unit area (kg/m^{2}s) in relation with pool diameter (m) of the studies presented in Table 8. The results for the FB20 and FB30 of the present work are also included. It is observed that the burning rates of both pans are in accordance with the results reported in the literature (Blinov and Khudiakov,1957 and Drysdale, 2011) in terms of the regression rate (mm/min) over pool diameter (m) for different liquid fuels. Very small diameter pool fires (<0.1 m) are governed by conduction and burning rate decreases until convection regime is established. Convection is the dominate heat transfer mechanism for pool fire diameters up to 0.2 m, at which transition from convection to radiation occurs (Babrauskas, 1986). For larger diameters, radiation becomes the dominate mechanism and the burning rate increases until reaching a plateau for diameters larger than 1 m. The present study also focuses on pool fires which are in the transition and radiation dominant regime because these fires are of particular interest in building fires as discussed in (Babrauskas, 1986). The three regimes are identified in Fig. 3.15 for ethanol. As discussed in (Ditch et. al., 2013), fuel properties (such as sootiness, heat of gasification etc.) are responsible for the exact pool diameter points when those transitions occur.

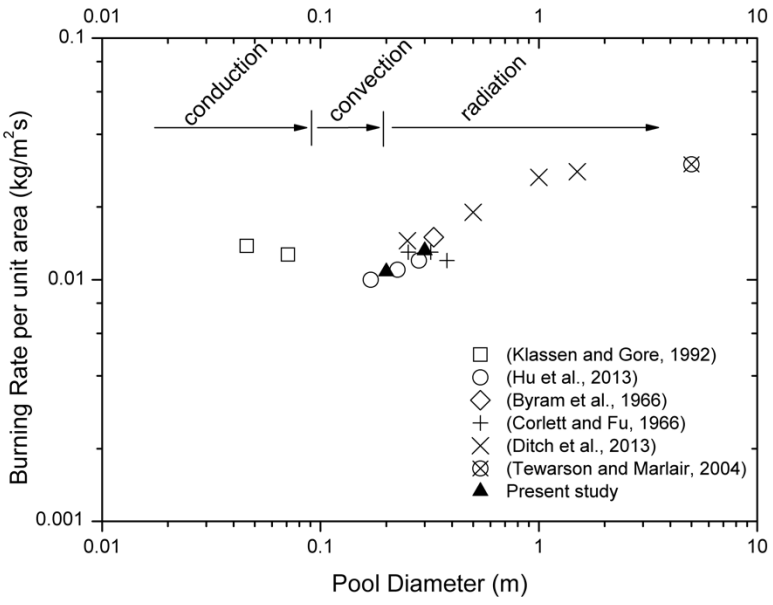

Figure 3.15 Burning rate per unit area in relation to pool diameter for free-burn ethanol experiments.

According to Zabetakis and Burgess (1961), Eq. 3.2 was proposed for liquid pool fires burning under quiescent conditions, which is transformed to Eq. 3.3 in case of

alcohols as they have a constant limiting burning rate per unit area (kg/m^{2}s). According to Babrauskas (1983) this value for ethanol is 0.015 kg/m^{2}s.

$$\dot{m}'' = \dot{m}''_{\infty}(1 - \exp(-k\beta D)) \quad \text{(kg/m}^2\text{s)} \tag{3.2}$$

$$\dot{m}'' = \dot{m}''_{\infty} \tag{3.3}$$

According to Eq. 3.2-3.3, the burning rate per unit area of the free-burn experiments of the current work is calculated as follows:

- 20 cm diameter pan: 0.00034 (kg/s) / 0.0314 (m^2) = 0.011 kg/m^{2}s
- 30 cm diameter pan: 0.00092 (kg/s) / 0.0706 (m^2) = 0.013 kg/m^{2}s

It is observed that the calculated value of the 20 cm diameter pan is 26% lower than the predicted value and for the 30 cm diameter pan is 13% lower, which is believed to be due to constant height of fuel surface (lip effect is minimised) inside the pan and to the water-cooled walls of the pans.

3.4.3 Gas Temperatures Inside the Enclosure

In total, thirty-six stainless steel sheath thermocouples of 1.5 mm bare bead diameter were used for measuring gas temperature evolution inside the enclosure. Type-K thermocouple wires were used as its operating temperature is up to 1100^{o}C, which was expected in some cases. The thermocouples were vertically spaced along the height of the enclosure on six thermocouple trees, 5 cm from the side wall. The highest and the lowest thermocouple on each thermocouple tree are 2 cm from the ceiling and 2 cm from the floor respectively. The vertical displacement between the thermocouples and the location of the thermocouple trees inside the enclosure are shown in Figs. 3.16 and 3.17. It is noted that the thermocouple tree within Box A was placed 5 cm from the opening.

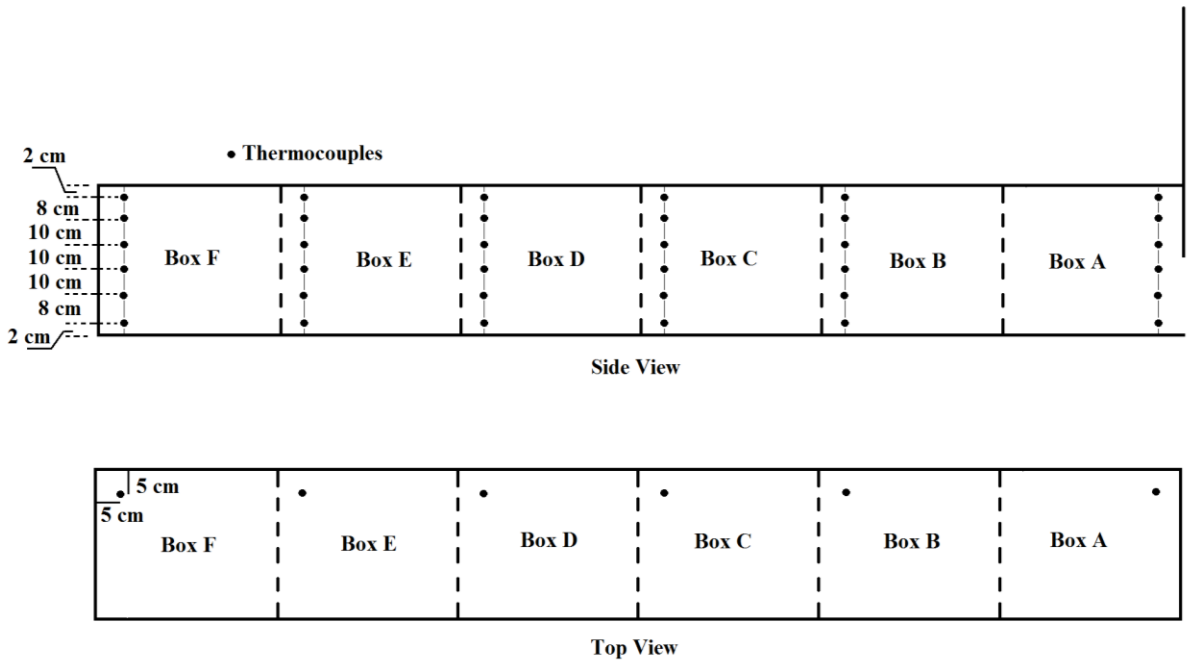

Figure 3.16 Location of the thermocouples inside the corridor.

Figure 3.17 The side wall of the corridor with thermocouples adjusted on it.

3.4.4 Heat Flux

Heat fluxes were measured on the façade of the corridor and on the floor inside the enclosure. Generally, heat flux gauges, such as Gardon gauges, are used for measuring heat fluxes on a surface, however they are very expensive especially and thus it is impractical to use them for measuring the heat flux on a large surface. In this work, steel plate heat flux meters originally used by Lee (Lee, 2006 and (Lee et. al., 2007) were used. They are significantly cheaper but yield results comparable

with those by Gardon gauges for enclosure and façade fires (Lee, 2006), (Lee et. al., 2007), (Tofilo et al., 2004). The steel plate meters have spot-welded thermocouples on the unexposed-to-fire surface and they are embedded into insulation boards. The heat fluxes, using the temperature measurements, are then deduced by solving the three-dimensional conduction equation for both the steel plate and the insulation, as described in detail by Zhang and Delichatsios (2009).

In total, twenty-seven steel plate meters were installed on the façade of the enclosure. At height of 72.5 and 87.5 cm from ground, two Gardon gauge meters were placed at a position symmetrically to two of the steel plate meters (5 cm apart) as shown in Fig. 3.18 in order to check the accuracy of the steel plate metres. Six steel plate meters were embedded into the floor of the corridor, as shown in Fig. 3.19. In boxes B to E, one steel plate meter was placed on the floor at the centre of each box and, depending on the location of the pan, two other meters were inserted in either Box A or F. The locations of the steel plate meters for both pan-location cases are shown in Fig. 3.20.

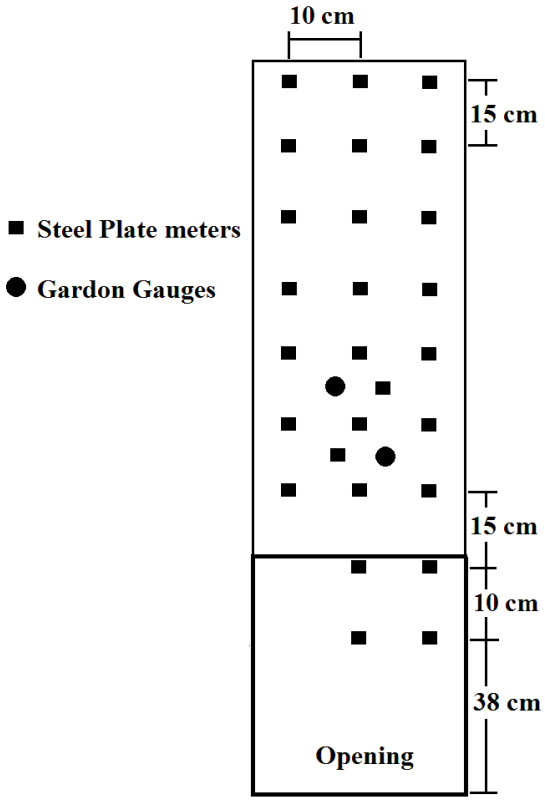

Figure 3.18 Location of the steel plate meters and the Gardon gauges on the façade.

Figure 3.19 Steel plate heat flux meters placed close to the opening of the corridor.

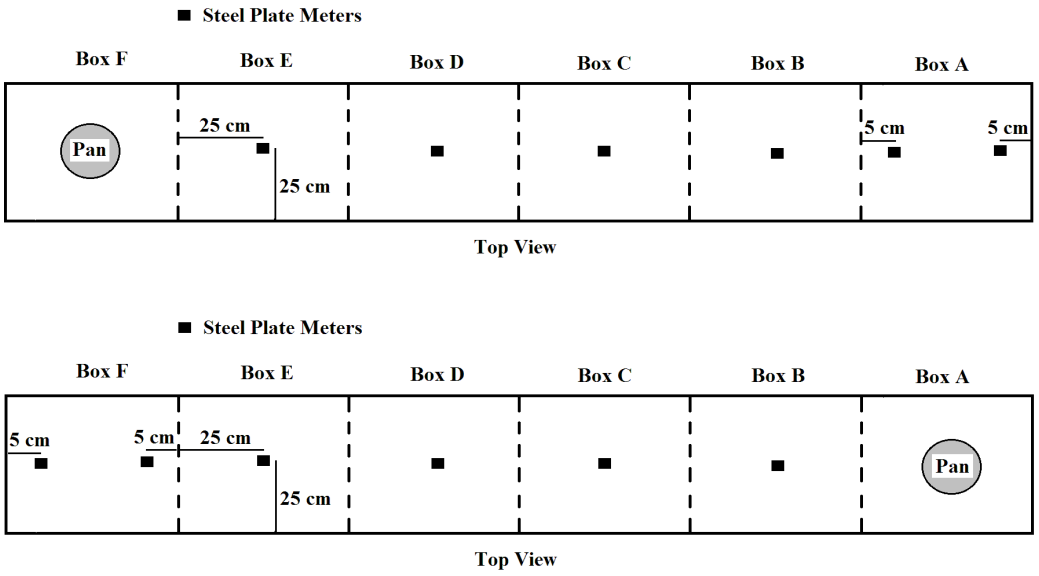

Figure 3.20 Location of the Steel Plate Heat Flux meters on the floor of the corridor, when the pan was located in Box F (up) and Box A (down).

3.4.5 External Flame Height Using a CCD Camera

The flame height was measured using a CCD camera coupled with the flame presence probability method, was used by many researchers (Audouin et al., 1995; Lee, 2006; Beji, 2009; Asimakopoulou, 2016). A comparison with other methods was made by Lee (Lee, 2006) showing that this method is reliable for calculating flame presence on the façade of an enclosure. A CCD camera (JVC KY-F55B) and an in-house developed MATLAB code were used to determine the height of the flames coming out of the corridor through the opening.

The camera was placed in front of the opening-façade side. Every picture/frame collected by the CCD camera is of a given number of pixels. Those pixels have

individual intensity values of 0 to 255. The value 0 is defined as black and the value 255 is defined as white. The minimal intensity of flames is then described by a threshold value (110) (Audouin et al., 1995). Afterwards, comparison of all pixels' intensity values with the threshold value takes place. So, if one pixel's intensity value is above the threshold's value the pixel is assigned the 1 value means the flame is present. Otherwise, flame is absent and pixel is assigned the 0 value. Finally, the flame presence probability is given by the following equation:

$$P_{x,y} = \frac{1}{N}\sum_{1}^{N} I_{bin} \tag{3.4}$$

where:

$P_{x,y}$ is the flame presence probability in every pixel

N is the total number of images/frames used in the code

I_{bin} is the 0 or 1 value assigned to each pixel in every image

3.4.6 Temperature of In- and Out-Flowing Water of the Pans' Water-Cooled Circuit

A water-cooling circuit was used for cooling down the pans' walls during the experiments. A 6 mm copper pipe was wrapped around each pan's walls for flowing water and cooling down the pans. The temperature of the water at the inlet and outlet of the wrapped pipe was measured using K-type thermocouples of 1 mm bead diameter. Temperature measurements were logged every 6 s.

3.4.7 Estimation of Measurements' Uncertainties

It is highly recognised the importance of investigating uncertainties which arise in every experimental work. In this work, as recommended in (Dieck, 1997) and (Nakos, 2004), the ASME method of error analysis (ASME, 1998) is used. According to this method, the total (expanded) uncertainty, U_T, of a measurement is the combination of two elementary uncertainties and is given by Eq. 3.5. The elementary uncertainty B_T, is the total 'systematic' uncertainty of the individual 'systematic' uncertainty sources ($B_{1,2,...}$) and is often constant during the experiment. The elementary uncertainty S_T is the total 'precision' uncertainty of the individual 'precision' uncertainty sources ($S_{1,2,...}$). Both uncertainties are calculated by the root-

sum-square (RSS) method as given in Eqs. 3.6 and 3.7. The factor k in Eq. 3.5 is the 'coverage' factor depending on the confidence interval (σ) needed and is usually of values 2 or 3 (2σ or 3σ), aiming to achieve a 95% or 99% confidence interval respectively. This work a factor of k=2 was used.

$$U_T = \pm k((B_T/2)^2 + {S_T}^2)^{1/2} \tag{3.5}$$

$$B_T = (B_1^2 + B_2^2 + B_3^2 \ldots)^{1/2} \tag{3.6}$$

$$S_T = (S_1^2 + S_2^2 + S_3^2 \ldots)^{1/2} \tag{3.7}$$

Thermocouples were used for measuring gas temperatures and back-surface temperature of the steel plate heat flux meters. All thermocouples were connected to the data acquisition system via extension wires. Bare-bead thermocouples have no 'precision' error, so S_T =0 (Nakos, 2004). Regarding systematic uncertainty, thermocouples have standard calibration uncertainty of ±2.2ºC or ±0.75% (whichever is greater). Because those values are of 99% coverage, systematic error of ±1.5ºC or ±0.5% is taken into account for achieving 95% confidence interval. As reported by Nakos (Nakos, 2004) the systematic error is also introduced by the presence of extension wires, which is assumed to be ±0.5%. He also suggested an error due to temperature change along the pin of the connectors of wires but this error is too small comparing to others, so it is neglected. Another source of uncertainty in a bare-bead thermocouple is due to radiation. No investigation of radiation losses was made in this work due to time and resource constraints, so values of similar experiments were considered. Brohez et al. (2004) introduced a correlation using smaller diameter thermocouples placed close to each main thermocouple used in the experiments. This method was also used in (Ukleja 2012) for estimating radiative losses in specific locations of the same experimental rig with this work. It was finally taken an error of -6% to 0% into account. As the same experimental rig and instrumentation was used in this work as that in (Ukleja, 2012) the same value was used for radiative losses of thermocouples used inside the corridor. An additional ±2% uncertainty is reasonable taken into account, as a result of other minor errors considered such as those in connection with the acquisition

logger, the noise etc (Nakos, 2004). The Gardon gauge heat flux meters have an initial calibration uncertainty of ±2.2% reported by the manufacturer. In addition, other significant sources of error in heat flux meters are non-linearity and sensitivity error. Values of ±2% and ±1% of full range were used respectively. Heat release rate was measured by the oxygen calorimetry method in the hood using an analyser developed by Dark Star Ltd. The instrumentation has an uncertainty of ±3% and the flow rate uncertainty is 5%. In addition, the gases used for the calibration of the hood are of ±5% accuracy. The balance used for estimating the mass of the remaining fuel at the fuel delivery system has a standard calibration uncertainty of ±3%. Ethanol used in the experiments is of ±2% purity uncertainty. Considering pipe connections and stability of the fuel delivery system, an additional ±3% random error is reasonably taken into account. A summary of all the estimated uncertainties for the sensors used in this work is shown in Table 9.

Table 9 Summary of uncertainty analysis for the sensors used in this work.

Sensor	**Uncertainty Type**	**Systematic (B_i) or Precision (S_i) Uncertainty**	**Total Expanded Uncertainty (U_T)**
Thermocouples	Standard Calibration Uncertainty	±0.5% or ±1.5°C	-6.4% to 2.1%
	Extension Wires	±0.5%	
	Radiation Losses	-6% to 0%	
	Random	±2%	
Gardon gauge meters	Standard Calibration Uncertainty	±2.2%	±4.3%
	Non-linearity	±2%	
	Sensitivity	±1%	
	Random	±3%	
Hood analyser	Instrumentation Uncertainty	±3%	±7.7%
	Exhaust Flow Rate	±5%	
	Accuracy of gas standards for calibration	±5%	
Balance	Standard Calibration Uncertainty	±3%	±4.7%
	Random	±3%	
	Fuel Purity	±2%	

3.5 List of Experiments Conducted and Final Layout

More than 65 experiments were conducted in this work. Three parameters were investigated, namely the pool fire's size, the location of the pool fire and the opening's dimensions of the enclosure. In addition, for comparison purpose, experiments in quiescent conditions (free-burn) of the same pool fire sizes were also conducted and discussed earlier. In order to uniquely identify each of the 34 different cases based on the location, the size of the pan and the opening dimensions, each case was given a unique name which starts with the location of the pan (either FR for front box or BC for back box location), followed by the size of the pan (20 for the 20 cm diameter pan or 30 for the 30 cm diameter pan) and ended with the opening dimensions W x H. For example, the case having the 30 cm pan at the back box and the 25 x 25 opening will be referred to as BC30W25xH25. A full list of the experiments conducted and the parameters studied in this work is given in Table 10.

Before each experiment, calibration of HRR measurement on the hood was conducted. Fuel was ignited at the centre of the pan using a lighter. For most of the tests, the fire reached the steady-state according to the HRR measurement. The tests were allowed to run a few minutes after the fire reaches the steady state in order to calculate the average results. There are however a few cases (large ventilation factors), in which no steady state was achieved because the HRR became excessively high and the test had to be terminated in order not to damage the walls of the corridor. No experiment was run for more than 45 mins.

The final layout of the experimental set-up used in this work is schematically shown in Figs. 3.21 and 3.22. Figure 3.21 shows the set-up that was used in experiments with the pool fire source at the front box (Box A) of the corridor and Fig. 3.22 shows the set-up which was used in experiments with the pool fire source at the rear box (Box F) of the corridor.

Table 10 List of parameters experimentally investigated, followed by the name for each case.

Pan Size	Pan Location	W_o x H_o (m)	$A_oH_o^{1/2}$	Experiments
20 cm	Free-burn	N.A.	N.A.	FB20
30 cm	Free-burn	N.A.	N.A.	FB30
20 cm	FRONT (Box A)	0.1 x 0.1	0.0032	FR20W10xH10
		0.15 x 0.15	0.0087	FR20W15xH15
		0.1 x 0.25	0.0125	FR20W10xH25
		0.2 x 0.2	0.0179	FR20W20xH20
		0.25 x 0.25	0.0313	FR20W25xH25
		0.3 x 0.3	0.0493	FR20W30xH30
		0.5 x 0.25	0.0625	FR20W50xH25
		0.5 x 0.5	0.1767	FR20W50xH50
30 cm	FRONT (Box A)	0.1 x 0.1	0.0032	FR30W10xH10
		0.15 x 0.15	0.0087	FR30W15xH15
		0.1 x 0.25	0.0125	FR30W10xH25
		0.2 x 0.2	0.0179	FR30W20xH20
		0.25 x 0.25	0.0313	FR30W25xH25
		0.3 x 0.3	0.0493	FR30W30xH30
		0.5 x 0.25	0.0625	FR30W50xH25
		0.5 x 0.5	0.1767	FR30W50xH50
20 cm	REAR (Box F)	0.1 x 0.1	0.0032	BC20W10xH10
		0.15 x 0.15	0.0087	BC20W15xH15
		0.1 x 0.25	0.0125	BC20W10xH25
		0.2 x 0.2	0.0179	BC20W20xH20
		0.25 x 0.25	0.0313	BC20W25xH25
		0.3 x 0.3	0.0493	BC20W30xH30
		0.5 x 0.25	0.0625	BC20W50xH25
		0.5 x 0.5	0.1767	BC20W50xH50
30 cm	REAR (Box F)	0.1 x 0.1	0.0032	BC30W10xH10
		0.15 x 0.15	0.0087	BC30W15xH15
		0.1 x 0.25	0.0125	BC30W10xH25
		0.2 x 0.2	0.0179	BC30W20xH20
		0.25 x 0.25	0.0313	BC30W25xH25
		0.3 x 0.3	0.0493	BC30W30xH30
		0.5 x 0.25	0.0625	BC30W50xH25
		0.5 x 0.5	0.1767	BC30W50xH50

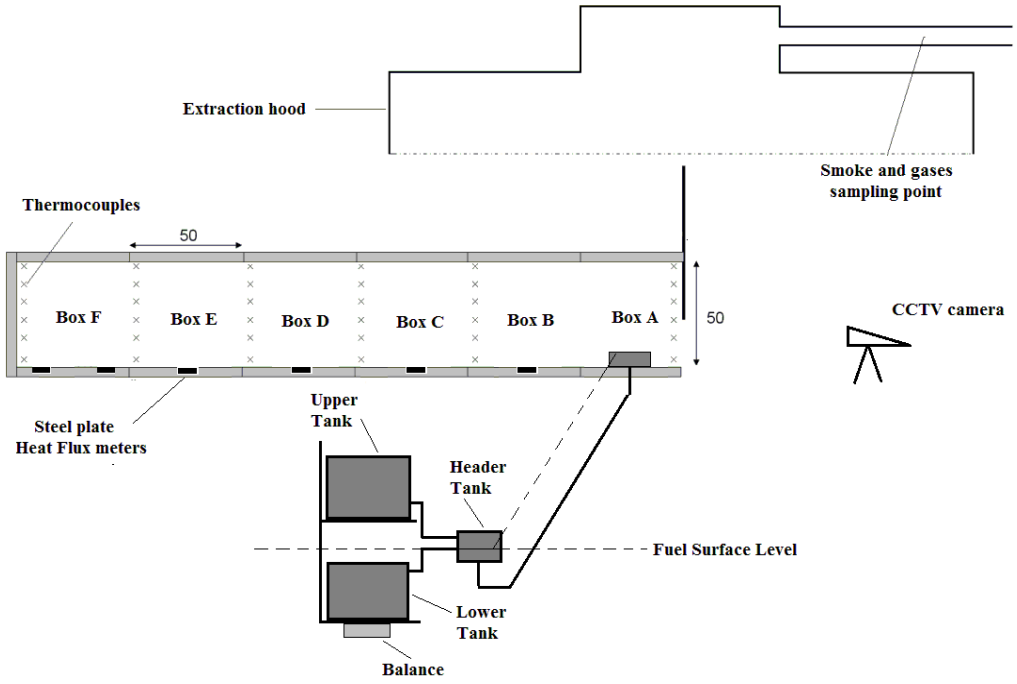

Figure 3.21 Sketch of the experimental layout with the pool fire placed at the front box of the corridor.

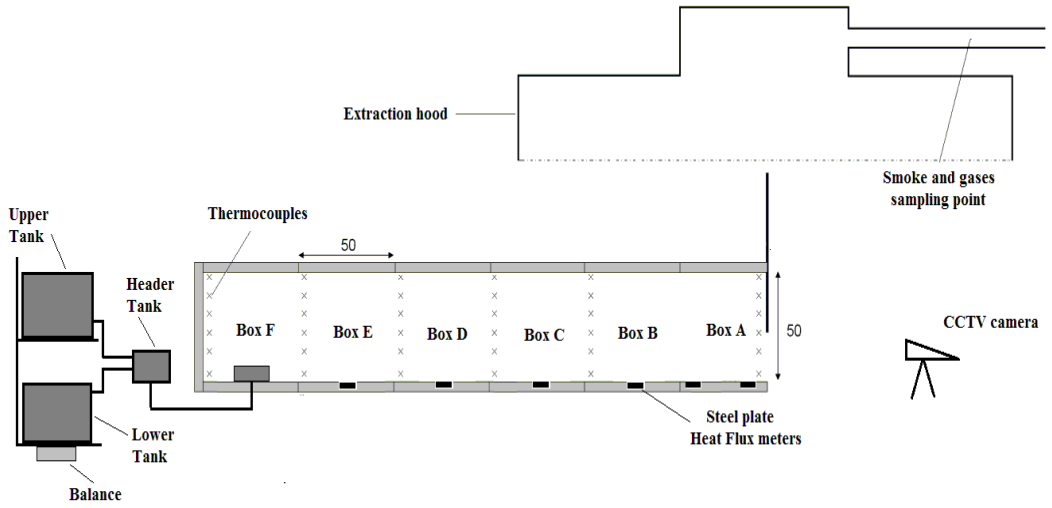

Figure 3.22 Sketch of the experimental layout with the pool fire placed at the rear box of the corridor.

3.6 Experimental procedure

Before every experiment conducted, the following procedure was followed:

- An hour before the start of the experiment, calibration of the gas analyser was taken place using a small gaseous burner.

- The data logging channels were checked to ensure that they register appropriate and reasonable readings.
- The upper tank of the fuel delivery and level maintenance system was filled with ethanol and the fuel pan inside the compartment was then filled too. Water was let flow inside the pan's water-cooling circuit.
- Water was let flow from a bath inside the Gardon gauge meters, which were placed on the façade in order not to damage them.
- Temperature and humidity of the interior of the lab were recorded.
- After everything was checked, the data logging system was started. After 1.5 min the fuel was ignited at the centre of the fuel surface using a lighter. For the cases when the pan was placed at the rear end of the corridor, the rear end wall was opened before ignition to have access to the pan for the ignition. After ignition the rear end wall was closed immediately.

3.7 Conclusions

This experimental work included small-scale experiments in a three-metre long corridor-like enclosure having a cross section 0.5 m x 0.5 m and a façade extended above the front panel of the enclosure, using ethanol pool fires as fire source. Three parameters were investigated, namely the opening dimensions, the pan's size and the pan's location. In total, eight opening dimensions, two pan sizes and two pan locations were examined. Fuel surface level inside the pan was kept constant during the experiments by using a newly designed fuel delivery and level maintenance system. An extensive sensor network was used to monitor the temporal variation of several important physical parameters, such as mass loss and heat release rate, temperatures and heat fluxes inside the corridor and on the façade, gases and smoke production outside the enclosure. Videos were also recorded by a CCD camera facing the façade to determine the height of the external flame. The test procedure was also described.

CHAPTER 4

POOL FIRES PLACED AT THE FRONT OF THE CORRIDOR-LIKE ENCLOSURE

4.1 Introduction

In this experimental study, ethanol pool fires were used as the fire source to investigate the effects of pool diameter and opening dimensions on the fire dynamics within a corridor-like enclosure and the subsequent façade fires. The pool fires were placed at the front of the corridor, close to the opening. The experimental results in this series are discussed later in this chapter, including the following:

i. Heat release rate
ii. Mass loss rate
iii. Combustion efficiency
iv. Temperatures in the interior of the enclosure
v. Heat fluxes on the floor of the enclosure
vi. External flame height
vii. Heat fluxes on the façade of the rig

The following section of the chapter presents a summary of the experiments conducted. In section 4.3, the repeatability of the experimental results is discussed. Section 4.4 describes the experimental observations and presents the experimental results. Finally, in Section 4.6, a summary of all findings is given followed by future recommendations.

4.2 Experimental Set-up

This chapter presents the experiments carried out by placing the pool fires inside the Box A of the corridor-like enclosure, where the opening is located. The pans were placed in the middle of the front box, at 0.25 m from the opening. The measurements taken were described in Chapter 3 and include MLR and HRR measurements, temperature profiles inside the corridor, heat fluxes on the floor and on the façade and heights of flames emerging through the opening of the enclosure. The layout of the experimental rig used for the experiments of pool fires at the Box A of the enclosure is given in Fig. 4.1.

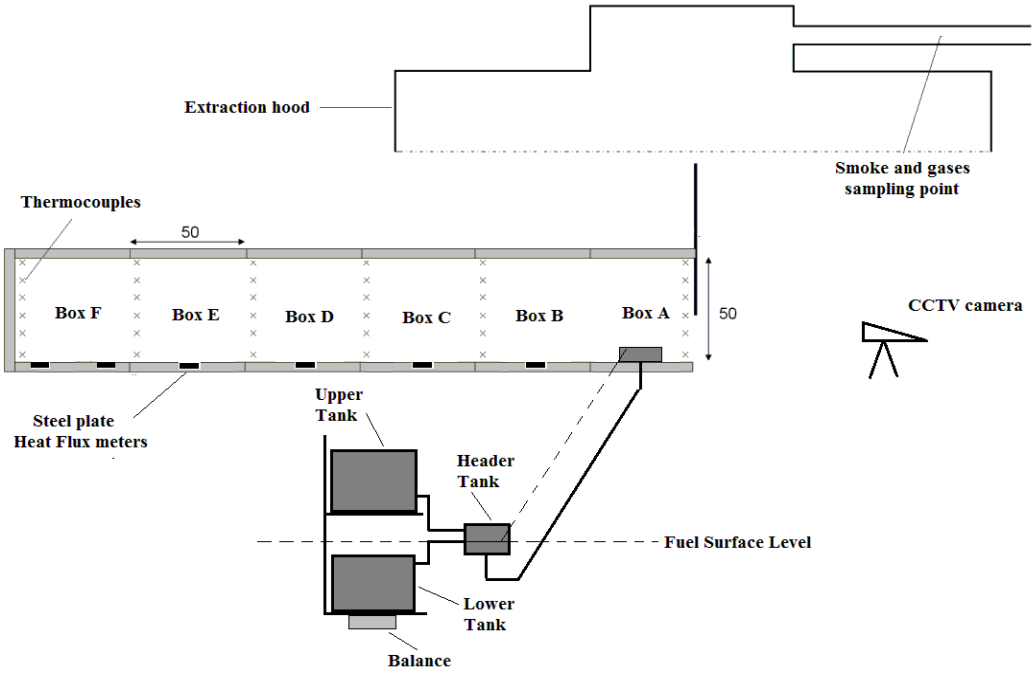

Figure 4.1 Sketch of the experimental layout with the pool fire placed at the front box (Box A) of the corridor.

In total, 16 cases were studied using eight different opening dimensions and two different diameter pans. A summary of the experiments conducted is given in Table 11. It is noted that more than one experiments were conducted for each case in order to achieve repeatable results. The duration of the experiments varied depending on the HRR measurements attained from the oxygen depletion system. Because the aim of this work is to study the steady-state period of pool fires inside the corridor-like enclosure, each experiment ran for a short period of time after HRR has reached a steady value. In general, a period of 2 to 3 minutes was considered for averaging the results in the steady-state period. As reported in Chapter 3, none of the experiments was left for more than 45 minutes in order not to damage the experimental rig's walls. As shown in Table 11, there are three cases, namely FR20W30xH30, FR20W50xH25 and FR30W50xH50, in which no steady-state conditions were achieved. In these cases, experiments had to be stopped for not damaging the rig as more time was needed for burning under steady-state conditions. In those cases, instead of the average steady-state values, the final values of the result profiles before the end the experiment were used in the analysis although those values are expected to further increase.

Table 11 Summary of the experiments conducted using the pool fires at the front box of the enclosure.

Pan Size (cm)	W_o x H_o (m)	$A_oH_o^{1/2}$	1500x $A_oH_o^{1/2}$	Experiments' Names	Duration of experiment (s)	Steady-state conditions achieved	Flames out
20	0.1x0.1	0.0032	4.8	FR20W10xH10	180	Self-extinction	N
	0.15x0.15	0.0087	13.1	FR20W15xH15	2400	Yes	N
	0.1x0.25	0.0125	18.8	FR20W10xH25	2400	Yes	N
	0.2x0.2	0.0179	26.7	FR20W20xH20	2400	Yes	Y
	0.25x0.25	0.0313	46.5	FR20W25xH25	2700	Yes	Y
	0.3x0.3	0.0493	73.5	FR20W30xH30	2400	No	Y
	0.5x0.25	0.0625	93.8	FR20W50xH25	2400	No	Y
	0.5x0.5	0.1767	265.1	FR20W50xH50	1200	Yes	N
30	0.1x0.1	0.0032	4.8	FR30W10xH10	150	Self-extinction	N
	0.15x0.15	0.0087	13.1	FR30W15xH15	1800	Yes	N
	0.1x0.25	0.0125	18.8	FR30W10xH25	2400	Yes	Y
	0.2x0.2	0.0179	26.7	FR30W20xH20	1200	Yes	Y
	0.25x0.25	0.0313	46.5	FR30W25xH25	1200	Yes	Y
	0.3x0.3	0.0493	73.5	FR30W30xH30	1200	Yes	Y
	0.5x0.25	0.0625	93.8	FR30W50xH25	1200	Yes	Y
	0.5x0.5	0.1767	265.1	FR30W50xH50	1800	No	Y

4.3 Experimental Results

4.3.1 Repeatability tests

The MLR and HRR profiles, gas temperature profiles of two locations in the interior of the corridor and heat flux profiles of two locations -on the floor and on the façade of the corridor- were selected as repeatability indicators. Table 12 shows the operational conditions of the two test cases, namely FR20W50xH50 and FR30W20xH20.

Table 12 Summary of the operational conditions of the selected test cases for repeatability.

Test case	FR20W50xH50		FR30W20xH20	
	Test 1	Test 2	Test 1	Test 2
W_o x H_o (m)	0.5 x 0.5	0.5 x 0.5	0.2 x 0.2	0.2 x 0.2
T_∞ (°C)	15.1	14.7	12.1	12.4
RH (%)	46	45	67	65
t_{dur} (s)	1200	1200	1200	1200
$1500A_oH_o^{1/2}$ (kW)	265.1	265.1	26.7	26.7

Profiles of HRR and MLR for the selected test cases are plotted in Fig. 4.2. As demonstrated in Fig. 4.2, the two test cases exhibited good repeatability. MLR calculated by mass loss data and HRR measured in the hood are almost identical for both cases. In addition, temperature profiles measured at two different locations in the upper hot gas layer inside the corridor are shown in Fig. 4.3, on the left for

FR20W50xH50 and on the right for the FR30W20xH20 test cases respectively. The heat flux profiles measured by steel plate heat flux meters in the middle of Box B are shown in Fig. 4.4, on the left for FR20W50xH50 and on the right for the FR30W20xH20 test cases respectively. Both Figures 4.3 and 4.4 highlight very good repeatability regarding gas temperature and heat flux measurements for both cases selected. All the other cases with the fire source placed inside the Box A have similar trends.

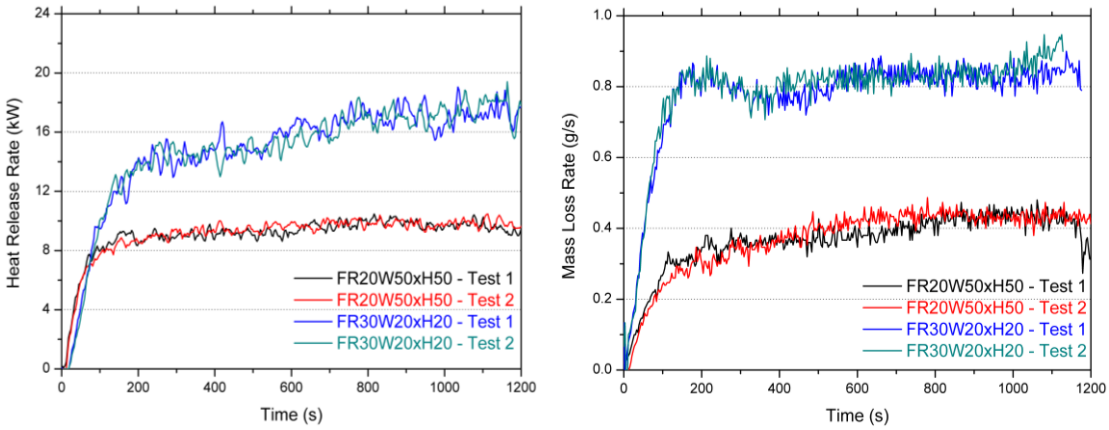

Figure 4.2 HRR profiles (left) and MLR profiles (right) of two identical tests for the two test cases investigated for repeatability.

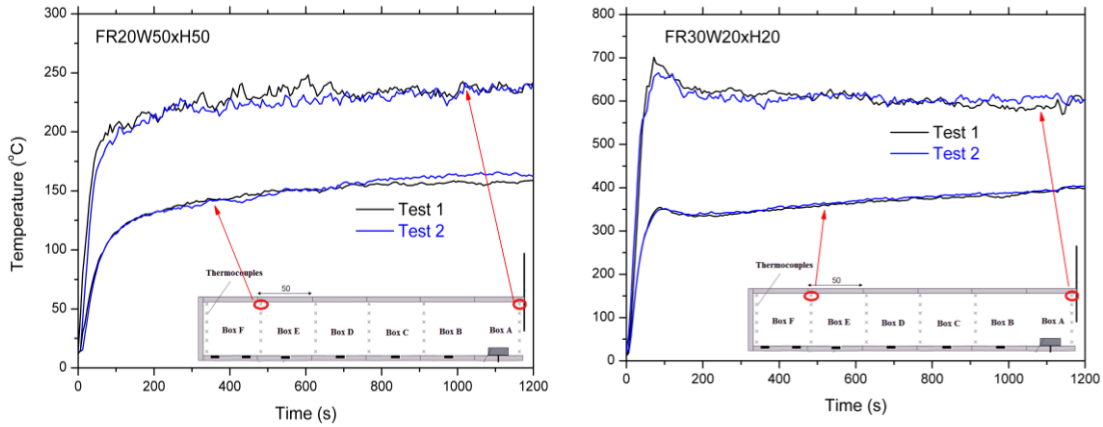

Figure 4.3 Temperature profiles measured 2 cm from ceiling in Box A and Box E of two identical tests for the FR20W50xH50 (left) and FR30W20xH20 (right) test case.

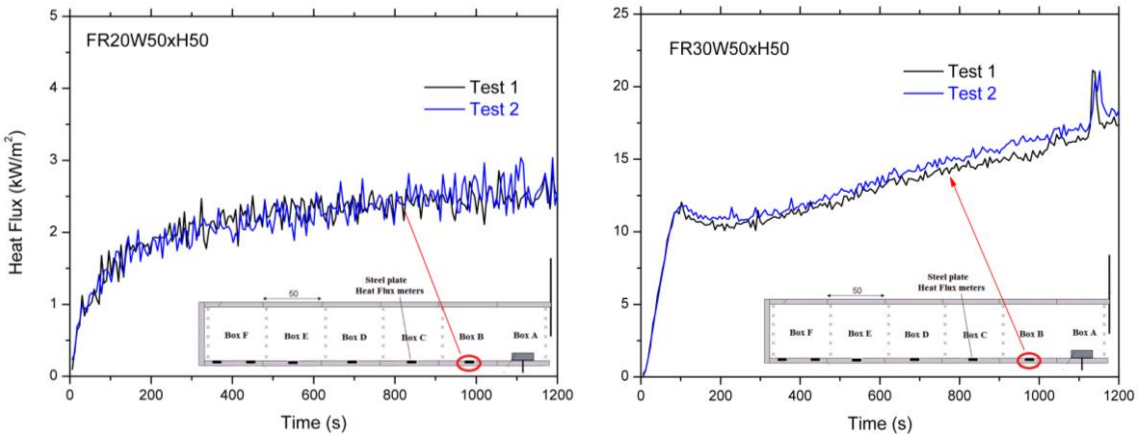

Figure 4.4 Heat Flux profiles measured in the middle of Box B of two identical tests for the FR20W50xH50 (left) and FR30W20xH20 (right) test case.

4.3.2 General burning behaviour

Before detailed analysis of the experimental measurement data (gas temperature, heat fluxes, flame height), some general observations will be made based on video recordings and the MLR and HRR measurements. The following observations were made with respect to (i) the opening's dimensions (in terms of ventilation factor) and (ii) the size of the pan (in terms of diameter of the circular pan)

- For the lowest ventilation factor (opening dimensions 0.1m x 0.1m), the fire self-extinguished as very limited amount of fresh air enters the compartment and reaches the fuel surface even if the pans were very close to the opening.
- For ventilation factors ($m^{5/2}$) up to 0.02 (i.e., opening dimensions 0.15m x 0.15m, 0.1m x 0.25m and 0.2m x 0.2m), the fire sustained. In the three cases, flames ejected through the opening: FR20W20xH20, FR30W10xH25 and FR30W20xH20.
- For ventilation factors up to 0.1, the fire sustained too. In all cases using the 30 cm diameter pan, flames ejected through the opening very quickly after ignition. In contrast, using the 20 cm diameter pan, flames came out of the enclosure only in FR30W25xH25 case. In the two cases using the 20 cm diameter pan with 0.3m x 0.3m and 0.5m x 0.25m openings, no steady-state conditions were achieved after 40 min of burning.
- For the largest ventilation factor, the burning behaviour of the case FR20W50xH50 with the 20 cm pan was similar to the free-burn case (will be

discussed later). In comparison, using the 30 cm pan, no steady-state conditions were achieved after 30 min of burning.

A summary of the burning behaviour for all cases using the two pans and eight ventilation openings are shown in Fig. 4.5. Detailed analysis for each case is followed in next subsections.

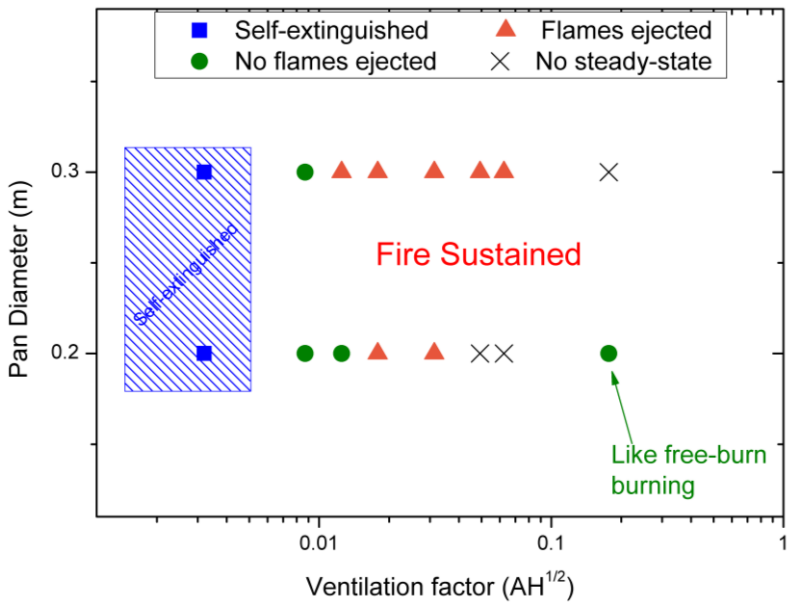

Figure 4.5 Fire behaviour depending on the ventilation factor and the size of the pool fire for all cases placing the fire source close to the opening.

4.3.3 Self-extinguished fire

Fire was self-extinguished in both cases of pans with the 0.1m x 0.1m opening (i.e. FR20W10xH10 and FR30W10xH10). In both cases, the fire was self-extinguished after 3-4 min of burning.

4.3.3.1 HRR, MLR and combustion efficiency

The actual HRR measured in the hood and the theoretical HRR profile for the FR20W10xH10 case are shown in Fig. 4.6. It is observed that both theoretical and measured HRR initially increase with the measured one reaching about 2kW. The theoretical HRR reaches a peak at 8 kW, but the combustion efficiency is too low (around 0.2) for the fire to sustain. Both HRRs drop suddenly indicating self-extinguishment of the fire. Similar finding was observed using the 30 cm dia. pan. Because the opening's dimensions are very small, not enough air enters through the

opening, thus there is not enough oxygen for combustion near the fuel surface of the pool fire.

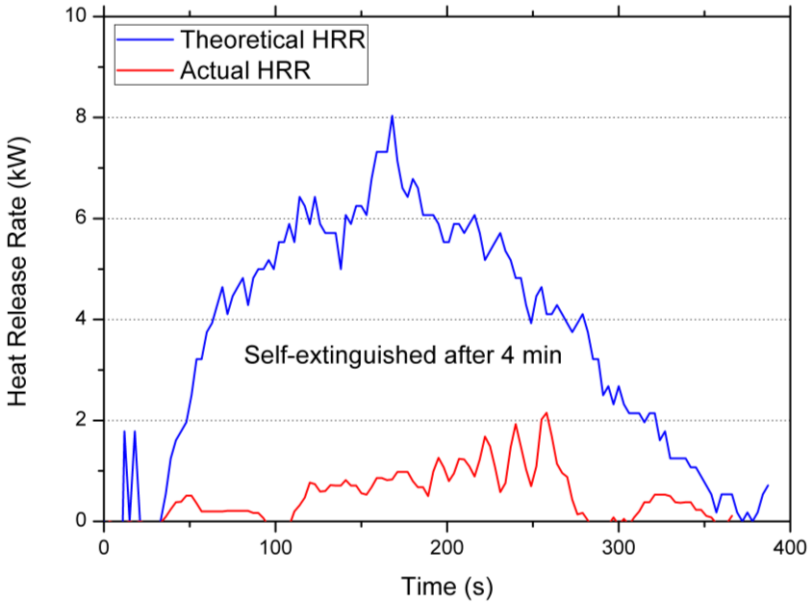

Figure 4.6 HRR profiles for the FR20W10xH10 case.

In addition to limited air entering the compartment, it is believed that the physical dimensions of the pans could also contribute to the self-extinguishment. The height of the opening (0.1 m) is slightly larger than the pans' walls (rim at 0.065 m) which would act like a physical boundary preventing the fresh air from reaching the fuel surface. An image taken moments before fire's self-extinguishment is shown in Fig. 4.7 for the FR30W10xH10 case.

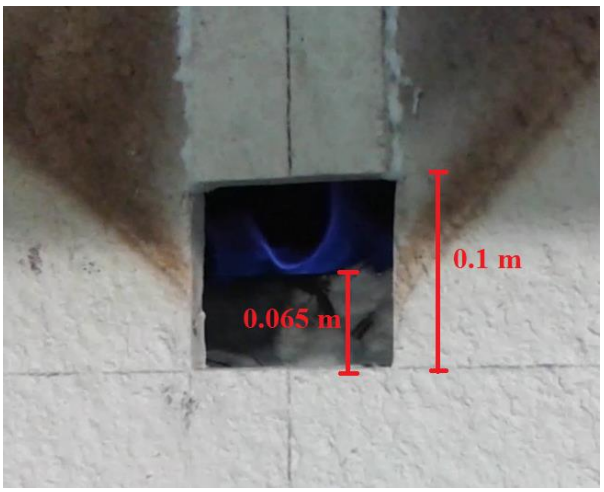

Figure 4.7 Side taken image of fire few seconds before self-extinguishment. Dimensions of opening height and pan rim height are also depicted. Image from FR30W10xH10 case.

4.3.3.2 Temperature measurements from the interior of the corridor

Temperature evolution profiles inside each box (A-F) from bottom (T1) to top (T6) are shown in Fig. 4.8 for the case FR20W10xH10. In consistence with the low values of HRR measurement, temperatures are very low too. Temperatures initially increase due to combustion of air initially in the compartment, but subsequently decreases sharply after the extinguishment of the fire .

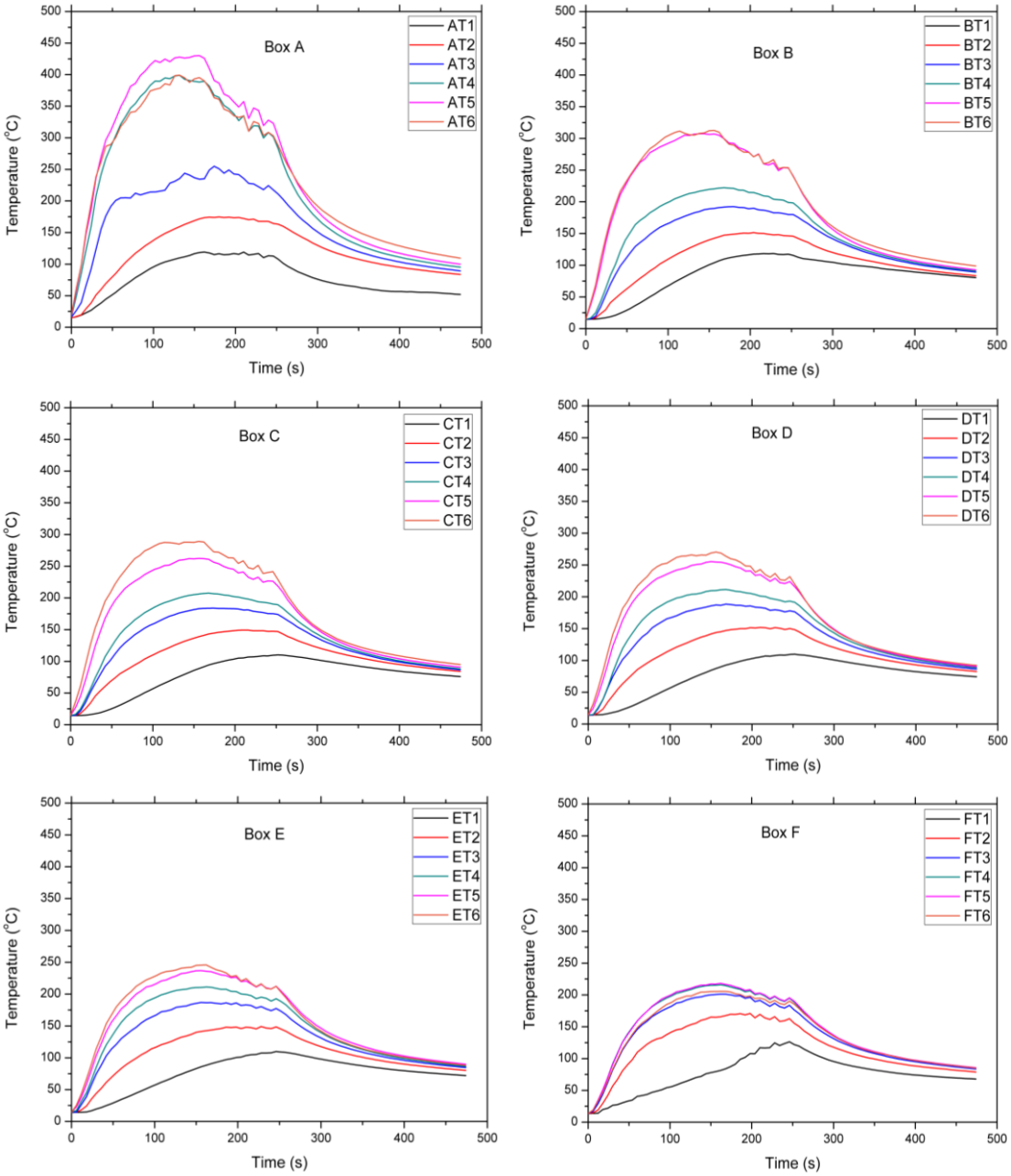

Figure 4.8 Temperature evolution profiles from bottom to top inside each box (Box A where pool fire was placed to Box F at the rear end) for case FR20W10xH10.

4.3.3.3 Heat flux measurements on the floor of the corridor

Heat fluxes were measured in the middle of the floor inside Box B, C, D and E and in two locations on the floor of Box F (F2 placed 5 cm and F1 placed 45 cm from the rear wall of corridor respectively. Heat flux evolution profiles in each box are depicted in Fig. 4.9. Similar to temperature profiles, heat fluxes in all locations firstly increase but then suddenly decrease because of self-extinguishment.

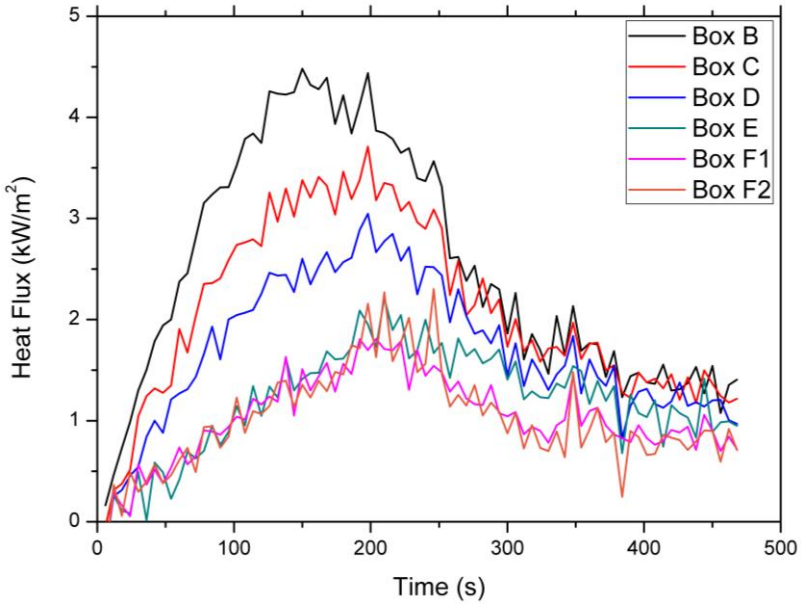

Figure 4.9 Heat Flux evolution profiles in six locations on the floor of the corridor for FR20W10xH10 case.

4.3.4 Unsteady fires

In three cases with large opening dimensions, no steady-state conditions were reached: FR20W30xH30, FR20W50xH25 and FR30W50xH50.

4.3.4.1 HRR, MLR and combustion efficiency

Figure 4.10 shows the comparison of the experimental HRR and the one calculated based on MLR for the case FR30W50xH50. It can be seen that both theoretical and actual HRRs keep increasing after 30 min, when the experiments had to be terminated for not damaging the rig. Initially, the theoretical and actual HRRs are almost similar, indicating a combustion efficiency close to unity, but after 400 s, the combustion efficiency reduces. The actual HRR increases to nearly 70kW after 30 min of burning but still no steady-state burning is achieved.

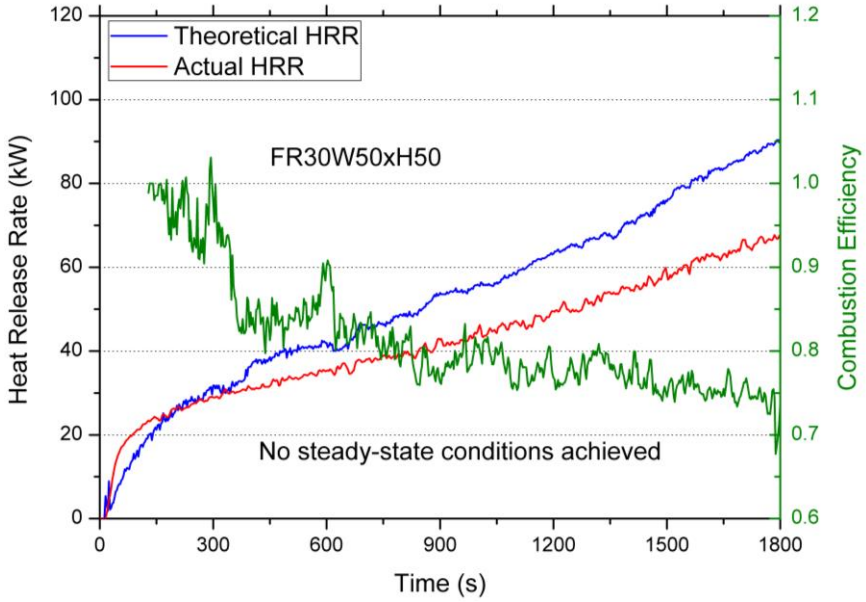

Figure 4.10 HRR profiles for the FR30W50xH50 case.

4.3.4.2 Temperature measurements from the interior of the corridor

Temperature evolution profiles from the interior of the enclosure (Boxes A-F) for FR20W50xH25 at different heights (T1-bottom to T6-top) are shown in Fig. 4.11. Similar to HRR, temperature at every location increases too. Figure 4.11 also indicates that there is more mixing at the rear of the corridor (Box F) indicated by the small temperature difference between the bottom and top locations. This phenomenon is also observed for the case, when the fire sustained and steady-state conditions were established and for which more details on this behaviour will be further discussed.

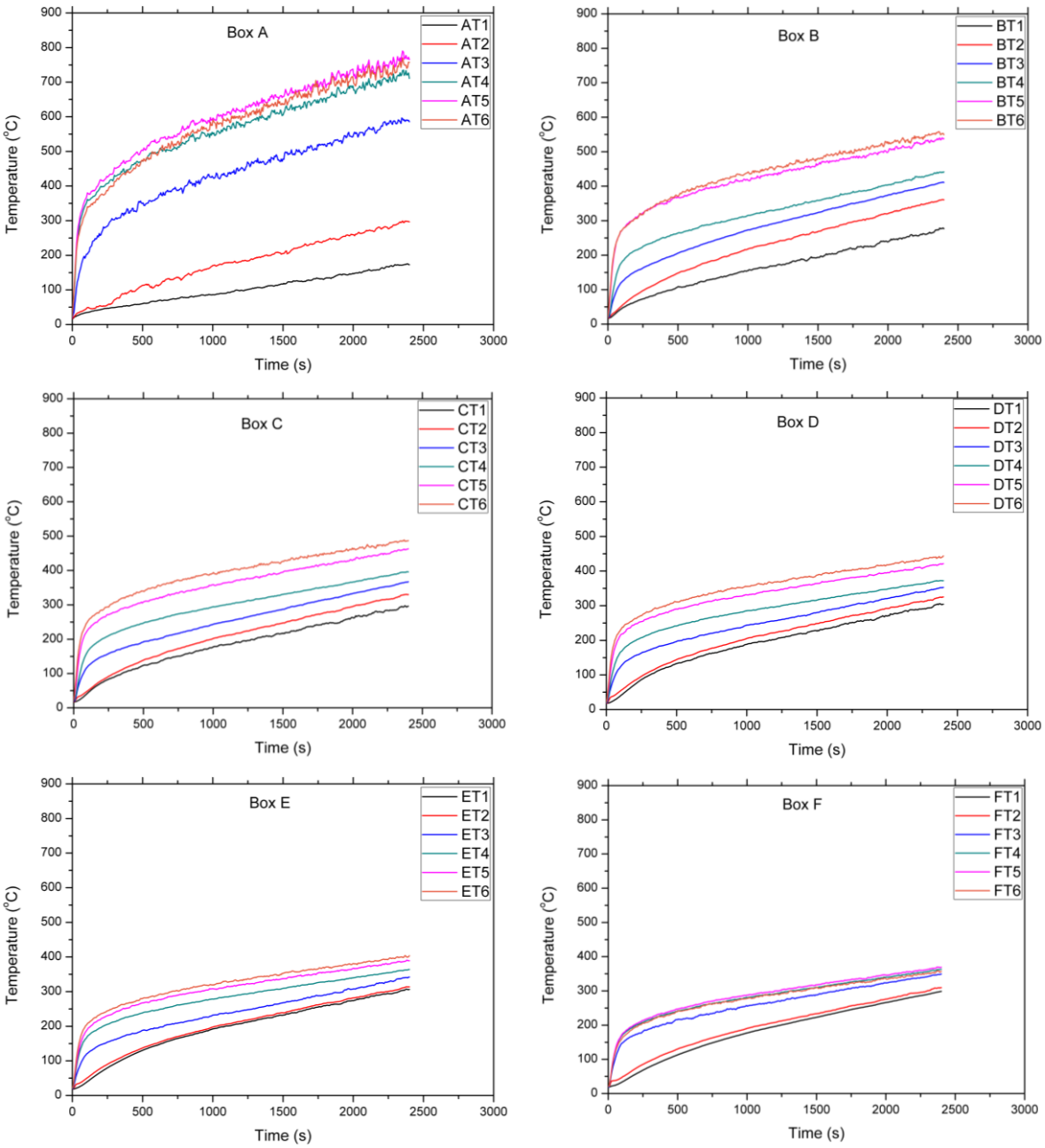

Figure 4.11 Temperature evolution profiles from bottom to top inside each box (Box A where pool fire was placed to Box F at the rear end) for case FR30W50xH50.

4.3.4.3 Heat flux measurements on the floor of the corridor

Heat Fluxes on the floor of the corridor inside each box are plotted in Fig. 4.12. In every location, heat flux increases. As expected, the heat flux in Box B (i.e., closest to the pool fire) achieves significantly higher values having a maximum value around 60 kW/m^2 near the end of the test.

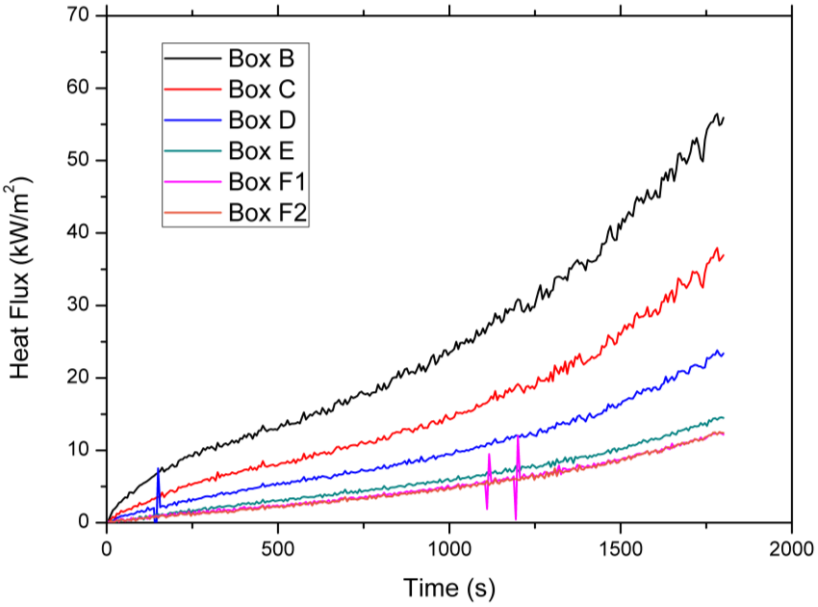

Figure 4.12 Heat Flux evolution profiles in six locations on the floor of the corridor for FR30W50xH50 case.

4.3.5 Steady fire without flame ejection

For this case, with relatively small ventilation factors, burning of pool fires was taking place only inside the corridor enclosure and no flames ejected. Steady-state conditions were established and the HRR became constant near the end of the test.

4.3.5.1 HRR, MLR and combustion efficiency

Both the theoretical and actual HRRs for one of those cases, FR20W15xH15, is shown in Fig. 4.13. Initially, a growth period is observed for about 360s and then HRR increases until it become steady at about 1600s indicating the onset of the steady-state period. Combustion efficiency was less than 0.8 during the steady-state burning period g. It is also noted that both theoretical and actual HRR are always less than the maximum heat release rate inside an enclosure applied under ventilation-controlled conditions (Delichatsios et. al., 2004; Yamaguchi and Tanaka, 2005), which for this case is calculated as 13.1 kW (=$1500A_oH_o^{1/2}$). Similar trends were found for other cases in this category, namely FR20W10xH25 and FR30W15xH15. These results along with visual observations confirm that ventilation-controlled conditions are not reached in these cases as the combustion is controlled by the availability of the fuel.

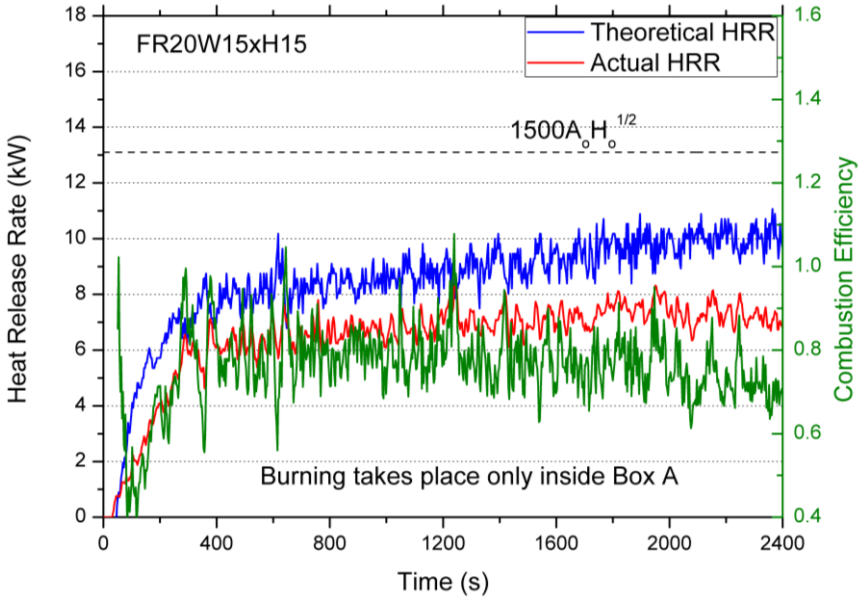

Figure 4.13 HRR profiles for the FR20W15xH15 case.

4.3.5.2 Temperature measurements from the interior of the corridor

Temperature evolution profiles for one of the cases (FR20W15xH15) are depicted in Fig. 4.14. Temperatures at all locations inside the corridor enclosure increase during the experiment, except for the two top locations inside Box A (see temperatures AT5 and AT6). These two temperatures increase until steady-state conditions are established and subsequently become constant at around 600ºC. The time when they became constant corresponds to the one when the actual HRR became constant (see Fig. 4.13) indicating the start of the steady-state burning period. The highest values were recorded inside Box A, close to the pool fire.

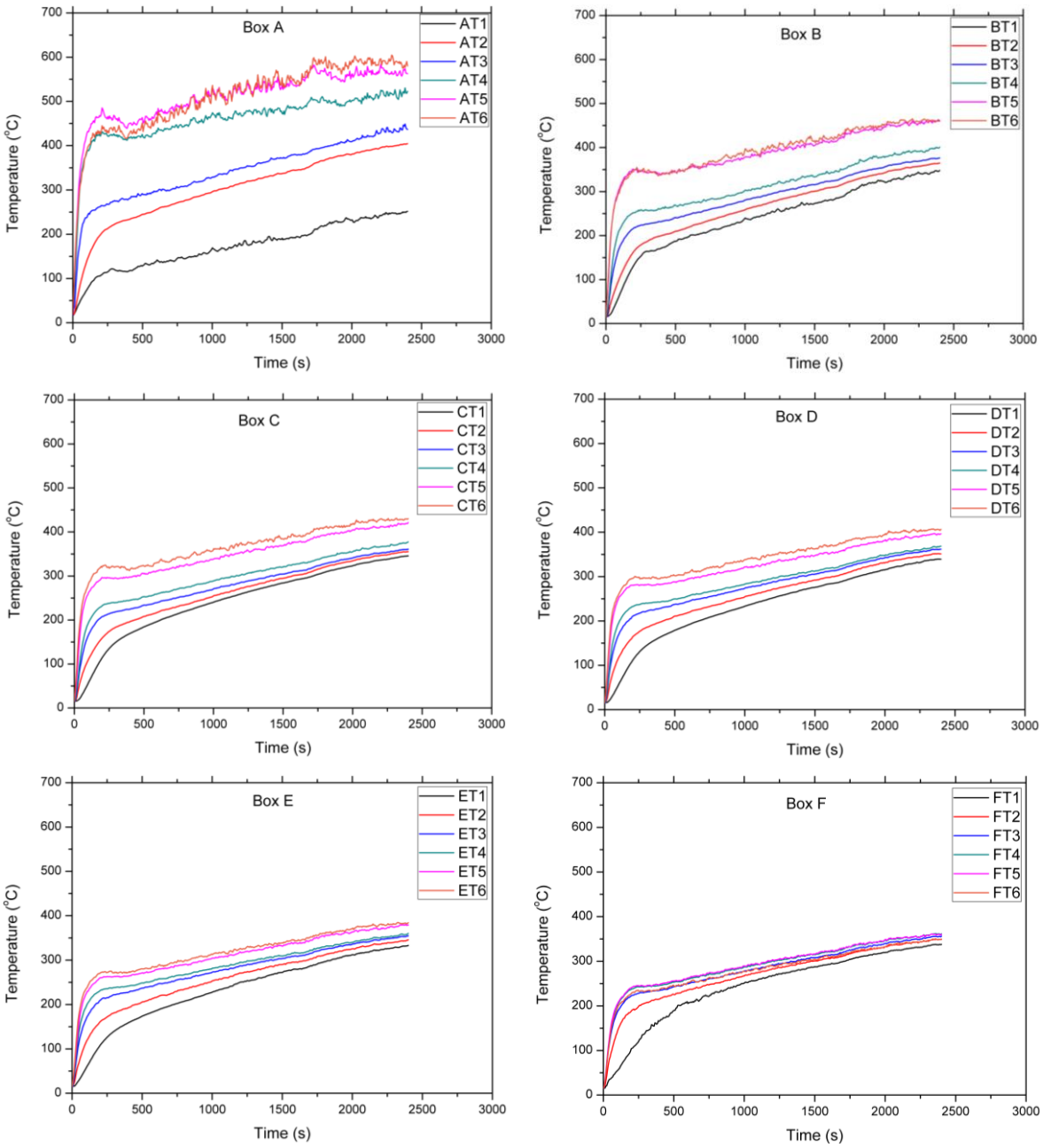

Figure 4.14 Temperature evolution profiles from bottom to top inside each box (Box A where pool fire was placed to Box F at the rear end) for case FR20W15xH15.

Figure 4.15 shows the temperature recordings at the top and bottom locations (T6 and T1 respectively) for case FR20W15xH15 at three different times: 60, 1000 and 2000s, corresponding to the growth period, the period just before steady burning and steady-state period respectively. At 60s, there is a clear distinction in gas temperature between the cold and hot gas layers over the whole length of the corridor. At t=1000s, this distinction becomes smaller indicating more mixing. The results also show that the temperature difference decreases with an increase in the distance to the

pool fire and near the rear end of the corridor the difference is only 25ºC. Finally, during the steady-state period (t=2000s) the hot gas near the rear end of the corridor (Box F) is completely well mixed indicated by nearly the same temperature at the top and bottom locations.

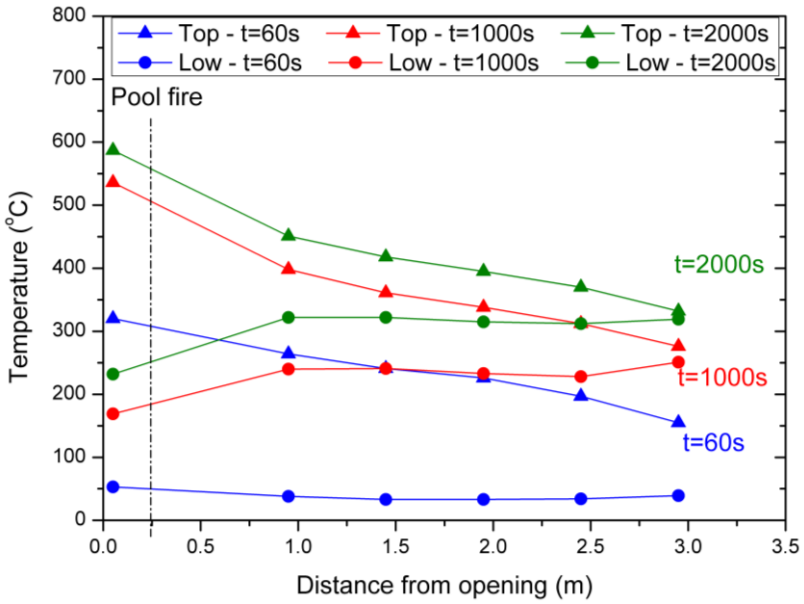

Figure 4.15 Temperature at the top and the low locations over the distance from the opening for case FR20W15xH15 in three time steps: 60, 1000 and 2000s.

Same observations were made for the other cases using the 20 cm pan and slightly larger ventilation factors (0.1m x 0.25m opening - FR20W10xH25). The only difference is that temperatures for the case with a larger ventilation factor are higher than those with the smaller ventilation factor. Top temperatures inside Box A and Box F for the two cases are depicted in Fig. 4.16. The temperatures for both cases inside Box A became steady after 2000 s, with the one of larger ventilation factor (0.10 x 0.25 opening) being higher 50ºC.

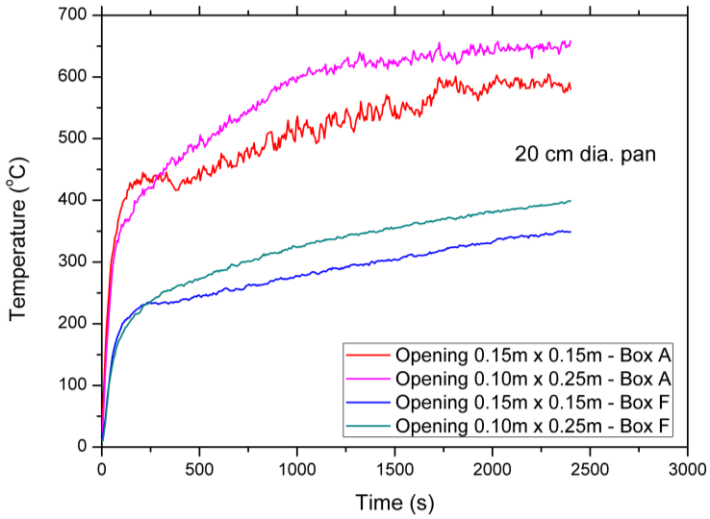

Figure 4.16 Comparison of the top temperature evolution profiles inside Box A and Box F, considering same pan size and two different openings.

In order to illustrate the influence of pan size, the top temperatures in Box A and Box F are depicted in Fig. 4.17 for cases with the same opening FR20W15xH15 and FR30W15xH15. It is observed that using the 30 cm dia. pan a peak is recorded rapidly a few seconds after the ignition (see top temperature in Box A and Box F), and then temperature increases as noted for the smaller pan cases. The top temperature inside Box A using the smaller pan was found higher than that using the larger pan during the steady-state period. However, inside Box F similar temperatures were recorded.

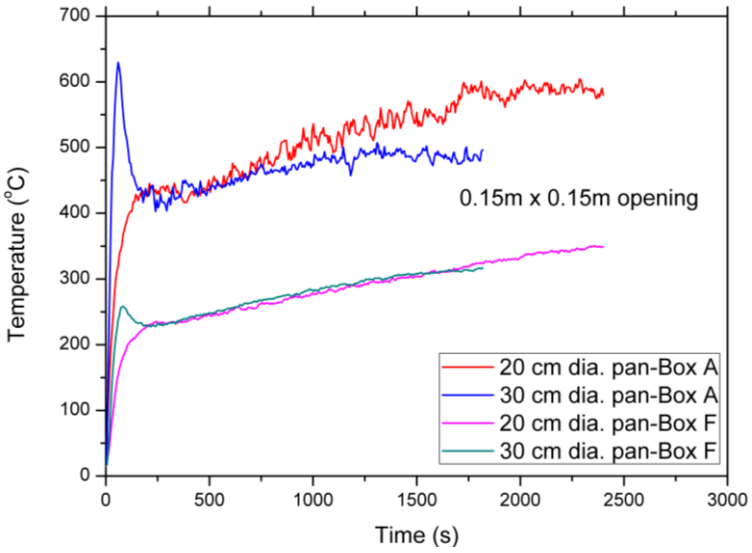

Figure 4.17 Comparison of the top temperature evolution profiles inside Box A and Box F, considering same opening size (0.15m x 0.15) and two different pan sizes.

4.3.5.3 Heat flux measurements on the floor of the corridor

The heat flux measurement profiles on the floor of the corridor enclosure are depicted in Fig. 4.18. Inside all boxes, except Box A where no measurement was conducted, heat flux increases with time. The lowest heat flux was measured inside Box F far from the pool fire and the closer to the fire box the higher heat fluxes.

The heat flux measurements can be explained by the burning behaviour described based on HRR and temperature profiles. Heat flux inside Box B (close to the pool fire) are shown in Fig. 4.19, together with the temperature at the top location in the same box and HRR. The growth and the steady-state period are also noted. During the growth period all the heat fluxes increase rapidly, followed by a slower increase until steady-state conditions are established. At this point, HRR and top temperature become steady, but because temperatures at other heights still increase, a further increase of heat flux is observed. In other boxes, heat flux increases as the gas temperatures continue to increase during the experiment.

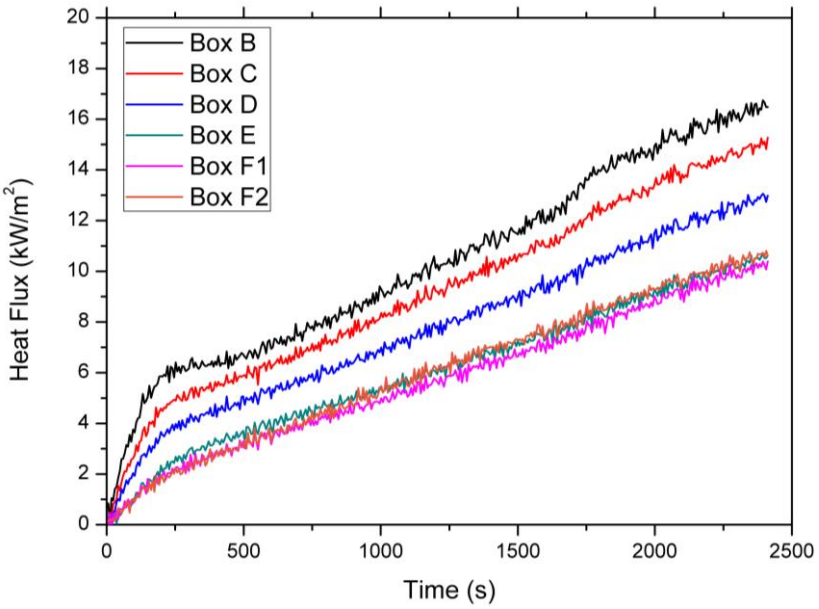

Figure 4.18 Heat Flux evolution profiles in six locations on the floor of the corridor for FR20W15xH15 case.

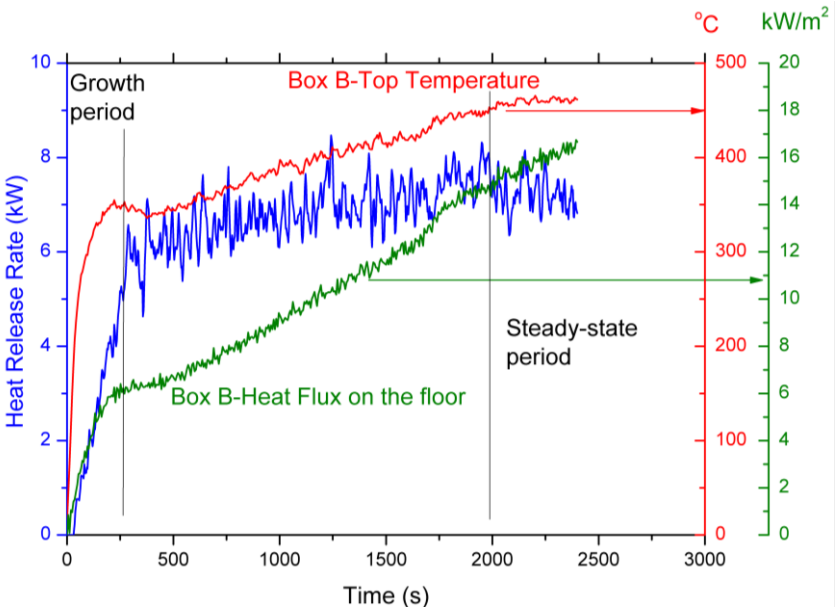

Figure 4.19 HRR, top temperature in Box B and heat flux inside Box B evolution profiles for FR20W15xH15.

4.3.6 Like free-burn case

As depicted in Fig. 4.5, the MLR for very large ventilation factors is very similar to that of free-burn cases. In the present experimental work this was observed only for the case using the smaller pan and fully-open (0.5m x 0.5m).

4.3.6.1 HRR, MLR and combustion efficiency

The HRR of case FR20W50xH50 is shown in Fig. 4.20 along with the free-burn HRR. It is observed that HRR of the corridor experiment is similar to the free-burn case using the same pan and becomes steady after 4 min. For a period of about 10 min the theoretical HRR is close to actual HRR, indicating combustion efficiency is close to unity. After this period, combustion efficiency drops by about 12%. In this case, no flames appeared out of the corridor and burning was taking place only inside Box A. This behaviour is different from the case when using the 30 cm dia. pan and same opening, which has much higher MLR that that of the free-burn case. This is attributed to the ceiling effect, as the flame height of the 30cm pan case is higher than the ceiling height. The flames reached the ceiling shortly after ignition and subsequently spread under the ceiling, and thus radiation feedback to fuel surface was significantly larger and finally flames ejected through the opening. No ventilation-controlled conditions are established in these cases, as none of the theoretical HRR reach the maximum heat released inside the enclosure (= 265.1

kW). This behaviour is particularly shown in Fig. 4.21, the images taken at 180, 600, 900 and 1200 s after ignition for FR20W50xH50 and FR30W50xH50. The difference on the flame structure for the two different pans using the largest opening dimensions is shown at different time intervals. While using the small pan the burning takes place only inside the fire source box without touching the ceiling, with the larger pan flames touch the ceiling and appear out of the enclosure.

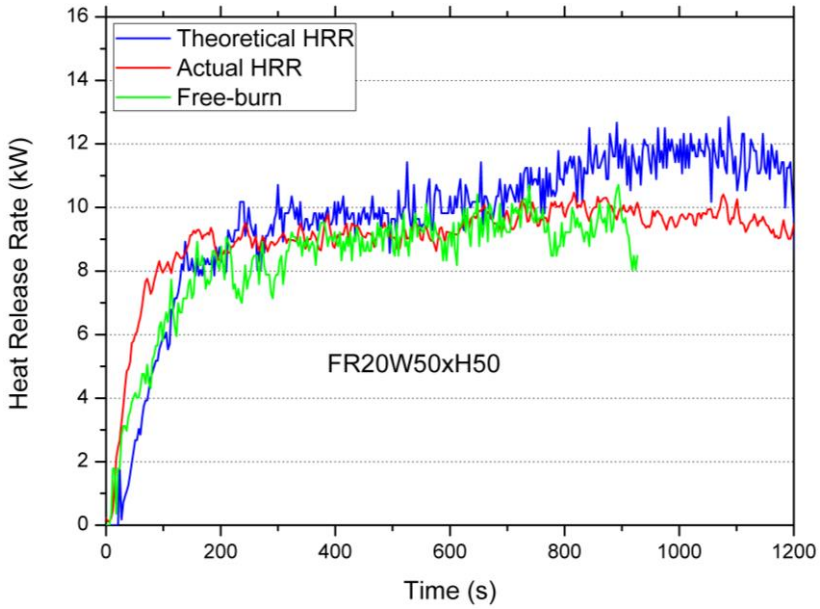

Figure 4.20 HRR profiles for the FR30W50xH50 case. Free-burn HRR is also plotted.

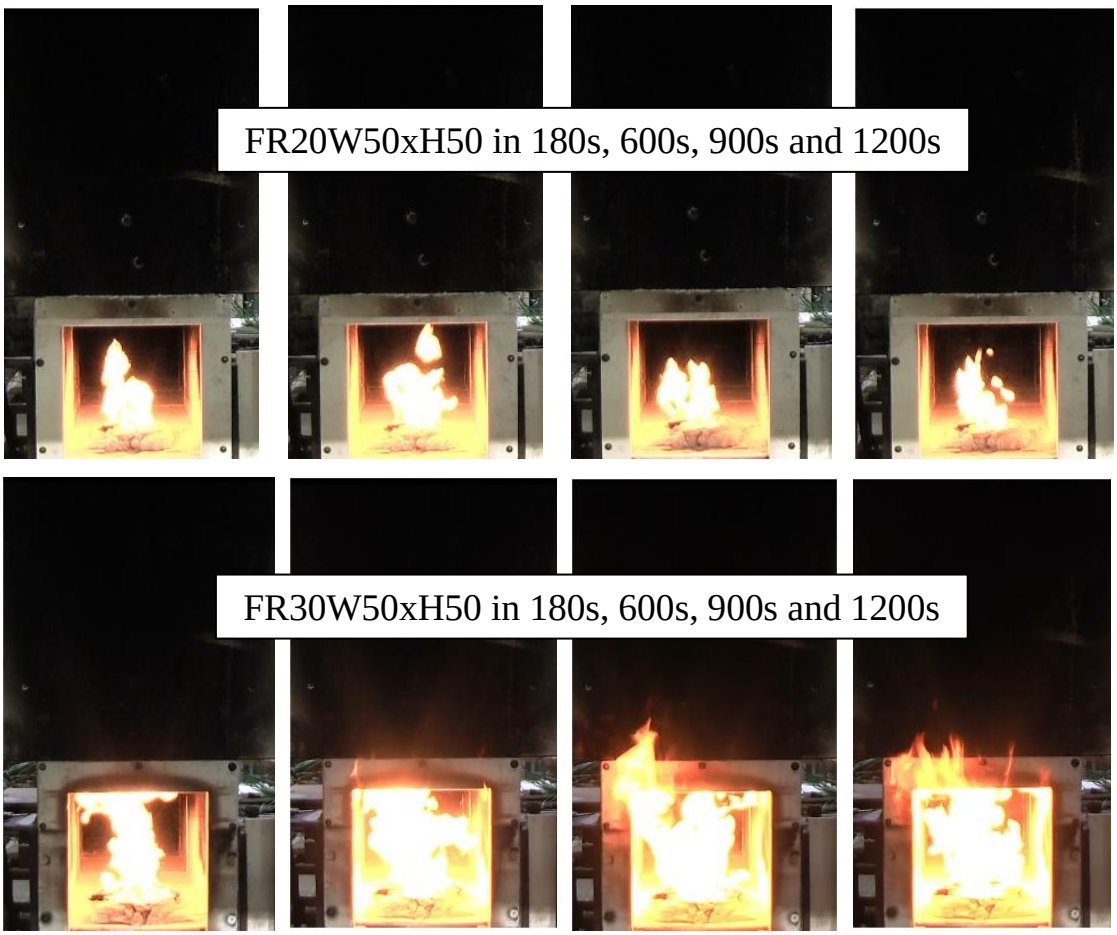

Figure 4.21 Images taken in different time steps showing the progress of the flame structure for the cases FR20W50xH50 and FR30W50xH50, using the largest opening factor and the two pans.

4.3.6.2 Temperature measurements from the interior of the corridor

The temperature evolution profiles for FR20W50xH50 are given in Fig. 4.22. Temperatures during the steady-state period (after 660 s.) became constant but values are significantly low, less than 250ºC. It is especially highlighted by the temperature difference between the upper hot gas layer and the cold air layer close to the floor. There is fresh air entering the corridor from the lower layer and gas temperature even at the rear end of the corridor does not exceed 65ºC. Average temperatures during the steady-state period are plotted against height inside the corridor in Fig. 4.23. A clear stratification is observed over the length of the corridor as temperatures are not homogeneous over the height, resulting in a 'weak' hot gas layer of low temperature values with minor radiation feedback to the surface of the fuel. The formation of the upper layer is observed at a height of 20-30 cm from the floor. Therefore, the temperature profiles of the hot gas layer are in accordance with the HRR profiles

shown in Fig. 4.20. As expected, the largest difference between the upper and lower layers was observed in Box A, where the pool fire was located.

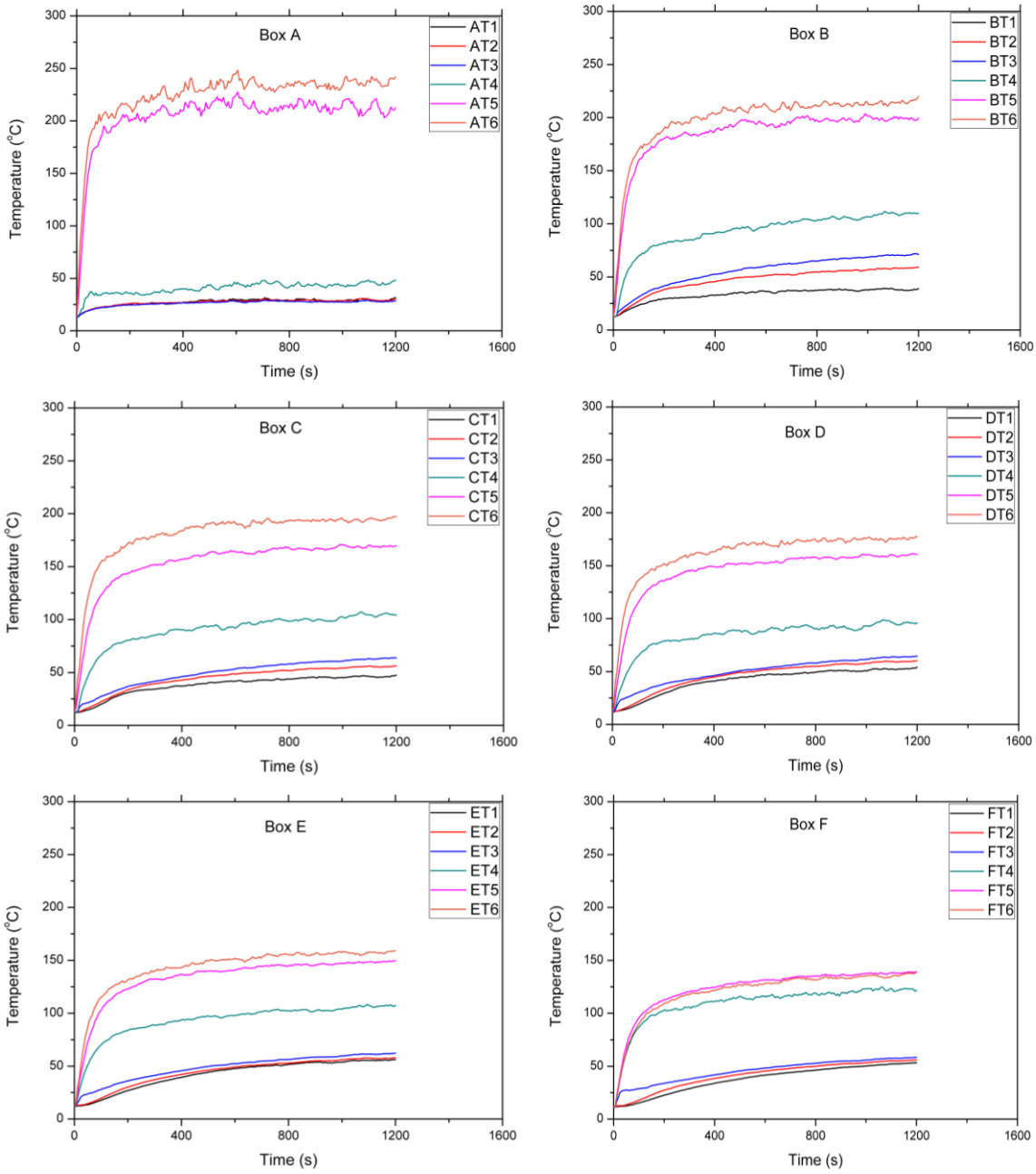

Figure 4.22 Temperature evolution profiles from bottom to top inside each box (Box A where pool fire was placed to Box F at the rear end) for case FR20W50xH50.

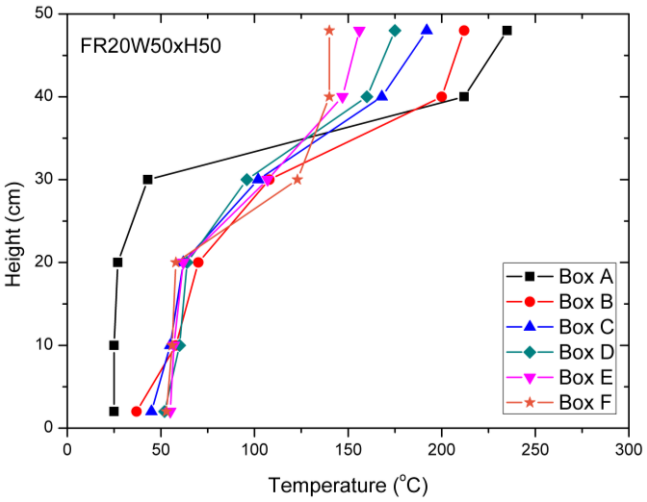

Figure 4.23 Gas temperature distribution inside each box of the enclosure for case FR20W50xH50.

4.3.6.3 Heat flux measurements on the floor of the corridor

Heat flux evolution profiles for the FR20W50xH50 and FR30W50xH50 cases are plotted in Fig. 4.24, on the left and right respectively. Using the smaller pan, heat fluxes on the floor of the corridor are very low, as the gas temperature measurements are low as shown in Figures 4.22 and 4.23. The heat flux inside Box B, which is closest to the pool fire, became steady at 2.5 kW/m^2 and heat flux decreases towards the rear end of the corridor.

The presence of a thin hot gas layer of low temperatures, according to temperature profiles, is the reason for the steady heat flux profiles. This is the main difference between the two different size pans with the fully-open opening, as in FR30W50xH50 case heat fluxes were found to increase because of a thick hot gas upper layer radiating back to the floor of the corridor. It is noted here that in Box B the heat flux using the larger pan was measured 60kW/m^2 before the end of the experiment and was still increasing.

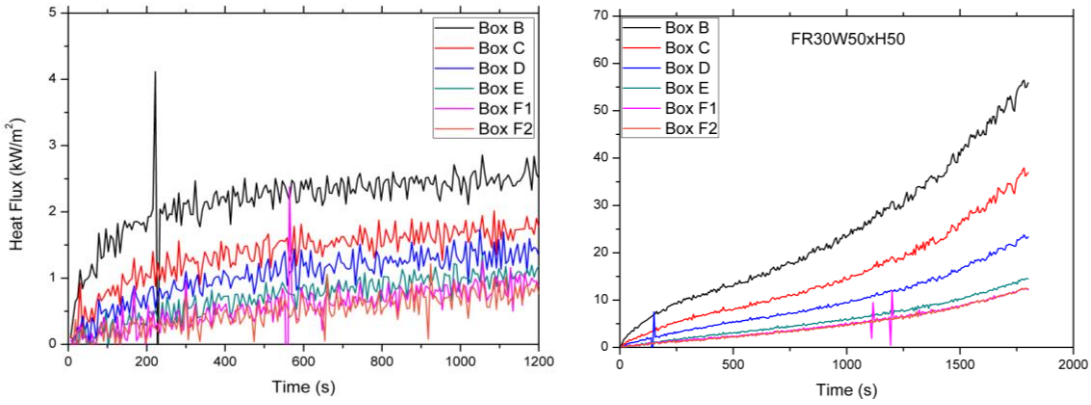

Figure 4.24 Heat Flux evolution profiles in six locations on the floor of the corridor for FR20W50xH50 (left) and FR30W50xH50 (right) cases.

4.3.7 Steady fire with flame ejection

The most common phenomenon observed is that of flames ejecting through the opening and projected on the façade, as it was observed in eight out of sixteen cases studied with the pool fire placed inside Box A.

4.3.7.1 HRR, MLR and combustion efficiency

The theoretical and actual HRRs of FR30W25xH25 case are depicted in Fig. 4.25. Initially a growth period is observed which lasts about 2 minutes. In this period, the fire is fuel-controlled and HRR increases rapidly. The theoretical and actual HRRs are similar and the combustion efficiency is close to unity. After the growth period flames were ejected through the opening and HRR continues to increase. Then, HRR becomes constant (about 31 kW) after 14 minutes when steady-state conditions are established, and flames burn constantly outside. Qualitatively, similar results were found for cases using the 20 cm dia. pan. The difference observed with the cases using the 20 cm dia. pan was that the time needed before flames ejected is significantly longer. When flames start to appear outside, a sudden increase of HRR (by a few kW) occurs and then HRR becomes constant again. As the pan is smaller (thus initial burning rate and HRR), it takes a lot more time to heat up the gases inside the corridor and corridor walls to reach the steady-state. Figure 4.26 show the HRR results for the case using 20 cm dia. pan and the same opening (0.25m x 0.25m). It is observed that using the same opening, the larger the pan, the higher HRR measured during the steady-state period. It is interesting to note here that the actual HRR in both cases never reached the theoretical HRR), even after flames

appeared outside. Combustion efficiency is close to unity during the growth period but afterwards it reduces even after flames were ejected through the opening. These results may indicate that unburnt fuel remains inside the corridor and not all of it burns outside. In all cases when flames ejected through the opening the actual HRR never reached the maximum heat released inside the enclosure, as given in Table 11 for each case.

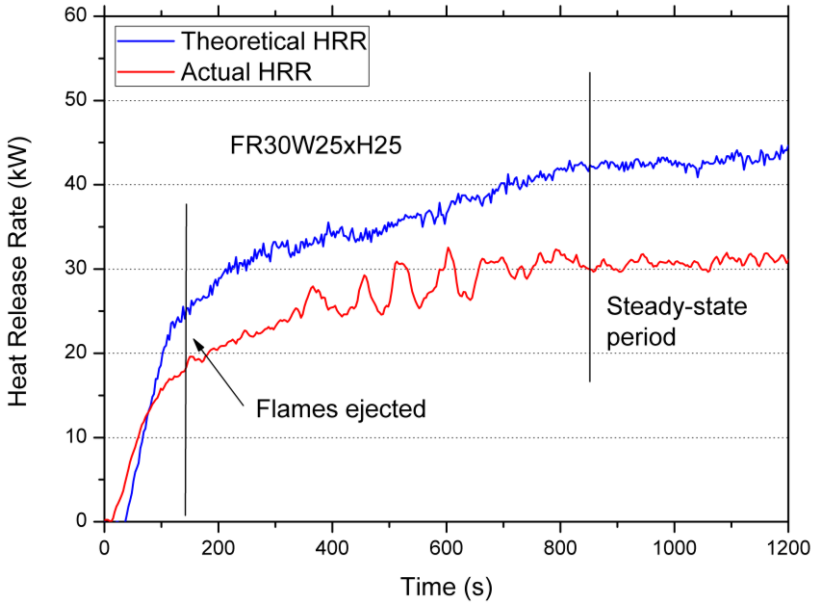

Figure 4.25 HRR profiles for the FR30W25xH25 case.

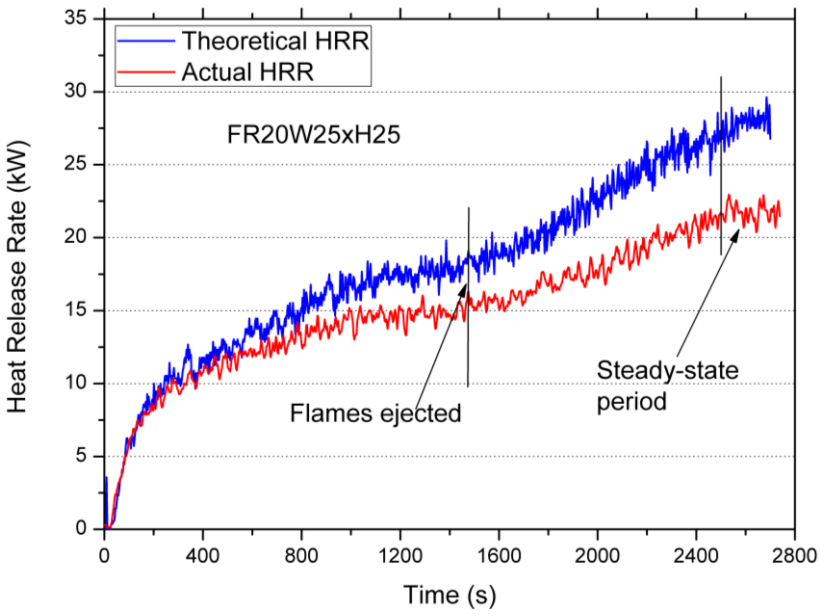

Figure 4.26 HRR profiles for the FR20W25xH25 case.

4.3.7.2 Temperature measurements from the interior of the corridor

Temperature evolution profiles from the interior of the corridor for the cases using the 0.25m x 0.25m opening, namely the FR30W25xH25 and FR20W25xH25 cases, are shown in Fig. 4.27 and 4.28 respectively. It is observed that at all locations except inside the Box A where the pool fire is located, temperatures increase even when HRR becomes steady. Thus, more time was needed for establishing steady-state conditions inside the corridor. Good agreement of the time to reach steady-state conditions in Box A was found between the HRR and the upper layer temperature measurements. In both cases, the top temperature reaches more than 600^{o}C while in the lower location it only reaches 300^{o}C and 450^{o}C using the 30 cm dia. and the 20 cm dia. pan respectively. The temperatures of the two lower locations inside Box A (see AT1 and AT2 profiles of Fig. 4.27-4.28) indicate the existence of the cold lower layer, as they are 150-300^{o}C less than the top temperature.

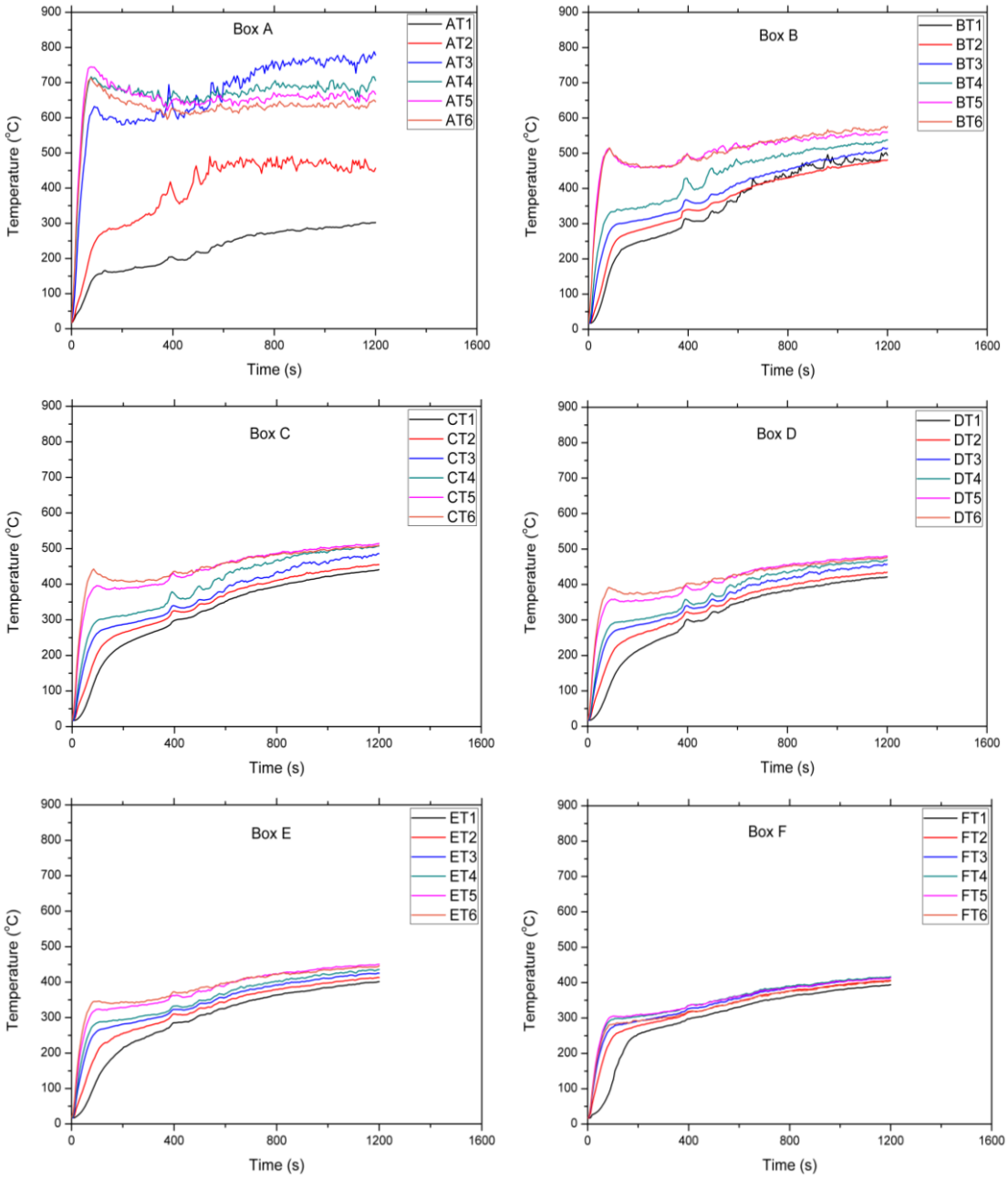

Figure 4.27 Temperature evolution profiles from bottom to top inside each box (Box A where pool fire was placed to Box F at the rear end) for case FR30W25xH25.

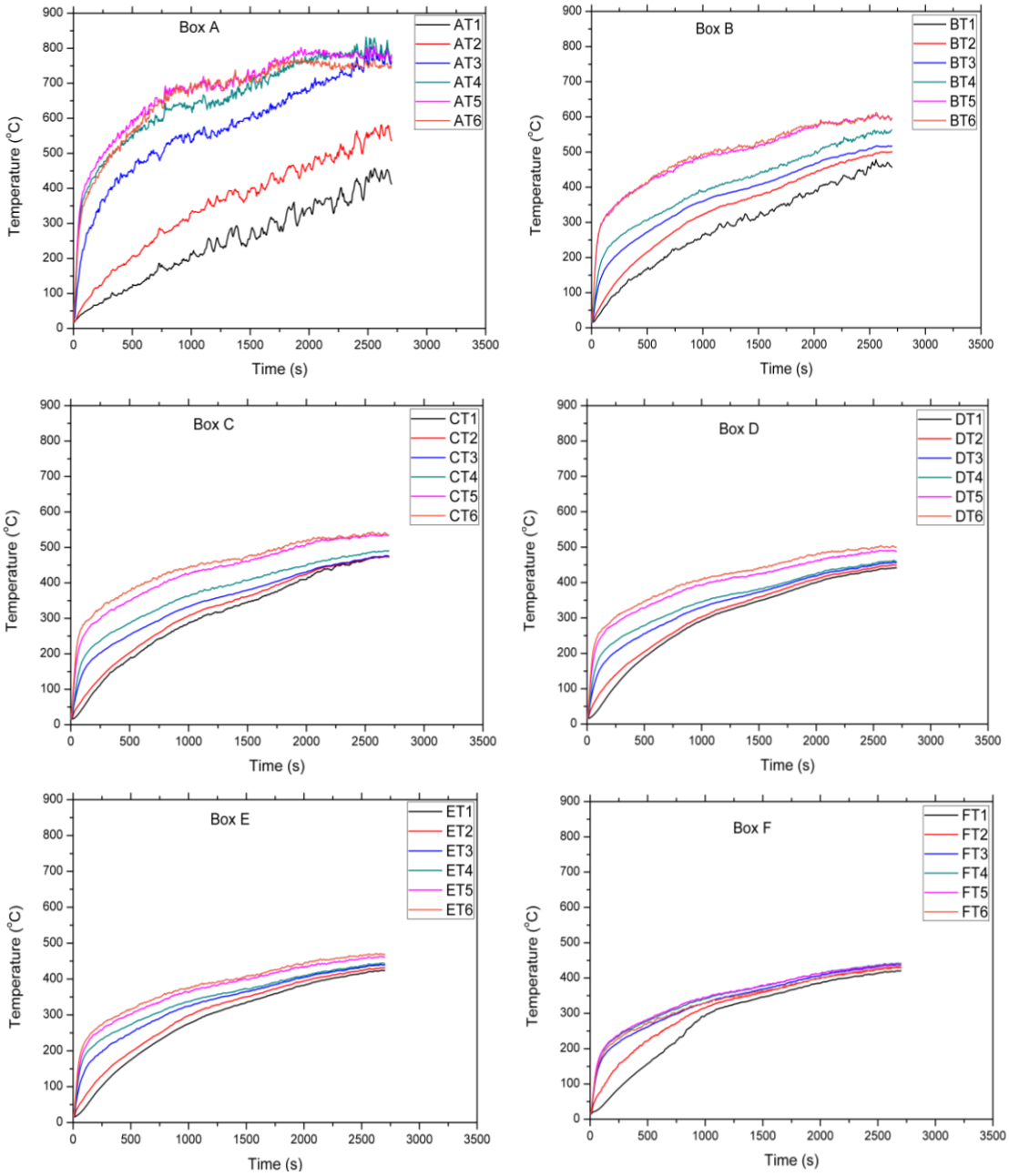

Figure 4.28 Temperature evolution profiles from bottom to top inside each box (Box A where pool fire was placed to Box F at the rear end) for case FR20W25xH25.

As temperature increases inside the corridor, three different times were selected for detailed analysis of temperatures of the top and lower locations in terms of the distance from the opening. Since the experiment with the 30 cm dia. pan lasted half the time of the experiment using the 20 cm dia. pan, different times were selected for each case but always considering the HRR regimes discussed above. The data are depicted in Fig. 4.29 and 4.30 for FR30W25xH25 and FR20W25xH25 respectively. Regarding the case using the 30 cm dia. pan, it is observed that in Box A, closer to

the opening, the temperature at the top location during the growth period is as high as that during the steady-state period. This can be explained by the peak temperature observed during the growth period after 70 s from ignition. Same observation was made for all cases using the large pan as discussed earlier. However, using the 20 cm dia. pan, the top temperature gradually increases during the growth period, with similar trends noted for the HRR data. In both cases, a distinctive cold layer is observed during the growth period in the whole length of the corridor with temperatures up to 110^{o}C. As the fire grows, this temperature increases and there is increasing mixing between the lower and upper layers. Eventually, during the steady-state period there is a clear distinction between the upper and lower layers only in Box A, where fresh air enters the compartment. For both cases, moving towards the rear end of the corridor leads in less stratification and more mixing as the difference between the top and lower locations decreases. This difference is completely eliminated in Box F during the steady-state period (see green lines) for both cases.

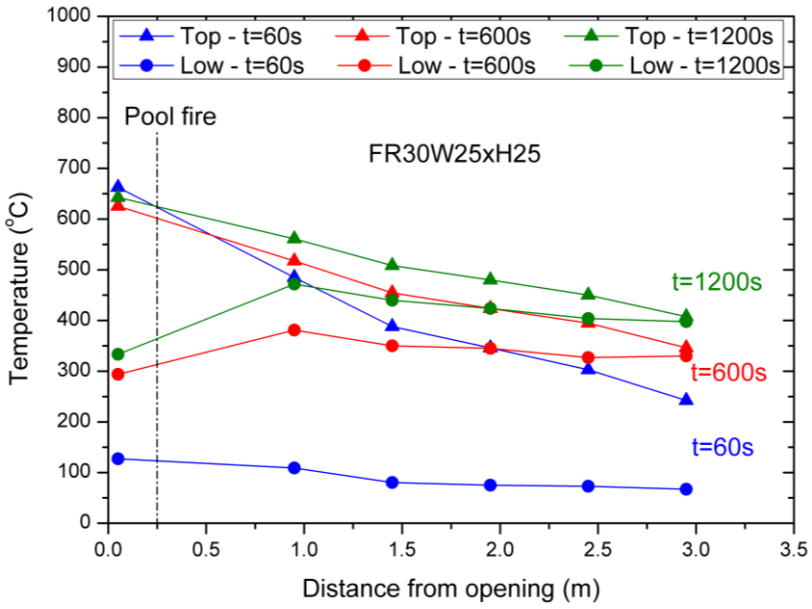

Figure 4.29 Temperature at the top and the low locations over the distance from the opening for case FR30W25xH25 in three time steps: 60, 600 and 1200s.

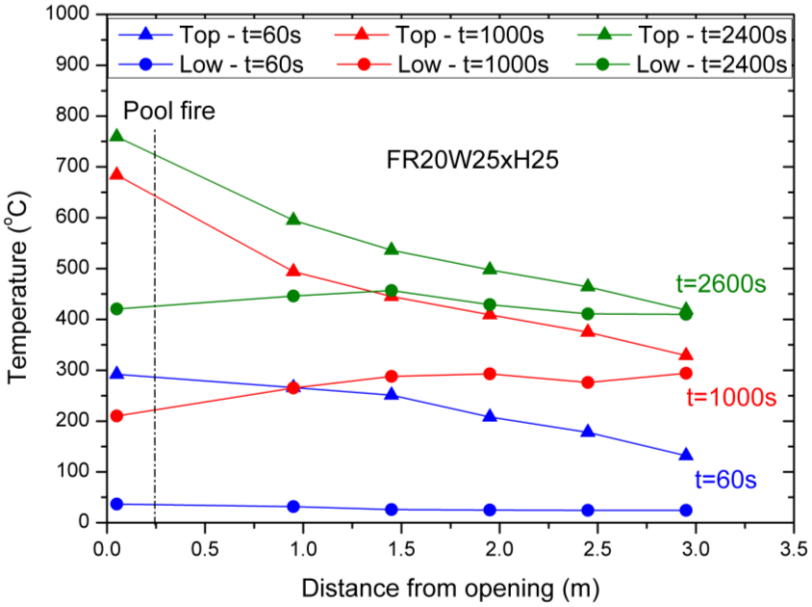

Figure 4.30 Temperature at the top and the low locations over the distance from the opening for case FR20W25xH25 in three time steps: 60, 1000 and 2600s.

The vertical distribution of the average steady-state temperature inside Box A for all cases when flames appeared outside is depicted in Fig. 4.31. The temperatures become steady at each vertical position. The results for FR30W50xH50 are not included because no steady-state conditions were established inside the corridor. A similar trend is observed for all cases. The gas temperatures inside the fire box are not vertically uniform during the fully developed stage. As depicted in Fig. 4.31, an increase in the opening dimensions, thus ventilation factor, results in an increase of the average hot gas temperature in the upper layer. Another interesting observation is that for the same opening higher temperatures were observed for the smaller pan in the fire box.

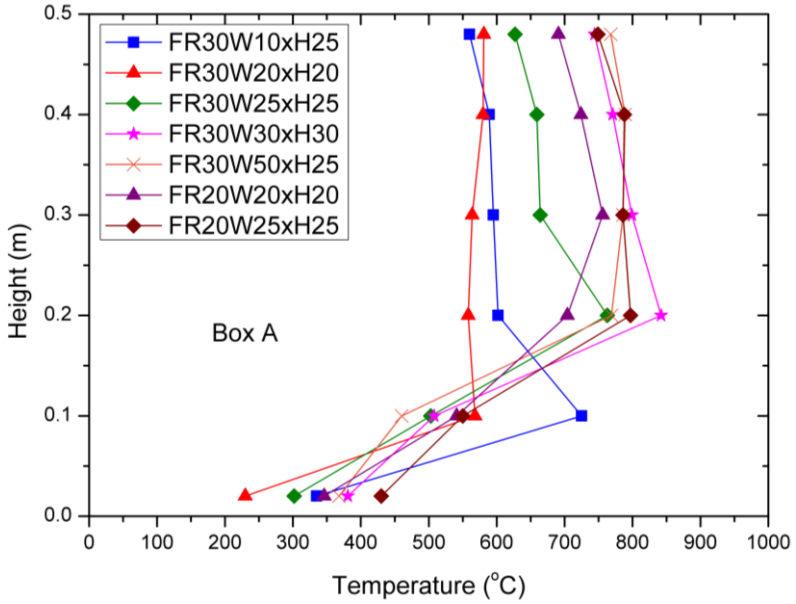

Figure 4.31 Vertical temperature distribution during steady-state period inside the Box A of the cases where flames appeared outside.

In summary, for the cases with steady burning and ejecting flame, the following observations can be made for the temperatures inside the corridor (see Fig. 4.27-4.31):

- The steady-state gas temperature inside the box where the pool fire was placed is not uniform over height. In other boxes, more time was needed for temperature to become steady.
- More mixing and less stratification was found during the steady-state period inside the rear end of the corridor (Box F). Temperature difference between the top and lower locations inside each box decreases as the distance from the opening increases. At the rear end this difference is not more than 25°C.
- For the cases of the same opening, higher gas temperatures were observed for the case with a smaller pan size.
- For the cases of the same pan size, gas temperatures increase with an increase in the opening dimensions (see Fig. 4.31).

4.3.7.3 Heat flux measurements on the floor of the corridor

The heat flux measurements are shown in Figs. 4.32 and 4.33 for FR30W25xH25 and FR20W25xH25 respectively. Using the 30 cm dia. pan, the heat fluxes inside Boxes B-F increase with time similar to temperatures. The same peaks observed in

the temperature profiles are also observed in the heat flux profiles occurring at the same time. Using the smaller pan, no peaks were observed but again heat fluxes follow the trends of the temperature profiles. In this case, heat fluxes inside Boxes B-D have values of 35, 26 and 21 kW/m^2 respectively. In both cases, the closer to the pool fire, the higher heat flux. The heat fluxes at the two locations inside Box F are similar. The higher heat flux recorded using the smaller pan inside Box B can be explained by the higher temperature inside this box for the cases of the smaller pan with the same opening as discussed earlier. Although heat flux profiles did not reach steady-state in every box, all heat flux measurements follow the same trend of temperature profiles. Where the burning takes place (closer to the opening in this case) there are higher temperatures in the upper hot smoke layer. Although in this work no measurements of temperature of the floor were made, is assumed that because temperature very close to the floor is low comparing to the hot gas layer (radiative contribution), thus convective contribution to the incoming heat flux is considered low compared to the radiative one from the hot gas layer. Accurate measurement of such contribution would need details regarding the material properties and temperature measurements on the floor rather than the gas temperatures considered here. Additionally, it has to be noted that gas temperatures were taken not in the middle of the corridor's width but close to the side wall which also could play a role in the present discussion. Based on these considerations only qualitative analysis is given regarding the radiative contribution on the heat flux.

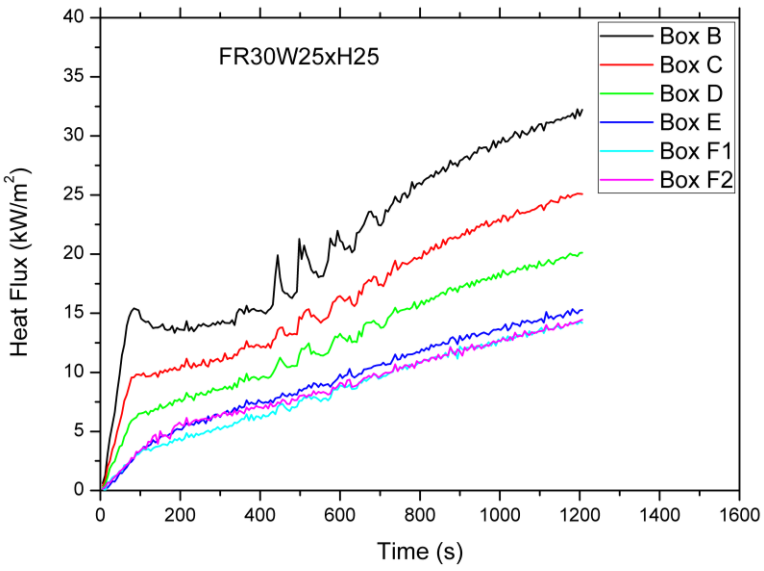

Figure 4.32 Heat Flux evolution profiles in six locations on the floor of the corridor for FR30W25xH25 case.

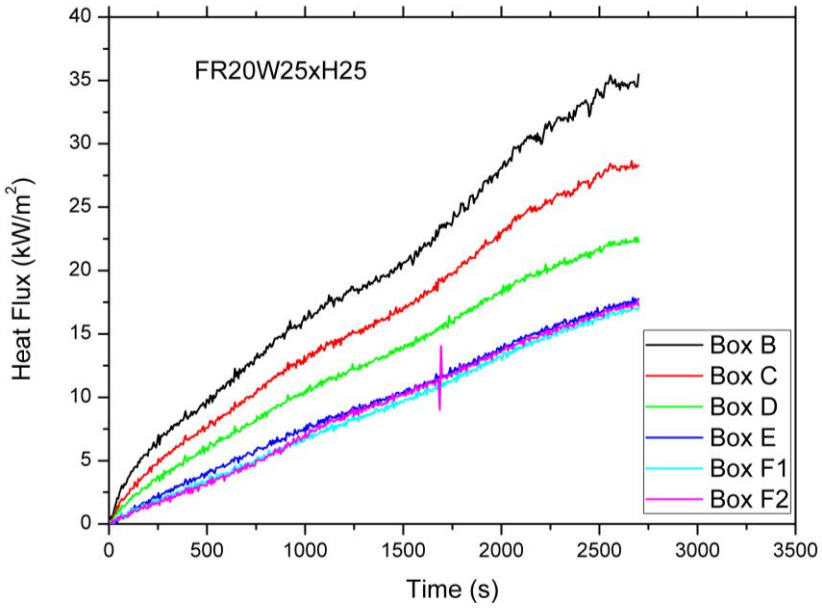

Figure 4.33 Heat Flux evolution profiles in six locations on the floor of the corridor for FR20W25xH25 case.

Figure 4.34 compares the heat flux profiles inside the Box B (closer to pool fire) for all cases. It is observed that an initial heat flux peak occurred in all cases using the 30 cm dia. pan. The heat flux seems to increase as the ventilation factor increases. The heat fluxes continue to increase during the experiments, due to the fact that no steady conditions were reached inside all the boxes except the fire box. Similar observations can be made for the two cases using the 20 cm dia. pan.

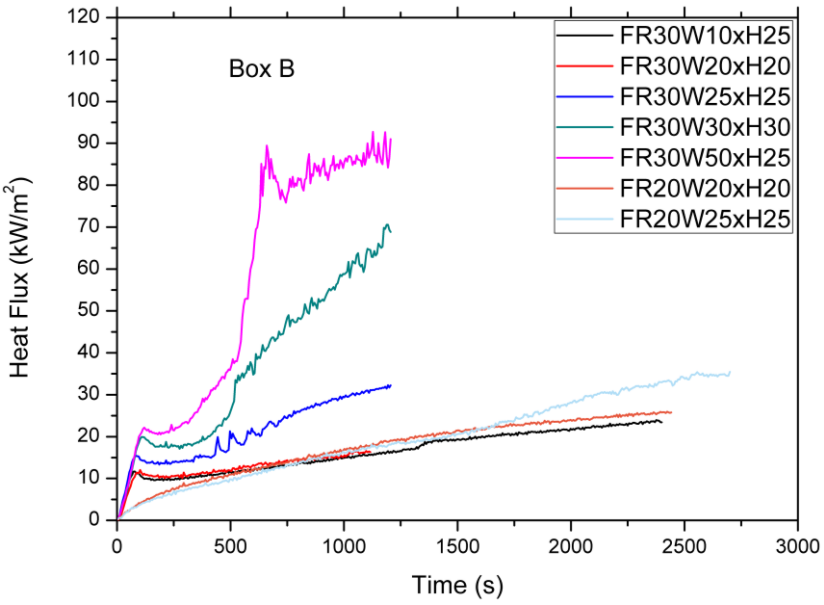

Figure 4.34 Heat flux profiles inside Box B for all cases where flames appeared outside.

4.3.7.4 External flames

This section presents flame height and heat flux experimental results for the cases when the flame ejected through the opening. The cases in which the flames came out are summarised in Table 13, along with the times (min) when the flames first appeared and became visible on the façade.

Table 13 Cases with flame ejection and time (min) they first appeared and became visible on the façade.

Cases with flame ejection	Time (min)
FR20W20xH20	26
FR20W25xH25	25
FR30W10xH25	7
FR30W20xH20	7
FR30W25xH25	2
FR30W30xH30	1
FR30W50xH25	1
FR30W50xH50	12

4.3.7.4.1 Flame Height

Flame height was calculated using the procedure described in (Audouin et al., 1995; Lee, 2006; Beji, 2009). For all cases, the reference level for the external flame height is considered to be the position of the neutral plane corresponding to 0.5H above the bottom of the opening (Beji, 2009; O' Connor, 2016). The intermittency over the flame height from the neutral plane for the case FR30W25xH25 is shown in Fig. 4.35. Based on Zukoski's criterion (Zukoski et. al., 1980), the mean flame height corresponds to an intermittency of 0.5. The maximum and continuous flame heights can be obtained similarly from the same figure, having the flame intermittency equals to 0.05 and 0.95 respectively.

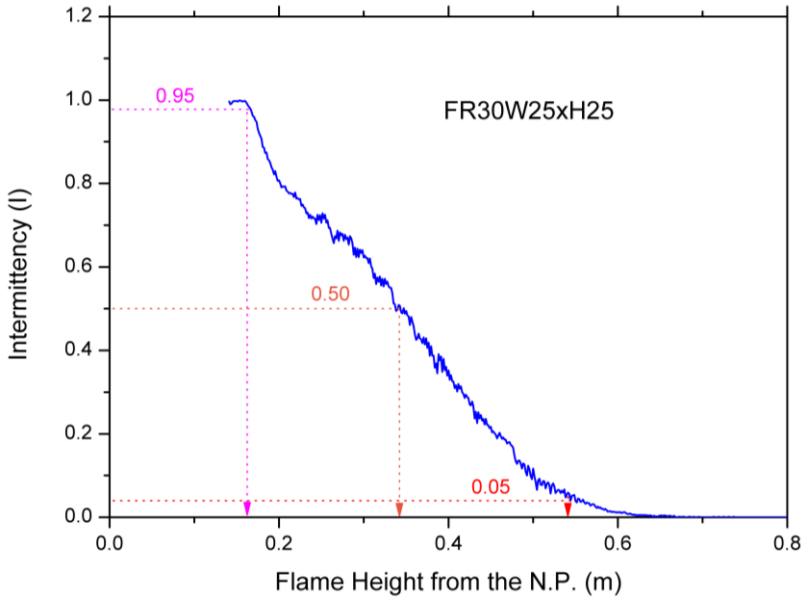

Figure 4.35 Intermittency against flame height for the FR30W25xH25 case. The location of maximum (I=0.05), mean (I=0.5) and continuous (I=0.95) flame height are also shown.

Following the same procedure as shown in Fig. 4.35, the location of the (mean) flame height is illustrated in Fig. 4.36 showing the experimental flame height against the theoretical HRR for all the cases when flames appeared outside the corridor. It is noted that the case FR30W50xH50 is not included as (i) it never reached steady-state burning and (ii) the maximum flame height is off the centreline of the facade. The main observation is that the flame height increases as the theoretical HRR increases. In addition, the flame height seems to be independent of the pan size, as for similar theoretical HRR the flame height is similar for both pans. It is interesting to note here that defining the heat released outside the enclosure was not feasible for these cases, as the flames came out shortly after ignition. Therefore, the flames extended towards the opening and no steady period of burning before they come out was noticed. As will be explained in next chapter, this is the main difference with cases in which the pans were located far from the opening and a plateau of HRR was reached before flame ejection. Subsequently, it was decided to plot the theoretical HRR (thus, burning rate) with flame height.

In Fig. 4.37, the flame height contours are shown for all cases. As expected, the external flame for all cases is nearly symmetrical with respect to centreline on the façade. The maximum flame height is also along the centreline of the faced except for the fully-open case FR30W50xH50, in which flames emerge as two separate

flames. This result clearly highlights the important influence of the opening dimensions on the flame behaviours.

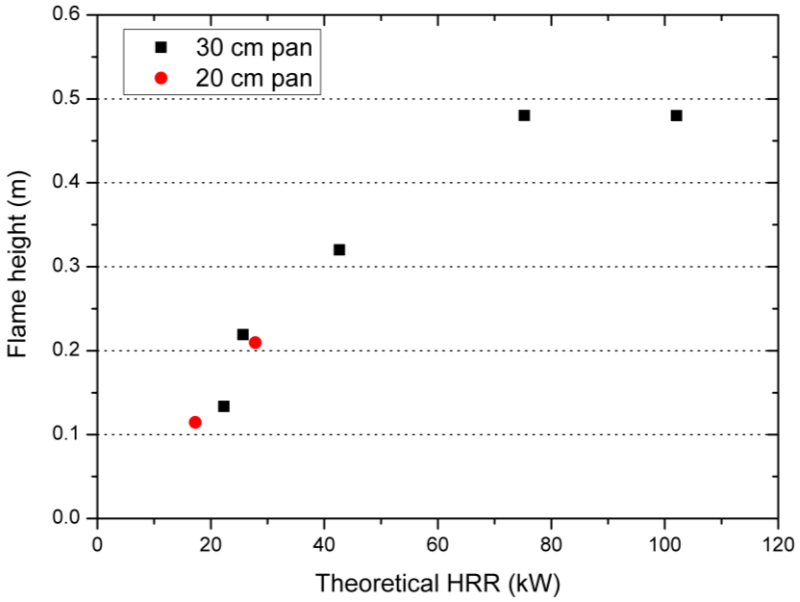

Figure 4.36 Mean flame height against theoretical HRR for cases using both pans.

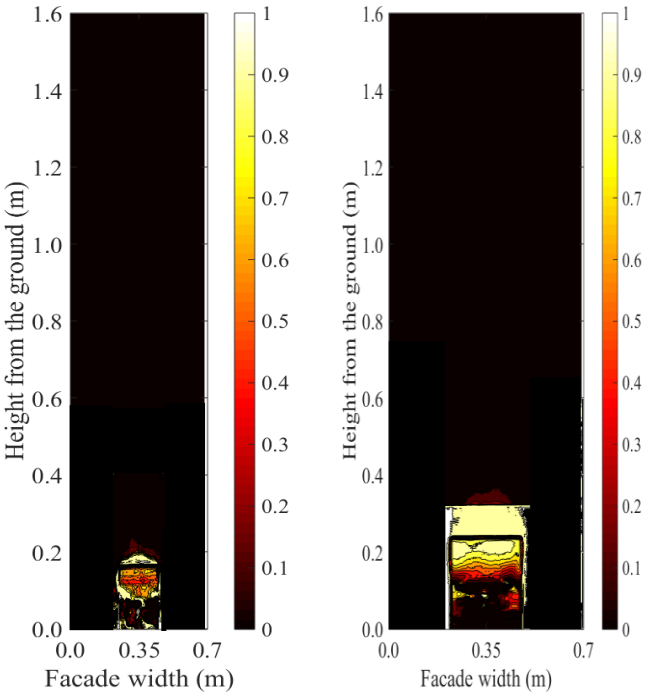

FR20W20xH20 FR20W25xH25

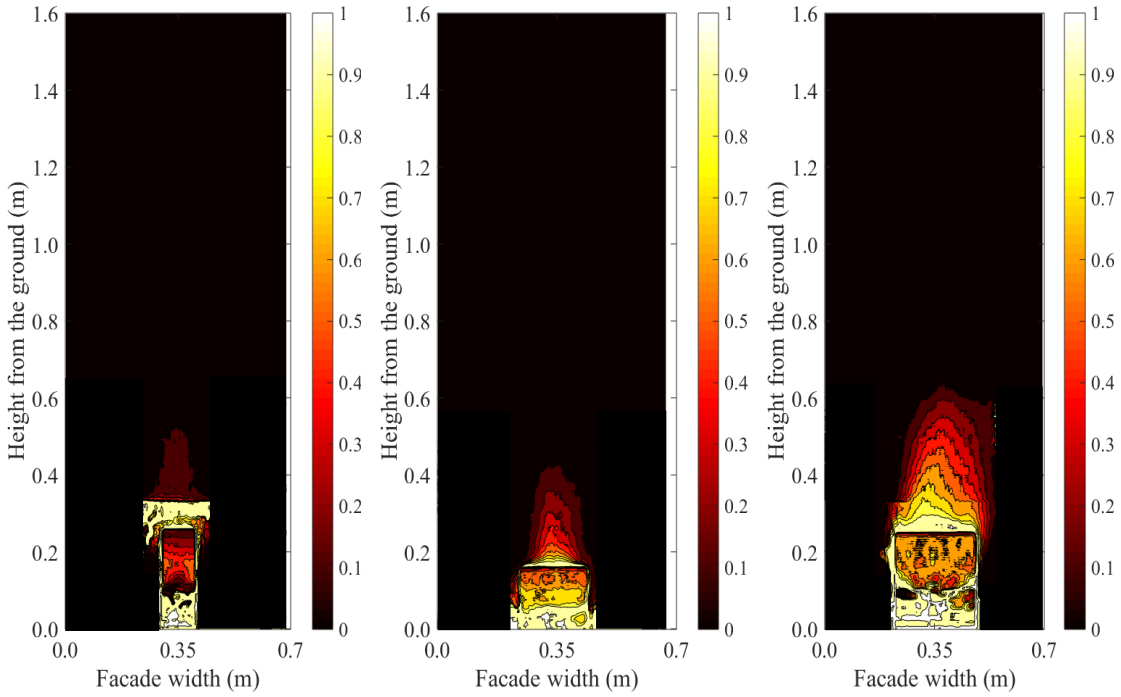

FR30W10xH25 FR30W20xH20 FR30W25xH25

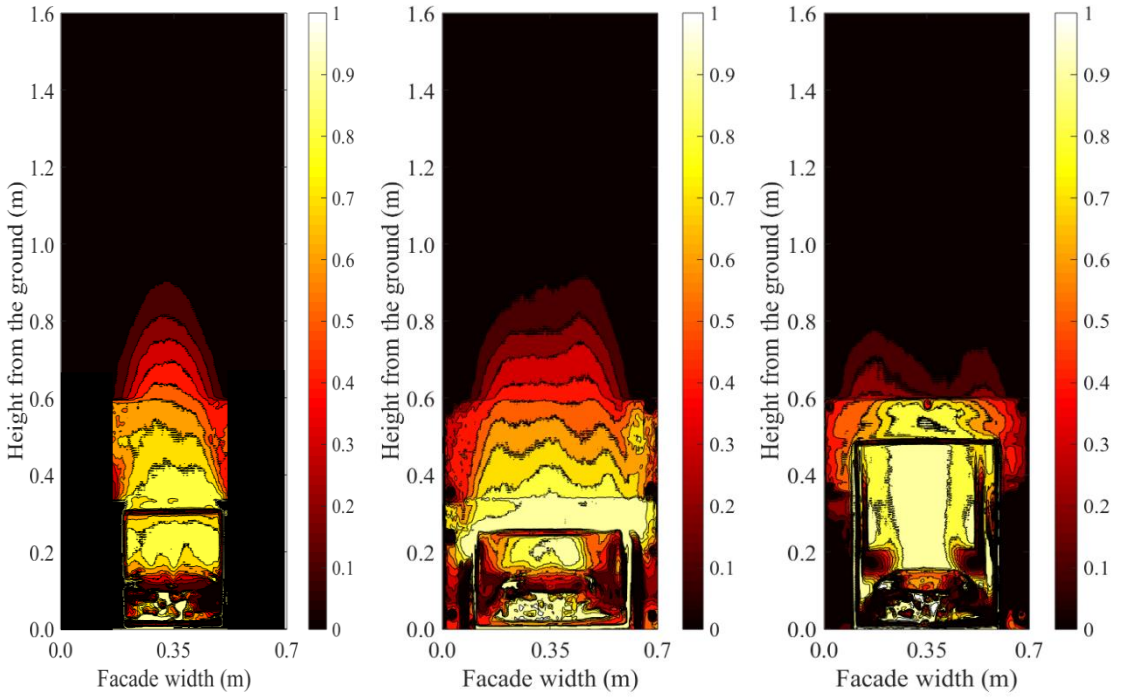

FR30W30xH30 FR30W50xH25 FR30W50xH50

Figure 4.37 Intermittency contours for all cases.

4.3.7.4.2 Heat Flux on the facade

Figure 4.38 depicts the heat flux measured at different positions on the façade for the two cases, FR20W25xH25 and FR30W30xH30 respectively. It is observed that, in both cases, the heat flux measured along the centreline is higher than the ones measured at the same height but 10 cm from the centreline. This is expected according to observations regarding the symmetry of the flame height as discussed earlier based on Figs. 4.35-4.37. In both cases, the heat fluxes on both sides of the centreline are similar. Therefore, it is reasonable to assume that the centreline can be considered as the symmetry axis for heat exposure of the façade, except for the FR30W50xH50 case, in which the maximum heat fluxes are off the centreline, as shown in Fig. 4.39. This finding highlights the importance of the width of the opening in addition to the ventilation factor to the heat exposure of the facade.

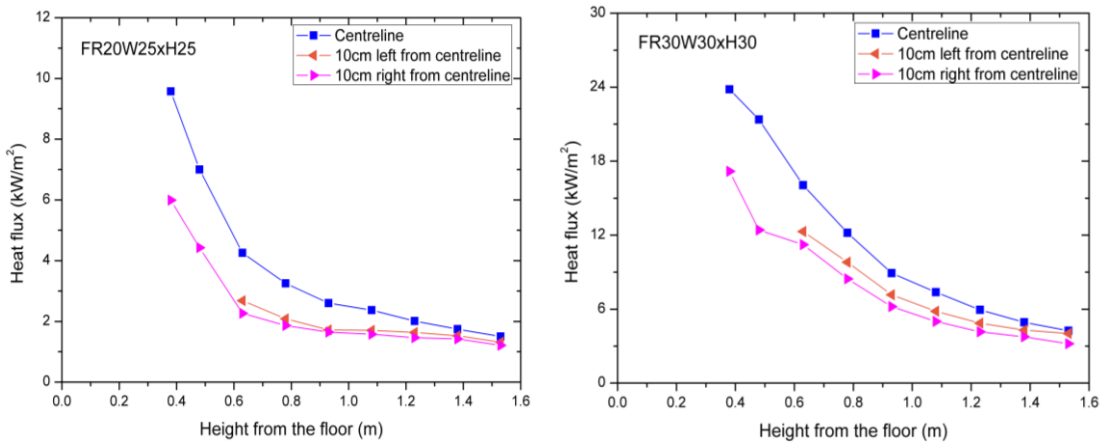

Figure 4.38 Heat flux distributions along the centreline above the opening for FR20W25xH25 (left) and FR30W30xH30 (right) case.

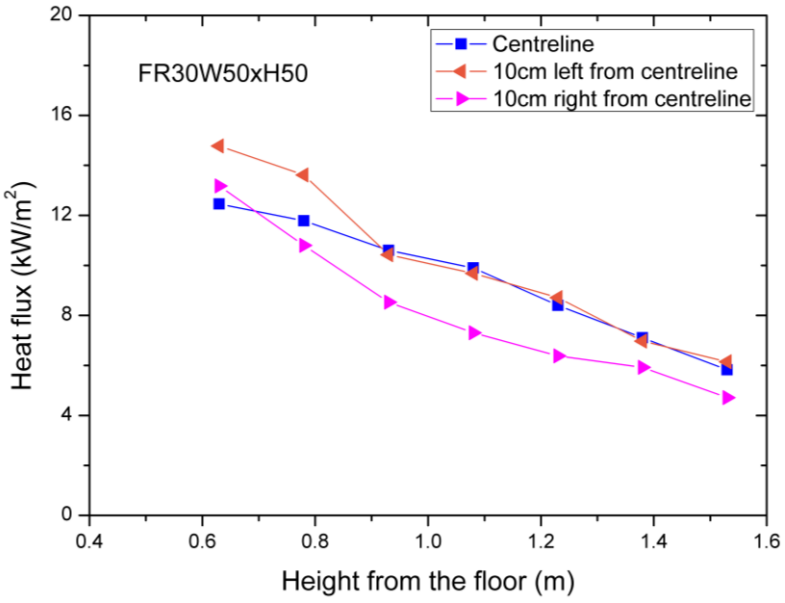

Figure 4.39 Heat flux distributions along the centreline above the opening for FR30W50xH50 case.

Figure 4.40 depicts the vertical distribution of the heat fluxes measured along the centreline of the façade for all test cases in which flames ejected through the opening. Similar distributions are observed for all cases, except for the case FR30W50xH50. It is shown that the measured heat fluxes decrease with increasing height as expected. Also, for the same pan size, the heat fluxes in the centreline increase as the opening dimensions (e.g. ventilation factor) increase.

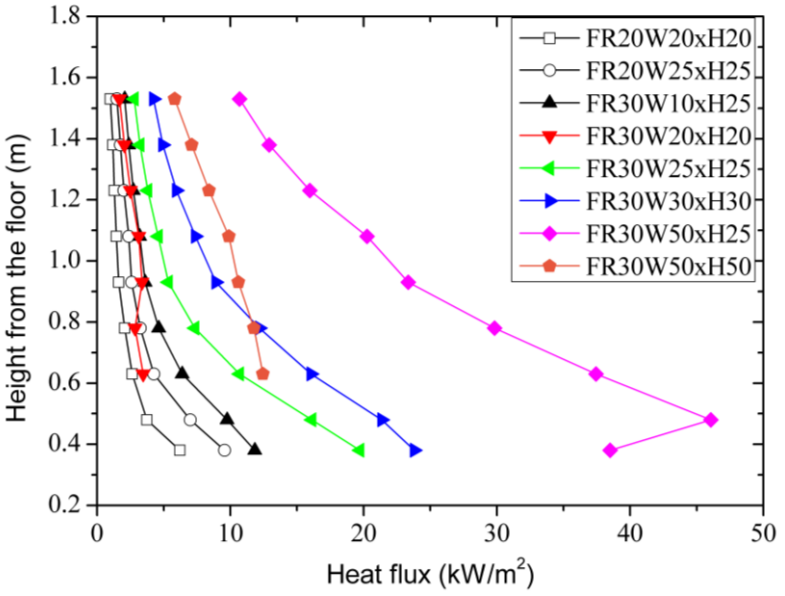

Figure 4.40 Heat flux distributions along the centreline above the opening for all cases.

4.4 Discussion and Analysis

4.4.1 Time to steady-state conditions

As the main objective of this work is to study burning behaviour of pool fires inside the corridor-like enclosure during the steady-state burning period, it is important to establish steady-state conditions. After HRR becomes steady the average values of HRR and MLR can then be calculated. The time needed to reaching steady-state burning varies for each case and is summarised in Table 14. Clearly, the size and location of the pool fire, and the opening factor all play an important role in whether steadying burning conditions can be achieved and, if yes, the time needed to reaching steady-state conditions.

Table 14 Summary of time needed for steady-state conditions established in each case.

Pan Size (cm)	**W_o x H_o (m)**	**$1500A_oH_o^{1/2}$**	**Experiments' Names**	**Duration of experiment (s)**	**Time to steady-state conditions (s)**	**Flames out**
20	0.1 x 0.1	0.0032	FR20W10xH10	180	Self-extinction	N
	0.15 x 0.15	0.0087	FR20W15xH15	2400	1974	N
	0.1 x 0.25	0.0125	FR20W10xH25	2400	1794	N
	0.2 x 0.2	0.0179	FR20W20xH20	2400	2094	Y
	0.25 x 0.25	0.0313	FR20W25xH25	2700	2487	Y
	0.3 x 0.3	0.0493	FR20W30xH30	2400	>2400	Y
	0.5 x 0.25	0.0625	FR20W50xH25	2400	>2400	Y
	0.5 x 0.5	0.1767	FR20W50xH50	1200	660	N
30	0.1 x 0.1	0.0032	FR30W10xH10	150	Self-extinction	N
	0.15 x 0.15	0.0087	FR30W15xH15	1800	630	N
	0.1 x 0.25	0.0125	FR30W10xH25	2400	1605	Y
	0.2 x 0.2	0.0179	FR30W20xH20	1200	803	Y
	0.25 x 0.25	0.0313	FR30W25xH25	1200	801	Y
	0.3 x 0.3	0.0493	FR30W30xH30	1200	759	Y
	0.5 x 0.25	0.0625	FR30W50xH25	1200	693	Y
	0.5 x 0.5	0.1767	FR30W50xH50	1800	>1800	Y

As shown in Table 14, the time needed for steady-state conditions to be established inside the corridor-enclosure is mainly affected by the size of the pan. Using the larger pan (30 cm dia.) it took much less time to reach steady-state burning than that in the cases with the smaller pan (20 cm dia.), due to the fact that more time is

needed for the gases in the corridor and the walls of the enclosure to be heated up with a smaller pan (thus small heat release rate). Using the smaller pan, the temperatures inside Box A (where the pool fire was placed) at different vertical locations, increase progressively until they reach a constant value. In comparison, using the larger pan, temperatures inside Box A reached their peak value almost immediately after ignition (only one min after), then a small decrease was observed until reaching a constant value. This behaviour is depicted in Fig. 4.41, showing the temperature evolution measured at 2 cm below the ceiling of Box A for two cases having same opening dimensions but different pan sizes.

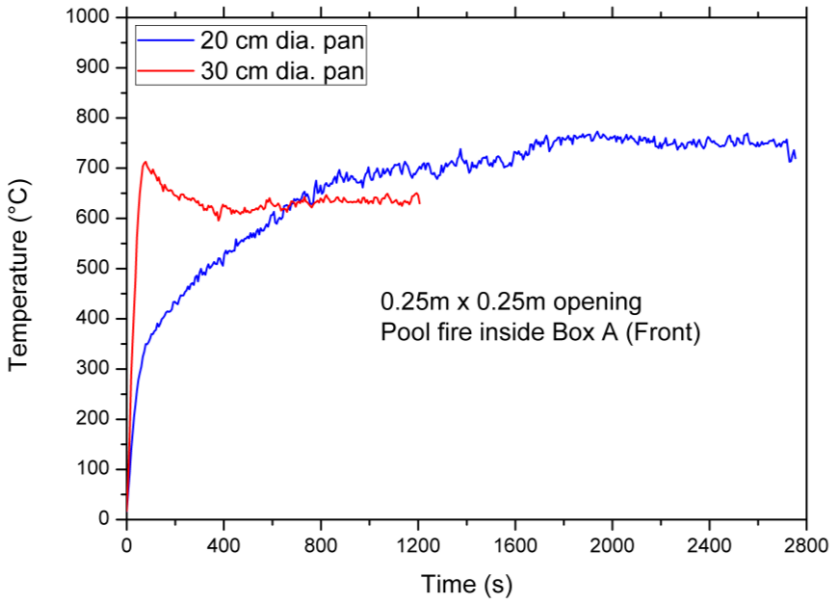

Figure 4.41 Temperature histories measured 2 cm below ceiling inside the Box A (where pool fire was) for cases FR20W25xH25 and FR30W25xH25.

Another influence is the geometry of the opening, thus the ventilation factor, but it was validated only in the cases using the smaller pan -20 cm dia. The time to steady-state was found to increase as the ventilation factor increases. Temperature histories of the upper layer inside the Box A (2 cm below ceiling) and heat flux measurements on the floor of the enclosure at a 0.5m distance from the pan are depicted in Fig. 4.42 for four different opening geometries, 0.15, 0.2, 0.25 and 0.5m respectively. As the width of the opening increases higher temperatures and heat fluxes are observed. The higher temperature of the hot gas layer under the ceiling enhances pyrolysis and the higher heat flux on the floor results faster evaporation of the fuel.

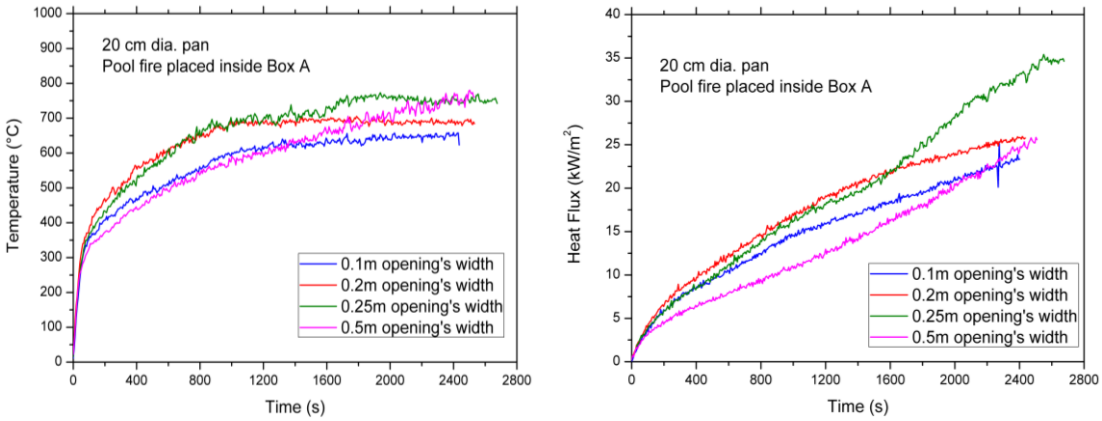

Figure 4.42 Temperature histories measured 2 cm below ceiling inside the Box A, where the pool fire was located (left) and heat flux on the floor at 0.5m from the pan (right) for different opening widths using the 20 cm dia. pan.

According to Table 14, no strong influence of opening size was found to affect the time needed to steady-state conditions in the case of the larger pan (30 cm dia.), as the time period before steady-state burning was scattered.

4.4.2 MLR and HRR

The MLR is plotted against the ventilation factor both normalised by the fire area (equals to the surface area of the fuel pan) in Fig. 4.43. Results of the free-burn cases are also plotted. It is noted that average values during the steady-state period are used. In three cases, FR20W30xH30, FR20W50xH25 and FR30W50xH50, the final values were used because they didn't reach steady-state burning and MLR was still increasing at the end of the experiments. The trend of the data follows that by other researchers (Delichatsios et. al., 2004; Quintiere, 2006; Drysdale, 2011; Delichatsios, 2014) as presented in Chapter 2. For smaller openings MLR increases almost linearly with the ventilation factor until reaching a critical point corresponding to the transition from ventilation- to fuel-controlled fires. After that point, MLR decreases as the ventilation factor increases until it becomes constant for very large openings similar to free-burn MLR. The distinction between the two regimes, 'Regime I' (ventilation-controlled) and the 'Regime II' (fuel-controlled) as formally referred in (Gross and Robertson, 1965) and (Thomas et al., 1967) was difficult to be made in this experimental series as some experiments didn't reach steady-state conditions as mentioned before. This distinction was however observed by incorporating data from

experiments with pool fires placed at the rear end of the corridor as will be discussed in the following chapters.

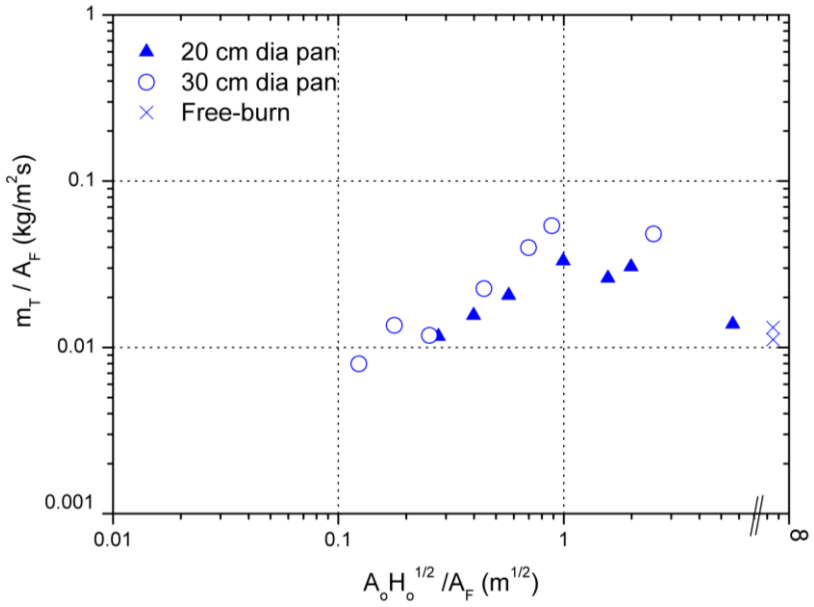

Figure 4.43 Mass loss rate over ventilation factor, both normalised by the fire area.

As depicted in Fig. 4.43, the normalised MLR of the experiments using the 30 cm diameter pan was found larger than the cases using the smaller pan, thus increase of pan size enhanced MLR. Finally, as mentioned in the previous section, the MLR of FR20W50xH50 case is very close to free-burn cases and burning takes place only inside the Box A.

4.4.3 Combustion Efficiency

Combustion efficiency is calculated by the following equation, Eq. 4.1:

$$\eta = \dot{Q}_{act}/\dot{Q}_{th} \tag{4.1}$$

The theoretical HRR was calculated using Equation 3.1 by multiplying the mass loss rate with the effective heat of combustion of ethanol 26780 KJ/kg (99% pure ethanol was used). The actual HRR was measured by oxygen depletion in the 3m x 3m collection hood.

Figure 4.44 plots the combustion efficiency of the experiments during steady-state burning period against the ventilation factor for each case. The experiments

conducted having the 0.1m x 0.1m opening are not included as the fire was self-extinguished. In general, with low ventilation factors (which in the current study corresponds to 0.15m x 0.15m, 0.1m x 0.25m and 0.2m x 0.2m-sized openings) combustion efficiency is 0.7 to 0.78. The lowest combustion efficiency, 0.55, was found for the FR30W15xW15 case, the only experiment using the 30 cm dia. pan when flames didn't appear out of the enclosure. In that case, burning took place only inside Box A due to limited oxygen availability. According to visual observations (see Fig. 4.45), burning was taking place more on the edges of the pan rather than on the whole surface of fuel. It was clear that not sufficient air was getting into the corridor through the opening for complete combustion of fuel. This case is similar to the cases of self-extinguishment, but the fire finally sustained during the experiment.

As opening dimensions increase, thus there is more oxygen available for combustion, a slight increase of combustion efficiency is observed, within the range 0.74 to 0.8. As expected, the highest values of combustion efficiency were for the fully-open opening, 0.5m x 0.5m. Using the 30 cm dia. pan combustion efficiency reached 0.77 and with the 20 cm dia. pan efficiency calculated 0.87 but both were less than the combustion efficiency which was measured in free-burn cases (0.97). It is therefore deduced that there is more available oxygen getting into the corridor through the opening for combustion as the ventilation factor increases. It needs to be reminded here, that using the smaller pan, burning was similar to the one in free air as discussed in §4.3.6, thus combustion efficiency is expected to be high.

It is also noted that because the pans are located very close to the opening, the influence of the incoming and outcoming air flows is more difficult to be evaluated as air reaches the fuel surface very quickly after entering the enclosure. Flows inside the corridor having the fire source at the rear end were studied in the past (Ukleja, 2012) and specific patterns have been proposed (change of flows behind the travelling flame). Future works with fire sources close to the opening and measurements of air inflows and outflows would provide great insights into the fundamental research of corridor fire dynamics.

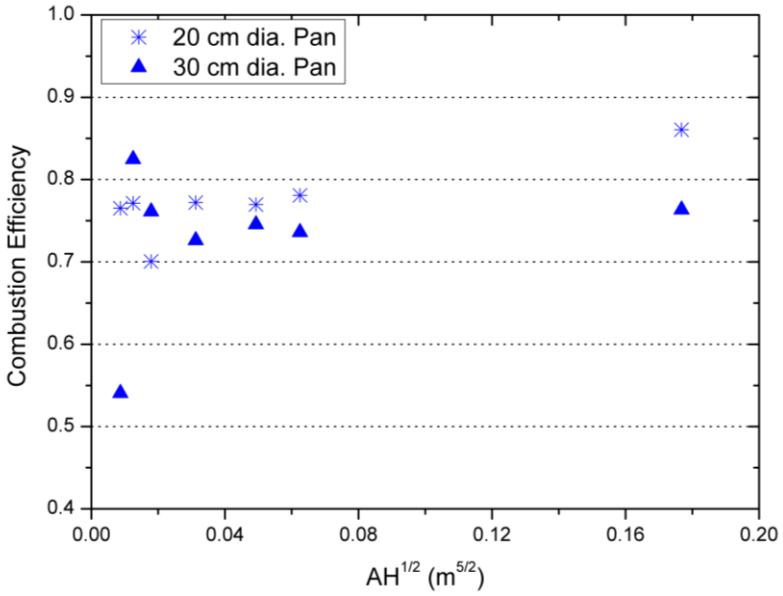

Figure 4.44 Combustion efficiency versus ventilation factor for all the cases fire sustained.

Figure 4. 45 Images taken during FR30W15xH15 case which was of very low combustion efficiency.

4.5 Conclusions

A parametric experimental investigation of the fire dynamics in a reduced-scale corridor-like enclosure and the heat exposure on the facade was performed in this chapter. The pool fire source was placed inside Box A -close to the opening- and effects of pool and ventilation size were studied. The findings relied on visual observations, theoretical and actual HRR profiles, temperature and heat flux distribution within the enclosure and flame height and heat flux measurements on the façade of the enclosure.

The main findings of this chapter are:

1. The time needed for steady-state conditions to be established inside the enclosure is mainly influenced by the size of the pan, as using the larger pan the gas inside and corridor walls of the enclosure are heated up faster, therefore steady conditions are established in a shorter period. Ventilation factor was also found to affect the time needed for steady conditions, but it needs to be further investigated.
2. Steady-state temperature distributions were found to be non-uniform along the height of the corridor-enclosure, showing a clear distinction between the upper hot and lower cold layers, especially closer to the opening (see §4.3.7). Also, it was found that for the cases with the same opening, higher gas temperatures were observed for the case with the small pan.
3. As discussed in §4.4.2 the steady-state MLR for smaller openings increases almost linearly with the ventilation factor until reaching a critical point corresponding to the transition from ventilation- to fuel-controlled fires. Then, the MLR decreases as the ventilation factor increases until it becomes constant for very large openings similar to free-burn MLR. In addition, it was found that pan size also influences slightly the normalised burning rate, with higher normalised burning rates found with the large pan size.
4. The combustion efficiency was found to increase with an increase in the ventilation factor, as using larger opening sizes more oxygen enters the corridor being available for combustion. It is also noted that the higher values of combustion efficiency for both pans were observed using the fully-open opening. The pan size was also found to strongly affect the combustion efficiency, as higher values were found for the smaller pan (0.75-0.86) opposed to the ones found using the larger pan (up to 0.76).
5. Regarding the flames ejecting through the opening, the flame height was found to increase with an increase in the HRR. It was also shown that heat fluxes on the façade were higher on the centreline of the exposed façade for all cases, except the one using the fully-open opening and the larger pan. In this particular case, the flames emerge through the opening as two separate flames, thus the major heat exposure of the façade was off the centreline.

CHAPTER 5

POOL FIRES PLACED AT THE REAR END OF THE CORRIDOR-LIKE ENCLOSURE

5.1 Introduction

In Chapter 4, results are presented for the cases when the burner was placed close to the opening. This chapter, results will be presented for the cases when the pool fires were placed at the rear end of the corridor, far from the opening. The experimental results include the following:

i. Heat release rate
ii. Mass loss rate
iii. Combustion efficiency
iv. Temperatures in the interior of the enclosure
v. Heat fluxes on the floor of the enclosure
vi. External flame height
vii. Heat fluxes on the façade

The following section of the chapter presents a summary of the experiments conducted and the measuring equipment used. In section 5.3 the repeatability of the experimental results is discussed. In addition, all the experimental observations and results are presented. Section 5.4 presents comparative discussions of the results. Finally, in Section 5.5, a summary of all findings is given followed by future recommendations.

5.2 Experimental Set-up

The pool fire was placed in the middle of the rear box (Box F), i.e., the centre of the pool is 0.25 m from the rear wall of the corridor or 2.75 m to the opening. The measurements taken were described in Chapter 3 include MLR, HRR, temperature profiles inside the corridor, heat fluxes on the floor and on the façade and heights of flames emerging through the opening of the enclosure. The layout of the experimental rig used for this series of experiments is shown in Fig. 5.1.

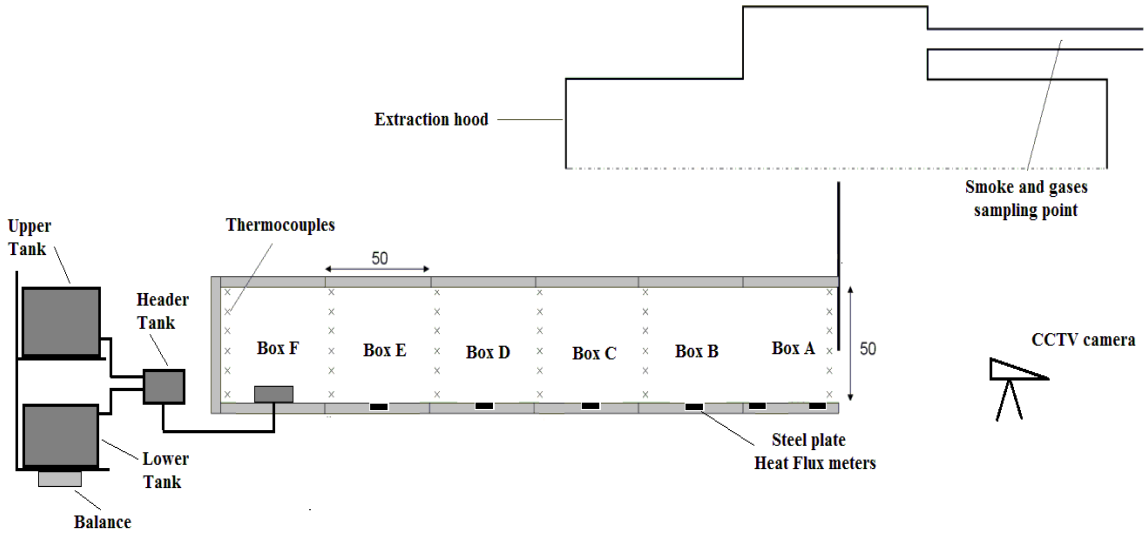

Figure 5.1 Sketch of the experimental layout with the pool fire placed at the rear box (Box F) of the corridor.

In total, 16 cases were studied using eight different opening dimensions and two pan sizes. A summary of the experiments conducted is given in Table 15. It should be noted that more than one experiment were conducted for each case in order to achieve repeatable results. The duration of the experiments varied depending on the HRR measurements. Because the aim of this work is to study the steady-state period of pool fires inside the corridor-like enclosure, each experiment ran for a short period of time after HRR has reached a steady value. In general, a period of 2-3 min. was considered for averaging the results of the steady-state period. As reported in Chapter 3, none of the experiments was left for more than 50 min in order not to damage the experimental rig's walls.

Table 15 Summary of the experiments conducted using the pool fires at the rear box of the enclosure.

Pan Size (cm)	W_o x H_o (m)	$1500A_oH_o^{1/2}$	Experiments' Names	Duration of experiment (s)	Steady-state conditions achieved	Flames out
20	0.1 x 0.1	4.8	BC20W10xH10	210	Self-ext.	N
	0.15 x 0.15	13.1	BC20W15xH15	2520	Yes	N
	0.1 x 0.25	18.8	BC20W10xH25	3000	Yes	N
	0.2 x 0.2	26.7	BC20W20xH20	3000	Yes	N
	0.25 x 0.25	46.5	BC20W25xH25	2280	Yes	Y
	0.3 x 0.3	73.5	BC20W30xH30	2100	Yes	Y
	0.5 x 0.25	93.8	BC20W50xH25	2220	Yes	Y
	0.5 x 0.5	265.1	BC20W50xH50	2100	Yes	N
30	0.1 x 0.1	4.8	BC30W10xH10	240	Self-ext.	N
	0.15 x 0.15	13.1	BC30W15xH15	1800	Yes	N
	0.1 x 0.25	18.8	BC30W10xH25	1800	Yes	N
	0.2 x 0.2	26.7	BC30W20xH20	2040	Yes	N
	0.25 x 0.25	46.5	BC30W25xH25	1800	Yes	Y
	0.3 x 0.3	73.5	BC30W30xH30	1080	Yes	Y
	0.5 x 0.25	93.8	BC30W50xH25	1200	Yes	Y
	0.5 x 0.5	265.1	BC30W50xH50	960	Yes	Y

5.3 Experimental Results

5.3.1 Repeatability tests

To demonstrate the repeatability of the tests, two test cases namely BC20W20xH20 and BC30W50xH50 are chosen. Table 16 shows the operational conditions of these test cases. The MLR and HRR profiles, gas temperature profiles of two locations in the interior of the corridor and heat flux profiles of two locations -on the floor and on the façade of the corridor are shown in Fig. 5.2-5.4.

Table 16 Summary of the operational conditions of the selected test cases for repeatability.

Test case	BC20W20xH20		BC30W50xH50	
	Test 1	Test 2	Test 1	Test 2
W_o x H_o (m)	0.2 x 0.2	0.2 x 0.2	0.5 x 0.5	0.5 x 0.5
T_{amb} (°C)	18.2	18.6	16.5	15
RH (%)	92	85	73	74
t_{dur} (s)	3000	2880	1200	1500
$1500A_oH_o^{1/2}$ (kW)	26.7	26.7	265.1	265.1

Figure 5.2 shows the HRR and MLR profiles for the selected test cases. The HRR measured is almost identical for both cases. Regarding the MLR in Fig. 5.2 (right), the two test cases also exhibit good repeatability. Further comparisons are made for hot gas temperatures at two locations (Fig. 5.3) and heat fluxes in the middle of Box

D (Fig. 5.4). Both sets of results show very good repeatability. All the other cases with the fire source placed inside Box F have similar trends.

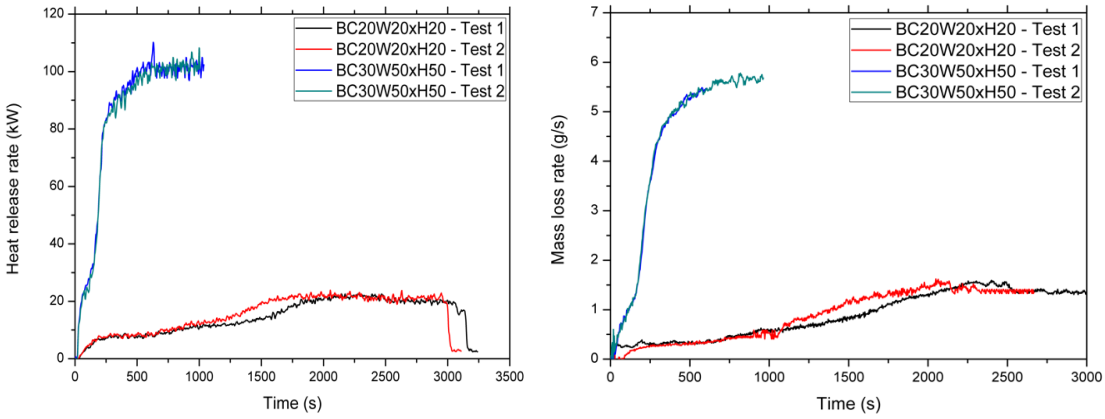

Figure 5.2 HRR profiles (left) and MLR profiles (right) of two identical tests for the two test cases investigated for repeatability.

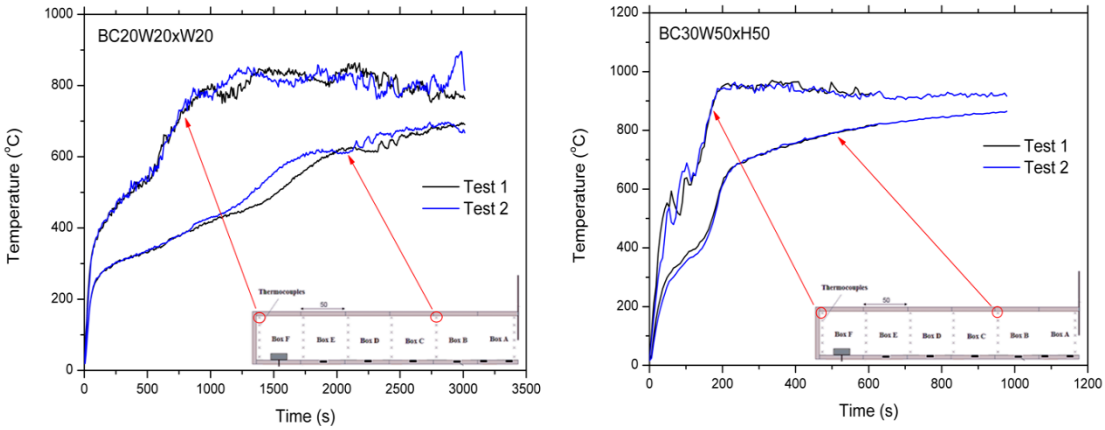

Figure 5.3 Temperature profiles measured 2 cm from ceiling in Box B and Box F of two identical tests for the BC20W20xH20 (left) and BC30W50xH50 (right) test case.

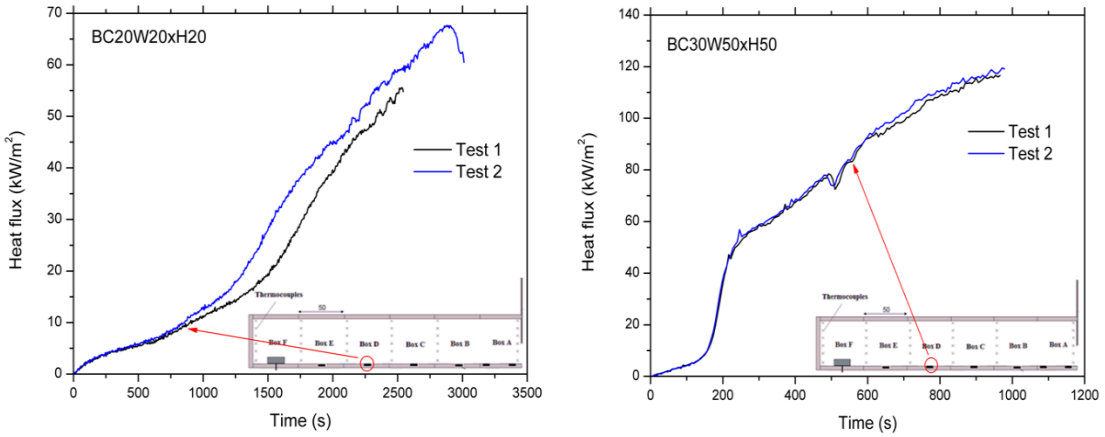

Figure 5.4 Heat Flux profiles measured in the middle of Box D of two identical tests for the BC20W20xH20 (left) and BC30W50xH50 (right) test case.

5.3.2 General burning behaviour

Before detailed analysis of the experimental measurement data (gas temperature, heat fluxes, flame height), some general observations will be made based on video recordings and the MLR-HRR measurements. The following observations were made with respect to (i) the opening's dimensions (in terms of ventilation factor) and (ii) the size of the pan (in terms of diameter of the circular pan):

- For the lowest ventilation factor (opening dimensions 0.1m x 0.1m), fire was self-extinguished as not sufficient fresh air (thus oxygen) was reaching the fuel surface which was far from the opening. As a result, fire didn't sustain for more than 3 min. Same behaviour was reported for both pan sizes used.
- For low ventilation factors (openings with W x H: 0.15 x 0.15, 0.1 x 0.25 and 0.2 x 0.2 m^2), burning took place only inside the corridor and no flames were observed outside the enclosure. Steady-state conditions were established inside the fire-box in all cases.
- Another case with no ejected flames through the opening was the BC20W50xH50, using the 20 cm dia. pan and the fully-open opening. It was observed that burning of this case is similar to the free-burn case, indicated by the same HRR as the one measured in free-burn conditions.
- For the larger openings of W x H (m^2): 0.25 x 0.25, 0.3 x 0.3, 0.5 x 0.25 and 0.5 x 0.5 (only using the large pan) flames ejected through the opening before steady burning was achieved.

A summary of the burning behaviour for all cases using the two pans is shown in Fig. 5.5.

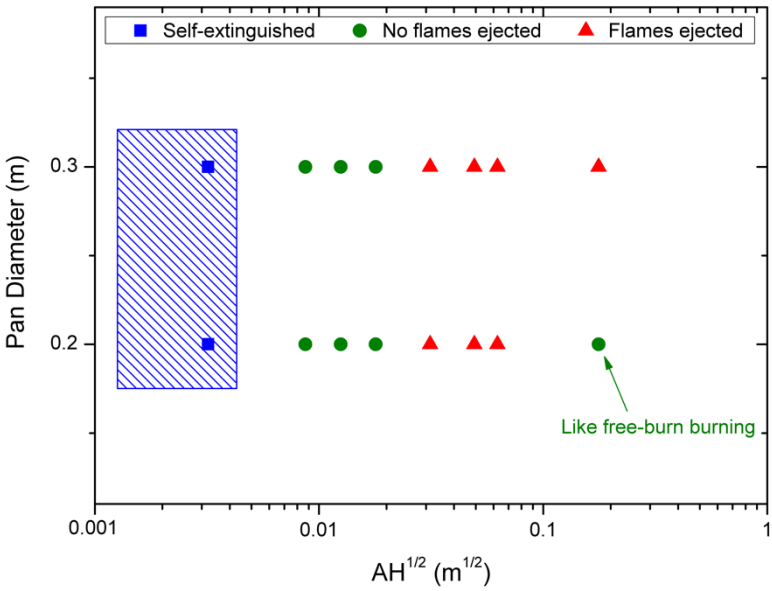

Figure 5.5 Fire behaviour depending on the ventilation factor and the size of the pool fire for all cases placing the fire source close to the rear end of the corridor.

In the next subsections, more detailed analysis of the pool fire behaviours is presented with respect to Fig. 5.5, considering:

i. Theoretical HRR which is calculated by multiplying the mass loss rate ($\dot{m}_f$) by the heat of combustion of ethanol (ΔH_C=26.78 MJ/kg):

$$\dot{Q}_{th} = \dot{m}_f \times \Delta H_C \tag{5.1}$$

ii. Measured HRR based on oxygen consumption in the hood;

iii. Temperature profiles measured with six thermocouple trees (one in each box) at six heights above the floor. Detailed positions of the thermocouples inside the corridor enclosure are given in Chapter 3. In the figures showing the temperature evolution, the profiles start from bottom (T1) to the top (T6) vertically placed location.

iv. Heat flux profiles on the floor of the corridor enclosure at six different locations; four in the middle of Boxes B-E and two in Box A at 5 and 45 cm distance from the opening

v. Flame height of ejected flames and heat flux measurements on the façade for the cases when flames ejected through the opening. Detailed positions of the heat flux measurements are given in Appendix B.

5.3.3 Self-extinguished fire

Fire was self-extinguished in both cases of pans with the 0.1m x 0.1m opening (i.e. BC20W10xH10 and BC30W10xH10). The dimensions of the opening and the distance of the pool fire from the opening restrained the availability of oxygen. In both cases, the fire was self-extinguished after 3-4 minutes of burning.

5.3.3.1 HRR, MLR and combustion efficiency

The actual HRR measured in the hood and the theoretical HRR profile for the BC30W10xH10 case are shown in Fig. 5.6. It is observed that the actual HRR initially increases reaching about 8kW, but this was not enough for the fire to sustain. This is followed by a sudden drop of the HRR indicating self-extinguishment of the fire. Similar finding was observed using the 20 cm dia. pan, but with less HRR measured before the extinguishment of the fire.

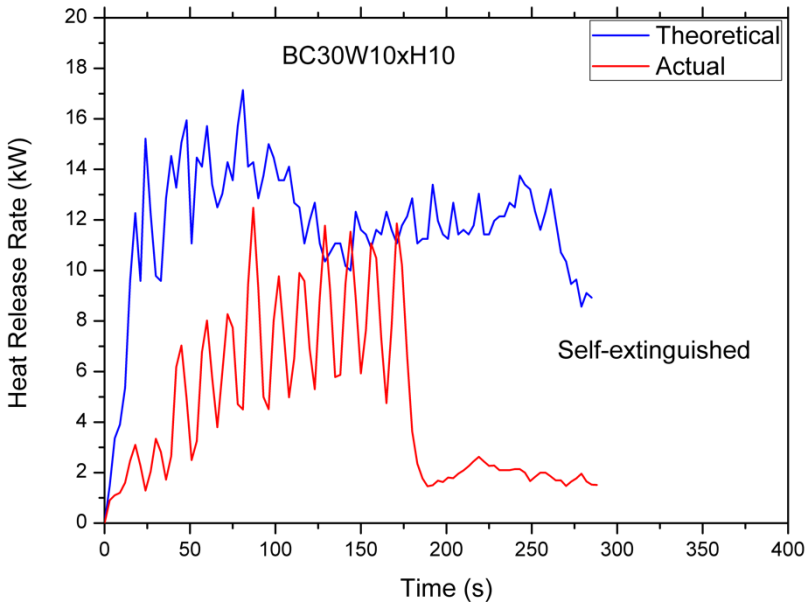

Figure 5.6 HRR profiles for the BC30W10xH10 case.

5.3.3.2 Temperature measurements from the interior of the corridor

Temperature evolution profiles inside each box (A-F) from bottom (T1) to top (T6) of the case BC30W10xH10 are shown in Fig. 5.7. In consistence with the low values of HRR measurements, temperatures are also very low. Temperatures initially increase due to the combustion of air in the enclosure, but subsequently decreases

sharply after the extinguishment of the fire. Inside the fire box, the temperature closer to the ceiling (see FT6) reaches about 600 ^{o}C.

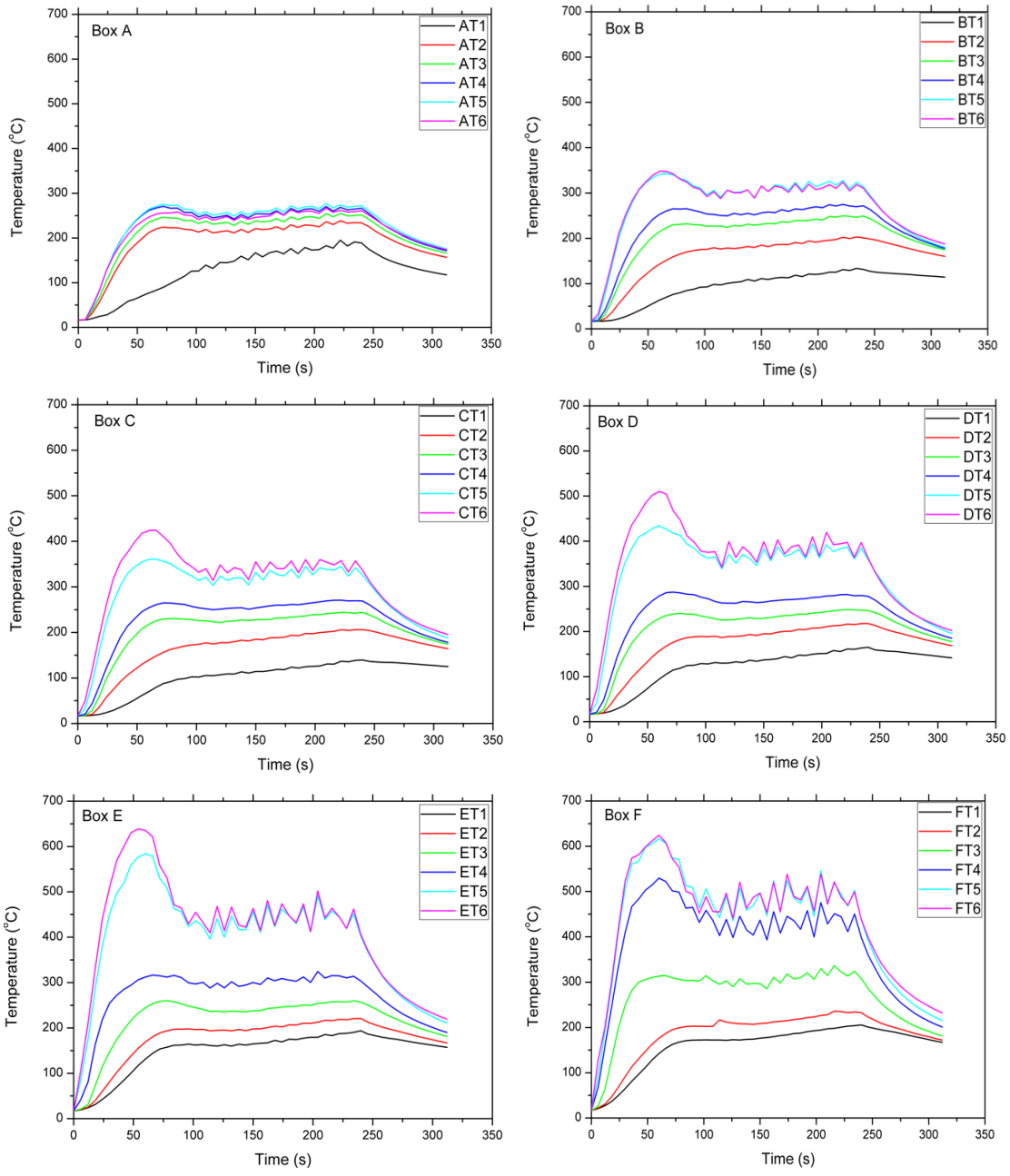

Figure 5.7 Temperature evolution profiles from bottom to top inside each box (Box A where the opening was to Box F at the rear end where pool was placed) for case BC30W10xH10.

5.3.3.3 Heat flux measurements on the floor of the corridor

Heat fluxes were measured in the middle of the floor inside Box B, C, D and E and in two locations on the floor of Box A (A1 placed 5 cm and A2 placed 45 cm from the opening of the corridor respectively. Heat flux evolution profiles in each box are

depicted in Fig. 5.8. Similar to temperature profiles, heat fluxes in all locations, firstly increase and then become nearly constant followed by a sudden decrease due to self-extinguishment. Maximum heat fluxes are found in Boxes D and E and the heat flux decreases towards the opening indicating that flame remains close to the rear end of the corridor.

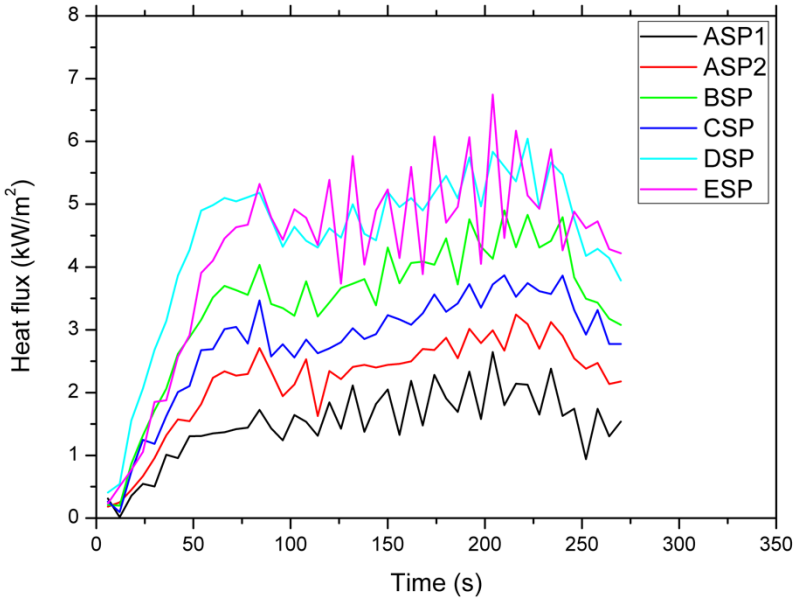

Figure 5.8 Heat Flux evolution profiles in six locations on the floor of the corridor for BC30W10xH10 case.

5.3.4 Steady fire without flame ejection

In six cases, burning was taking place only inside the corridor and no flames appeared out of the enclosure. Those cases were of small openings, which are W (m) x H (m): 0.15 x 0.15, 0.1 x 0.25 and 0.2 x 0.2. Regardless the pan size, no flames ejected and only smoke was noticed to exit the corridor through the opening. According to HRR measurements, steady-state conditions were established in all cases.

5.3.4.1 HRR, MLR and combustion efficiency

By using the HRR measured in the hood (actual) and the theoretical one calculated by Eq. 5.1, we can calculate the overall combustion efficiency, η, as:

$$\eta = \frac{\dot{Q}_{act}}{\dot{Q}_{th}} \tag{5.2}$$

Figure 5.9 shows the HRR profiles together with combustion efficiency for the BC20W20xH20 case. Two distinct regions can be identified from Fig. 5.9 as summarised in Table 17.

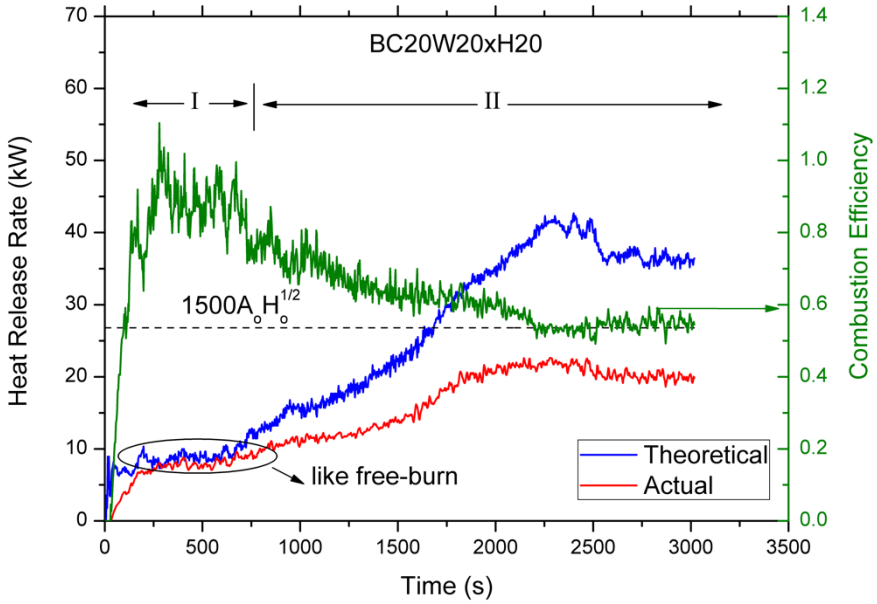

Figure 5.9 HRR profiles for the BC20W20xH20 case.

Table 17 Distinct regions considering the fire conditions established inside the corridor according to Fig. 5.9.

	Region I	Region II
Flames appear out of the opening	No	No
Fire scenario	Fuel-controlled	Ventilation-controlled
Actual HRR	All HRR inside the enclosure	HRR inside the enclosure

- Region I

  Initially, both the theoretical and actual HRRs are close to that for the free-burn case about 9kW (see Chapter 3). During this period, which lasts around 700 s for this particular case, the fire is fuel-controlled and the combustion efficiency is close to unity, similar to the free-burn (FB20) case. This result indicates that during this period all the fuel is consumed inside the enclosure.

- Region II

  In region II, the fire is ventilation-controlled and HRR increases progressively with time before a quasi-steady state is achieved at around

2500s. The increase of HRR is due to the increase of temperature of the hot gas layer and compartment walls and also the increase of the depth of the hot gas layer, which result in larger radiation feedback from the flame and the walls of the enclosure to the surface of the fuel.

The theoretical HRR becomes significant higher than the measured value and the combustion efficiency decreases gradually to a constant value of about 0.55, implying that there is a significant amount of unburnt fuel inside the enclosure as no external burning was observed. The theoretical HRR exceeds the stoichiometric (maximum) rate of heat released inside an enclosure as given by the following expression (Yamaguchi and Tanaka, 2005; Lee et. al., 2007; Delichatsios, 2014):

$$\dot{Q}_{st,in} = \dot{m}_a \Delta H_{air} = 3000 \times 0.5 A_o \sqrt{H_o} = 1500 A_o \sqrt{H_o} \quad (5.3)$$

It is interesting to notice that the actual HRR during this region is however less than the stoichiometric rate of heat released inside the enclosure. More discussion for this observation will be given in Section 5.4.

Figure 5.10 shows the fire development inside the corridor for the case BC20W20xH20 at different times and the following observations can be made:

a) 300 s after ignition. Fire burns like free-burn case. As shown in Fig. 5.9, the HRR is close to 9.1kW which is similar to the steady-state HRR of the free-burn case. Combustion efficiency is nearly one.
b) 700 s after ignition. Fire increases in size and the flame impinges on the ceiling and the HRR starts increasing.
c) 1200 s after ignition. Fire continues to increase and flames spread under the ceiling and reach the side walls. HRR increases and combustion efficiency decreases.
d) 1500 s after ignition. Fire is everywhere inside the fire box (Box F) and HRR increases. Combustion efficiency keeps decreasing.
e) 2100 s after ignition. Fire detachd from the pool surface and propagates towards the opening, seeking oxygen for combustion. HRR still increases with combustion efficiency less than 0.6.

f) 2700 s after ignition. Steady-state conditions are established with HRR being about 20 kW. The combustion efficiency is about 0.55 during the steady-state period.

g)

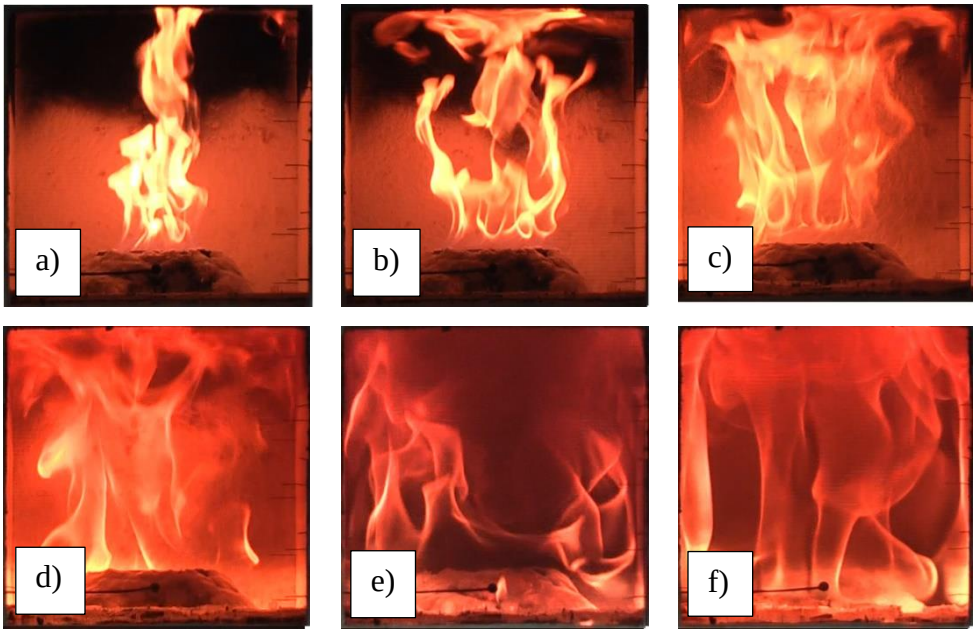

Figure 5.10 Fire development inside the corridor for case BC20W20xH20.

Using the 20 cm dia. pan and smaller openings, 0.15 x 0.15 and 0.1 x 0.25 (m^2), the HRR measured in the hood during the steady-state period was 10.3kW and 18 kW respectively, as shown in Fig. 5.11. It is highlighted here that using the 0.15 x 0.15 (m^2) opening the fire didn't become ventilation-controlled, as the theoretical HRR didn't reach the stoichiometric heat released inside the enclosure.

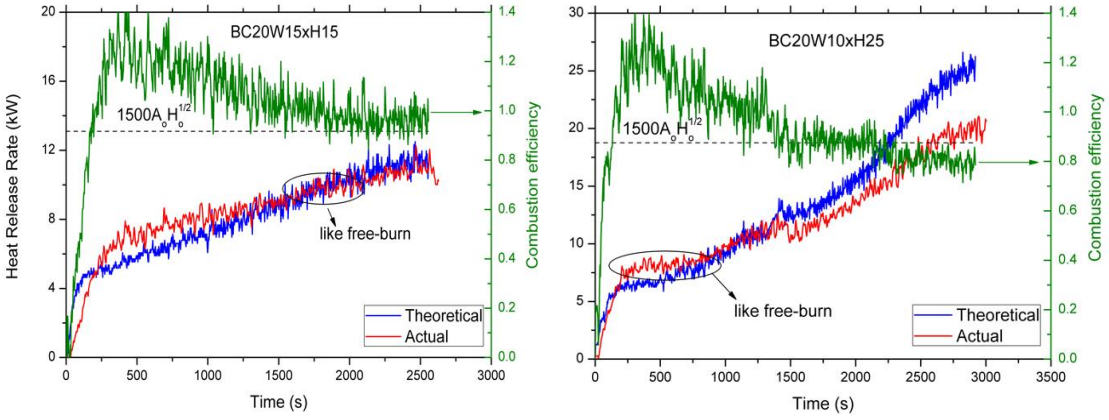

Figure 5.11 HRR profiles for the BC20W15xH15 and BC20W10xH25 cases.

Different behaviours were observed using the larger pool fire (30 dia. pan) and the same opening. HRR profiles for BC30W20xH20 case are depicted in Fig. 5.12. The main difference using the larger diameter of the pan is observed during the initial period (Region I). In BC30W20xH20 case, the HRR increases rapidly and Region I lasts less than 120s. During this period, HRR didn't reach the free-burn burning plateau, as the steady-state HRR was slightly less than the free-burn case. Using the 0.2 x 0.2 (m^2) opening the HRR became steady after 180 s at around 23 kW. The theoretical HRR increases after a point when it starts to decrease reaching steady-state after 1250 s. It is noted that the free-burn HRR for the 30 cm dia. pan was measured 24.1 kW as reported in Chapter 3. Using smaller openings, 0.15 x 0.15 and 0.1 x 0.25 (m^2) the HRR measured in the hood was 12 kW and 20 kW respectively (see Fig. 5.13). Both cases became ventilation-controlled, as the theoretical HRR was higher than the stoichiometric heat released inside the enclosure. It needs to be noted here that in most cases, initially the combustion efficiency was higher than unity, which is due to the error of measuring mass loss via the balance, as the balance needs some time to become steady initially.

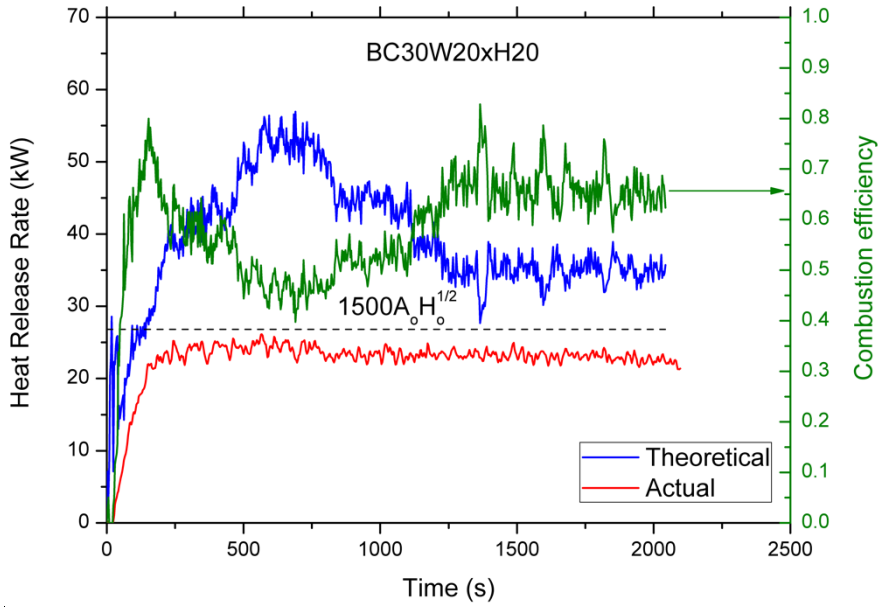

Figure 5.12 HRR profiles for the BC30W20xH20 case.

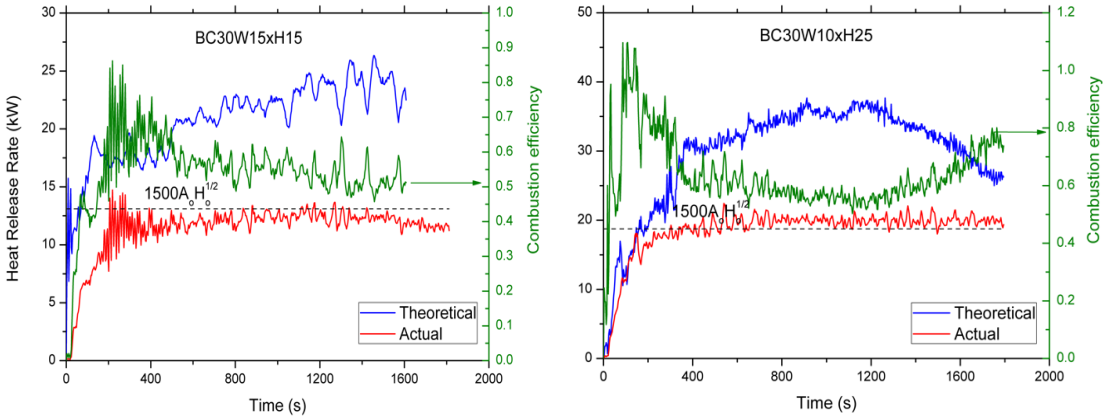

Figure 5.13 HRR profiles for the BC30W15xH15 and BC30W10xH25 cases.

As expected, it took more time for steady-state conditions to establish using the smaller pan (20 cm dia.) than using the larger one. The smaller fuel surface area means smaller mass burning rate (thus heat release rate), which in turn result in lower gas temperatures and heat feedback from the hot gas and flame to the fuel surface.

5.3.4.2 Temperature measurements inside the corridor

Temperature evolution profiles for the cases BC20W20xH20 and BC30W20xH20 are depicted in Fig. 5.14 and 5.15 respectively for different (six) vertical positions. The following observations can be made:

- During the initial growth period temperatures at all locations increase. The fire is fuel-controlled and the difference between the top (T6) and the lower (T1) is substantial. This behaviour denotes that there is fresh air entering the enclosure in the lower cold layer.
- After the growth period, no peak is observed and the temperatures in all boxes continue to increase, except those inside Box F where the pool fire was placed. The temperatures inside the fire box (F) increase in relation to the HRR, reaching their peaks when the HRR becomes steady. After that, gas temperatures decreased by 100-150^{o}C before becoming constant again. The decrease of temperature is consistent with the observation in Fig. 5.10 that flame detaches from the burner and moves towards the opening. The temperature at the highest and lowest positions in Box F during the steady-state period were 770^{o}C and 725^{o}C respectively indicating less stratification. The highest value (900^{o}C) was recorded in the top location inside Box E,

which indicates the region where most combustion takes place. The temperatures inside Boxes A to D continue to increase indicating that the flame extends towards the opening but the HRR is low and the extension of the flame does not reach the opening.

These profiles are clearly shown in Fig. 5.16, with the temperature profiles in the top locations inside each box are plotted. The flame movement towards Box E is depicted with the peak observed in Box F after 2250 s. This denotes that flame detached from the pool and moved to Box E.

Similar observations can be made for the BC30W20xH20 case, using the same opening but with a larger pool diameter. The temperature profiles are depicted in Fig. 5.15. After the over-ventilated period of growth where temperatures were rising, a peak was observed inside Boxes F-D. Subsequently, the temperatures decrease and finally become steady. As explained earlier, this behaviour indicates flame detachment from the burner and propagation towards the opening as the peak moves from Box F to D. Fire stays in Box D and is extended towards the opening. In Box A, lower temperatures were observed because flames don’t reach the opening. This is depicted in Fig. 5.17, showing the top temperatures profiles of BC30W20xH20.

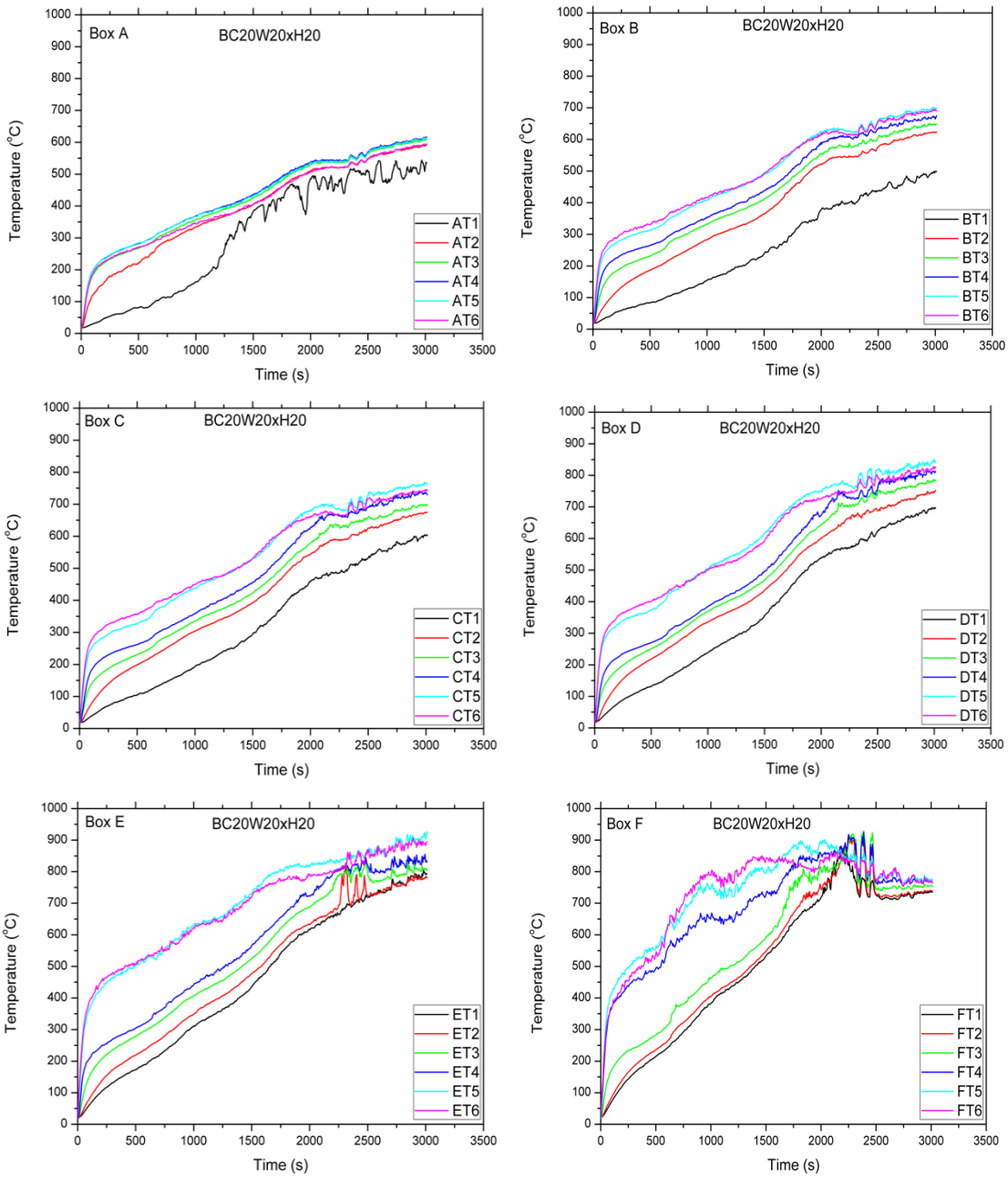

Figure 5.14 Temperature evolution profiles from bottom to top inside each box (Box A where the opening was to Box F at the rear end where pool was placed) for case BC20W20xH20.

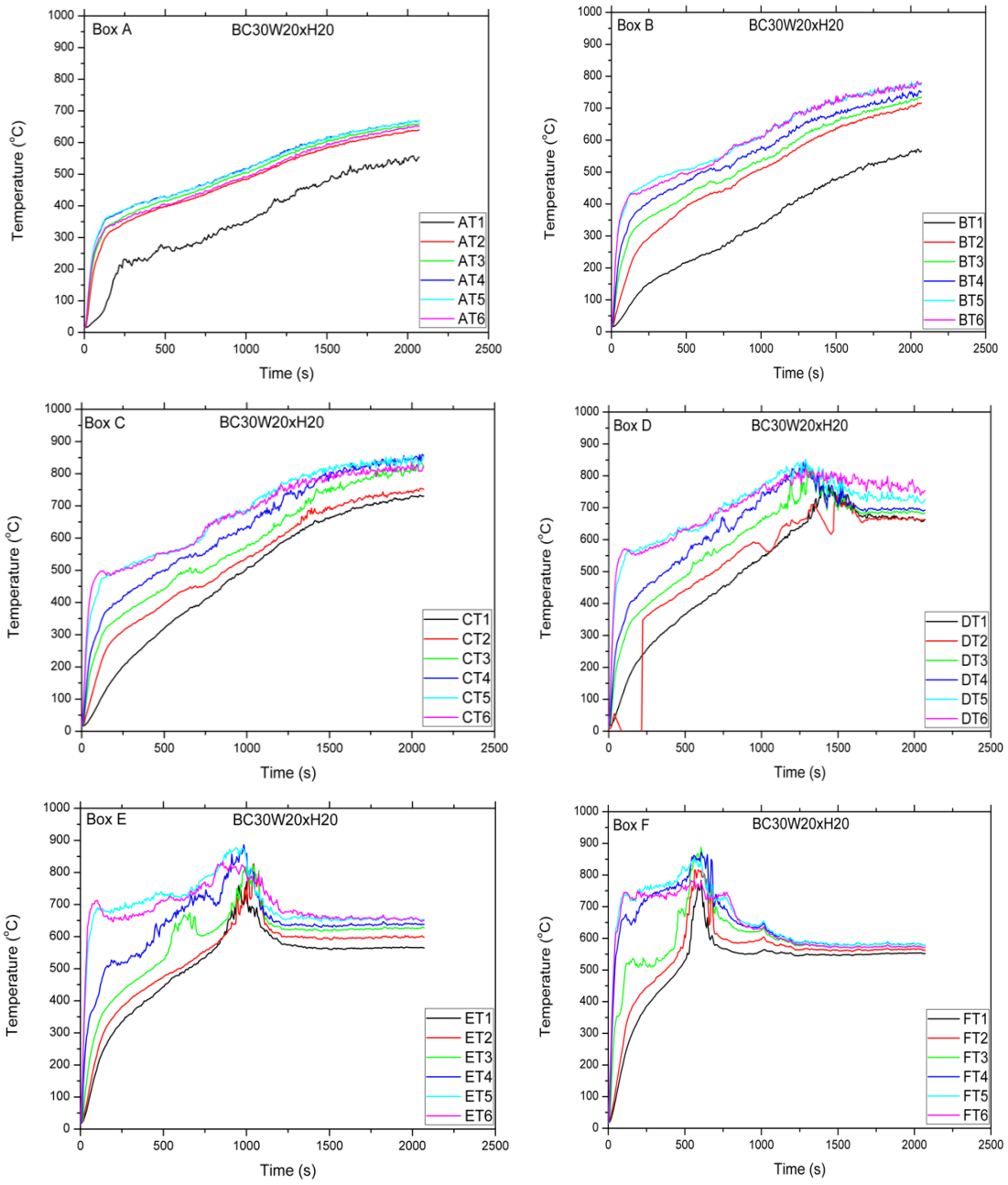

Figure 5.15 Temperature evolution profiles from bottom to top inside each box (Box A where the opening was to Box F at the rear end where pool was placed) for case BC30W20xH20.

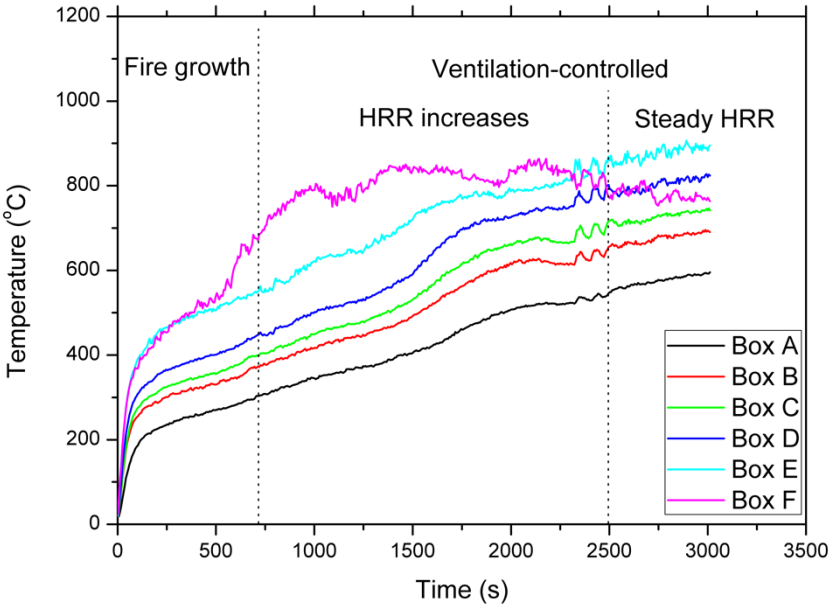

Figure 5.16 Temperature evolution at top location inside each box for BC20W20xH20 case.

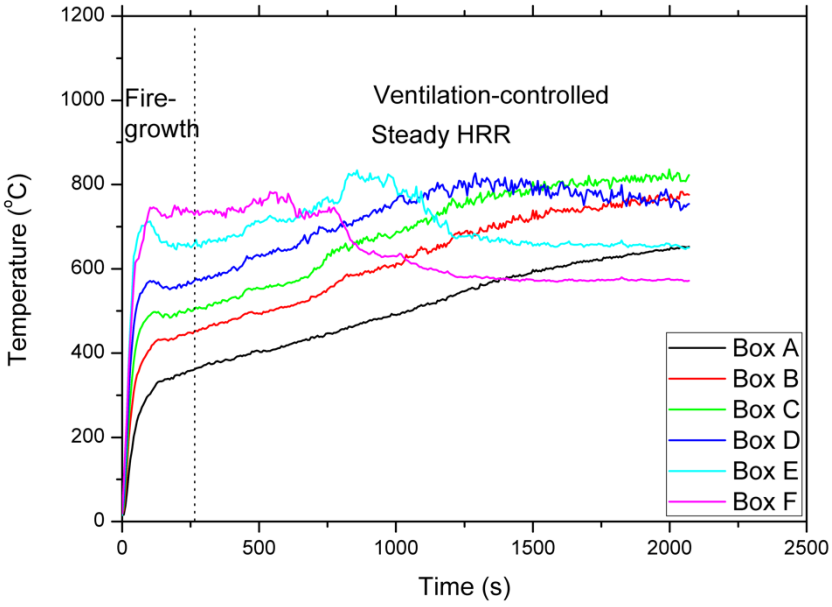

Figure 5.17 Temperature evolution at top location inside each box for BC30W20xH20 case.

The transition from over-ventilated to under-ventilated fire conditions inside the enclosure is depicted in Fig. 5.18 -5.19, showing the temperature at the top and bottom locations in each box at three different times., i.e., 60, 750 and 2000s. At 60s, for both cases with the 0.2 x 0.2 m^2 opening it is in the growth period. The temperature difference between the top and bottom layers is high, over 200°C. This difference denotes the presence of cold air entering the enclosure in the lower layer. Due to the difference in the burning rate, the times needed for the HRR to become

steady is different for the two cases, BC20W20xH20 and BC30W20xH20, having values of 2000s and 750s respectively. Temperatures increase and the fire becomes under-ventilated. Temperatures in all locations continue to increase and the temperature difference between the top and bottom layers decreases. Finally, when steady-state conditions are established inside the fire box, the temperature difference inside Box F was less than 80ºC, indicating more mixing of the cold air and the hot gases at this location.

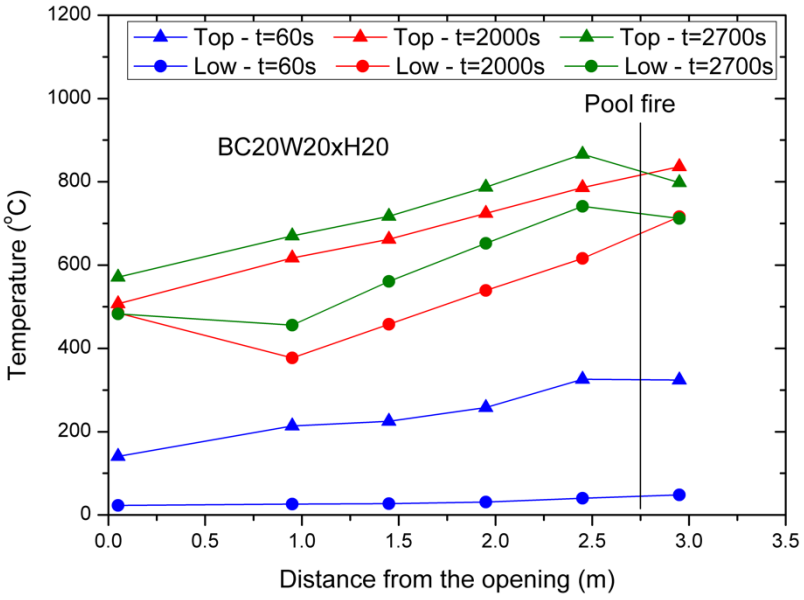

Figure 5.18 Temperature at the top and bottom layers over the distance from the opening for case BC20W20xH20 in three time steps: 60, 2000 and 2700s.

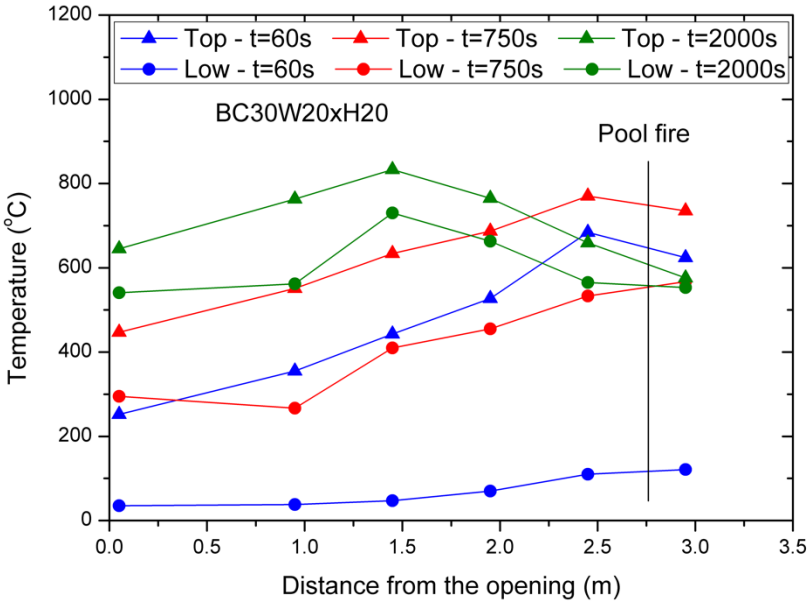

Figure 5.19 Temperature at the top and the low locations over the distance from the opening for case BC30W20xH20 in three time steps: 60, 750 and 2000s.

5.3.4.3 Heat flux measurements on the floor of the corridor

Heat flux histories for the BC20W20xH20 case are depicted in Fig. 5.20. In all boxes (except in Box F, where measurement was infeasible) the heat fluxes increase continuously with time. This behaviour is consistent with the observation in the temperature histories inside the Boxes A-E as shown in Fig. 5.14. The heat flux closer to the fire (Box E) reaches 75kW/m^2 after 3000s. The heat flux decreases with distance towards the opening, with the lowest heat flux measured inside Box A, closer to the opening, which are also consistent with the temperature data.

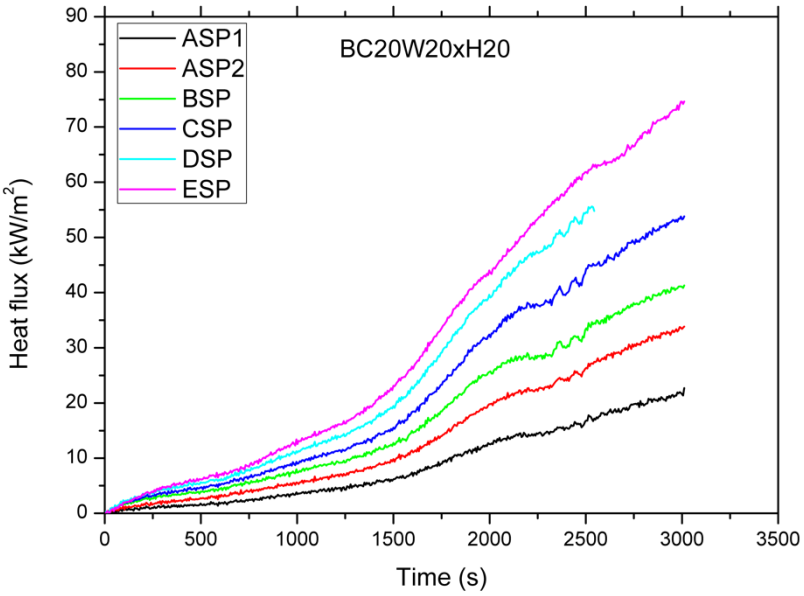

Figure 5.20 Heat Flux evolution profiles in six locations on the floor of the corridor for BC20W20xH20 case.

Using the 30 cm dia. pan and the same opening, similar behaviour to the temperature profiles was observed for the heat flux measurements. As depicted in Fig. 5.21, the heat flux in Box E reaches a peak, and then decreases reaching 35kW/m^2. The same peak was observed in the temperature measurement inside Box E as shown in Fig. 5.15. A peak is also observed for the heat flux inside Box D, occurring at the same time as with the temperature peaks in the same box. The fact that the maximum heat flux occurring in Box D confirms previous observation that the flame detaches from the burner and the base of the flame is located in Box D with the flame front moving towards the opening.

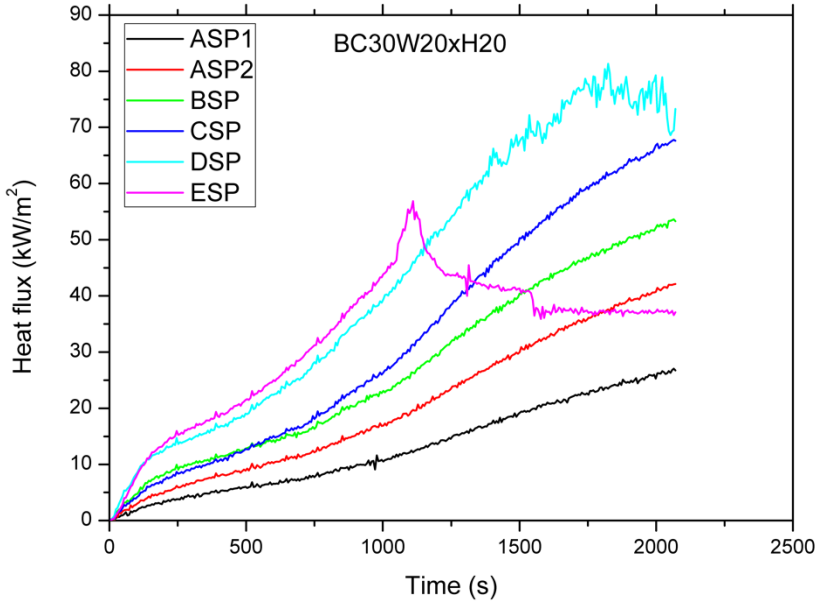

Figure 5.21 Heat Flux evolution profiles in six locations on the floor of the corridor for BC30W20xH20 case.

5.3.5 Like free-burn case

As discussed in (Delicahtsios et. al., 2004; Drysdale, 2011; Delichatsios, 2014) for very large ventilation factors and small HRRs in relation to the size of the enclosure, the MLR tends to be like the MLR of free-burn cases. In the present experimental work this was observed only using the smaller pan and the fully open opening (0.5m x 0.5m).

5.3.5.1 HRR, MLR and combustion efficiency

Heat release rate histories (theoretical and measured) for the case BC20W50xH50 are shown in Fig. 5.22. The measured HRR of the free-burn case (FB20) is also plotted for comparison. The overall combustion efficiency based on the theoretical and actual HRRs of BC20W50xH50 is shown in the same plot. Since the theoretical HRR doesn't exceed the stoichiometric heat released inside the enclosure ($1500AH^{1/2}$ = 263.1 kW), the fire is fuel-controlled. It is observed that the actual HRR of the corridor experiment is similar to that for the free-burn case and also to the theoretical one. The overall combustion efficiency is close to unity. In this case no flames appeared out of the corridor and burning is taking place only inside Box F (see Fig. 5.23).

It is worth mentioning that the fire behaviour using the 30 cm dia. pan and same opening is significantly different. After ignition, the flame reaches the ceiling very quickly and appears outside the enclosure just 3 min after the ignition. The gas temperatures in the gas layer are very high resulting in larger radiation feedback to the fuel surface. Whilst the case BC30W50xH50 is still well ventilated, the present results indicate that whether a flame will eject from the opening depends not only on the ventilation factor but on the HRR (with respect to the dimensions of the enclosure); more results of this case will be discussed in more detail in the section describing experiments where flames appeared outside.

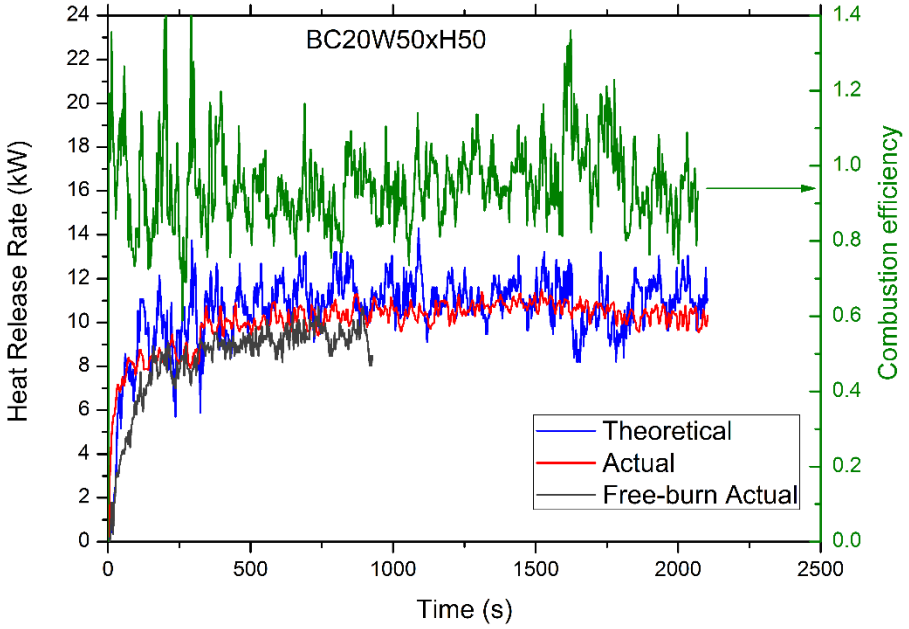

Figure 5.22 HRR profiles for the BC20W50xH50 case.

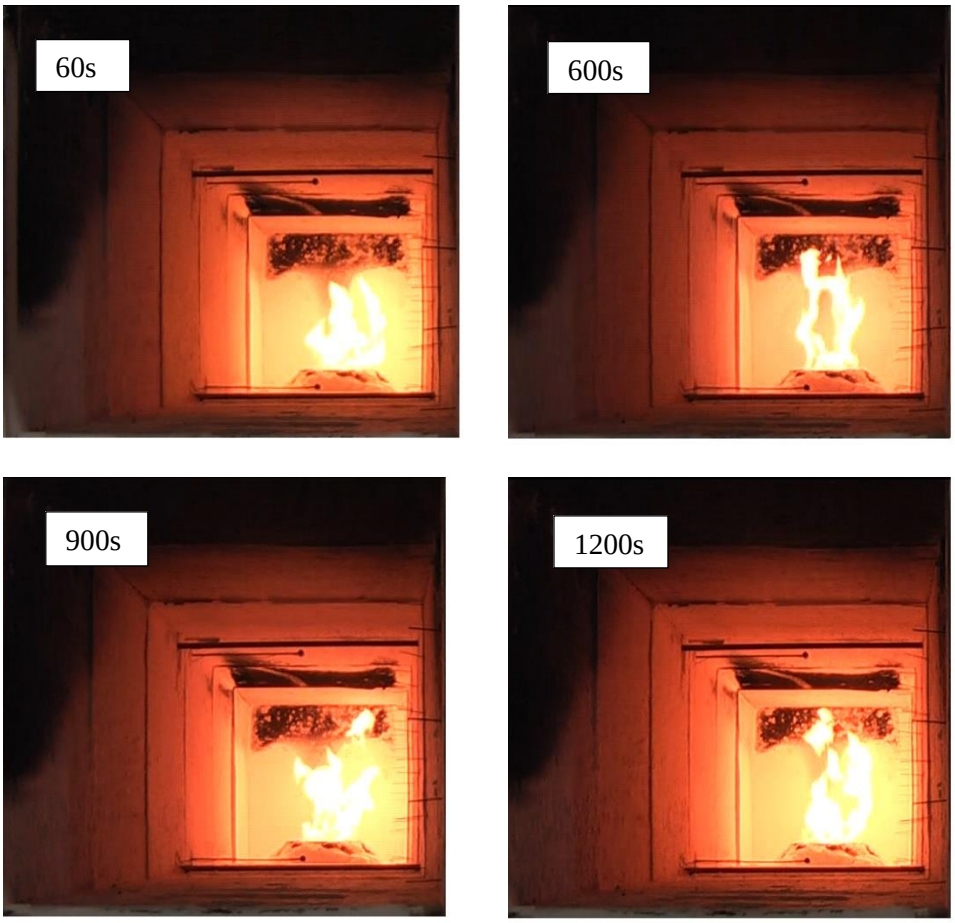

Figure 5.23 Fire development inside the enclosure for BC20W50xH50 case.

5.3.5.2 Temperature measurements from the interior of the corridor

The temperature evolution profiles for the BC20W50xH50 case are given in Fig. 5.24. Temperatures during the steady-state period (after 1400s) became constant but values are significantly low, less than 400^{o}C. The temperatures inside Box A closer to the opening are less than 250^{o}C in the upper layer. The difference between the upper hot gas layer temperature and the cold air layer close to the floor is significant. There is fresh air getting into the corridor from the lower layer and gas temperature even at the rear end of the corridor does not exceed 100^{o}C. Average temperature values during the steady-state period are plotted against height in Fig. 5.25. A clear stratification is observed over the length of the corridor as temperatures are not homogeneous over the height, resulting in a two-layered zone with a ‘weak’ hot gas layer of low temperature values and minor radiation feedback to the surface of the fuel. The formation of the upper layer is observed at a height of 20-30 cm from the floor.

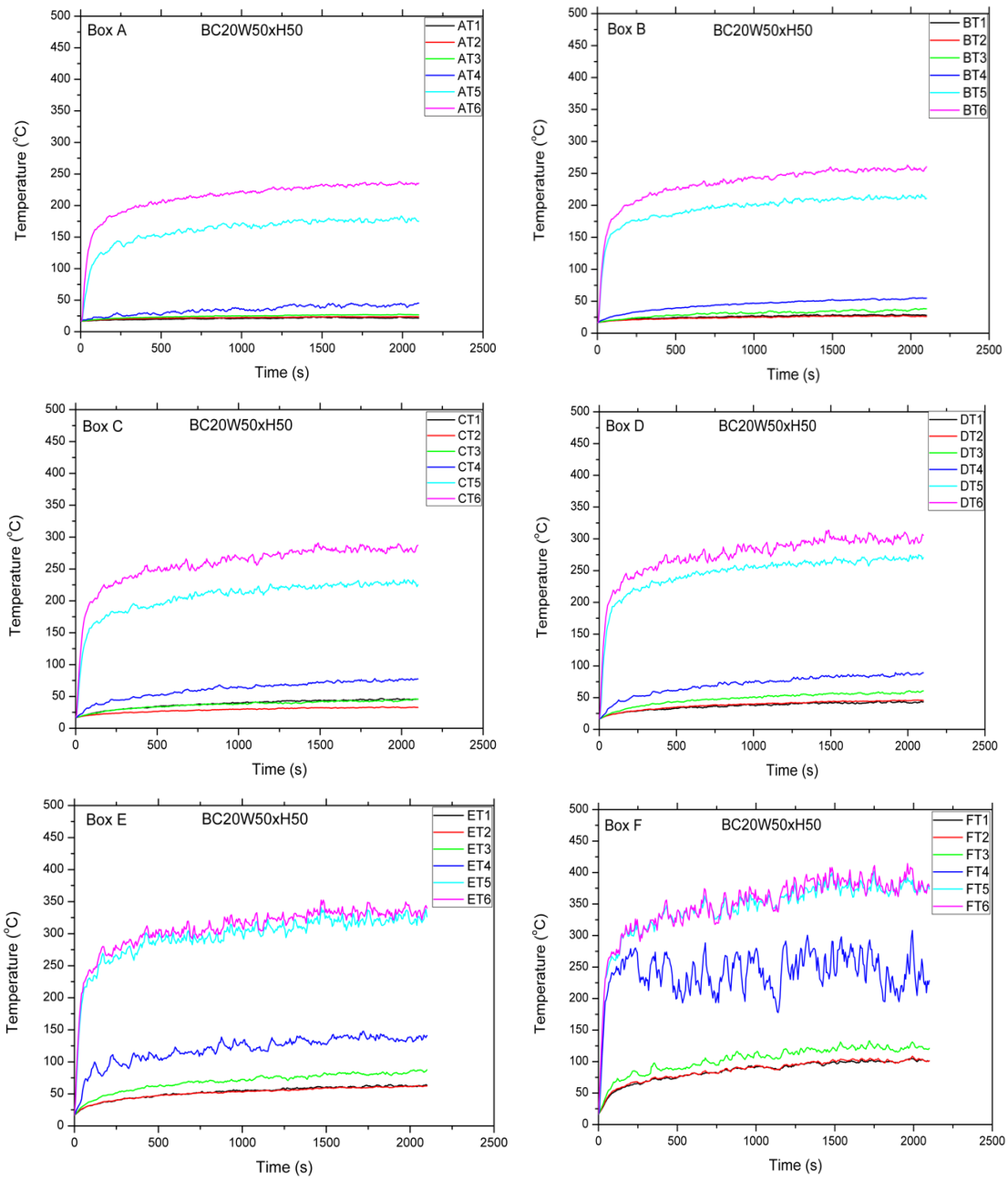

Figure 5.24 Temperature evolution profiles from bottom to top inside each box (Box A where the opening was to Box F at the rear end where pool was placed) for case BC20W50xH50.

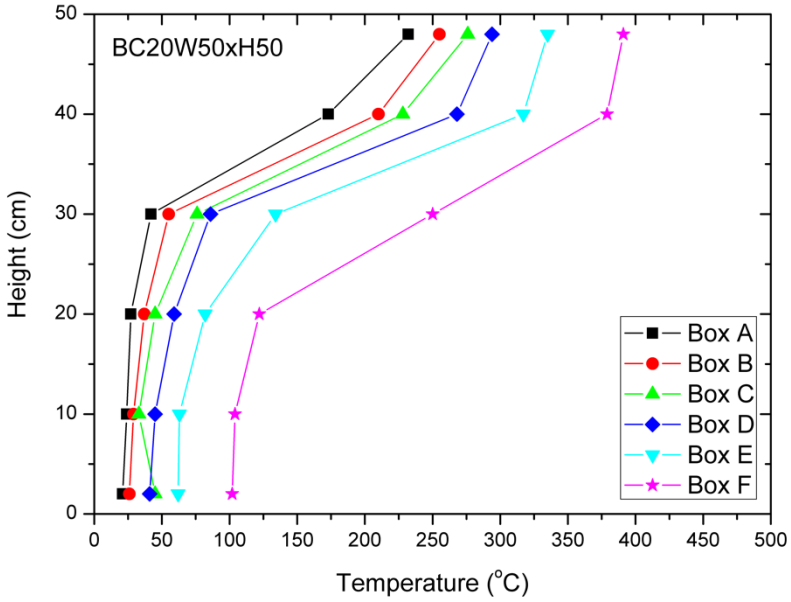

Figure 5.25 Gas temperature distribution inside each box of the enclosure for case BC20W50xH50.

5.3.5.3 Heat flux measurements on the floor of the corridor

Heat flux evolution profiles measured on the floor of the corridor for the BC20W50xH50 case are plotted in Fig. 5.26. Heat fluxes are very low in accordance with the low temperature measurements presented above.

The heat flux inside Box E, which is closest to the pool fire, reaches 3.2 kW/m^2 and moving towards the opening of the corridor heat fluxes decrease to 0.7 kW/m^2. The presence of a thin hot gas layer of low temperatures, according to temperature results, is the reason for the low heat fluxes as radiation feedback from the hot gas layer to the floor surface is very low. This is the main difference using the two different size pans with the fully-open opening, as in BC30W50xH50 case heat fluxes are found to increase because of a thick hot gas upper layer radiating back to the floor of the corridor. This will be discussed later for the case with external burning.

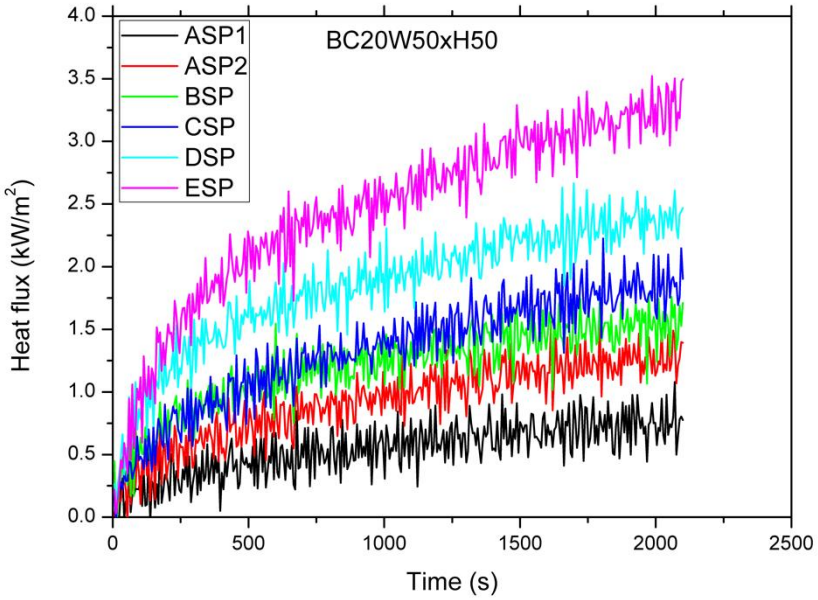

Figure 5.26 Heat Flux evolution profiles in six locations on the floor of the corridor for BC20W50xH50 case.

5.3.6 Steady fire with flame ejection

In experiments using the 0.25 x 0.25, 0.3 x 0.3 and 0.5 x 0.25 (m^2) opening and the largest opening with the large diameter pool fire (BC30W50xH50 case) the flame was ejected through the openings. The burning behaviour of these cases is explained in the following subsections.

5.3.6.1 HRR, MLR and combustion efficiency

The HRR profiles (theoretical and actual) for the two different pan diameter cases using the 0.3 x 0.3 (m^2) opening are depicted in Figs. 5.27 and 5.28. The maximum HRR inside the enclosure which equals to $1500AH^{1/2}$ (Yamaguchi and Tanaka, 2005; Lee et. al., 2007; Delichatsios, 2014) is also plotted for comparison, along with the combustion efficiency, η, calculated using the Eq. 5.2.

Three distinct regions are observed as depicted in Figs. 5.27 and 5.28. These three regions are presented in the Table 18 and discussed below.

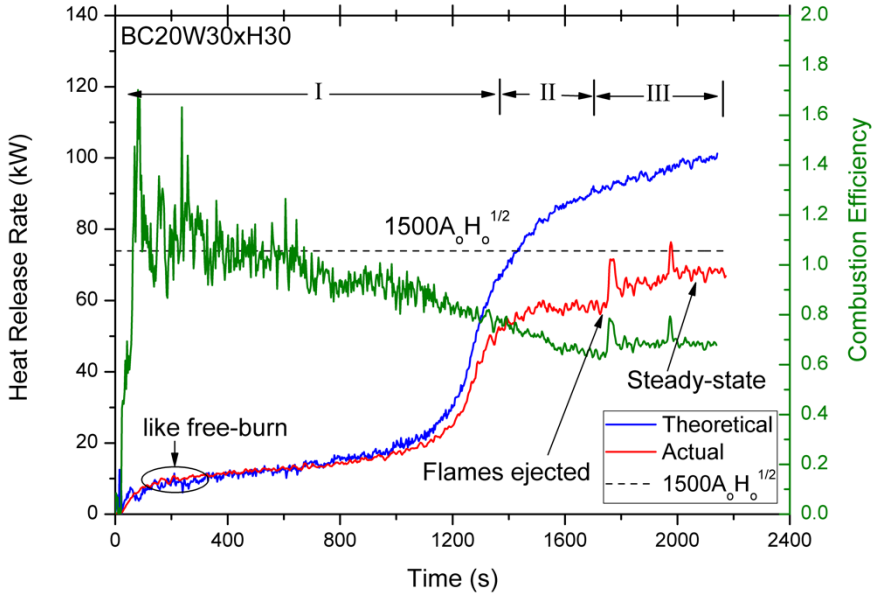

Figure 5.27 HRR profiles for the BC20W30xH30 case.

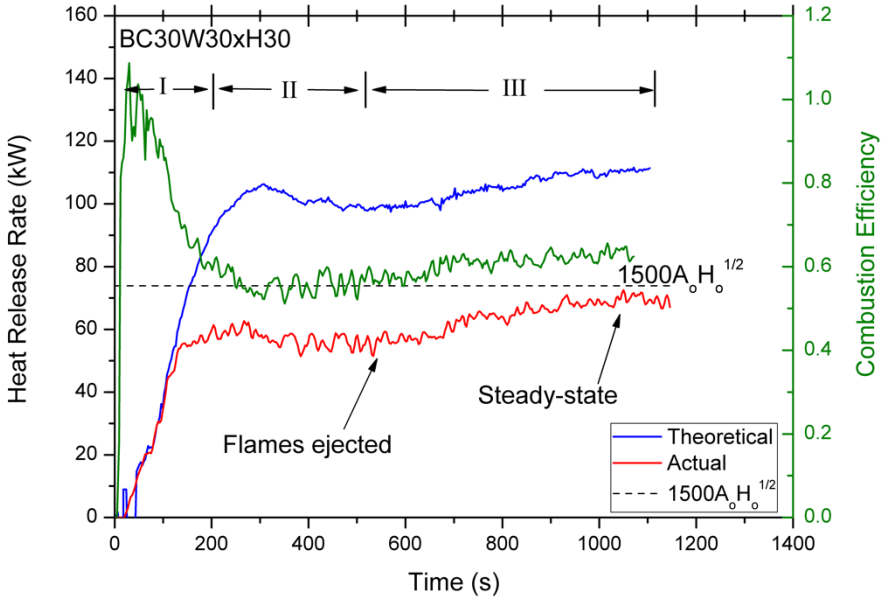

Figure 5.28 HRR profiles for the BC30W30xH30 case.

Table 18 Distinct regions considering fire conditions established inside the corridor according to Fig. 5.27-5.28.

	Region I	Region II	Region III
Flames ejected through the opening	No	No	Yes
Fire scenario	Fuel-controlled	Ventilation-controlled	External Burning
Actual HRR	All HRR inside the enclosure	All HRR inside the enclosure	HRR inside and outside the enclosure

- Region I

  After the ignition of the pool fire, the actual and theoretical HRRs are almost identical, i.e. the combustion efficiency is close to unity. During this period the fire grows and all the fuel is consumed within the enclosure. Thus, the fire is fuel-controlled in this region and all the HRR is released inside the enclosure. The difference for the cases using the same opening but different pan sizes is that in the case of the larger pan this period is much shorter. Using the larger pan there is a rapid increase of HRR a few seconds after ignition. In these cases, the fire increases firstly to the free-burn HRR, keeps constant for a couple of minutes and then further increase for a longer period.

- Region II

  After the growth period, in Region II, the actual HRR reaches a plateau and stays constant for a few minutes (3-4 min). At the end of 'Region II' flames ejected through the opening, thus there was unburnt fuel emitted outside the enclosure. This is confirmed by the observation that the theoretical HRR is larger than the actual one. During this period the fire has become ventilation-controlled and the HRR inside the enclosure depends on the flow rate of air coming into the enclosure through the opening. The actual HRR in this Region is found to be less than the maximum rate of heat released inside an enclosure as given by the Eq. 5.3 (Yamaguchi and Tanaka, 2005; Lee et. al., 2007; Delichatsios, 2014). This observation was also made for the cases presented earlier of steady fire without external burning. More discussion on this observation is given in Section 5.4.

- Region III

  During 'Region III', the actual HRR increases because flames start appearing outside the enclosure due to the burning of the unburnt fuel that has escaped from the enclosure. This increase in HRR is followed by a plateau indicating that steady-state conditions are established. However, even after the flames steadily burn outside (steady-state period), the actual HRR never reached the theoretical one, implying incomplete combustion. The combustion efficiency during this steady-state period is calculated for all cases and will be presented in the next section.

Same burning behaviour is observed for all cases using the openings 0.25 x 0.25 and 0.5 x 0.25 (m^2). The actual and theoretical HRR profiles for the cases BC20W25xH25, BC30W25xH25, BC20W50xH25 and BC30W50xH25 are depicted in Fig. 5.29. Same regions can be observed for all cases with respect to the pool fire's size. As observed, all cases became ventilation-controlled during 'Region II' with the theoretical HRR becoming higher than the maximum heat released inside the enclosure.

It is noted that using the 20 cm dia. pan, the fire burned for a couple of minutes as in free-burn conditions during the fire growth period before the enclosure effects become significant. The time for the flame ejecting from the opening is much shorter in cases using the 30 cm dia. pan than the 20 cm dia. pan with the same opening dimensions.

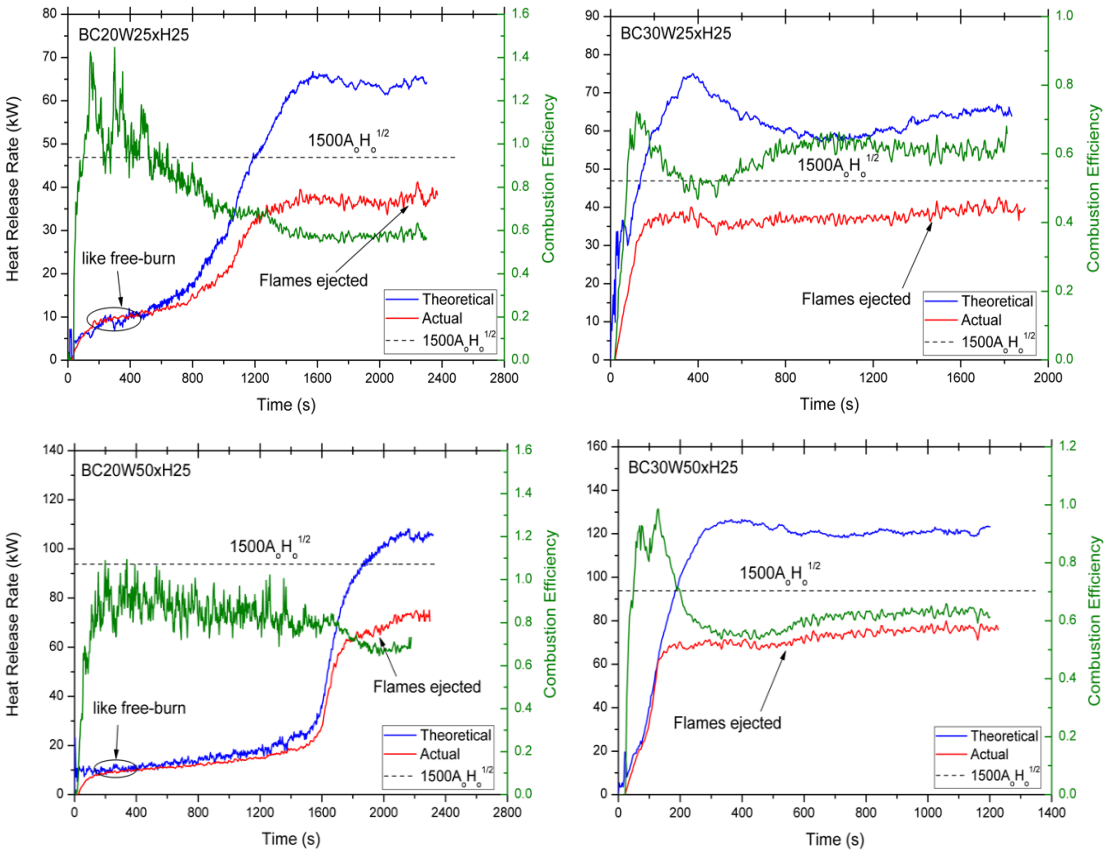

Figure 5.29 HRR profiles for the BC20W25xH25, BC30W25xH25, BC20W50xH25 and BC30W50xH25 case.

As discussed in the previous section, using the fully-open opening, 0.5 x 0.5 m^2, and the 20 cm dia. pan, the fire was burning like in free-burn conditions. However, this is not the case using the larger pool fire size. The HRR profiles for the BC30W50xH50 case are given in Fig. 5.30. The HRR increases during the growth period and the flames ejected through the opening just 4 min after the ignition. The HRR further increases and finally becomes steady after almost 10 min. As the maximum heat released inside the enclosure for this opening is 263.1 kW, the fire, even though the flames comes out, is still fuel-controlled as the theoretical HRR never reached this value. This result highlights the importance of the size of the enclosure in studying under-ventilated fires. In terms of combustion efficiency, it is close to one during the growth period and then decrease as the flame comes out and finally becomes constant (about 0.7) during the steady-state period. More discussion on mass loss rate and combustion efficiency of all cases will be present later when comparing all cases during the steady-state period.

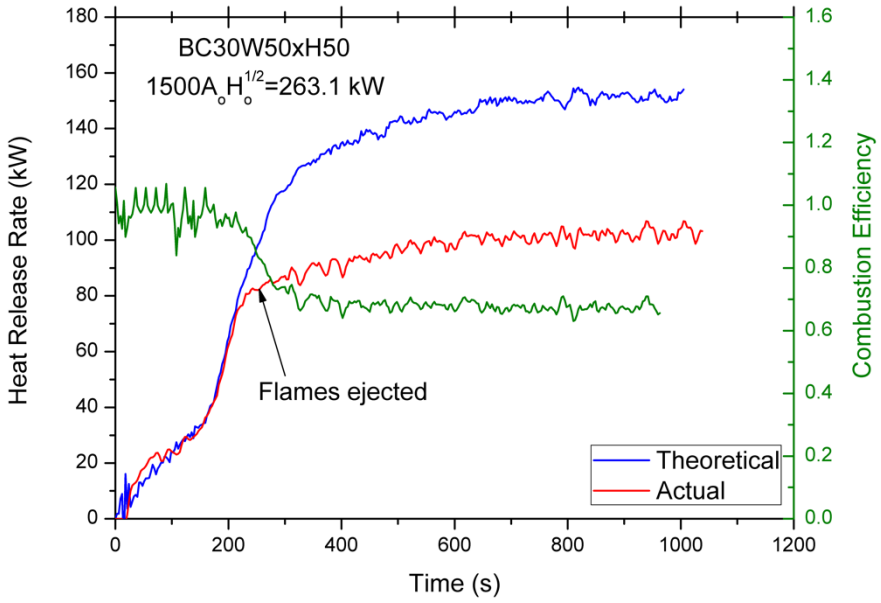

Figure 5.30 HRR profiles for the BC30W50xH50 case.

5.3.6.2 Temperature measurements from the interior of the corridor

Temperature evolution profiles for the cases BC20W30xH30 and BC30W30xH30 are depicted in Fig. 5.31-5.32. Figure 5.31 displays temperature evolution profiles for the BC20W30xH30 case, using the 20 cm dia. pan and the 0.3 x 0.3 (m^2) opening. The following observations can be made for the temperature profiles in relation to the HRR measurements:

- During the initial growth period temperatures at all locations increase. The fire is fuel-controlled and the difference between the top (T6) and the bottom (T1) is substantial.
- After the growth period, i.e., during 'Region II', no temperature peak is observed. The temperatures in all boxes continue to increase, except the ones inside the fire box (Box F). The temperatures inside Box F reaches a peak at the start of this region and then they slightly decrease before becoming steady. During this period burning was taking place only inside the enclosure. This peaks of temperature can be used to indicate that the flame detaches from the pool, moving towards the opening and seeking oxygen available for combustion. Thus, fire stays in Box E and combustion occurs in this box and flame extends towards the opening. Behind the flame, in Box F, decrease of the temperature implies that only hot gas and smoke is present. More discussion on the flame propagation is followed in the next section.

- After the flames appeared outside of the enclosure at the start of 'Region III', the temperatures inside the Box F became steady. It is worth noting that in the other boxes temperature profiles weren't steady yet and were still increasing. Inside the fire box (F), temperatures are 1000^{o}C and 910^{o}C at the top and bottom positions respectively indicating less stratification.

Similar observations are made for the BC30W30xH30 case, using the same opening but larger pool diameter. The temperature profiles are depicted in Fig. 5.32. After the over-ventilated period of growth, a peak was observed inside Box F. After this peak the temperatures decrease and finally become steady. As explained earlier, this behaviour denotes flame detachment from the pool region and propagation towards the opening as the peak moves from Box F to Box E. It is finally noted that a decrease of the steady-state temperatures inside Box F was observed using the same opening and the larger diameter pan.

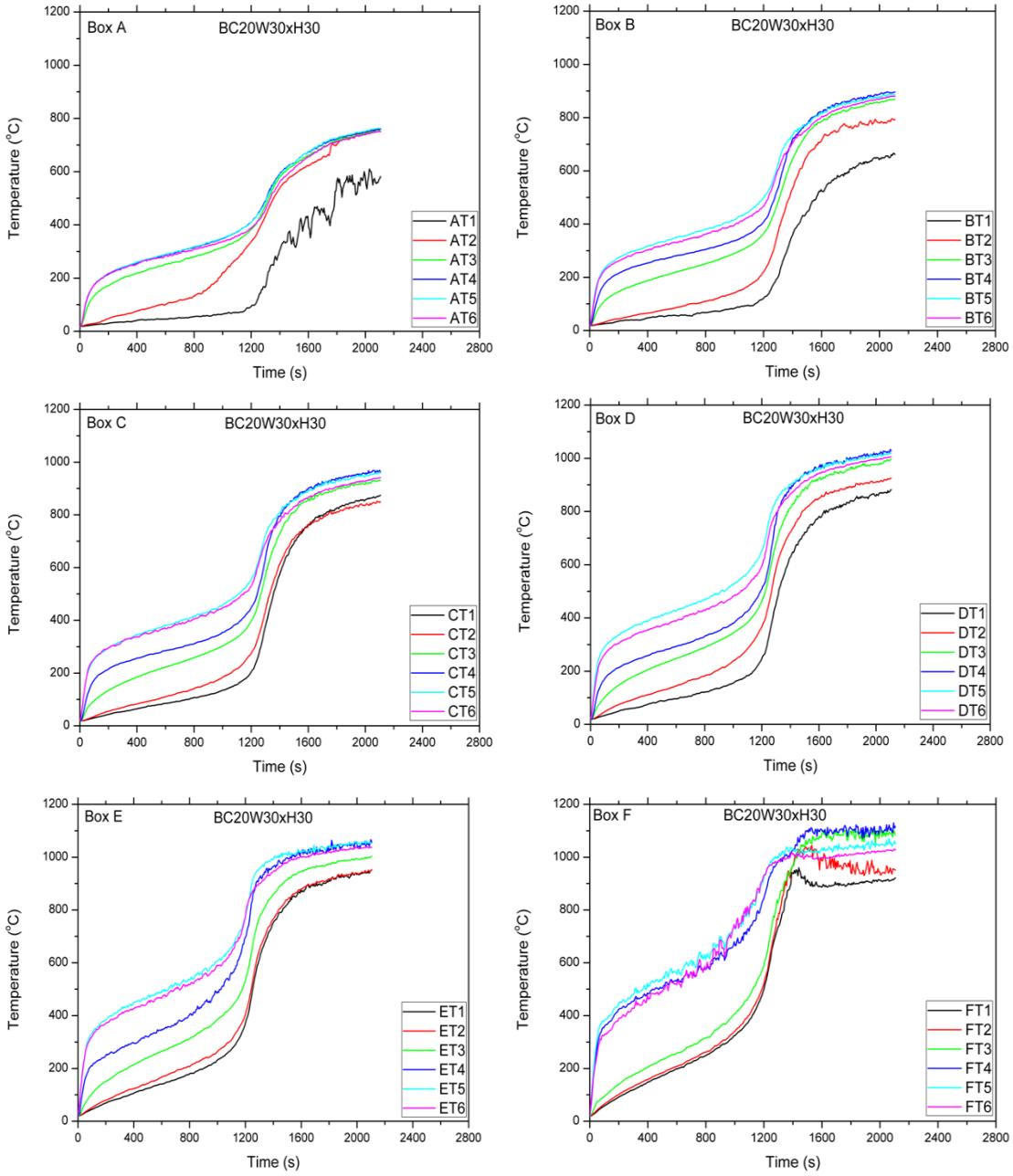

Figure 5.31 Temperature evolution profiles from bottom to top inside each box (Box A where the opening was to Box F at the rear end where pool was placed) for case BC20W30xH30.

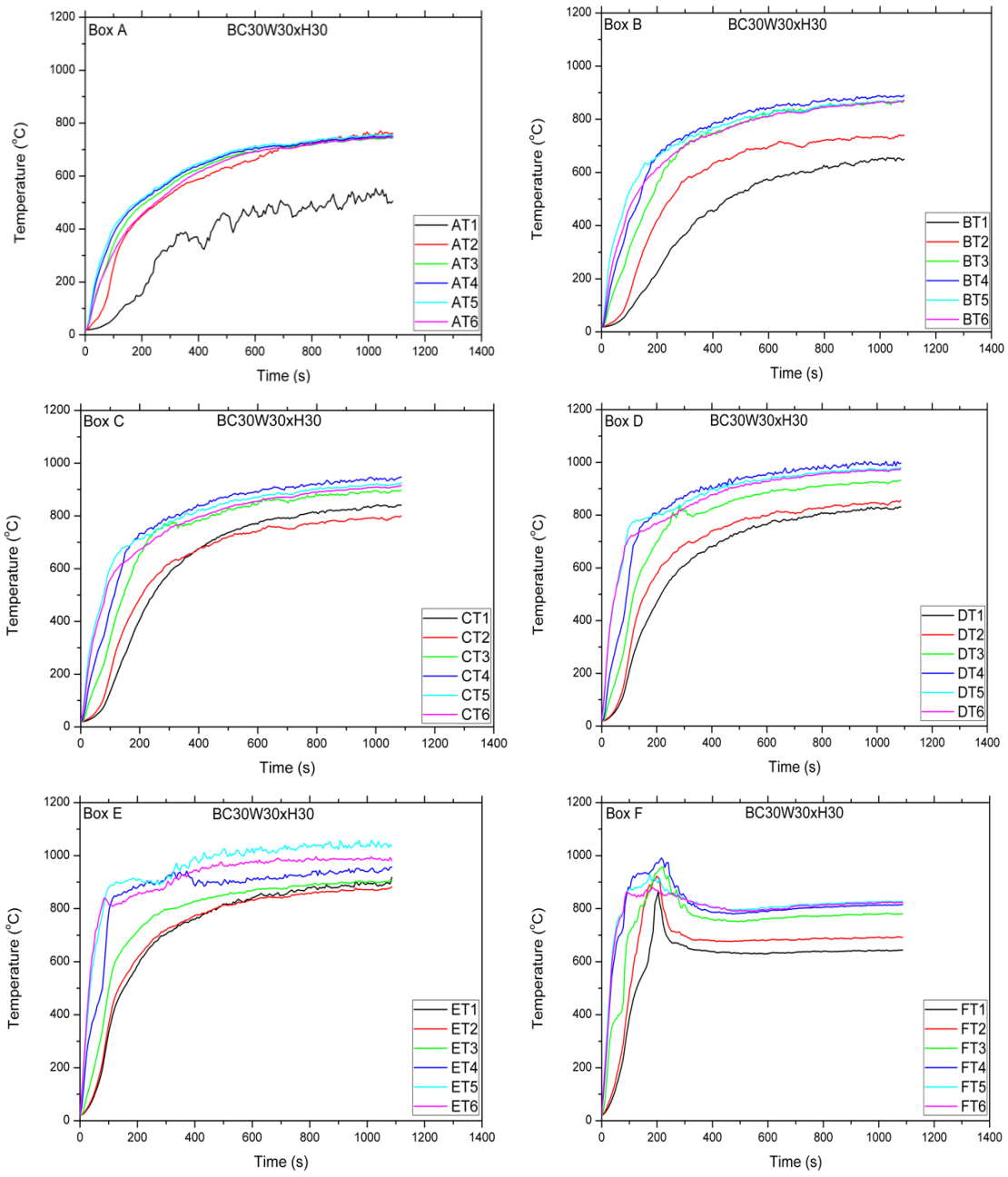

Figure 5.32 Temperature evolution profiles from bottom to top inside each box (Box A where the opening was to Box F at the rear end where pool was placed) for case BC30W30xH30.

The three stages described above are shown in Fig. 5.33-5.34 with respect to the measured HRR presented earlier. During the ventilation-controlled stage, the peak temperature is moving towards the opening, which can be explained by the fact that the flaming region detaches from the burner and then migrates towards the doorway where oxygen is available. In the cases discussed, this movement (peak of temperature measurement) was only observed from Box F to Box E. After the flames came out of the enclosure, it seems that they have filled the upper layer of the

enclosure and burning takes place inside all boxes except Box F. Thus, the flames are extended towards the opening and appearing outside the enclosure. This is different from the work of Beji (2009) using a gaseous burner using the same enclosure. Beji (2009) investigated ventilation-controlled fires with flames appearing outside the enclosure, noting that there was a progressive movement of the flame from the rear towards the opening during 'Region II', until the flames came out. Thus, peaks of temperature measurements were observed in every box before the flames appeared outside. In this work, movement of the flame region was observed towards the Box E and only in case BC30W25xH25 movement until Box D was noted, as depicted in Fig. 5.35.

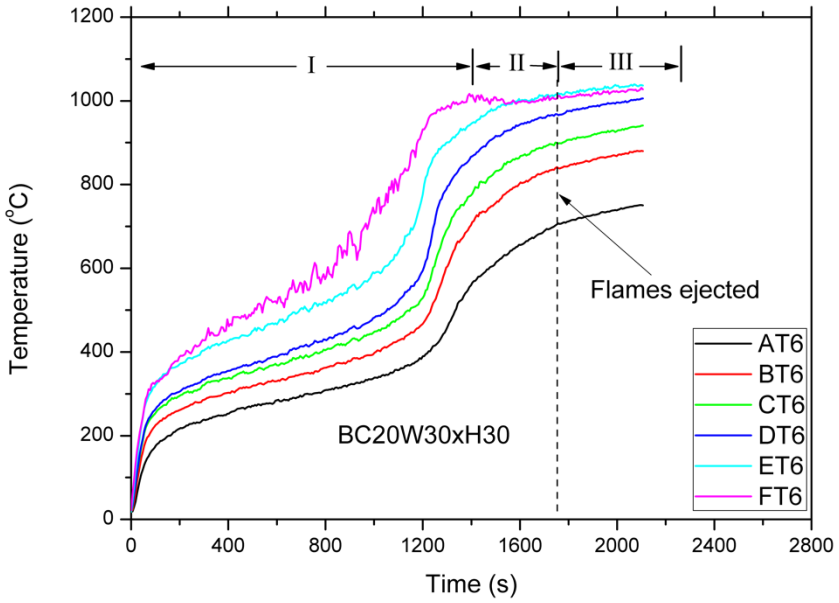

Figure 5.33 Temperature evolution at top location inside each box for BC20W30xH30 case.

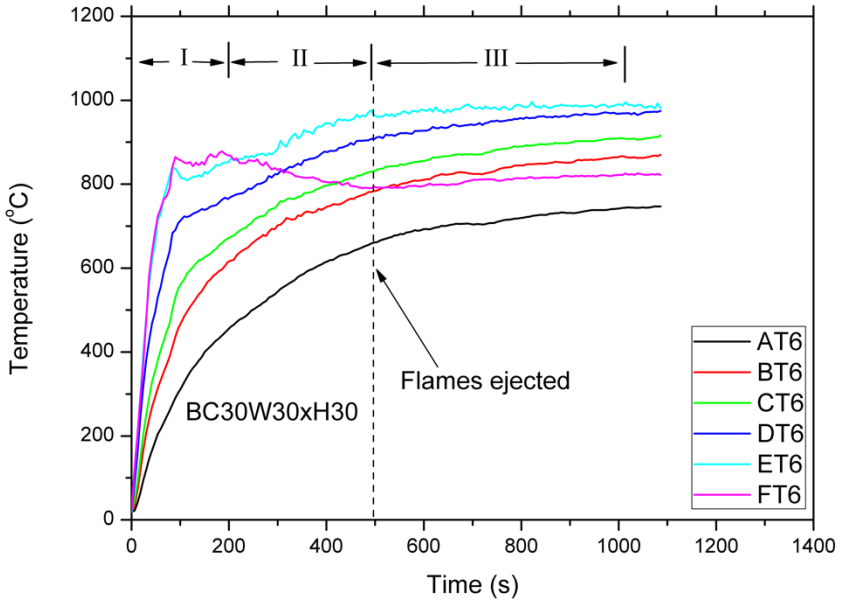

Figure 5.34 Temperature evolution at top location inside each box for BC30W30xH30 case.

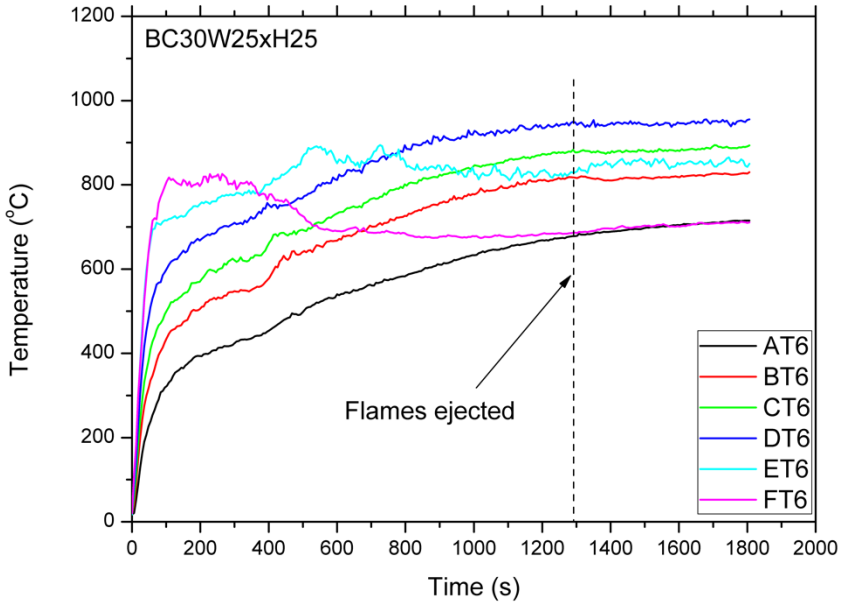

Figure 5.35 Temperature evolution at top location inside each box for BC30W25xH25 case.

The temperature distribution over height during the steady-state period for case BC30W30xH30 is depicted in Fig. 5.36. The temperature distribution is layered, being uniform above the half-opening height. Below this point, the temperatures in every box are low, indicating that air entering the corridor. It is also observed that the upper layer temperatures inside Box F is less than in the other boxes except Box A. This is because of the flame detachment from the pool and movement towards the opening. As flames moves from Box F to Box E, only hot gases are present in Box F

and thus temperature decreases. Inside Box E, higher temperatures were measured in the upper layer, due to the presence of burning in this box. In Box A, with fresh air coming inside the enclosure, the lower cold layer is very clear and the difference with the upper layer is almost 250^{o}C. Towards Box E (where combustion mainly occurs) this difference decreases, as more oxygen is consumed closer to the fire. Similar observations were made for all cases, highlighting nearly non-uniform temperature distribution over the height of the corridor. In addition, the higher temperatures are always measured in the box in which flame was moved to.

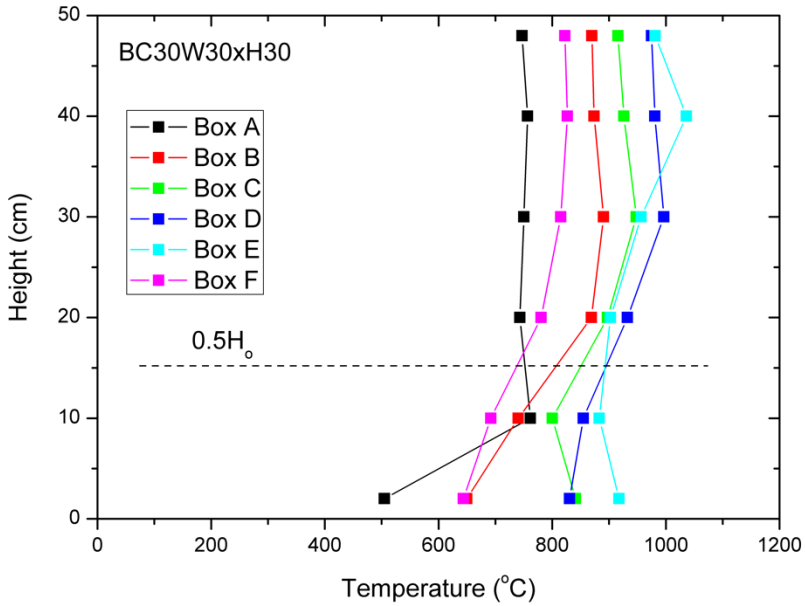

Figure 5.36 Vertical temperature distribution during steady-state period inside along the corridor for the BC30W30xH30 case.

The temperature distribution over height in Box A and Box F for all cases in which the flame came out is depicted in Fig. 5.37. In Box F (right), the temperatures are higher for cases using the smaller pan, but always increase with increasing ventilation factor. This observation is explained based on the heat losses; as the opening size decreases, heat losses are bigger resulting in lower temperatures. As expected, the upper layer temperatures closer to the opening (left), are the lowest, between 600-700^{o}C for all cases. In every case, the fresh air entering the enclosure is shown by the lower temperatures below the half-opening height.

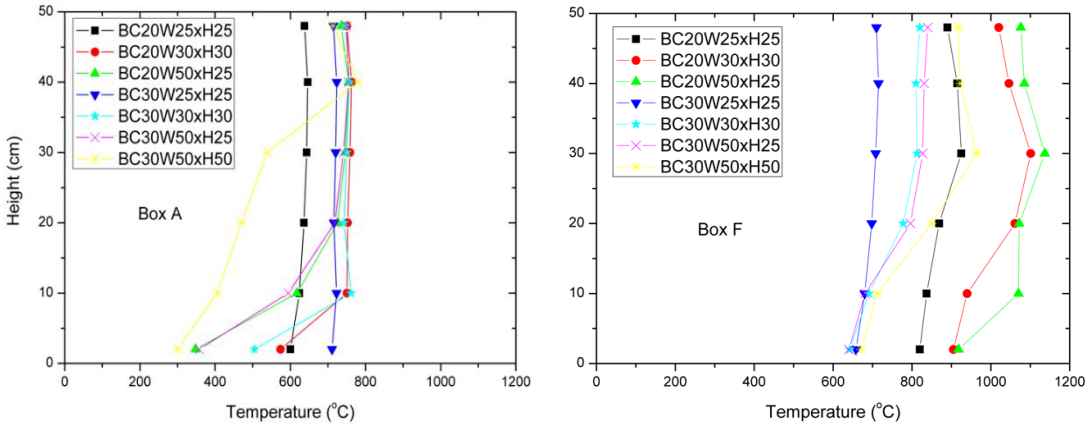

Figure 5.37 Vertical temperature distribution during steady-state period inside the Box A and Box F of the cases where flames appeared outside

In summary, under ventilation-controlled conditions, the following observations can be made for the temperatures inside the corridor:

- The steady-state gas temperature profiles inside enclosure are not uniform over height. Instead, it is a two-zone layered temperature distribution, being uniform only above the half-opening height level.
- Inside the fire box, temperatures are less than in other boxes, due to flame detachment from the pool and movement towards the opening seeking available oxygen for combustion. The movement of the flame was observed up to either Box E or Box D, in which the highest temperatures are found for different cases.
- For the cases of the same pan size, steady-state gas temperatures increase with a increase in opening dimensions, as heat losses become higher.

5.3.6.3 Heat flux measurements on the floor of the corridor

The heat flux measurements are shown in Fig. 5.38 and 5.39 for BC30W30xH30 and BC20W30xH30 respectively. For the smaller pan, the heat fluxes always continue to increase. Initially, the increase is slow following the HRR and temperature results. A rapid increase is followed, as the fire becomes ventilation-controlled and after the flames come out, the increase rate is reduced again. The heat flux decreases with a decrease in the distance to the opening. Using the larger pan, the heat fluxes in all boxes initially increase rapidly, as HRR does. Then, after growth period, the rate of

increase decreases until flames are ejected through the opening. Finally, a further decrease on the increase rate denotes ‘Region III’, in which the flames burn outside.

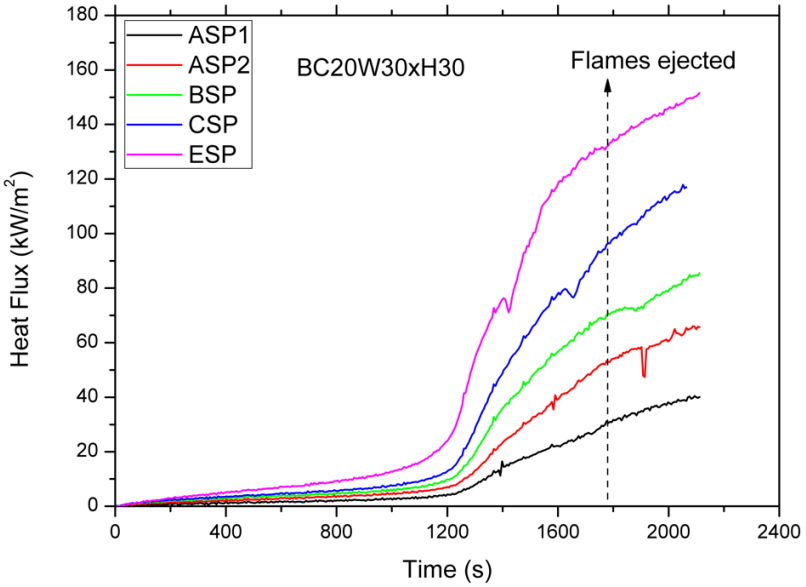

Figure 5.38 Heat Flux evolution profiles in six locations on the floor of the corridor for BC20W30xH30 case.

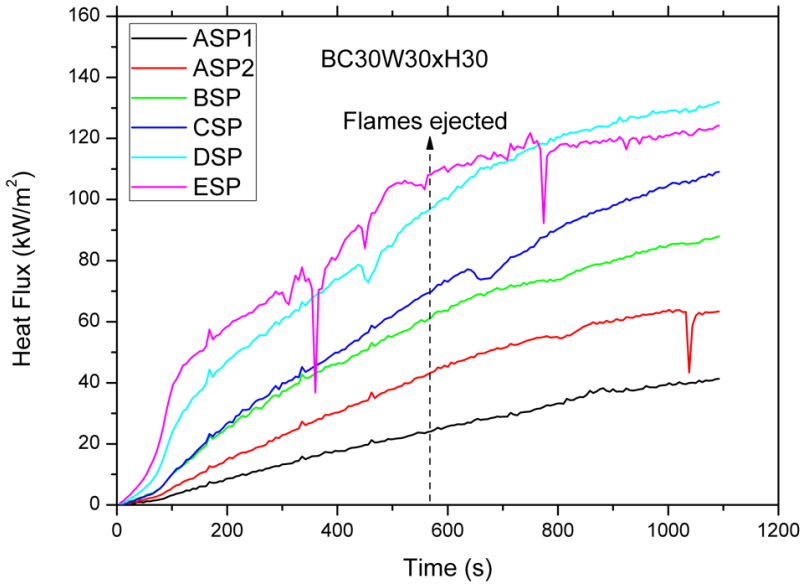

Figure 5. 39 Heat Flux evolution profiles in six locations on the floor of the corridor for BC30W30xH30 case.

Heat flux measurements for different opening dimensions (e.g. ventilation factor) but same pool size (20 cm dia.) are depicted in Fig. 5.40. It shows that as the ventilation factor increases the heat flux closer to the pool fire increases. This behaviour follows

the HRR and the steady-state temperature distribution trends as discussed above. Increase of the ventilation factor results in an increase of the burning rate, thus an increase of HRR. Therefore, as the ventilation factor increases the steady-state temperature inside the corridor increases, since the heat losses increase. In general, heat flux measurements follow the temperature profiles, as radiation from the upper hot layer is the primary heat feedback mechanism to the floor as discussed in previous chapter.

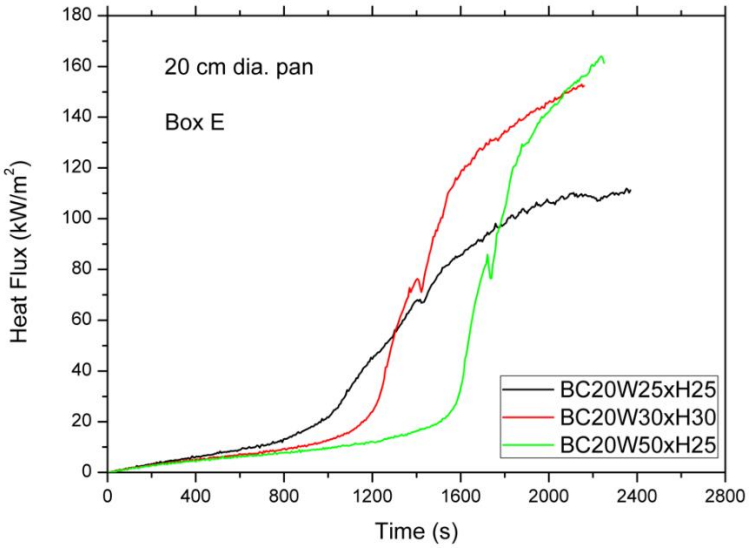

Figure 5.40 Heat flux profiles on the floor of Box E for cases using the 20 cm dia. pan but different openings.

5.3.6.4 External flames

This section gives flame height and heat flux experimental results for the cases where the flame ejected through the opening. Table 19 summarises all the cases and the time when flames appeared outside.

Table 19 Cases with flame ejection and time (min) they first appeared and became visible on the façade.

Cases with flame ejection	Time (s)	Fire conditions
BC20W25xH25	35.5	Ventilation-controlled
BC20W30xH30	28.5	Ventilation-controlled
BC20W50xH25	30.5	Ventilation-controlled
BC30W25xH25	22	Ventilation-controlled
BC30W30xH30	8.5	Ventilation-controlled
BC30W50xH25	5	Ventilation-controlled
BC30W50xH50	3.5	Fuel-controlled

5.3.6.4.1 Flame Height

The same procedure as presented in §4.3.7.4.1 was followed to calculate the mean (I=0.5), the maximum (I=0.05) and the continuous flame height (I=0.95) according to intermittency (Zukoski et. al., 1980). The relationship between the intermittency and the flame height from the N.P (=0.5H_o) for the BC20W30xH30 and BC30W30xH30 cases is shown in Fig. 5.41. The mean, continuous and maximum flame heights for both cases are also indicated on the figure.

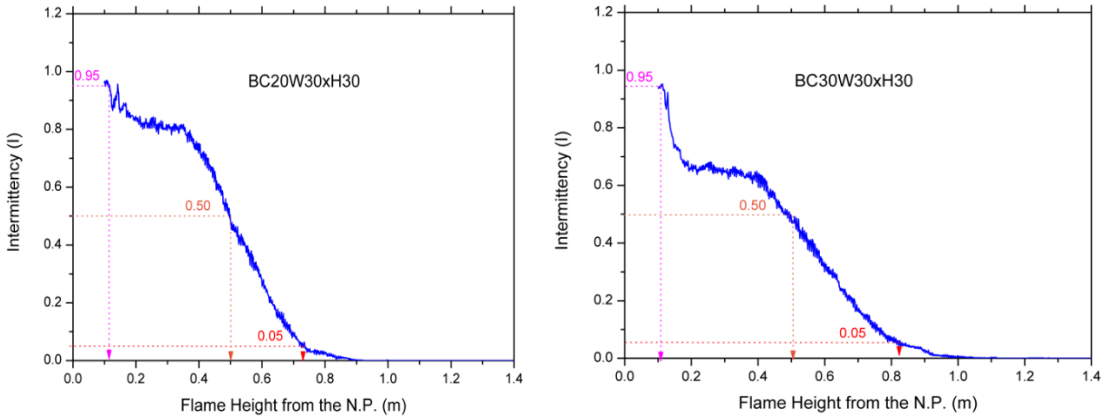

Figure 5.41 Intermittency against flame height for the BC20W30xH30 (left) and BC30W30xH30 (right) case. The location of maximum (I=0.05), mean (I=0.5) and continuous (I=0.95) flame height are also shown.

Using the same procedure, the (mean) flame height for every case is depicted against the theoretical HRR in Fig. 5.42. The case BC30W50xH50 is not included in the plot, as it was fuel-controlled as discussed in §5.3.6.1. It is observed that the mean flame height increases with the theoretical HRR for the ventilation-controlled cases. The only exception was the BC20W50xH25 case, which may be attributed to possible underestimation of the flame height using the image processing technique as presented in Chapter 3. In all ventilation-controlled cases the mean flame height was observed on the centreline of the façade above the opening, as the contours of all cases show in Fig. 5.43.

Regarding the fuel-controlled case, BC30W50xH50, the resulted external flame was observed to emerge as two separate fire plumes (see Fig. 5.43 and Fig. 5.45-right). This behaviour is due to the large opening dimensions which equals to a fully-open

side opening. In this case, there is no wall above the opening, thus the only boundary is the ceiling and fire is ejected freely through the entire width of the opening.

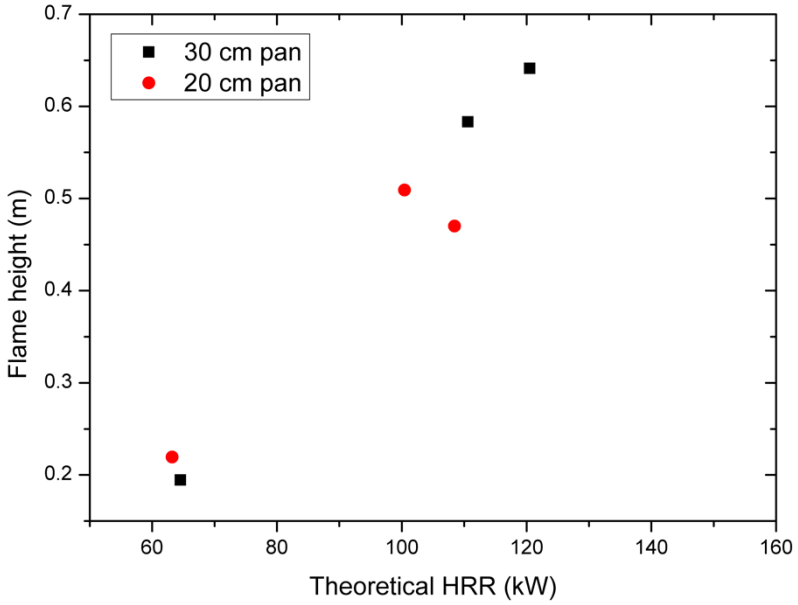

Figure 5.42 Mean flame height against theoretical HRR for cases using both pans.

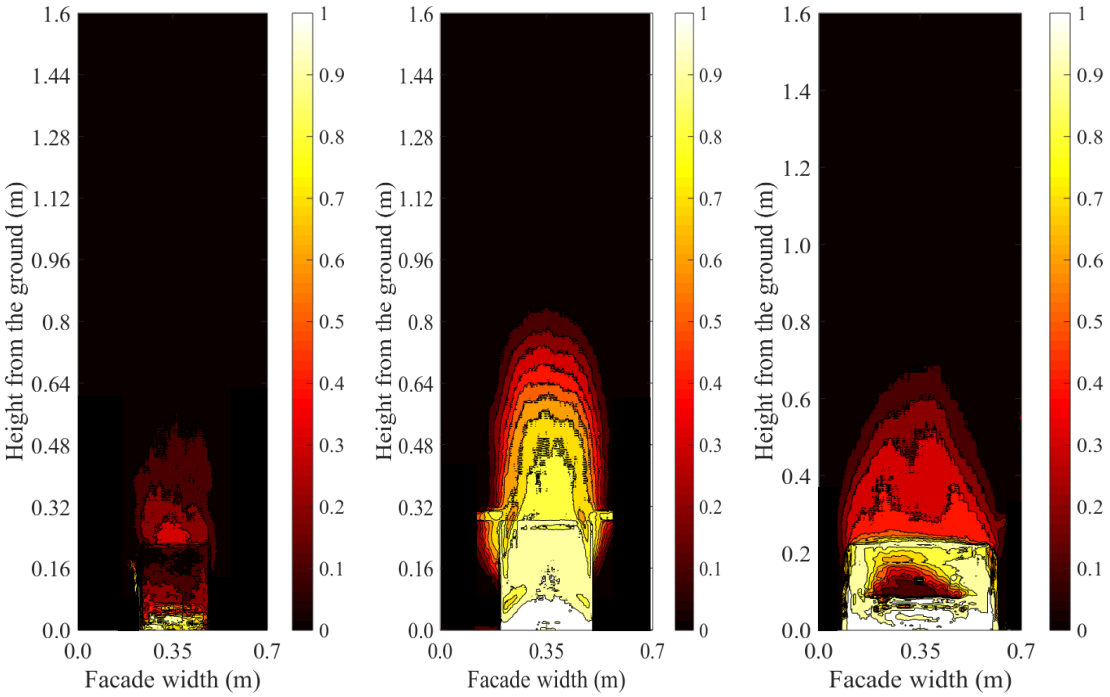

BC20W25xH25 BC20W30xH30 BC20W50xH25

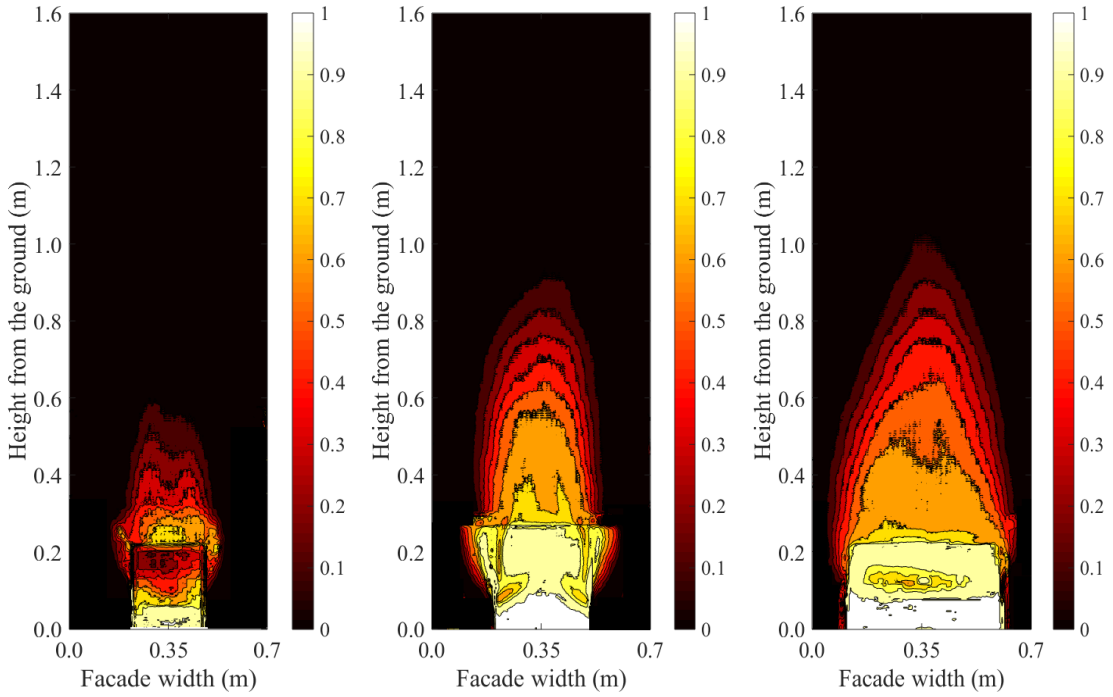

BC30W25xH25 BC30W30xH30 BC30W50xH25

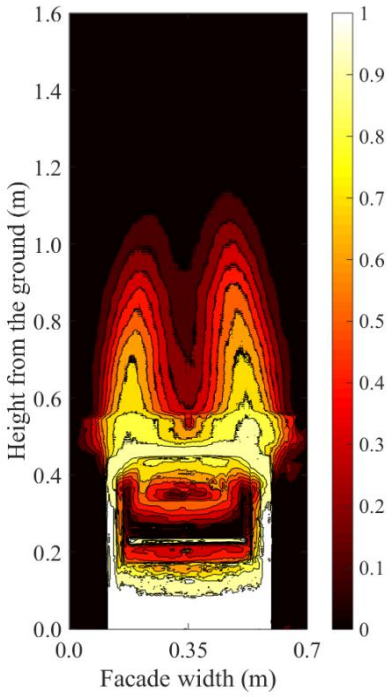

BC30W50xH50

Figure 5.43 Intermittency contours for all cases.

5.3.6.4.2 Heat Flux on the façade

Figure 5.44 depicts the heat flux measured at different positions on the façade for two cases, BC20W30xH30 (left) and BC30W30xH30 (right) respectively. It is observed that, in both cases, the highest heat flux is located along the centreline and the heat fluxes measured at 10cm to the right or left of is higher than the ones measured 10 cm from the centreline. This is expected according to observations regarding the symmetry of the flame height as discussed earlier based on contours depicted in Fig. 5.43. In both cases, the heat fluxes 10cm to the right or left of the centreline are similar, thus it is reasonable to assume that the centreline can be considered as the symmetry axis for heat exposure of the façade, except for the BC30W50xH50 case. Due to the fire plume emerge observed in this case (see last contour of Fig. 5.43 and Fig. 5.45-right), the highest heat flux values, are off the centreline, as shown in Fig. 5.45, in contrast to other cases. This finding highlights the importance of the width of the opening in addition to the ventilation factor to the heat exposure of the facade.

Figure 5.46 depicts the vertical distribution of the heat fluxes measured at the centreline of the façade for all test cases in which flames ejected through the opening. Similar distributions are observed for all cases, except again for the BC30W50xH50. It is shown that the measured heat fluxes decrease with increasing height as expected. Also, for the same pan size, the heat fluxes in the centreline increase as the opening dimensions (e.g. ventilation factor) increase.

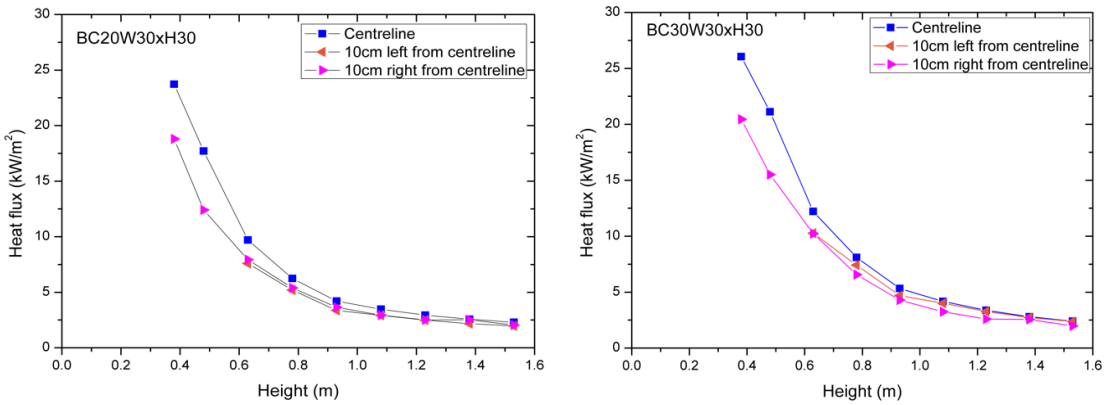

Figure 5.44 Heat flux distributions along the centreline above the opening for FR20W25xH25 (left) and FR30W30xH30 (right) case.

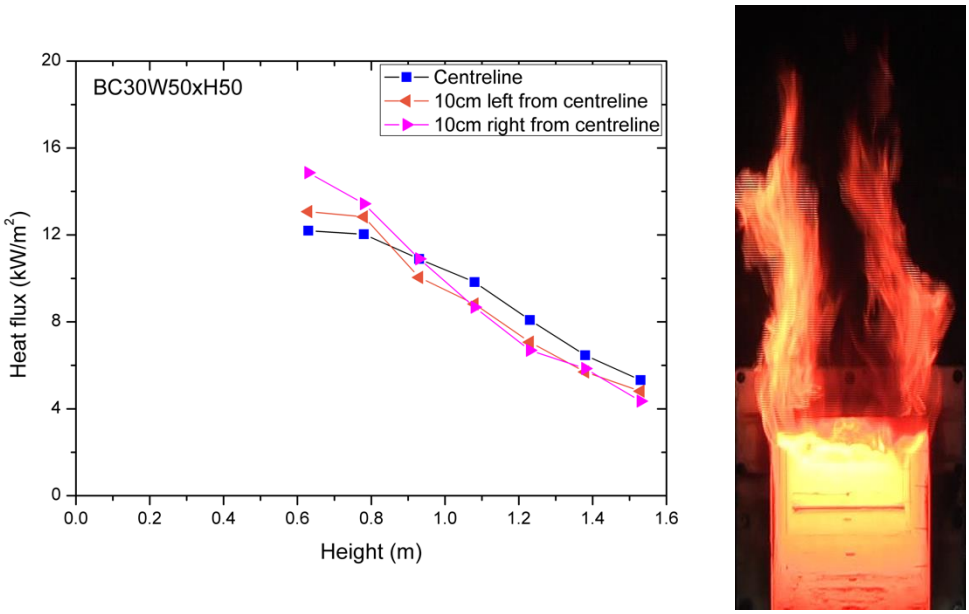

Figure 5.45 Heat flux distributions along the centreline above the opening for FR30W50xH50 case (left) and a frame taken after flames are established outside (right).

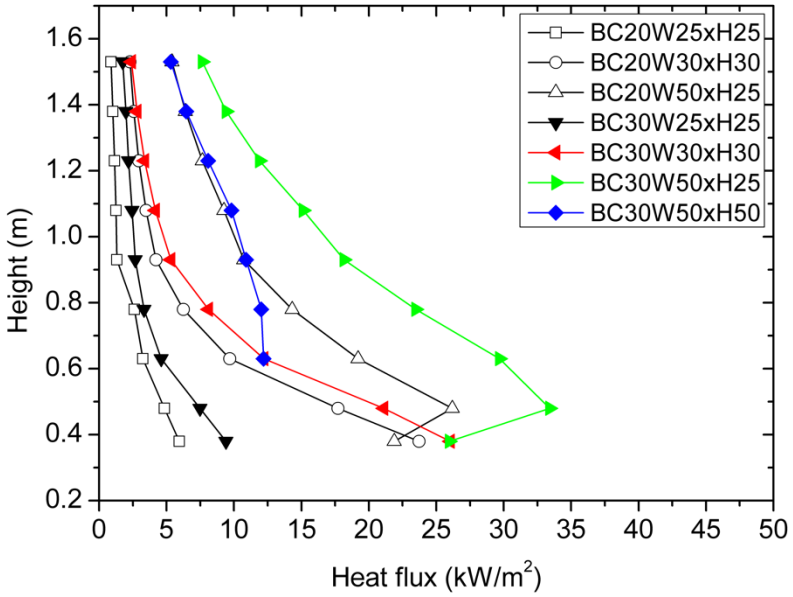

Figure 5.46 Heat flux distributions along the centreline above the opening for all cases.

5.4 Discussion and Analysis

5.4.1 Time needed before steady-state conditions established

The time needed for each case to reach steady-state burning is shown in Table 20.

Table 20 Summary of time needed for steady-state conditions established in each case.

Pan Size (cm)	$W_o x H_o$ (m)	$A_o H_o^{1/2}$	Experiments	Duration of experiment (s)	Time needed to steady-state conditions (s)	Flames out
20	0.1 x 0.1	0.0032	BC20W10xH10	210	Self-extinction	No
	0.15 x 0.15	0.0087	BC20W15xH15	2520	2385	No
	0.1 x 0.25	0.0125	BC20W10xH25	3000	2680	No
	0.2 x 0.2	0.0179	BC20W20xH20	3000	2490	No
	0.25 x 0.25	0.0313	BC20W25xH25	2280	2150	Yes
	0.3 x 0.3	0.0493	BC20W30xH30	2100	1990	Yes
	0.5 x 0.25	0.0625	BC20W50xH25	2220	1985	Yes
	0.5 x 0.5	0.1767	BC20W50xH50	2100	1430	No
30	0.1 x 0.1	0.0032	BC30W10xH10	240	Self-extinction	No
	0.15 x 0.15	0.0087	BC30W15xH15	1800	1120	No
	0.1 x 0.25	0.0125	BC30W10xH25	1800	660	No
	0.2 x 0.2	0.0179	BC30W20xH20	2040	1080	No
	0.25 x 0.25	0.0313	BC30W25xH25	1800	1580	Yes
	0.3 x 0.3	0.0493	BC30W30xH30	1080	900	Yes
	0.5 x 0.25	0.0625	BC30W50xH25	1200	850	Yes
	0.5 x 0.5	0.1767	BC30W50xH50	960	620	Yes

It is observed that the time needed for reaching steady-state conditions to be established inside the corridor-enclosure is affected primarily by the size of the pan, as using the larger pan takes less time to reach steady-state burning than that in the cases with the smaller pan. This is attributed to the difference in the time needed for the walls of the corridor and hot gas to be heated up. Temperature profiles of the upper hot layer inside the Box F, in which the pool fire was placed, also confirm this behaviour. Using the 20 cm dia. pan, the temperature at different vertical locations, increase progressively until they reach a peak value before the steady-state burning period. In comparison, using the larger pan, temperatures inside Box F reached their peak values significantly faster, followed by a small decrease before reaching a constant value during the steady-state burning period. This behaviour is depicted in Fig. 5.47, showing the temperature evolution measured at 2 cm below the ceiling of Box F for two cases having same opening dimensions (WxH: 0.2 x 0.2 m^2) but different pan sizes.

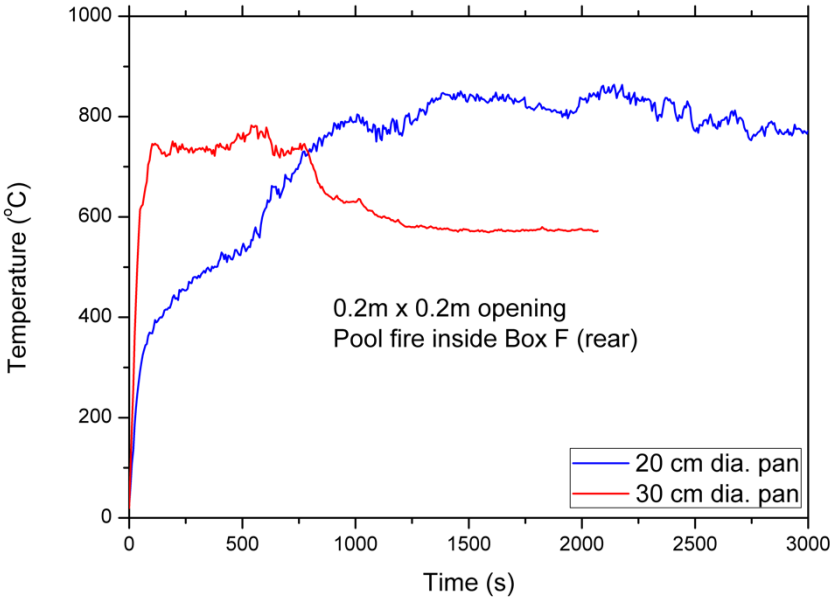

Figure 5.47 Temperature evolution measured at 2 cm below the ceiling of the Box F for two cases having same opening dimensions (0.2 x 0.2 m^2) but different pan size.

5.4.2 Fuel burning rate affected by the ventilation factor

Based on the results from previous sections, each case can be characterised as either fuel- or ventilation-controlled. Table 21 presents a summary of the fire scenarios for all cases, along with the theoretical HRR and stoichiometric HRR inside the enclosure.

Table 21 Summary of fire scenario for the experiments conducted.

Experiments	$A_oH_o^{1/2}$	$Q_{st,in}$ ($1500\ A_oH_o^{1/2}$)	Q_{th} (kW)	Fire scenario
BC20W10xH10	0.0032	4.8	-	Self-ext
BC20W15xH15	0.0087	13.1	11.2476	Fuel-controlled
BC20W10xH25	0.0125	18.8	25.1732	Vent-controlled
BC20W20xH20	0.0179	26.7	36.9564	Vent-controlled
BC20W25xH25	0.0313	46.5	63.2008	Vent-controlled
BC20W30xH30	0.0493	73.5	100.425	Vent-controlled
BC20W50xH25	0.0625	93.8	108.459	Vent-controlled
BC20W50xH50	0.1767	265.1	10.712	Fuel-controlled
BC30W10xH10	0.0032	4.8	-	Self-ext
BC30W15xH15	0.0087	13.1	23.5664	Vent-controlled
BC30W10xH25	0.0125	18.8	33.475	Vent-controlled
BC30W20xH20	0.0179	26.7	36.153	Vent-controlled
BC30W25xH25	0.0313	46.5	64.5398	Vent-controlled
BC30W30xH30	0.0493	73.5	110.6014	Vent-controlled
BC30W50xH25	0.0625	93.8	120.51	Vent-controlled
BC30W50xH50	0.1767	265.1	149.968	Fuel-controlled

Figure 5.48 plots $\dot{m}_T$ against the ventilation factor, $A_o H_o^{1/2}$, both normalised by the fire area (equals to the pan surface of the pool fires), A_f. Results of the free-burn cases of both pans are also plotted. For comparison purpose, data extracted from Bullen and Thomas (1978) who used ethanol pool fires in a cubic-like enclosure are also included. It is noted that in all cases with the 10 x 10 cm opening, the air flowing inside the corridor was not sufficient for the fires to sustain and they were self-extinguished after 3-4 min. Thus, data from experiments having the 10 cm x 10 cm opening are not included in the plot.

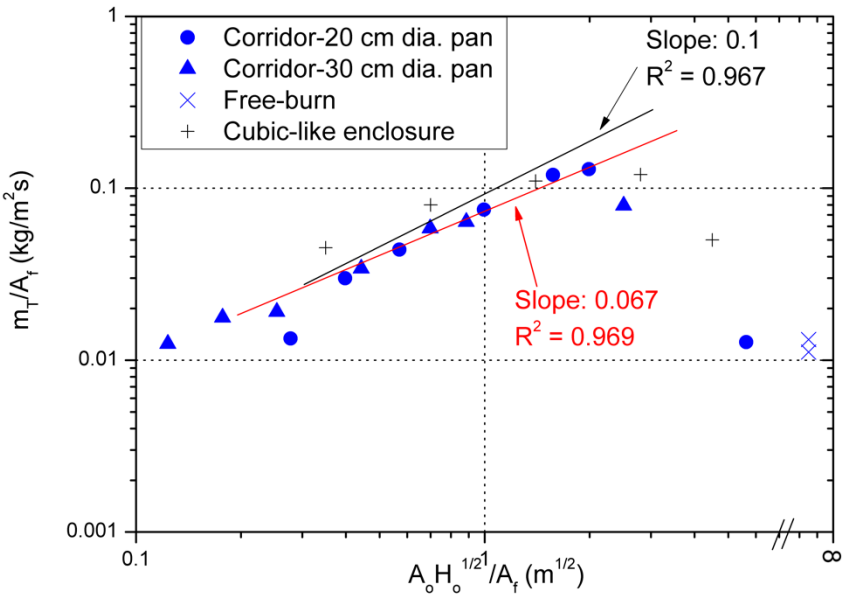

Figure 5.48 Mass pyrolysis rate against ventilation factor, both normalised by the fuel area for corridor-like enclosures of the present work compared with data (Bullen and Thomas, 1978) for cubic-like enclosures using ethanol as fuel.

As the ventilation factor increases, the normalized burning rate, $\dot{m}_T/A_f$, also increases until reaching a maximum value corresponding to the transition from ventilation- to fuel-controlled conditions, observed at about $A_o H_o^{1/2}/A_f = 2$. A further increase in the ventilation factor results in a decrease in $\dot{m}_T/A_f$, as the fire becomes fuel-controlled and finally, for very large ventilation factors, $\dot{m}_T/A_f$ approaches the free-burn burning rate. The trend of the data follows the one obtained in cubic-like enclosures for different fuels by many researchers (Kawagoe and Sekine, 1963; Thomas et. al., 1967; Delichatsios et. al., 2004; Drysdale, 2011; Delichatsios, 2014), as presented in Chapter 2. The data extracted for cubic-like enclosure coincides the

linear fit proposed in (Kawagoe, 1958; Kawagoe and Sekine, 1963) and verified by Delichatsios et. al. (2004) who suggested a slope of 0.1 in the ventilation-controlled regime, as Eq. 5.4 shows.

$$\frac{\dot{m}_T}{A_f} = 0.1\frac{A_o H_o^{1/2}}{A_f} \tag{5.4}$$

The experimental data of this work, for experiments in a 6:1 aspect ratio corridor-like enclosure having one end closed, indicate that a linear relation between the $\dot{m}_T/A_f$ and $A_oH_o^{1/2}/A_f$ still exists, as Fig. 5.48 shows. However, the proportional constant in the present work is 0.067 (Eq. 5.5), which is about 2/3 of the one obtained for cubic-like enclosures.

$$\frac{\dot{m}_T}{A_f} = 0.067\frac{A_o H_o^{1/2}}{A_f} \tag{5.5}$$

The current results are in accordance with previous experimental studies in corridors (Miyazaki and Watanabe, 1998; Cooke, 1998; Thomas and Bennetts, 1999; Delichatsios et. al., 2004) demonstrating that the burning rate in corridor-like enclosure is less than that in cubic-like enclosures under ventilation-controlled conditions. This difference was attributed to a decrease of the air inflow rate in corridor-like enclosures due to the non-uniform temperature distribution over height inside the corridors (Thomas and Bennetts, 1999; Yii et. al., 2007). This phenomenon will be further discussed in the following subsections.

5.4.3 Heat release rate

The main difference between a gaseous burner fire source and a pool fire is that using a gaseous burner means that the mass burning rate can be controlled. Thus, the fire conditions within the enclosure, either fuel- or ventilation-controlled fire, are prescribed, as was done by Beji (2009) and Ukleja (2012) in order to achieve ventilation-controlled conditions. This is however not the case for a pool fire, as its burning rate depends on the heat feedback from the hot gas layer and compartment walls. Therefore, in the present experimental work, no prior knowledge regarding the fire scenario was available before the experiments.

5.4.3.1 Mass inflow rate and heat released inside an enclosure

As Kawagoe (1958) described in his model, during the fully-developed stage of a ventilation-controlled fire in a cubic-like enclosure, a well-mixed fire environment (uniform temperature) into the enclosure and an ambient environment of uniform temperature outside the enclosure are assumed. The hydrostatic pressure between these two environments generates the buoyancy forces which drive the vent flows. It is widely recognised (Rockett, 1976; Yamaguchi and Tanaka, 2005; Lee et. al., 2007; Drysdale, 2011; Delichatsios, 2014) that based on the initial assumption of a well-mixed fire environment, the air inflow into the enclosure strongly depends on the geometry of the ventilation opening. Thus, the air inflow rate through the opening, $\dot{m}_a$, is given:

$$\dot{m}_a = C \times A_o\sqrt{H_o} \tag{5.6}$$

where C is the ventilation coefficient, which for moderate sized openings is assumed to be 0.5 (Kawagoe, 1958; Steckler et. al., 1982; Yamaguchi and Tanaka, 2005; Lee et. al., 2007; Beji, 2009; Drysdale, 2011; Ukleja, 2012; Hurley, 2016).

The maximum stoichiometric heat released inside an enclosure, $\dot{Q}_{st,in}$, is calculated by multiplying the air inflow, $\dot{m}_a$, by the energy released per kilogram of air completely consumed inside the enclosure (about 3000kJ/kg) (Yamaguchi and Tanaka, 2005; Lee et. al., 2007; Drysdale, 2011; Delichatsios, 2014)

$$\dot{Q}_{st,in} = \dot{m}_a \Delta H_{air} = 3000 \times C \times A_o\sqrt{H_o} \tag{5.7}$$

Based on the maximum heat released inside an enclosure, a useful quantity for describing a fire as fuel- or ventilation-controlled can be defined as the Equivalence Ratio (φ) (Hurley, 2016). As reported in (Pitts, 1995; Gottuk and Lattimer, 2002; Hurley, 2016), φ defines the ratio of the fuel mass flux, $\dot{m}_T$, to the oxygen mass flux entering the enclosure, $\dot{m}_{O_2}$, divided by the fuel-to-oxygen stoichiometric ratio of the fuel, S. Inserting the heat released inside the enclosure, φ is calculated (Lee, 2006; Lee et. al., 2007; Ukleja, 2012) as follows

$$\varphi = \dot{Q}_{th}/\dot{Q}_{st,in} = \dot{m}_T \Delta H_c/(3000 \times C \times A_o\sqrt{H_o}) \quad (5.8)$$

When φ exceeds unity, the fire is considered ventilation-controlled; whereas when φ is less than unity, the fire is fuel-controlled. Clearly the accurate calculation of the Equivalence Ratio depends on the accuracy of measurement (or estimation) of the mass inflow rate into the enclosure. For example, as shown in Table 21, based on Eq. 5.8, BC20W15xH15 was found to be fuel-controlled, although would be expected to be ventilation-controlled based on Fig. 5.48. The HRR difference (of less than 2 kW) is suggested to be due to the uncertainty of measurement (see Chapter 3) for estimating the MLR and the HRR on the hood. But, as noted here, the values as attained are given for each case.

The validity of Eq. 5.7 in corridor enclosures of 6:1 aspect ratio having one end closed was investigated (Beji, 2009; Ukleja, 2012) using gaseous burners, showing good agreement. An example (Beji, 2009) is given in Fig. 5.49 for a gaseous burner placed at the rear end of the corridor enclosure and with a 0.1 x 0.25 (m^2) opening. The prescribed theoretical HRR (through the mass flow rate of the burner) was set to 30 kW to achieve ventilation-controlled conditions. The HRR measured in hood increases during the growth period and when the fire becomes ventilation-controlled it reached a plateau equal to the maximum heat released inside an enclosure (= $1500A_oH_o^{1/2}$) at 18.75 kW, which implies a ventilation coefficient of 0.5 and thus Eq. 5.7 is validated for this enclosure geometry with a gaseous burner as fire source. During this region, the theoretical HRR is higher than the measured HRR, indicating the fire is controlled by the ventilation and burning takes place only inside the enclosure. When flames ejected through the opening, the HRR increases to be almost the same as the theoretical one during the final steady-state period.

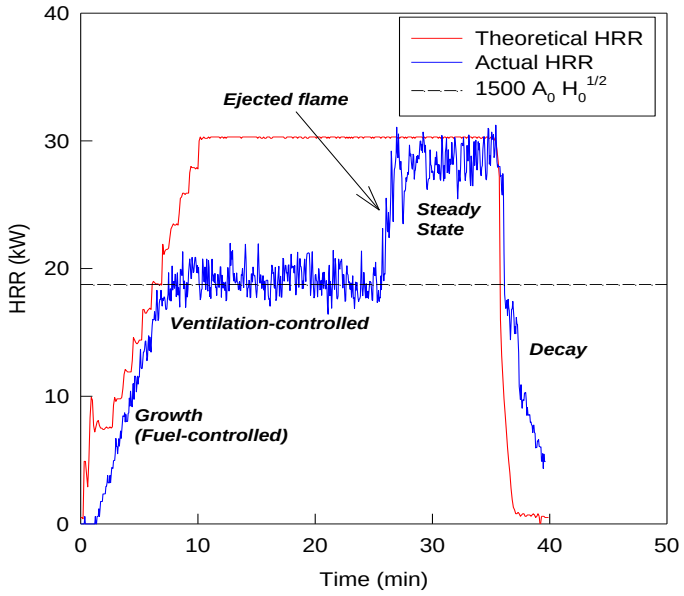

Figure 5.49 HRR profiles for a case using a propane burner inside Box F of the corridor and a 0.1 x 0.25 m^2 opening (Beji, 2009).

For enclosure fires using large openings and especially when the width of the opening is the same as that of the enclosure, several researchers (Thomas et. al., 1967; Yii et. al., 2007) have concluded that the ventilation coefficient, C, is less than 0.5. Thomas et. al. (1967) suggested two vent flow behaviours for small and large openings in a post-flashover fire and concluded that for small openings the vent flows are driven by the hydrostatic pressure difference between the upper hot gas layer of the interior of the enclosure and the cold ambient temperature outside the enclosure. On the other hand, using large openings the vent flows are driven by entrainment (smaller pressure difference). Different vent flow behaviours for small and fully-open wall openings were also observed by Thomas and Bennett (1999). They used liquid pool fires in a wide enclosure investigating the vent flows of an opening having the same height and varying widths. They found that the vent flows in fully-open wall opening are two-dimensional, but the flows become three-dimensional when the width of the opening is reduced. This was attributed to the flows on the vertical edges of the opening. Finally, Yii et. al. (2007) performed a simple numerical vent flow analysis based on line plume theory (Morton et. al., 1956; Karlsson and Quintiere, 2000; Drysdale, 2011) to investigate the influence of the opening's width on the mass inflow rate in enclosures and the ventilation coefficient. Based on previous experimental observations of Thomas and Bennetts (1999) for a uniformly distributed fuel load within an enclosure, a fire parallel to the

opening could be produced. A model was then proposed for estimating the ventilation coefficient C in post-flashover fires, based on the width fraction of the opening, W_o, to the enclosure's width, W_{enc}. He proposed that in enclosures with openings occupying a full wall, the ventilation coefficient C is less than the one proposed by Kawagoe (1958) due to the two-layer temperature distribution within the enclosure in ventilation-controlled fires. This finding was applied in two different configurations (see Fig. 5.50) signifying the direction of air entrainment into the flame, (i) fire source burns like a free-line plume fire (placed distant from or tangent to the wall) and (ii) fire burns like a wall line plume (attaching a wall) (Karlsson and Quintiere, 2000; Drysdale, 2011).

Figure 5.50 Plan view of a (i) free-line plume fire (left) and (ii) wall-line plume fire (Karlsson and Quintiere, 2000)

5.4.3.2 A simple approach for determining experimentally the ventilation coefficient in ventilation-controlled fires of the present work

It was shown in previous sections (§5.3.4.1 and §5.3.6.1) that in all ventilation-controlled cases the actual HRR measured in the hood after the growth period became constant for a couple of minutes reaching a plateau during 'Region II'. During this region, the theoretical HRR exceeds the maximum ventilation-controlled heat released inside the enclosure, indicating the transition from fuel- to ventilation-controlled fire. For the cases when flames ejected through the opening, the measured HRR further increases before reaching steady-state conditions. For the cases without ejected flames, burning takes place only inside the enclosure and the measured HRR remains constant. These results demonstrate that during 'Region II', the fire is ventilation-controlled ($\varphi>1$, Eq. 5.8) and the HRR was controlled by the amount of oxygen entering the enclosure through the opening. Thus, Eq. 5.7 can be applied for estimating the heat released inside the enclosure in such configuration.

In this work, for ventilation-controlled fires, the HRR plateau reached during 'Region II' is always lower than the one calculated by Eq. 5.7, i.e., the maximum ventilation-controlled heat released inside the enclosure. For example, BC20W30xH30 is presented in Fig. 5.51. While the maximum stoichiometric heat released inside the enclosure (Eq. 5.7) using the 0.3 m x 0.3 m opening is 73.9 kW, the plateau reached before flames ejected is lower. Since the HRR in this region is nearly constant, it is reasonable to assume that all oxygen is consumed within the enclosure during 'Region II'. For this reason, an average value (see circled line) of the measured (actual) HRR of 'Region II' is calculated as 57.4 kW.

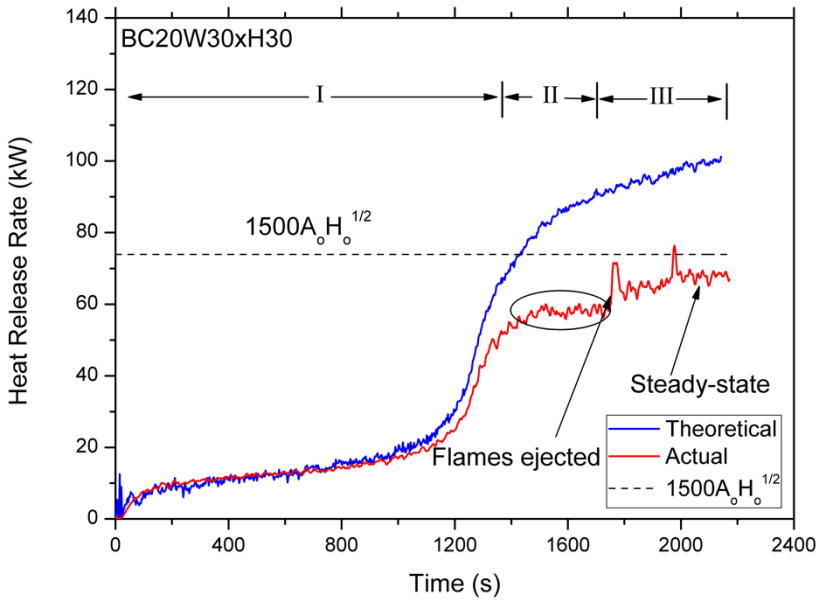

Figure 5.51 HRR profiles for BC20W30xH30 case.

Based on the previous observation regarding the HRR during 'Region II', the following two calculations of equivalence ratio are made:

- Using C=0.5 (maximum heat released inside the enclosure) and applying Eq. 5.7 to Eq. 5.8, the equivalence ratio is determined for each case.
- Using the average actual HRR during 'Region II', as calculated in Fig. 5.51, the equivalence ratio for each case is determined.

The comparison of the equivalence ratio, as calculated above using both ways, is plotted in Fig. 5.52. It is observed that for small opening dimensions, good agreement is reached, indicating that the assumption of C=0.5 is reasonably correct.

But, as the opening dimensions increase, the deviation from the ideal agreement becomes considerable.

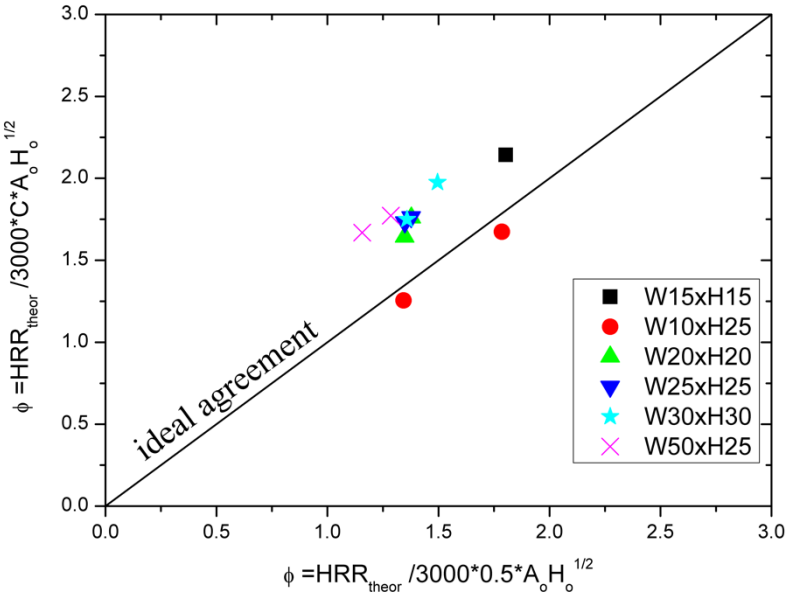

Figure 5.52 Verification of Eq. 5.7 using ventilation factor equal to 0.5 for all ventilation-controlled cases.

From Fig. 5.52, the measured ventilation coefficient is plotted in Fig. 5.53, against the ventilation factor. It is observed that for smaller ventilation factors, C tends to 0.5 showing good agreement with the Kawagoe (1958) approach. However, as the ventilation factor increases up to 0.06, the ventilation coefficient C is decreased being approximately 0.39 before reaching the lowest value of 0.35 for the 0.5 x 0.25 (m^2) opening.

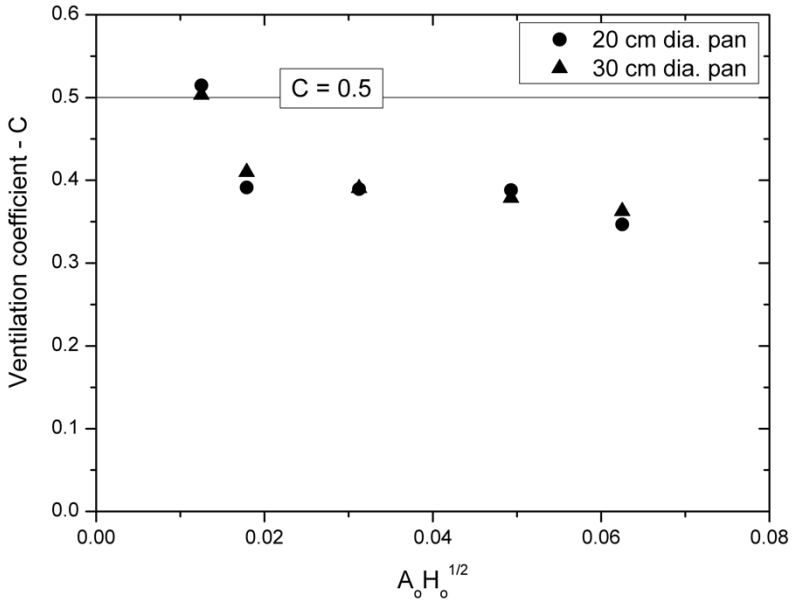

Figure 5.53 Ventilation coefficient, C, against the ventilation factor for all ventilation-controlled cases.

Finally, combining Eq. 5.5 and the results from Fig. 5.53 he mass pyrolysis rate in terms of the mass inflow rate is:

$$\dot{m}_T = 0.18\,\dot{m}_a \tag{5.9}$$

Delichatsios et. al. (2004) found that in cubic-like enclosures the mass pyrolysis rate equals to $0.22\dot{m}_a$, which is larger than the corresponding one calculated for corridor enclosures using data of the current work.

It is interesting here to compare the ventilation coefficient results of this work with the analysis of Yii (2002; 2007) presenting the relation of C with the width ratio W_o/W_{enc}. The results of the dimensionless, C/C_{max}, versus the width ratio W_o/W_{enc} are plotted in Fig. 5.54. Value of 0.5 was taken as C_{max} based on Kawagoe's model. It is observed that as the width ratio W_o/W_{enc} increases, the ventilation coefficient decreases, reaching very low value in cases when one wall of the enclosure is entirely open. Experimental results of the present study agree well with the trends of Yii's model for different line plume analogies, with the free-line plume fire (see Fig. 5.50) being reasonable closer to current findings, as no attachment of the pool to the wall was occurred within the corridor (Zukoski, 1995; Drysdale, 2011).

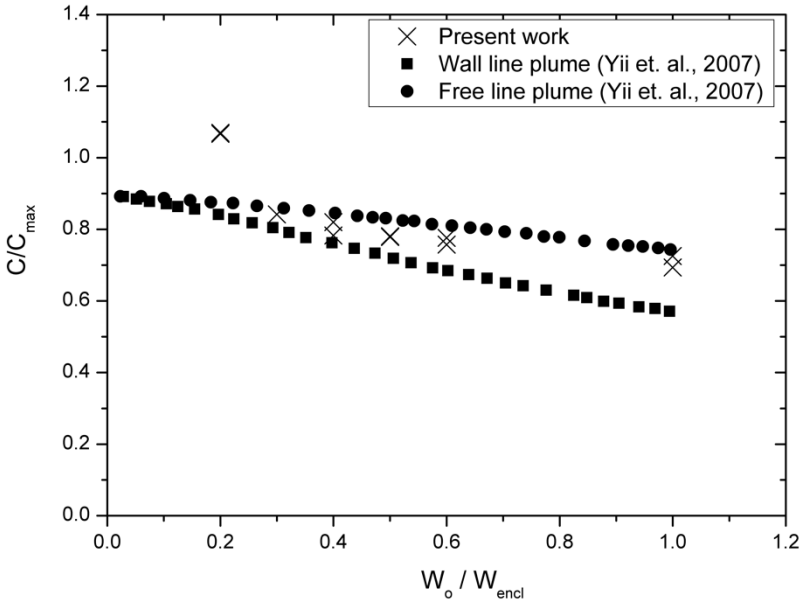

Figure 5.54 Ventlation coefficient ratio C / C_{max} plotted over the width ratio W_o/W_{enc}, for the experimental data of the present work and data obtained from (Yii et. al., 2007).

5.4.3.2.1 Heat released inside the corridor

The measured average heat released inside the corridor as calculated based in Fig. 5.51 against the ventilation factor is depicted in Fig. 5.55. It is revealed that a linear correlation is found between the average heat released inside the corridor and the ventilation factor. The value of 1110 kW/$m^{5/2}$ is 26% lower than the 1500 kW/$m^{5/2}$ which is widely proposed.

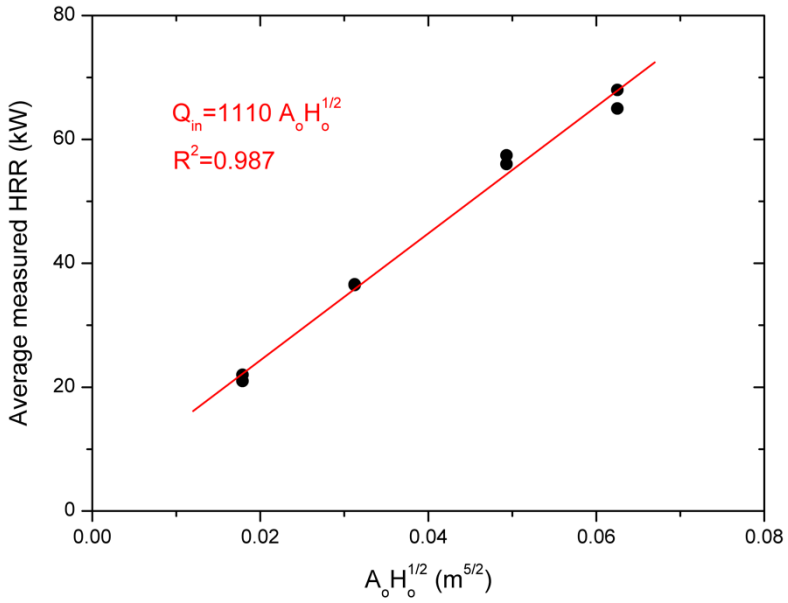

Figure 5.55 Linear correlation between the heat released inside the corridor and the ventilation factor.

5.4.3.2.2 Temperature distribution inside the corridor

The lower values of both mass pyrolysis rate and mass inflow rate found in corridor-like enclosures compared to cubic enclosures (see discussion related to Eq. 5.4 and 5.5) can be attributed to the formation of a two-layer temperature profile in the enclosure. To further support this, vertical distribution of the temperature profiles (time averaged over the steady-state period) inside the front (A) and the rear box (F) are plotted in Fig. 5.56 (left) and (right) respectively for all cases using the 30 cm dia. pan. In Box A, fresh air entraining through the opening results in lower temperatures compared to that in Box F. For the cases with greater ventilation factors, the temperature stratification is more intense, resembling clearly a two-layer zone distribution as the mass inflow rate through the opening is essentially entrainment driven. As the ventilation factor decreases, the interface between the hot and cold layers descends towards the floor and more mixing occurs, approaching the well-mixed scenario (Kawagoe, 1958). In these cases, the inflow rate inside the enclosure is restricted by the vent opening and the coefficient value, C, tends to the one proposed for cubic-like enclosures, namely 0.5 (see Fig. 5.53). Another point to be highlighted is that the temperatures seem more uniform close to the fire source, indicating more mixing occurring close to the pool fire.

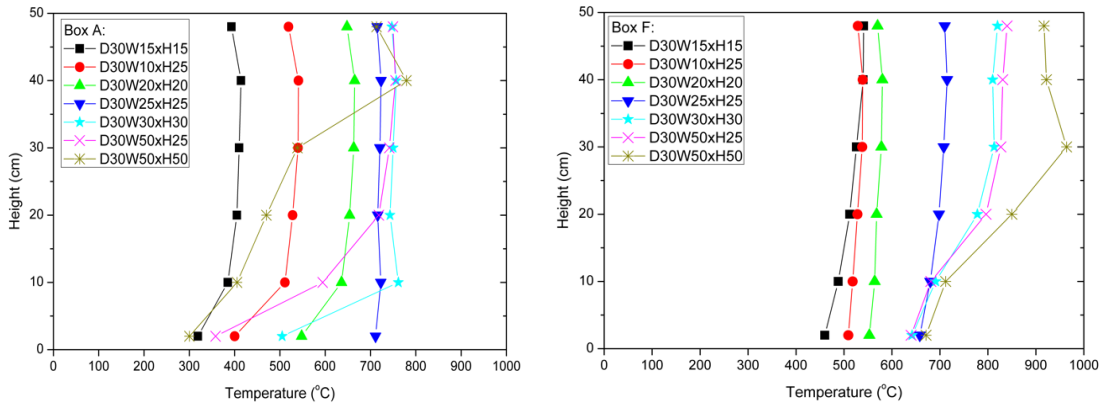

Figure 5.56 Time averaged over the steady state period gas temperature at the interior of the corridor enclosure for all test cases, in Box A (left) and Box F (right).

The present results clearly illustrate that temperature distribution in corridor enclosures cannot be considered uniform along the corridor, even under ventilation-controlled conditions, as is usually done for cubic enclosures (Kawagoe, 1958). Thus, value of 0.5 for the ventilation coefficient for calculating the mass inflow rate

through the opening should not be used in such fire scenarios. The opening size also has an importance influence on the temperature distribution inside the corridor – for small openings the vertical temperature distribution tends to uniform; whereas for larger openings it becomes layered. Based on the previous discussion regarding the temperature distribution affected by the opening size, the present experimental data are consistent with the finding by Yii (2002; 2007).

5.4.4 Detachment of flames from the pool and propagation along the corridor

Visual observations through the opening revealed that in most cases the flames detached from the pool surface, travelling towards the adjacent boxes before external burning occurred. Similar observations were made by (Beji, 2009; Ukleja, 2012) using the same corridor enclosure but with gaseous fuels. A slightly different phenomenon called ‘ghosting flames’ was reported in (Sugawa et. al., 1989; Audouin et al., 1997) using methanol and TBP/TPH liquid pool fires respectively and in (Most and Saulnier, 2011) using propane gaseous fuel. In these studies, the flames were observed lifting, completely separated from the pyrolysis zone, and travelling along the enclosure. However, as no lifting of flames was observed in the present work, the term ‘travelling flames’ (Beji, 2009; Ukleja, 2012) would better describe this phenomenon. Detachment of flames from the pool fire was observed in all ventilation-controlled cases, but not under fuel-controlled conditions.

5.4.4.1 Detachment of flames from the pool under ventilation-controlled conditions

This detachment of the flame is confirmed by detailed analysis of the gas temperature data. For the majority of the cases investigated in this work, the flames were found to detach from the pan after the initial growth period, moving towards the next box seeking fresh air. For some cases further propagation was followed towards the Box D or C.

Beji (2009) studied the rate of flame propagation towards the opening in a similar enclosure, by using the gas temperature data inside the corridor. Temperature measurements under the ceiling were used to indicate the presence of the flame. It was then assumed that in any given box, the peak of temperature recorded at the highest location indicated the passing of the flame through that point. It is noted that

the temperature measurements recorded cannot be considered as flame temperature measurements, but measurements of the gaseous products (Ukleja, 2012), as the flames do not always be in contact with the thermocouple probes as the gaseous products do. Finally, by overlapping those temperature measurements against time, Beji calculated the time (e.g. the propagation rate) needed from the transition of flames from one box to another. Moreover, the detachment of the flames from the burner was confirmed by a sudden decrease of temperature measurement at the top location inside the Box F. It has to be mentioned here that the measurements of temperature inside the corridor were taken in locations closer to the one side of the walls and not in the centreline along the corridor. This could introduce some uncertainty, as the fire source was placed on the centreline along the corridor. Similar methodology was also used by Pearson et. al. (2007) and Ukleja (2012).

The propagation velocity of the flames towards the opening of case BC30W20H20 is analysed as an example. The temperature profiles at all locations are depicted in Fig. 5.57 for each box. Figure 5.58 shows the temperature profiles of the top thermocouples inside each box. Based on the peak temperatures observed inside boxes F-D, the propagation of the flames as a function of time for this case is depicted in Fig. 5.59 The data follow a linear relation of a mean velocity of propagation of 0.12 cm/s. Similar velocity of propagation was found for the two other cases when flames reached box D, the BC30W10xH25 and BC30W25xH25 respectively.

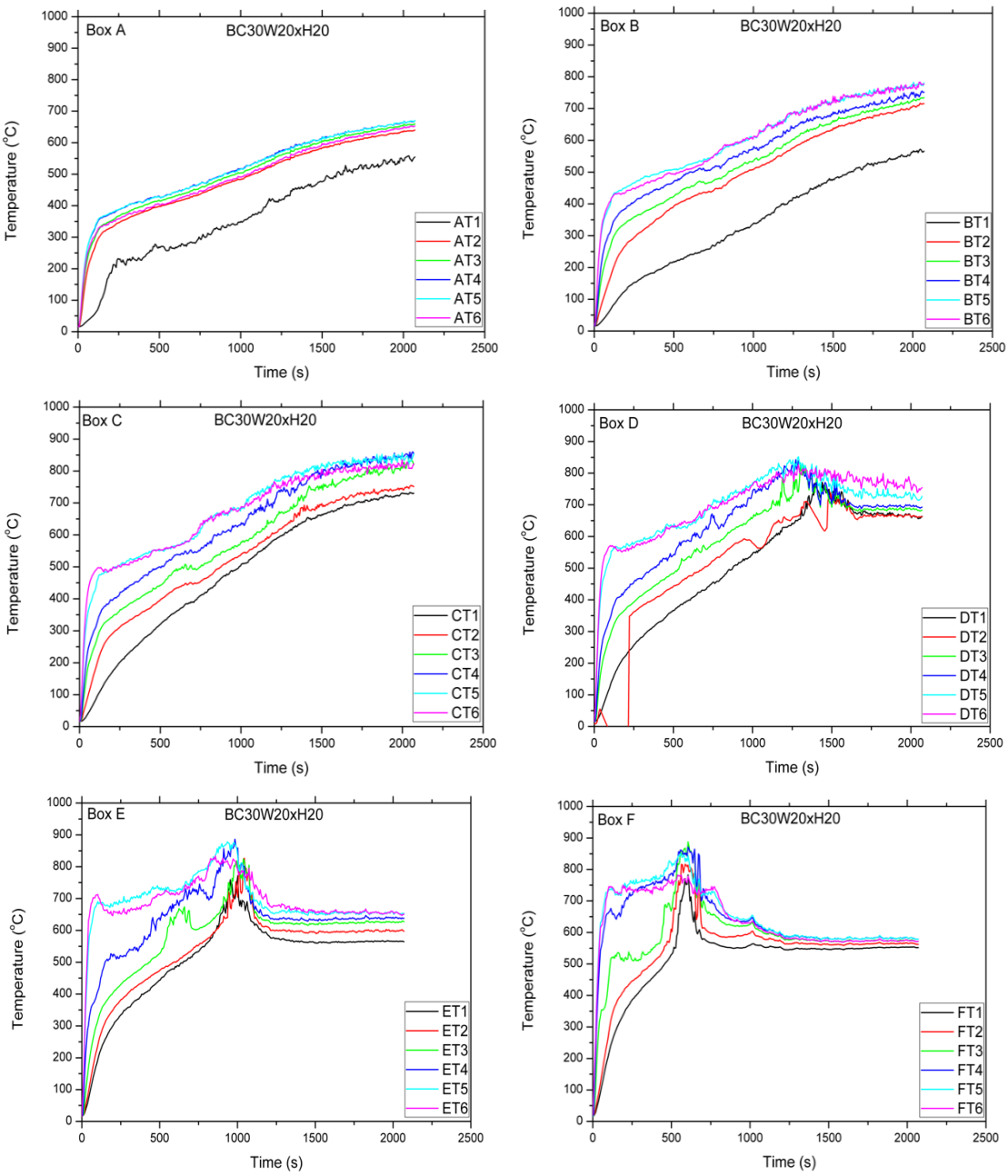

Figure 5.57 Thermocouple readings from all boxes along the corridor length as a function of time for case BC30W20xH20.

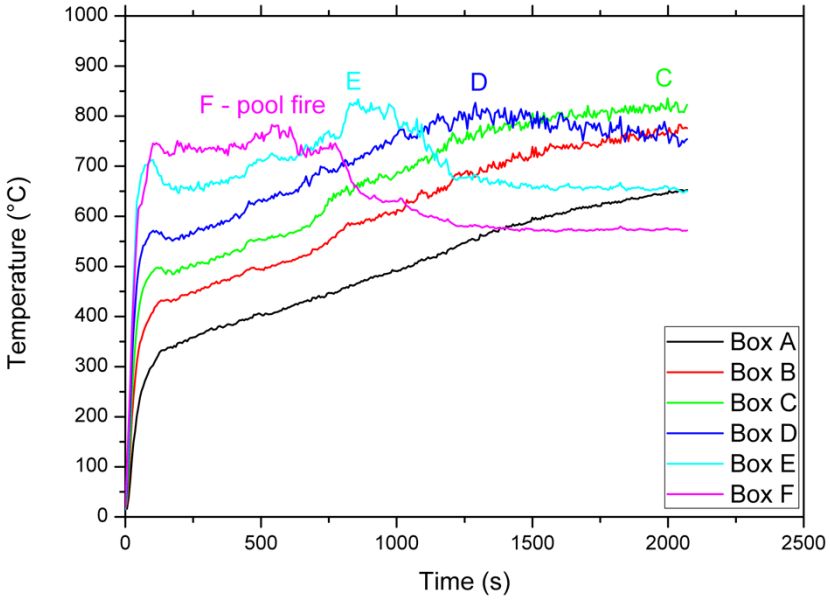

Figure 5.58 Top thermocouple reading from all boxes along the corridor length as a function of time for case BC30W20xH20.

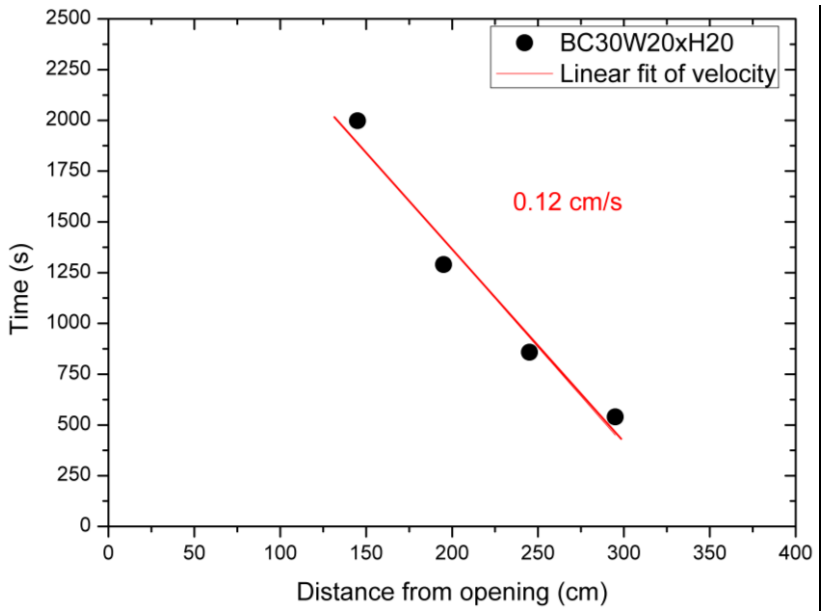

Figure 5.59 Propagation of flames along the enclosure as a function of time for BC30W20xH20 case.

5.4.4.2 Recirculation of gases behind the flames under ventilation-controlled conditions

Based on the discussion regarding the temperature distribution within the enclosure (see §5.4.3.2.2), no mixing occurs as the cold lower and the hot upper layer are clearly distinguished. This is due to the layered temperature distribution close to the opening. On the other hand, mixing may occur behind the flame region as indicated by the rapid reduce of the upper hot layer temperature after the flame has passed as

depicted in Fig. 5.58. The temperature distribution in the fire box becomes more uniform at different heights indicating more mixing of hot gases behind the flame region, which could be attributed to recirculation of gases behind the flames after they detach the burner and move towards the opening asproposed by Delichatsios (1990) and further experimentally confirmed by Audouin et. al. (1997) and Ukleja (2012).

Audouin et. al. (1997) reported traverse flows behind the ghosting flames as they moved from the fire source towards the opening. Figure 5.60 shows that initially a clear distinction between the upper and the lower layer exists. As the fire evolves, the flows reverse behind the fire source. When the detachment of flames occurs and flames propagate towards the opening, the flows remain reversed behind the flame region and temperature difference between the two layers becomes less than 100^{o}C.

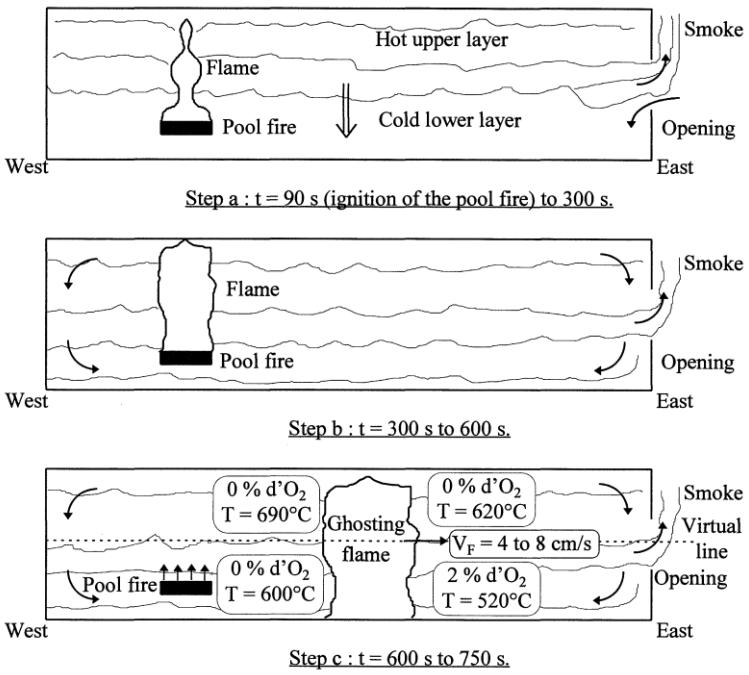

Figure 5.60 Reported traverse flows behind the ghosting flames (Audouin et. al., 1997)**.**

Ukleja (2012) measured the velocity of gas flows inside the corridor enclosure using bi-probes. He observed that when the travelling flames were passing through the location of the bi-probes the flows were reversing. A sketch of the proposed flows of that work is shown in Fig. 5.61.

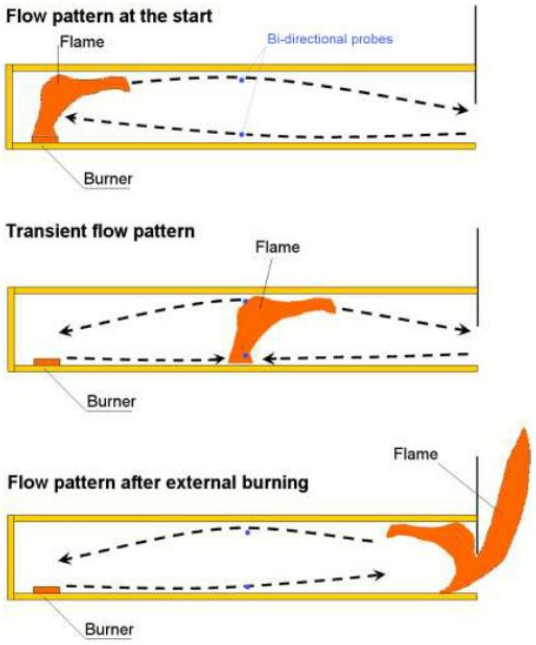

Figure 5.61 Flow patterns reported behind the travelling flames (Ukleja, 2012).

Similar recirculation of gases and flow patterns are expected in the present work owing to the detachment of flames from the pool and their movement towards the opening. The present results also show that ventilation-controlled conditions can be established even if non-uniform temperatures observed inside the corridor enclosure, as recirculation of gases and more mixing closer to the pool could help establish such conditions. More experimental studies measuring the flow velocities and reporting flow patterns prevail in a corridor for different fuel types could provide more insight to this interesting phenomenon.

5.4.5 No detachment of flames under fuel-controlled conditions

When fuel-controlled conditions prevailed within the corridor, no detachment of flames from the pool fire was detected. Thus, no data was presented in previous figures for $\varphi \leq 1$. An example for such a case was BC20W15xH15; for which $\varphi = 1$. Temperature profiles from top locations along the corridor for this case are shown in Fig. 5.62. The temperature profiles kept increasing in all boxes and no sudden decrease was noticed, indicating no detachment of flames from the pool. This finding was also complemented by visual observations through the opening of the corridor.

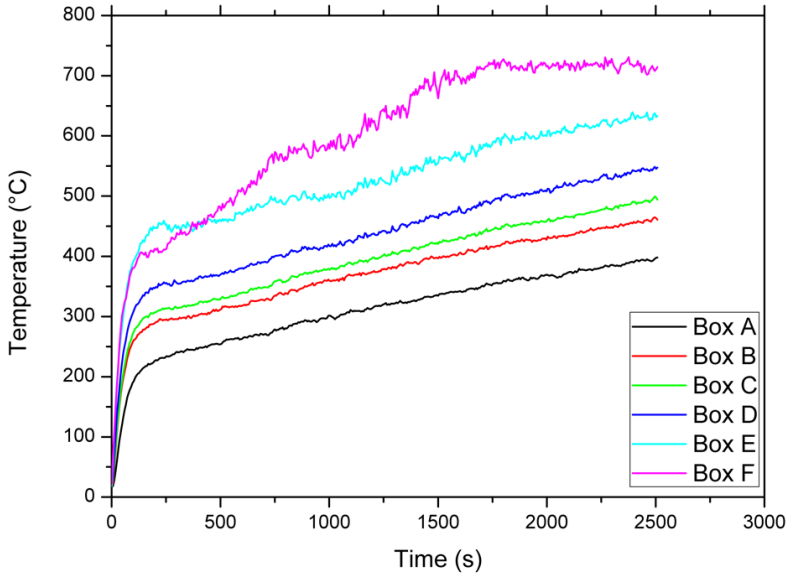

Figure 5.62 Top thermocouple reading from all boxes along the corridor length as a function of time for case BC20W15xH15.

5.4.6 Combustion efficiency

The combustion efficiency over the steady-state period based on the theoretical and the actual HRR is shown in Fig. 5.63 versus the ventilation factor. Data for the cases having the 0.1 x 0.1 m^2 opening are not plotted, since the fire was self-extinguished. The same trend was found for both pan sizes. It is observed that, as expected, the combustion efficiency of the fuel-controlled cases using the small pan (BC20W15xH15 and BC20W50xH50) was of the highest value, approaching unity. The higher value (0.7) was also found for the fuel-controlled case BC30W50xH50 using the larger pan. However, all the ventilation-controlled cases were of combustion efficiency less than 0.7. For the ventilation-controlled cases of both pan sizes, as the ventilation factor increases, the combustion efficiency increases too. This is attributed to the fact that more oxygen is available for combustion as more fresh air enters the corridor when increasing the opening size.

It is interesting now to show the combustion efficiency against the equivalence ratio, φ, as this was calculated in §5.4.3.2. The data for all the cases when fire sustained are plotted in Fig. 5.64. The data obtained show a good correlation between the combustion efficiency and the equivalence ratio; combustion efficiency reduces as the equivalence ratio increases from 1 to 2.5. The highest combustion efficiency was

found for the fuel-controlled cases. For most of the ventilation-controlled cases the combustion efficiency is between 0.5 and 0.67.

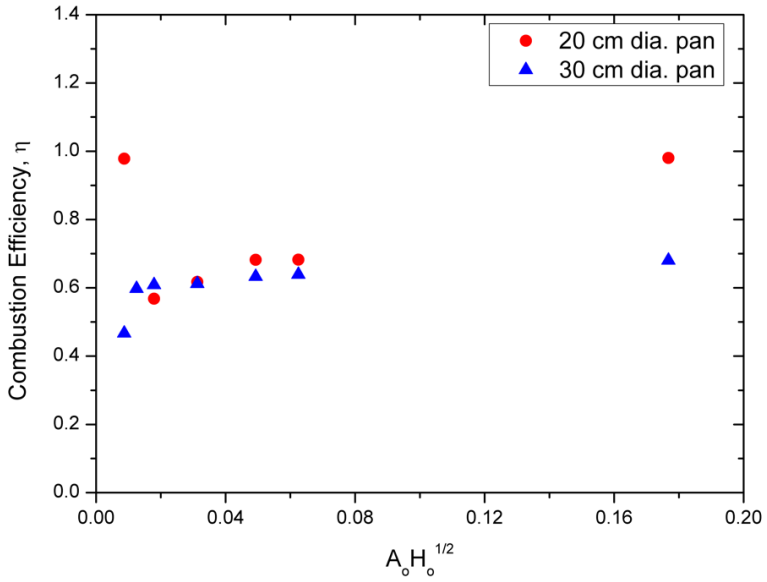

Figure 5.63 Combustion efficiency versus the ventilation factor for the cases that fire sustained and pool fire was placed at the rear end of the corridor.

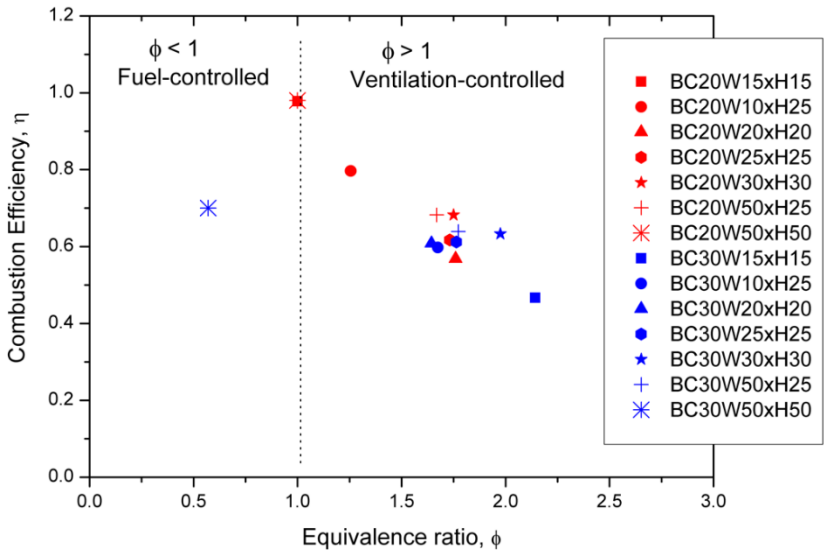

Figure 5.64 Combustion efficiency versus the equivalence ratio for the cases that fire sustained and pool fire was placed at the rear end of the corridor.

5.4.7 External burning

As explained in Chapter 2, external burning can occur in both ventilation-controlled and fuel-controlled fire scenarios. However, this section focuses on ventilation-

controlled fire scenarios as most of the cases were investigated using the pool fire close to the rear closed end of the corridor.

5.4.7.1 Heat release rate after ejection of flames

In a ventilation-controlled enclosure fire, façade flames are produced by the combustion of the unburnt fuel leaving the enclosure. Therefore, façade flames exist only if the total heat released is larger than the heat released inside the enclosure (Lee et. al., 2007; Drysdale, 2011; Delichatsios 2014).

In the corridor enclosure in which current investigation was performed it was found that the heat released inside the enclosure is lower than the 'classic' $1500A_oH_o^{1/2}$. Considering the values of ventilation coefficient, C, as they are depicted in Fig. 5.53, the flames are established outside the corridor if:

$$\dot{Q}_{act} > 3000 \times C \times A_o H_o^{1/2}$$

Until ignition of the fuel leaving the corridor, the HRR is constant (see Fig. 5.51) 'during Region II'. Thus, the excess HRR, $\dot{Q}_{ex}$, can be calculated as the difference between the steady heat release rate ($\dot{Q}_{act}$) in 'Region III' and that at the end of 'Region II'. The relevant values are shown in Table 22.

$$\dot{Q}_{ex} = \dot{Q}_{act} - 3000 \times C \times A_o H_o^{1/2} \quad (5.10)$$

Table 22 Measured (actual) and excess HRR for cases where flames appeared outside.

Test case	$\dot{Q}_{act}$ (kW)	$\dot{Q}_{ex}$ (kW)
BC20W25xH25	39.0	2.5
BC20W30xH30	68.5	11.1
BC20W50xH25	74.0	9.0
BC30W25xH25	39.5	2.9
BC30W30xH30	70.0	14.0
BC30W50xH25	77.0	9.0

It is interesting to note here that in all cases studied, the actual HRR measured in the hood is less than the theoretical HRR calculated from the fuel's mass loss rate (see Fig. 5.27-5.28). Thus, the combustion efficiency is less than unity as shown in Fig. 5.63. It is possible that part of the unburnt fuel leaving the corridor doesn't take part

in the combustion process which occurs outside. Thus, some fuel escape to the duct of the hood fast enough before mixing with oxygen.

5.4.7.2 Carbon monoxide concentration in the duct

After examination of the HRR data measured in the duct of the hood it was revealed that external burning follows a rapid decrease of the CO which is measured in the duct. The HRR and the carbon monoxide (CO) concentration in the duct for the cases in which flames were ejected are depicted in Fig. 5.65. The start of Region II corresponds to a transition from fuel-controlled to ventilation-controlled conditions where the combustion efficiency decreases due to insufficient oxygen availability. This also results in an increasing production of intermediate products, e.g. *CO*. During Region III, the concentration of intermediate combustion products, e.g. *CO*, exiting through the opening is decreased due to more complete combustion after external burning.

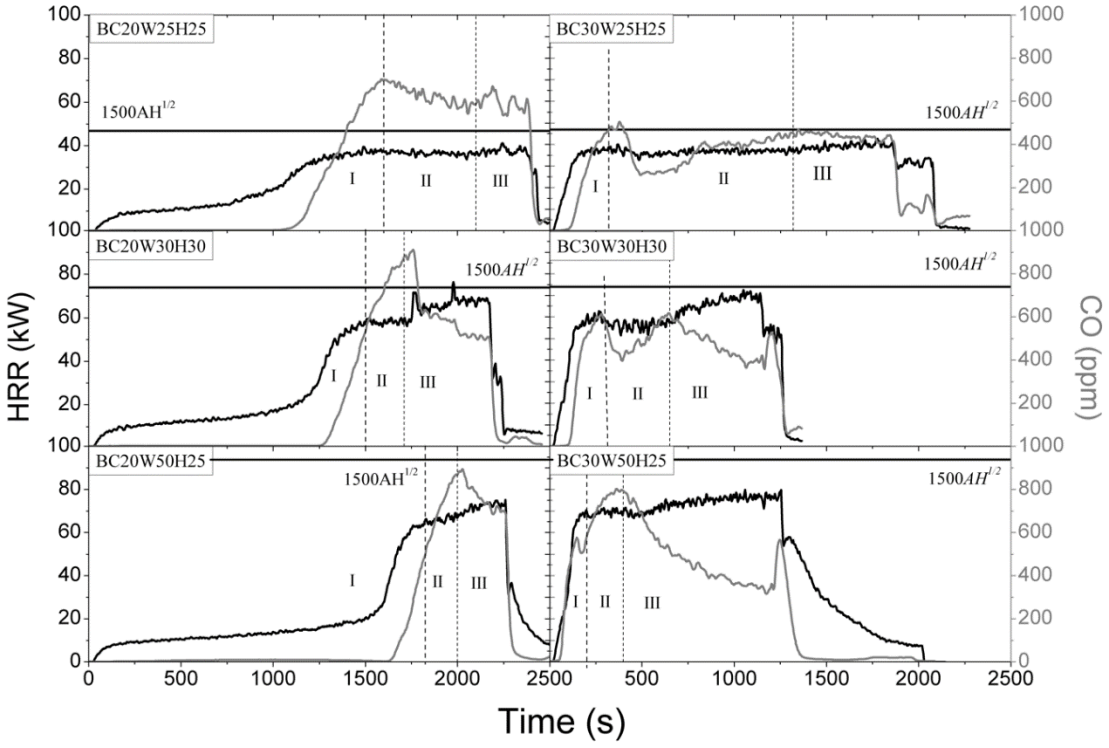

Figure 5.65 Temporal evolution of actual HRR and CO volume concentrations measured in the duct of the hood for ventilation-controlled test cases with flame ejection.

5.5 Conclusions

A parametric experimental investigation of the fire dynamics in a reduced-scale corridor-like enclosure and the heat exposure on the facade was performed in this chapter. The pool fire source was placed inside Box F -close to the closed end of the corridor- and effects of pool and ventilation size were studied. The findings relied on visual observations, theoretical and actual HRR profiles, temperature and heat flux distribution within the enclosure and flame height and heat flux measurements on the façade of the enclosure.

The main findings of this chapter are:

1. The time needed for steady-state conditions to be established inside the enclosure is mainly influenced by the size of the pan, as using the larger pan the walls of the corridor are heated faster, therefore steady conditions are established in a shorter period (§5.4.1). Similar behaviour was found using the pans inside the Box A as discussed in the previous chapter.
2. A linear relation between the $\dot{m}_T/A_f$ and $A_o H_o^{1/2}/A_f$ exists (Eq. 5.5 and Fig. 5.48) and the proportional constant in the present work for a 6:1 aspect ratio corridor is found about 2/3 of the one obtained for cubic-like enclosures.
3. The heat released inside the corridor for the ventilation-controlled cases was found lower than the 'classic' value $1500 A_o H_o^{1/2}$. For the current experiments the proportional factor was found 1110 instead of 1500 kW/m$^{5/2}$. This result is based on the finding that the ventilation coefficient, C, decreases for large openings; in the present study was found to be approximately 0.39 for most of the cases. This suggests that inflow air entering the corridor is less than the proposed given by Eq. 5.6.
4. The lower values of both mass pyrolysis rate and mass inflow rate found in the current study for corridor enclosures compared to the values proposed in literature for cubic-like enclosures (see discussion related to Eq. 5.4 and 5.5) are due to the formation of a non-uniform temperature profile inside the enclosure. Thus, it is suggested that the well-mixed fire environment (Kawagoe, 1958) does not properly describe the temperature formation inside the corridor and should be used cautiously.

5. Experiments of equivalence ratio higher than unity, under ventilation-controlled conditions, characterised by flame detachment; whereas no detachment was noticed during experiments under fuel-controlled conditions. In ventilation-controlled cases the flame was detached the pool propagating towards the opening. This observation reveals that the flames seek available oxygen for combustion moving towards the opening. Same finding was observed in previous experiments conducted using gaseous burner.
6. As expected, the combustion efficiency during steady-state period was found to increase as the ventilation factor increases, as there is more available oxygen for combustion. In addition, a linear relationship between the combustion efficiency and the equivalence ratio exists for $1<\varphi<2.5$.
7. A simple approach was followed for calculating the excess HRR in ventilation-controlled cases, used also in previous research. It was also validated that external burning resulted in a sudden decrease of carbon monoxide measured in the duct of the hood.
8. Regarding the flames ejecting through the opening, the flame height was found to increase with an increase in the theoretical HRR. It was also shown that heat fluxes on the façade were higher on the centreline of the exposed façade for all cases, except the one using the fully-open opening and the larger pan. In this particular case, the flames emerging through the opening were seen to emerge as two separate fire plumes, thus the major heat exposure of the façade was deviated from the centreline (see Fig. 5.45).

CHAPTER 6

COMPARATIVE ANALYSES OF EFFECTS OF POOL LOCATION AND FUEL TYPE

6.1 Introduction

It has been shown in previous chapters that the ventilation geometry and pool fire size play a significant role in the burning rate, HRR and thus, the fire dynamics of a pool fire within a corridor. In this chapter, further detailed analyses are presented to examine the effects of (i) fire location by comparing the results obtained in Chapters 4 and 5 with the fire located at the front and rear end of the corridor-like enclosure and (ii) fuel type by comparing the results obtained using liquid pool fires in this work with those obtained using gaseous fuels.

As highlighted by a number of researchers (Lee, 2006, Parkes, 2009; Drysdale, 2011) based on experiments using rectangular- or cubic-like enclosures, the location of a fire within the enclosure can also have a distinct effect on the fire development. In this work, this effect is addressed by placing the pool (i) at the rear end of the corridor (box F), far from the opening and (ii) at the first box of the corridor (box A), very close to the opening. The detailed results for these two cases have been presented in Chapters 4 and 5 respectively. In this chapter, a detailed comparison between the two cases is presented.

Another important effect, which will be discussed in this chapter, is the fuel type. Performing liquid (ethanol) pool fire experiments in a corridor enclosure is considered as a step further for investigating fire development within corridors, as using a simpler fire source such as a gaseous burner can only simulate simple fire scenarios in which the burning rate of the fuel is prescribed. However, this is not the case on real fire accidents, where the fire burns at an unknown rate. Consequently, appropriate comparisons are made between the present work with previous experimental works performed using the same enclosure but with a propane gaseous burner as the fire source (Beji, 2009; Ukleja, 2012), in order to highlight the effects of the fuel type on the fire dynamics in a corridor enclosure and subsequent externally venting flames (EVF).

Section 6.2 presents a summary of the experimental set-up for the experimental work performed using two different locations of the pool within the corridor, as well as that from previous work using a gaseous burner. In section 6.3, results and analyses

regarding the pool location effect are presented. Section 6.4 provides an analysis of the fuel type influence on the fire development within the corridor. Finally, in section 6.5, a summary of all findings is given.

6.2 Experimental Set-up

6.2.1 Experimental set-up of the present study considering two different pool locations

Experiments performed by placing the pool fires in the middle of two different boxes within the corridor: (i) at the front of the corridor (box A) and (ii) at the rear end of the corridor (box F). Thus, the distance between the opening and the centre of the pool fire was either (i) 0.25 or (ii) 2.75 m. Detailed description of the measurements taken can be found in Chapter 3. The layouts of the experimental rig used in the two different locations; Box A and Box F, are given in Fig. 4.1 and 5.1 respectively. A summary of the experiments conducted by placing the pool fires inside the front box (A) are given in Table 11 and inside the rear box (F) are given in Table 15, as presented in previous chapters. As reported in Chapter 3, none of the experiments was left for more than 50 min in order not to damage the experimental rig's walls. It is reminded that three cases of placing the pool inside Box A, namely FR20W30xH30, FR20W50xH25 and FR30W50xH50, did not reach steady-state conditions as explained in Chapter 4.

6.2.2 Summary of the experimental set-up of previous researches using gaseous burners as fire source in corridors

Beji (2009) and Ukleja (2012) performed experiments in the same corridor rig using a gaseous sandbox propane burner of dimensions 0.1 x 0.2 m^2 with its longer side being parallel to the opening, studying only ventilation-controlled fires by controlling the mass flow of fuel burning inside the enclosure. Table 23 shows a summary of the experimental set-up and the measurements performed in Beji (2009), Ukleja (2012) and the present study.

Table 23 Detailed summary of the experimental set-up and the measurements performed in Beji (2009), Ukleja (2012) and the present study.

	Beji (2009)	**Ukleja (2012)**	**Present study**
Fuel type/location	Propane/Front-Rear	Propane/Rear	Ethanol/Front-Rear
Opening dimensions, W_o x H_o (m^2)	0.10 x 0.25, 0.2 x 0.2, 0.25 x 0.10, 0.075 x 0.20	0.075 x 0.20, 0.075 x 0.30, 0.10 x 0.25, 0.2 x 0.2, 0.25 x 0.10	0.10 x 0.10, 0.15 x 0.15, 0.1 x 0.25, 0.2 x 0.2, 0.25 x 0.25, 0.3 x 0.3 0.5 x 0.25, 0.5 x 0.5
Measurements performed			
HRR in the hood	√	√	√
Gas temperature inside the enclosure	√	√	√
Gas temperature at the opening	√	X	X
Heat flux on the floor	√	X	√
Heat fluxes on the façade	√	X	√
Flame height	√	X	√
Concentration of gases inside the corridor	X	√	X
Smoke concentration inside the enclosure	X	√	X
Velocity of gases inside the corridor	X	√	X

6.3 Effects of fire location

6.3.1 Self-extinguishment of the fire

For all the cases using the smallest opening geometry, 0.1 x 0.1 m^2, the fire couldn't sustain for a long period after ignition and was self-extinguished. This observation was made regardless the pool location and the pool size. For example, the theoretical and actual HRR profiles for the cases FR30W10xH10 and BC30W10xH10 are depicted in Fig. 6.1. Using this opening, the fire was self-extinguished after 3 min with the pool fire placed in the front box and after 4 min with the pool fire placed at the rear end of the corridor. The HRR measured in the hood was larger with the pool fire placed at the rear, far from the opening, reaching 12kW, but it was not sufficient for the fire to sustain.

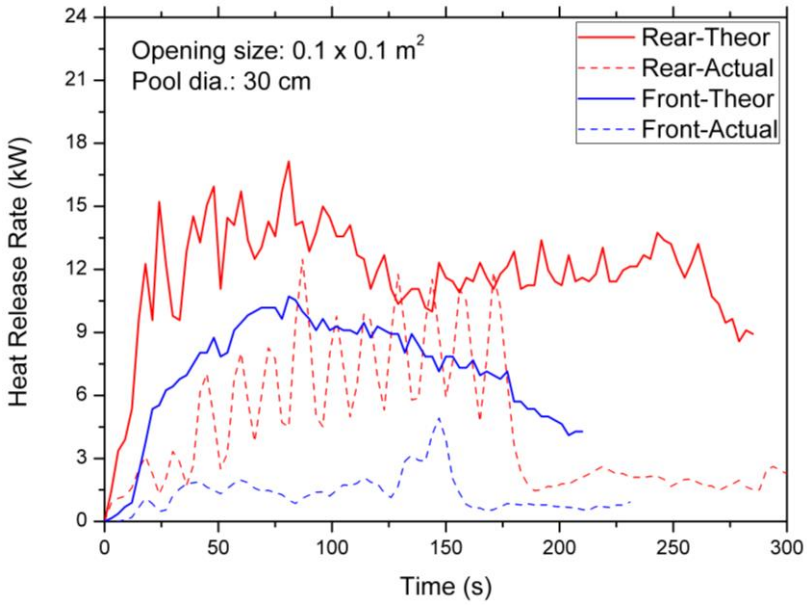

Figure 6.1 T|heoretical and actual HRR profiles for both pool fire locations using the 30 cm dia. pan and having the 0.1 x 0.1 m^2 opening; fire was self-extinguished.

When the fire was placed far from the opening, there was not sufficient air reaching the rear end of the enclosure to mix with the fuel for combustion. However, when the pool fire was placed inside the front box of the corridor, another possible reason for self-extinguishment was observed. As explained in §4.3.3.1, the height of the pan, could also contribute to the self-extinguishment. As the height of the opening (0.1 m) was slightly larger than the pans' walls (rim at 0.065 m), the wall of the pan acts like a physical boundary preventing the fresh air from reaching the fuel surface (see Fig. 4.7). For this reason, it would be interesting to perform experiments in the future with the pool fire surface flushed with the floor of the corridor to address more precisely this effect.

6.3.2 Burning rate and HRR

The MLR (g/s) during the steady-state period of burning are shown in Table 24 for all cases tested for both fire locations, which shows a significant effect of the fire location on the burning rate of the fuel, thus the burning behaviour of the fire within the corridor, with respect to the ventilation factor. The relative difference (%) of the MLR measured by placing the pans at the rear end of the corridor compared to the one measured with the pans placed at the front is also included.

Table 24 Mass loss rate (g/s) for all cases that fire sustained during steady-state period and its relative difference (%) moving the pans from the front box to the rear end of the corridor.

W_o x H_o (m^2)		0.15 x 0.15	0.1 x 0.25	0.2 x 0.2	0.25 x 0.25	0.3 x 0.3	0.5 x 0.25	0.5 x 0.5
$A_oH_o^{1/2}$		0.0087	0.0125	0.0178	0.0312	0.0492	0.0625	0.1767
20 cm dia. pan	**FRONT**	0.36	0.48	0.64	1.04	0.82*	0.96*	0.43
	REAR	0.42	0.94	1.38	2.36	3.75	4.05	0.40
	%	14	92	114	126	357	321	-8
30 cm dia. pan	**FRONT**	0.56	0.96	0.83	1.59	2.81	3.81	3.40*
	REAR	0.88	1.25	1.35	2.41	4.13	4.50	5.60
	%	56	30	62	51	46	18	64

*cases which did not get steady (end values taken into account -see Chapter 3).

Generally, it is observed that for both pan sizes the MLR increases as the pan was moved from the front to the rear. This result is due to a combined effect of the radiation enhancement from the rear wall of the corridor back to the fuel surface of the pan and higher gas temperatures as a result of reduced heat losses through the opening. This is clearly shown in Fig. 6.2 comparing the burning rate during steady-state period versus the ventilation factor, both normalised by the area of the pool. Results for free-burn cases are also included.

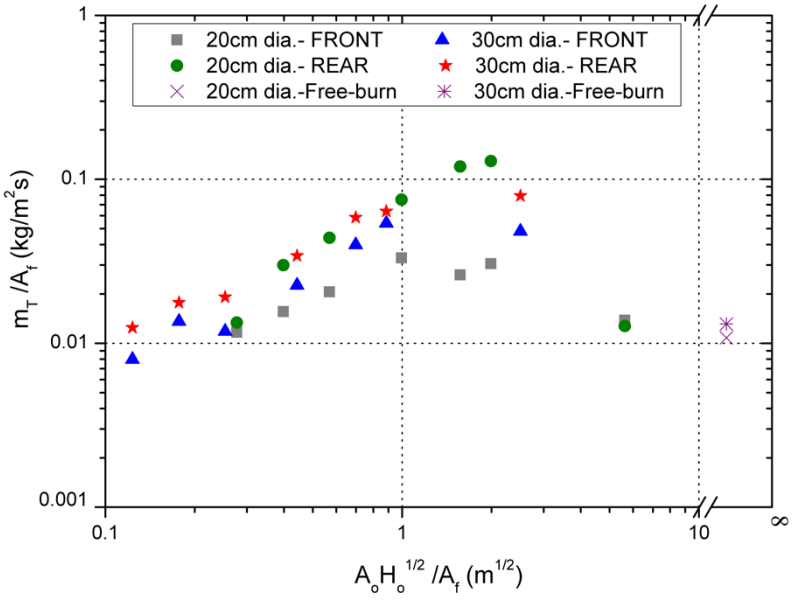

Figure 6.2 Mass pyrolysis rate against ventilation factor, both normalised by the fuel area for both locations and both pool sizes used in the present work.

It is observed that for all ventilation factors investigated, the burning rate of the cases with the pool fire at the rear box is higher than those with the pool fire close to the opening. Another possible reason maybe the leaning-over effect of the flame which has been observed previously in pool fires within rectangular enclosures (Steckler et. al., 1982; Parkes, 2009). According to this phenomenon, the incoming flows (air) through the opening could lean over the flame resulting in less radiation feedback from the flame back to the fuel surface. This result is explained by the fact that the area of the pool which is covered by flames decreases, as the incoming air forces the flame to lean-over towards the direction opposed to the opening. This phenomenon is of more importance at the front of the corridor, where the pool fire is closer to the opening; when the pool fire is placed at the rear end, the leaning-over effect pushes the flame to the rear wall of the corridor, enhancing radiation from the boundaries. Visual observations in this study also support this phenomenon.

The only cases in which no difference was found between the two locations are those using the smaller pan (20 cm dia.) with the fully-open opening. In both cases, the fire burns like in open-conditions with the steady-state burning rates similar to the free-burn value as shown in Fig. 6.4. This finding is further reinforced by gas temperature measurements along the corridor showing low temperatures at the lower cold layer. It is also noted that the burning rate against the ventilation factor for both locations

using the two pans follow the same trend as those reported in literature (Delichatsios et. al., 2004; Drysdale, 2011; Delichatsios, 2014). The burning rate initially increases with an increase of the ventilation factor, reaches a peak, and then decreases with a further increase of the ventilation factor until it becomes steady for very large openings.

To further investigate the effect of the location of the pool fire on the burning rate, it is useful to compare the results of all the cases using the same opening; 0.3 x 0.3 m^2. The mass loss rate histories for these cases are depicted in Fig. 6.3. The burning rate for the free-burn cases are also plotted for comparison.

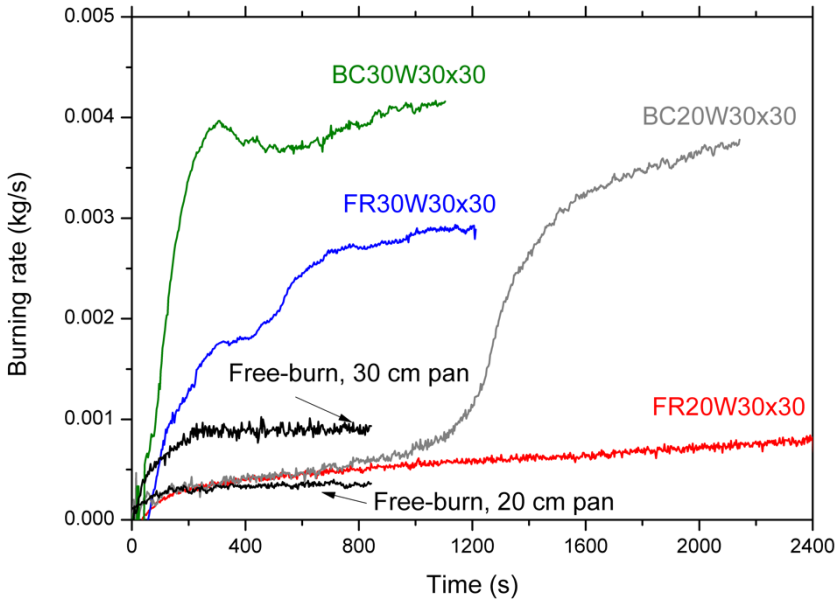

Figure 6.3 MLR histories for FR20H30xW30, FR30W30xH30, BC20W30xH30 and BC30W30xH30 cases.

By using the 20cm dia. pan inside the front box (FR20W30xH30), initially the fire burns in a similar manner to that in open conditions, but after 500 s. the burning rate starts to increase. Because the enclosure was not heated fast enough, the burning rate still increases even after 40 minutes of burning and no steady-state conditions were established within the box. This observation is further supported by the temperature evolution profiles of the highest and the lowest locations inside the boxes where the pool fire was located. The temperature profiles within Box A for the FR20W30xH30 case and inside Box F for the BC20W30xH30 case are compared in Fig. 6.4.

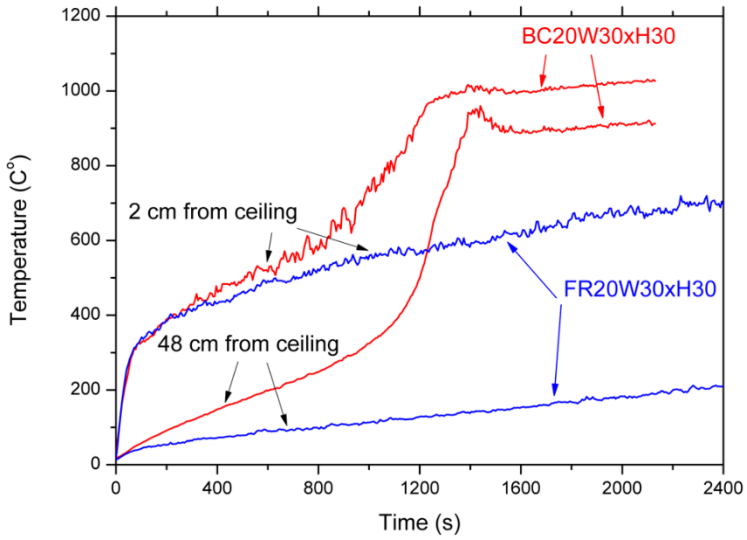

Figure 6.4 Temperature profiles inside Box A for FR20W30xH30 and Box F for BC20W30xH30 at the top and lower location.

The temperatures in both the upper and lower layers increase as a result of increasing mass loss rate/heat release rate but did not reach the steady state after 40minute. Regarding the BC20W30xH30 case, initially the mass loss rate is almost the same as that when the burner is located at the front indicating that there is no hot smoke layer providing extra heat feedback to the fuel surface. After the initial stage, the mass loss rate for the burner placed inside the rear box of the corridor increases up to about five to six times of that for the burner at the front, indicating the formation of the hot gas layer. The time of the increase of the mass loss rate corresponds to the one when the temperatures of the upper and lower layers inside the Box F become steady. For the same opening size, higher MLRs are always observed for the cases when the fire is located at the rear end of the corridor (Box F) in comparison to the cases when the pan was placed in Box A, showing major enhancement to the fire due to radiation feedback from corridor's walls, especially the back wall.

6.3.3 Combustion efficiency

As mentioned in previous chapters, the combustion efficiency of a pool fire is the ratio between the actual HRR (measured in the hood by oxygen consumption method) and the theoretical HRR which is required for complete combustion. In the case of pool fires, the theoretical HRR is estimated by multiplying the burning rate by the effective heat of combustion of the fuel (for ethanol: 26.78 MJ/kg). The combustion efficiency during the steady-state period of burning for all the cases

investigated with the pool fire placed in two different locations is depicted in Fig. 6.5 against the ventilation factor. The cases using the 0.1 x 0.1 m^2 opening are not included as they were self-extinguished. The results reflect the general behaviour of the combustion efficiency in an enclosure fire with respect to the ventilation factor, i.e., the combustion efficiency increases with increasing ventilation factor. The highest combustion efficiency for a given fire size and location is always achieved with the largest opening (0.5 x 0.5 m^2) as sufficient air enters the corridor and the fire is essentially fuel-controlled. The location of the pool fire also affects the combustion efficiency. For the same ventilation factor, it is the case when the fire is placed at the front box that has higher combustion efficiency. As was presented in previous chapter, when the pool fire is closer to the opening it is easier for fresh air to reach the fuel surface, thus burning taking place approaches free-burn combustion (0.97 for both pool sizes). The transition from fuel- to ventilation-controlled conditions while moving the pool towards the closed end of the corridor (far from the opening) explains the reduction of the combustion efficiency for the cases where the pool fire is inside the rear box.

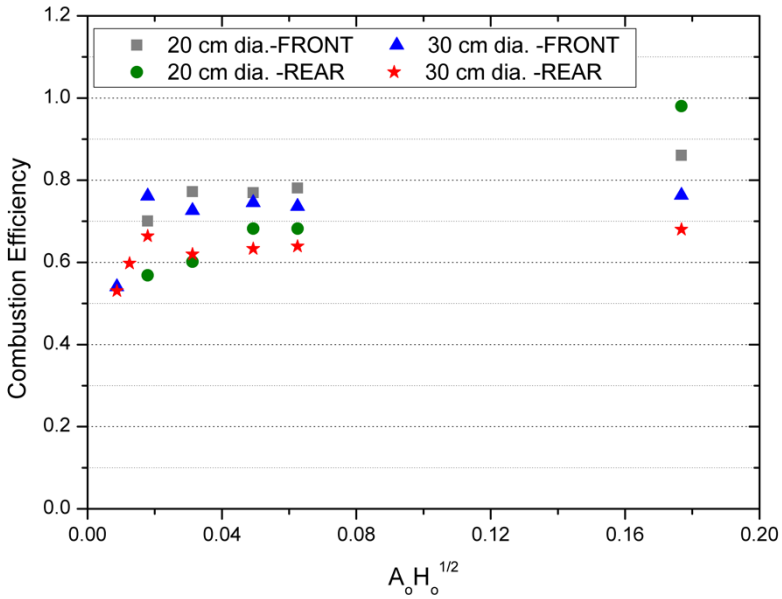

Figure 6.5 Combustion efficiency over ventilation factor for all the cases investigated in this series of experiments.

6.3.4 Gas temperatures and heat fluxes measured inside the corridor

After examining the gas temperature profiles for all different situations depicted in previous chapters, it appears that the temperature distribution inside the enclosure

strongly depends on the size of the opening and the pool's size. In order to evaluate the pool's location influence on the temperature distribution of the gases inside the corridor, the cases using the 30 cm dia. pan with the opening 0.3 x 0.3 m^2 are shown in Fig. 6.6. When the pool is placed close to the opening (Box A), the temperatures constantly increase inside all the boxes except for the one where the pool is (see Fig. 6.6-left). In Box A, steady conditions prevail and the temperatures in the upper layer at 2 cm below the ceiling (AT6) become constant at 750°C, while in the lower location (AT1), 48 cm below the ceiling, it is less than 400°C indicating clear distinction between the two layers. Towards the rear end of the corridor this difference (see FT1 and FT6 respectively) becomes insignificant indicating more mixing and less stratification far from the pool fire.

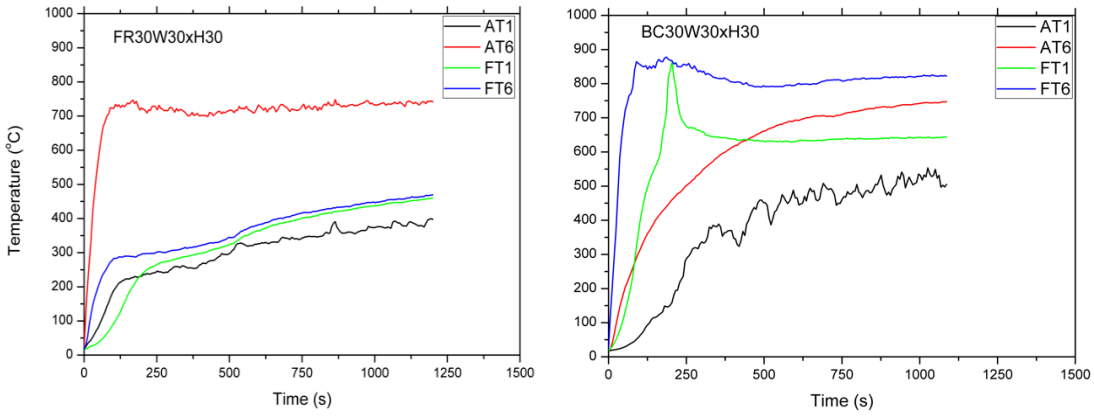

Figure 6.6 Temperature evolution recordings inside Box A and Box F at 2 and 4 cm below the ceiling for the cases FR30W30xH30 (left) and BC30W30xH30 (right).

When the pool is placed far from the opening (Box F), totally different transient profiles are observed regarding the temperature distribution within the enclosure due to the flame detachment and propagation towards the opening. As reported in Chapter 5, the temperatures of the upper location inside the fire box reach a peak and then decrease to a constant value due to flame detachment. This is followed by a temperature peak in Box E. This pattern of flame movement was observed in all the ventilation-controlled cases (see Fig. 5.58). The difference between the two locations of the pan are clearly shown in Fig. 6.7, in which a visualization of the temperatures inside the corridor is depicted for both cases. The temperatures depicted are at 120, 400 and 900 s. Clear distinction is noticed between the hot and cold layers especially at 400 s. This distinction still exists when steady conditions are prevailed (900 s).

The detachment of the flames is also observed for the BC30W30H30 case, as the highest temperatures during steady-state conditions are found inside Box D, 80 cm from the burner. The gaseous temperatures recorded during steady-state conditions inside the fire box are much higher in cases where the pool was placed at the Box F of the corridor. This is attributed to the location of the fire source, as when the pan was placed close to the rear end of the corridor the combustion takes place mainly inside the corridor. However, as shown in Chapter 4, when the pans were placed close to the opening, the flames are ejected shortly after ignition and most of the combustion takes place outside.

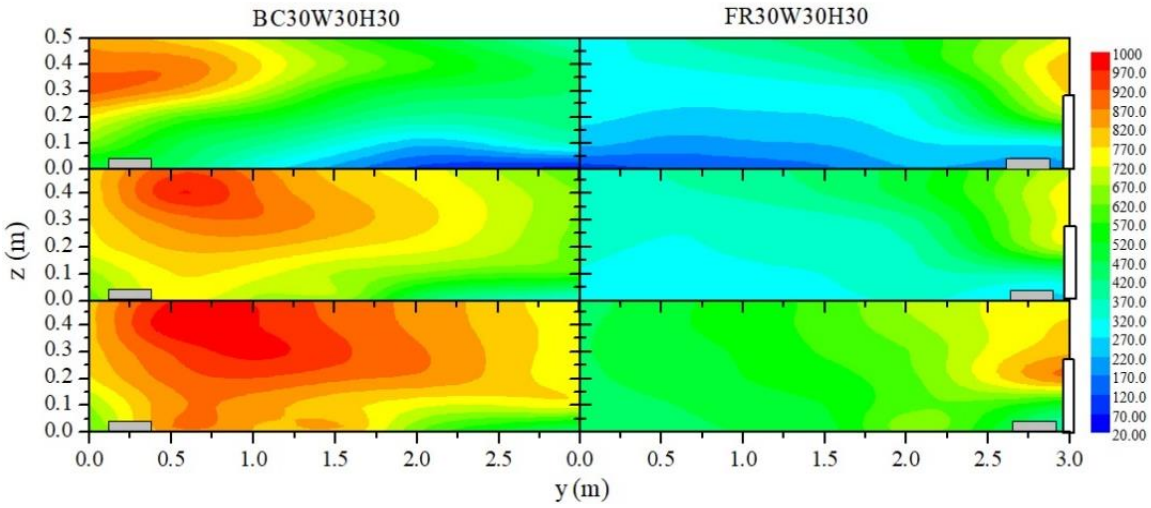

Figure 6.7 Spatial visualization of gaseous temperature at the interior of the corridor for test cases F30W30H30 (left) and B30W30H30 (right) for 120, 400 and 900s.

The temperature results are further supported by the heat flux measurements. Figure 6.8 show the heat fluxes inside Boxes B and F for the cases when the fire is located in Box A for two pool sizes but with the same opening (e.g. 0.25 x 0.25 m^2). When the pool fire was placed inside the front box (Box A), the heat fluxes in other boxes were observed to continuously increase. The heat flux inside Box B for both cases increases more rapidly than that in Box F (close to the rear end of the corridor) because pool was placed close to the opening, and thus burning takes place very close to the Box B. The maximum heat fluxes reached for the two cases were similar, but it took more time for the case with the smaller pool size to reach them due to the slower increase of the heat release rate in the corridor.

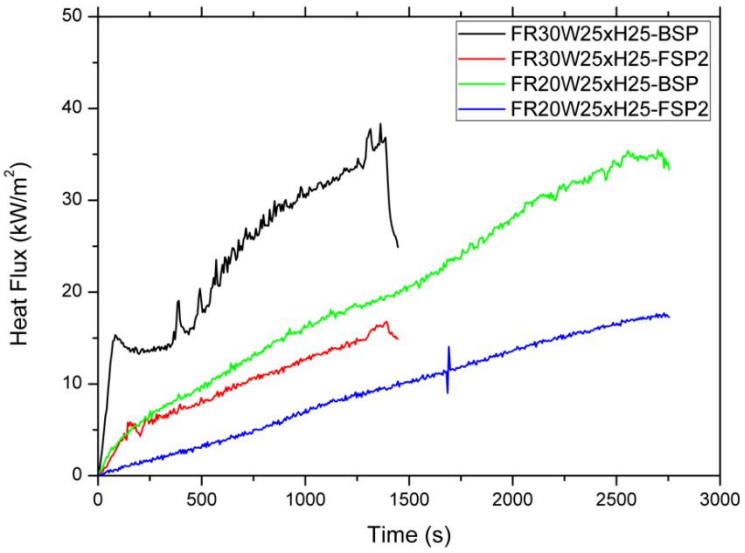

Figure 6.8 Heat flux evolution profiles from Boxes B and F for the cases FR30W25xH25 and FR20W25xH25.

The heat fluxes inside the Boxes A-E for the BC30W30xH30 case are depicted in Fig. 6.9. it can be noted that when the pool was placed inside the rear box (F), the heat fluxes inside the Boxes A-E also increase with time but in a rather different manner compare to that for the cases of the pools placed at the front. Initially, heat fluxes increase at a low rate, as HRR does during the growth period. A rapid increase is followed, as the fire became ventilation-controlled and after the flames come out, the increase rate is reduced. The level of heat flux decreases with increasing distance between the pool fire and the opening. The detachment of the flames from the pool and their movement towards the opening can be supported by the fact that the highest heat flux is found in Box D. This result is also consistent with the temperature profiles; the highest temperatures are recorded inside box D in which the flame was moved to after detachment from the pool. These findings indicate strong influence of the pool location on the fire development within the corridor. It is also interesting to note that higher heat fluxes are noted when the pool fire is closer to the closed end of the corridor than placed closer to the opening. This is due to more fresh air entering the corridor resulting in clear distinction between the upper hot and the lower cold layer within the corridor; temperature measurements of Fig. 6.7 further support this finding.

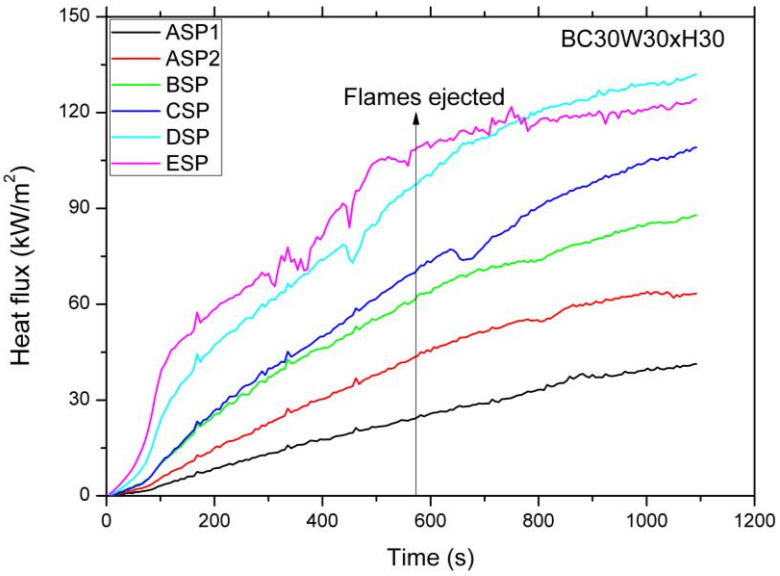

Figure 6.9 Heat flux evolution profiles for the case BC30W30xH30.

6.3.5 External burning

Investigation of the characteristics of the externally venting flames was implemented by measurements of the flame height and heat flux on the façade of the corridor. It was observed that pool location has a major impact on the time when flames appeared outside (see Tables 14 and 20). Using the same opening and placing the pan close to the opening, the flames came out through the opening earlier than by placing the pan close to the rear end of the corridor. The main reason for this behaviour is that in cases of pool fires close to the opening, the flames extended towards the opening and finally appeared outside. Therefore, defining the heat released outside the corridor was not feasible for such cases. On the other hand, for ventilation-controlled cases using the pans at the rear end of the corridor, the plateau of HRR (measured in the hood) which was observed before the flames came out (see Fig. 5.51), allowed an estimation of the heat released outside. It was found that for ventilation-controlled fires the flame height increases as the ventilation factor increases. An interesting phenomenon was observed for both fire locations using the fully-open opening (e.g. 0.5 x 0.5 m^2) that the external flame tends to emerge as two separate flame plumes. Regarding the pool location impact on the heat exposure of the façade, this behaviour using the fully-open opening resulted in higher heat flux off the centreline of the façade; opposed to the rest cases where highest heat flux is always found on the centreline of the façade regardless the pool location. Using the

same opening and pan size, higher heat flux values are found when the fuel pan was positioned in Box A, near the opening.

6.4 Fuel type effect in corridor enclosures

6.4.1 Fire conditions established inside the corridor

Because the main objective of all previous studies using gaseous fuels (Lee, 2006; Beji, 2009; Ukleja, 2012) was to investigate fire phenomena under ventilation-controlled conditions, the prescribed theoretical HRR was always set above the maximum heat released inside an enclosure ($>1500A_oH_o^{1/2}$). However, this is not the case in the present study, as the burning rate of pool fires depends on the radiative feedback of the hot gas layer and enclosure walls to the fuel surface and as a result it is not known prior to the experiment whether the burning conditions would be fuel- or ventilation-controlled . This major difference highlight one of the most important objectives in this work to provide insights into the burning behaviours of pool fires in corridor enclosures.

Figure 6.10 shows a comparison of the theoretical and actual HRRs obtained in the present study (FR30W20xH20) and that in (Beji, 2009) for the case with a maximum theoretical HRR of 30kW. For both cases, the opening size is 0.2 x 0.2 m^2 and the fire source is located inside Box A. The maximum heat release rate inside the enclosure for this opening is $1500A_oH_o^{1/2}$ = 26.78 kW. For the gaseous fuel, when the theoretical HRR of the fire exceeded this value, the fire became ventilation-controlled and flames appeared on the façade at 640s. On the contrary, for the FR30W20xH20 case in this work the theoretical HRR never exceeds the maximum heat released inside the enclosure; fire was fuel-controlled and external flames appeared on the façade after 7 min.

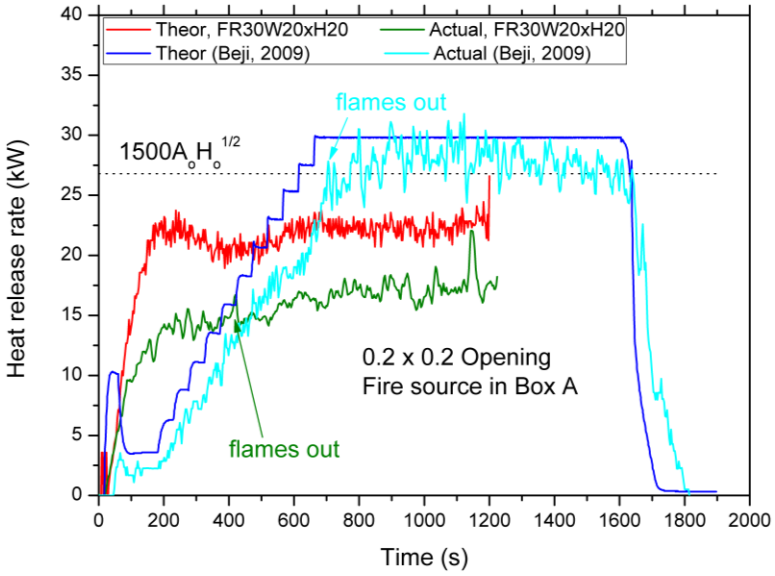

Figure 6.10 Temporal evolution of both theoretical and actual HRR for case FR30W20xH20 (present study) and Test No. 22 (Beji, 2009), using a 0.2 x 0.2 m^2 opening and fire source inside the Box A.

6.4.2 Self-extinguishment of fire

It was found in Beji (2009) that for a gaseous fuel the fire could not be sustained for low ventilation factors (<0.008) when the burner was placed far from the opening, as fresh air entering through the opening could not reach the rear end of the corridor for combustion. However, when the burner was located inside the Box A, fire was sustained even for the cases with low ventilation factors followed by external burning but with low combustion efficiency. By combining the results of Lee (2006) and his own data, Beji proposed that for low ventilation factors (up to 0.008) there is a critical distance between the burner and the opening (1.25m < d_c < 2.75m), beyond which the fire could not be sustained. This critical distance is found not to be applicable for the cases when a pool fire is used as fire source. In the present work, for low ventilation factors (in this study: 0.0081) the fire couldn't sustain, not only when the pool was placed far from the opening, but also when it was placed close to the opening at 0.25 m distance. It is also noted that the same observation was made for both pool sizes. This is due to the fact that the radiative heat feedback from the flame, hot gases layer and enclosure walls is not sufficient to vaporise the fuel. Another possible explanation is that the gaseous burner in (Beji, 2009) was flushed with the floor, whereas the rim of the pool fire is 65 mm from the floor (see discussion prior to Fig. 4.7). Therefore, not only the ventilation factor, but also the distance between the floor and the fuel surface should also be considered.

6.4.3 Fire development in corridor using moderate openings

Figure 6.11 shows a comparison of the theoretical and actual HRRs for the case BC30W10xH25 and those obtained in (Beji, 2009) with a similar theoretical HRR. The prescribed theoretical HRR (through the mass flow rate of the burner) in Beji (2009) was set to 30 kW. It can be observed that for the gaseous burner, the actual HRR increases during the growth period, Region I, and when the fire became ventilation-controlled reaching a plateau equal to the maximum heat released inside the enclosure for this opening (18.75 kW). During Region II, the theoretical HRR is higher than the measured HRR, indicating that the fire was controlled by ventilation as burning only takes place inside the corridor. At the end of this period, flames ejected through the opening, indicating the start of Region III. During the Region III, the actual HRR almost reaches the theoretical one.

In the test case BC30W10xH25 of the present study, during Region I, as the fire grows the theoretical and actual HRRs are almost identical and combustion efficiency is close to unity as all the fuel is consumed within the corridor. During Region II, the actual HRR gradually increases and eventually reaches the maximum heat released inside the enclosure, a behaviour also observed during Region II in experiments performed in (Beji, 2009). For this case, no flames were observed outside the enclosure (thus no Region III was noted), whereas for the gaseous burner flames ejected from the enclosure at around 1500s indicating the start of Region III.

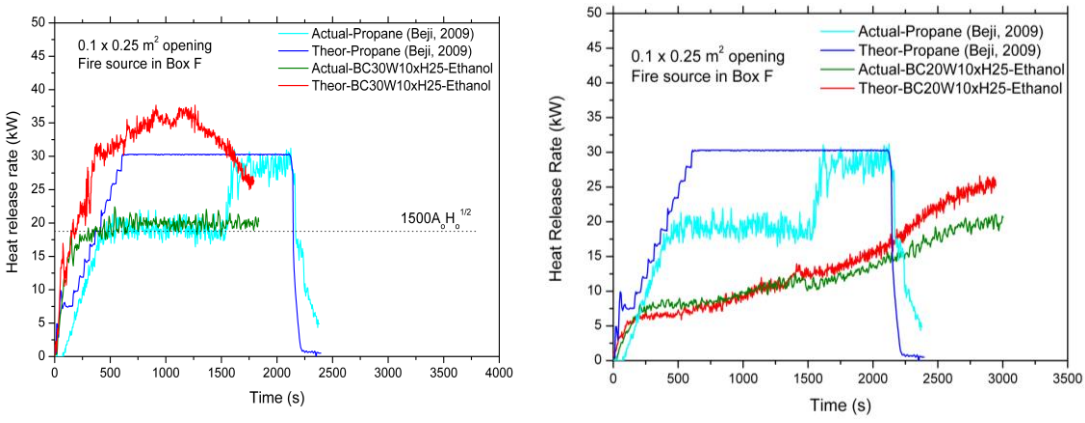

Figure 6.11 Temporal evolution of both theoretical and actual HRR for a case with the 0.1 x 0.25 m^2 opening using propane (Beji, 2009) and ethanol inside the Box F using the 30 cm pan (left) and the 20 cm pan (right) of present study.

Similar observations were found comparing the same test case of Beji's study with the case using the same opening but the smaller pan of this study, as depicted in Fig. 6.11 (right). Even though the time it takes to reach steady-state burning within the corridor is significantly longer using the small pan, the results agree well with previous observations with the larger pan size.

6.4.4 Flame detachment from burner and propagation towards the opening

As discussed in Chapter 5, when the pool fire was placed far from the opening, flame detachment from the burner was observed under ventilation-controlled conditions and flame was found to move towards the opening seeking available oxygen for combustion. This observation was made based on gas temperature measurements at the top location inside each box with the temperature peaks at these locations indicating the presence of the flame. The same method was used in (Beji, 2009; Ukleja, 2012) for gaseous fires, where it was found that the flame propagates along the corridor until it appears outside the enclosure and burning only takes place in the box close to the opening.

In comparison, when a pool fire is used as in this work, it was observed that the flame detaches from the pool surface and propagates towards the opening. However, there are still flames inside the enclosure and the flame anchors in Box C or Box D, even for the cases when burning was observed outside the corridor. This is due to the fact that as the flame moves away from the fire box, the temperature in the fire box decreases resulting in a decrease in the heat feedback to the fuel surface and as a consequence a reduction of the burning rate. These two effects compete against each other until a dynamic balance is reached. The top temperature profiles for the two cases investigated previously, using the 0.1 x 0.25 m^2 opening and fire source placed inside Box F are depicted in Fig. 6.12. As shown in the figure, the flame propagates towards the opening using the gaseous burner and the last peak in Box A indicates the time when the flames appeared outside the enclosure. However, using the pool fire the flame propagates up to Box C and burning takes place inside boxes C to A. In both cases, the temperature behind the flame decreases denoting the absence of the flame. These temperatures using gaseous fuel reach about 500^{o}C in all boxes (except for Box A where the flame is). Slightly higher temperatures were recorded for the liquid pool fire cases reach about 600^{o}C. Different trends on the temperature profiles

during the growth period are also noticed. Using the gaseous fuel, the temperatures constantly increase until a peak is observed and then decrease when flame moves towards the next box. In the pool fire case, there is a sudden increase of temperature during the growth period and then the temperature inside Box F becomes steady for almost 600 s before the detachment of the flame. Inside the other boxes, after the initial sudden increase, temperature keeps increasing steadily until reaching the peak.

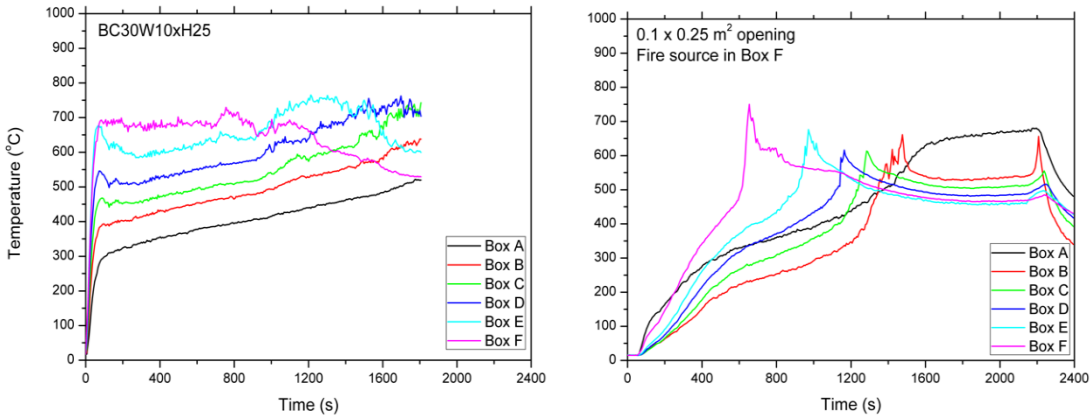

Figure 6.12 Temperature evolution at the top location of each box for two cases having same opening and burner location but different fuel; namely the BC30W10xH25 case of the present study (left) and the Test No. 3 of Beji's study (2009) (right).

Based on temperature measurements we were able to calculate the velocity of flame propagation towards the opening, as described in §5.4.4.1. The deduced velocity of flame propagation in this work is plotted in Fig. 6.13 against the equivalence ratio, φ, along with the data from previous work (Ukleja, 2012) using a propane gaseous burner as the fire source. It can be seen that the present results are comparable to those in (Ukleja, 2012). However, the present data are only for low equivalence ratio values due to the nature of fire and therefore further examination of cases using pool fires with larger equivalence ratios would be useful for a more complete comparison.

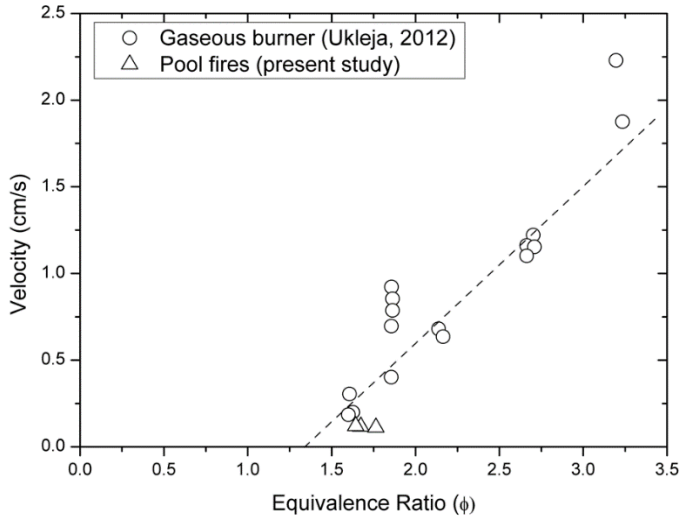

Figure 6.13 Velocity of flame propagation for pool fires (present study) and for gaseous burners (Ukleja, 2012) as a function of equivalence ratio (φ).

6.4.5 External burning

External burning is investigated with respect to the flame height and heat flux measurements on the façade for cases when flames appeared constantly outside the enclosure. As the correlation developed previously in (Lee et. al., 2007; Beji, 2009; Beji et. al., 2012) only apply to flames ejecting from a ventilation-controlled fire enclosure, only the same cases are considered here, i.e., the cases when the fire source was placed in Box F. Flame height and heat flux results of these cases were presented in §5.4.7.

6.4.5.1 Flame height

Using Froude scaling (Quintiere, 2006), Lee et. al. (2007) developed a correlation for the flame height of the flames emerging from a burning rectangular enclosure using a gaseous burner. This correlation was further validated by Beji (2009; 2012) using a gaseous burner in corridor enclosures. The same methodology is used in the present work to deduce the flame height correlation which is also compared with previous results using gaseous burners. The steps followed are described as follows:

1. Definition of the reference base level (i.e., the height of the neutral plane), Z_n. In enclosure fires, it is generally defined as 0.4 - 0.5 of the height of the opening, H_o (Lee et. al., 2007, Drysdale, 2011; Beji et. al., 2012;

Asimakopoulou et. al., 2015). In this work the neutral plane is considered $0.5H_o$.

2. Calculation of the length scale of the flame (Eq. 2.23a) based on previous work in enclosures using gaseous fuels (Lee et. al., 2007; Beji et. al., 2012; Delichatsios, 2014):

$$\lambda_1 = \left(A_0 \sqrt{H_0}\right)^{2/5}$$

3. Estimation of the dimensionless external heat release rate outside the enclosure, $\dot{Q}^*_{ex}$ using Eq 6.1. The estimation of the external HRR was discussed in §5.4.7.1. For the cases considered, the values of external HRR are shown in Table 5.8.

$$f\left(\dot{Q}^*_{ex}\right) = f\left(\frac{\dot{Q}_{ex}}{\rho_\infty c_p T_\infty \sqrt{g} {l_1}^{5/2}}\right) \tag{6.1}$$

4. Apply the correlation:

$$\frac{Z_f - Z_n}{l_1} = f\left(\dot{Q}^*_{ex}\right) \tag{6.2}$$

By performing the above procedure for all the cases with external burning , Fig. 6.14 plots the dimensionless flame height, Z_f/l_1, against the dimensionless external heat release rate $\dot{Q}^*_{ex}$. Additionally, experimental data of previous works using gaseous burner inside i) the same box of the corridor (Beji, 2009; Beji et. al., 2012) and ii) a rectangular enclosure (Lee et. al., 2007) of aspect ratio 1:1 to 3:1, are plotted for comparison. It is demonstrated that the present data applies to small values of $\dot{Q}^*_{ex}$, and the power dependence of the flame height, Z_f, normalised by the length scale, l_1, to the dimensionless HRR, $\dot{Q}^*_{ex}$, is 2/3. This finding agrees with the correlation proposed by Lee et. al. (2006; 2007) and Beji et. al. (2012) using limited data for $\dot{Q}^*_{ex}$<1. For $\dot{Q}^*_{ex}$>1, experimental results using gas burner from both rectangular and corridor geometries corroborate a 2/5 dependence on $\dot{Q}^*_{ex}$ (Lee et. al., 2007; Beji et. al., 2012). However, in this region, no data exist using liquid pool fire as the fire

source, thus verification of such correlation needs to be further investigated in the future.

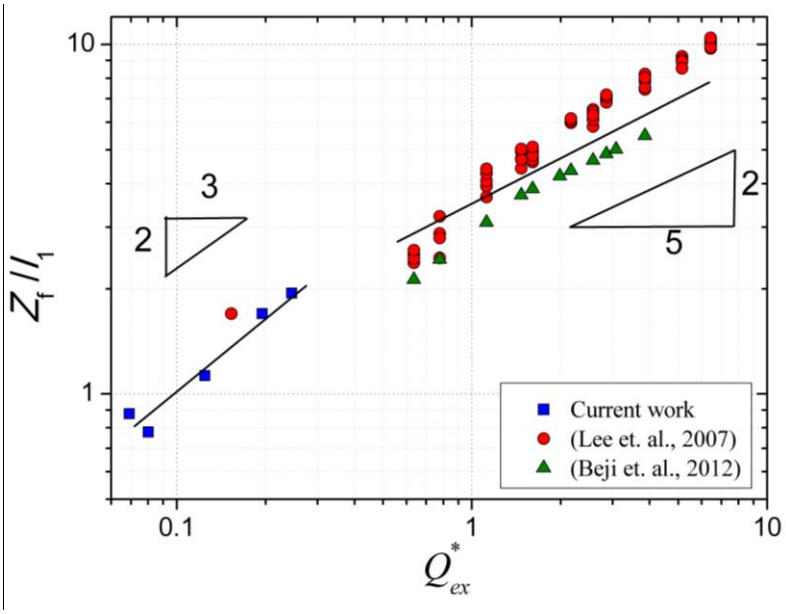

Figure 6.14 Dimensionless flame height, Z_f/l_1, against dimensionless HRR, $\dot{Q}^*_{ex}$, for experimental data of current work using liquid pool fires in corridors and previous works using gaseous burner in i) enclosure geometries of aspect ratio up to 3:1 (Lee et. al., 2007) and ii) corridors (Beji et. al., 2012).

6.4.5.2 Heat flux on the facade

According to Lee et. al. (2007) and Beji et. al. (2012), the experimental heat flux distribution along the centreline above the opening on the façade can be correlated with dimensionless height as:

$$\frac{\dot{q}'' Z_f}{\dot{Q}_{ex}/l_1} = f\left(\frac{Z}{Z_f}\right) \tag{6.3}$$

where $\dot{q}''$ is the heat flux at the centreline of the façade, Z_f is the flame height and Z is the location of each steel plate at the centreline of the façade both measured from the position of the neutral plane, $0.5H_o$, l_1 is the length scale proposed in (Lee et. al., 2007) and $\dot{Q}_{ex}$ is the external HRR as calculated in §6.4.5. The residual effect of the aspect ratio of the opening is accounted for (Lee et. al., 2007; Beji et. al., 2012) by using the exponential factor, $e^{0.6H_o/l_1}$.

The results of the dimensional analysis described above are depicted in Fig. 6.15 along with the data using gaseous burner (Lee et. al., 2007; Beji et. al., 2012) are plotted for comparison. The data is more scattering than that obtained using gaseous burners due to the difficulties in determining accurately the external heat release rate. However, two regions can be observed in Fig. 6.15. In the flame region (i.e., small values of Z/Z_f), the heat flux is constant. In the intermittent flame regime and buoyant plume (i.e., larger values of Z/Z_f), the heat flux decreases with height with a power dependence of -3/2. The following correlations exist for the heat flux for liquid pool fires:

$$\frac{\dot{q}'' Z_f e^{0.6H_o/l_1}}{\dot{Q}_{ex}/l_1} = 0.48 \qquad ; Z/Z_f < 0.7 \tag{6.4a}$$

$$= 0.31(Z/Z_f)^{-3/2} \qquad ; Z/Z_f \geq 0.7 \tag{6.4b}$$

The results agree reasonable well with the results of (Lee et. al., 2007) and (Beji et. al., 2012), as they are mainly located in the intermittent flame regime and buoyant plume regime where Z/Z_f >0.7. Additionally, the power dependence found is similar to these works.

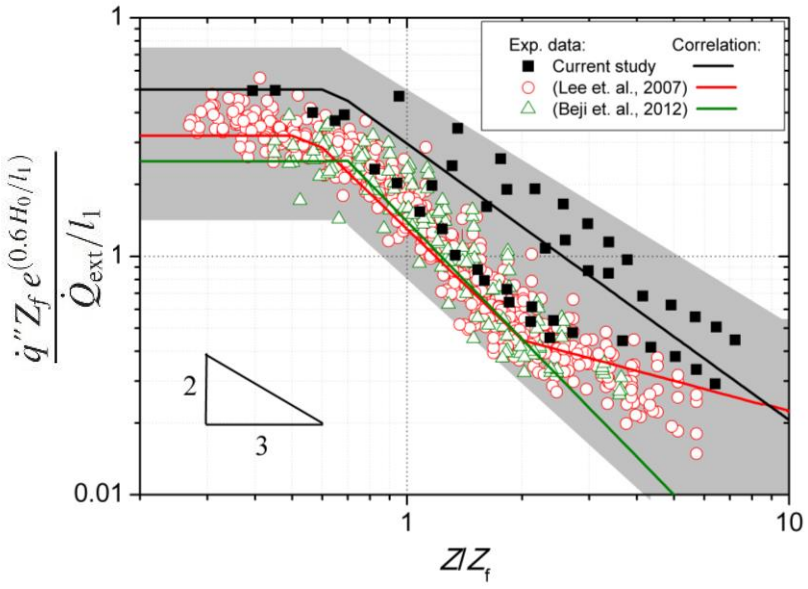

Figure 6.15 Dimensionless heat flux against dimensionless height for experimental data of current work using liquid pool fires in corridors and previous works using gaseous burner in i) enclosure geometries of aspect ratio up to 3:1 (Lee et. al., 2007) and ii) corridors (Beji et. al., 2012).

6.4.5.3 Extrapolation of experimental data to real-scale fire scenarios

It is of high importance to extrapolate the results of laboratory-scale fire experiments to full-scale fire tests, so a better understanding of real fire scenarios can be achieved.

One of the most well-known approach for this is the scaling theory which is used to translate small- and medium-scale experiments into corresponding large-scale systems. Scaling theory regarding fire dynamics has been studied in the past (Quintiere, 1989; 2006) and converts the values into dimensionless groups, depending on the geometric scale that is desired, and applying differential mass and energy conservation laws. The Buckingham Pi theorem (Quintiere, 2006) is implemented in order to scale the fire load in accordance to the dimensions of the experimental enclosure-façade configuration, by developing a complete set of dimensionless Π groups necessary to perform scaling of compartment fires. Based on the correlation developed in Eq. 6.4 regarding the heat flux in the centreline of the façade, it is important to ensure similarity in fire power (HRR) and the radiative heat transfer. According to this theorem, for ensuring similarity of fire power between the model (m) and the prototype (p) it is important to preserve the second group, Π_2, also called Zukoski number Q^*, expressing the ratio of fire power to the enthalpy rate (see eq. 2.8). Based on the Eq. 2.8, the relation between the fire power of the model and the prototype is:

$$\Pi_2 \equiv Q_m^* = Q_p^* \left(\frac{l_m}{l_p}\right)^{5/2} \tag{6.5}$$

Length scales l_m and l_p correspond to the physical dimensions of the model and the prototype system.

Similarity in radiative heat transfer is ensured by preserving the Π_7 group. Using the appropriate model for emissivity the scaling relation between the prototype and the model is:

$$\Pi_7 \equiv \frac{\sigma \varepsilon T_\infty^3}{\rho_\infty C_p \left(g\frac{l_m}{l_p}\right)^{1/2}} \rightarrow \varepsilon \propto \left(\frac{l_m}{l_p}\right)^{1/2} \tag{6.6}$$

As Quintiere (2006) noted, scaling theory in fire scenarios is not completed but it can be applied with assumptions and consideration in order to obtain valid results for large-scale geometries.

Another approach for gaining more insight of the fire dynamics of real-scale fire scenarios, by extrapolating experimental results of laboratory-scale experiments to large-scale more complex geometries has become the increasing trend of implementing CFD modelling. CFD tools are capable of providing information regarding the detailed characteristics of the flow (thermal) field inside and outside (thermal exposure of the façade) the enclosure. Data obtained from laboratory-scale experiments can be compared with numerical predictions using CFD models (such as FDS code -widely used in fire science) to evaluate their accuracy and validate the methodology chosen. Some recent works were based on FDS use solving numerically a form of the Navier-Stokes equations appropriate for low-speed, thermally driven flows; with an emphasis on smoke production and heat transfer from fires (Hwang et al., 2010; Jahn et al., 2011; Boehmer et al., 2009). Numerical work was also performed for corridor enclosures by Beji (2009) who found that FDS failed to predict cases like the configuration that corresponds to a burner placed at the back of the corridor with an opening size of 0.2×0.2 m^2 and a Heat Release Rate of 30 kW. In another study (Ukleja, 2012) it was shown that soot concentrations are underestimated in corridor enclosure geometries.

As CFD modelling has taken the forefront today and since, it is not easy to perform large-scale tests due to many constraints (cost), it is of high importance to properly use such models and develop accurate solutions for fire safety design in complex constructions used today.

6.5 Conclusions

The main conclusions regarding the parameters investigated in this chapter are summarised as follows.

1. The burning rate of pool fires is influenced by the location of the pool fire within the enclosure. It was found that the burning rate, and thus the HRR, is enhanced as the pool fire is moved towards the rear closed end of the

corridor, owing to the higher radiation feedback from the walls and the upper hot gas layer.

2. The temperature distribution inside the corridor strongly depends on the location of the pool fire and as well as on the size of the opening, regardless the type of fuel used. It was shown that only above the half height of the opening temperature becomes uniform along z axis. In addition, there was clear difference between the temperature recorded inside front and rear boxes depending on the location of pool fire. Thus, it is not possible to assume uniform temperature distribution for the interior of the corridor.
3. Fire development inside the enclosure for the same ventilation factor (e.g opening) can be completely different using a liquid pool fire comparing to a gaseous burner. Being able to control the fuel supply rate of gaseous fuels is easy to pre-define the conditions established within the corridor enclosure; either fuel- or ventilation-controlled. However, using a pool fire the burning rate is unknown, thus conditions established cannot be pre-defined. Controlling the HRR of the fire is useful investigating prescribed scenarios, but this could lead to inconsistent results in case of investigating more realistic scenarios.
4. Regarding the parameters affecting the conditions leading to self-extinguishment, for the pool fires it was found that, opposed to findings using gaseous fuels, the distance between the opening and the burner is not the only crucial parameter, but also the distance of the fuel surface and the floor. Future experiments should be performed to address this effect. In addition, for very small openings, using pool fires the fire was self-extinguished regardless the pool location, while for gaseous fuels this was not the case.
5. In the cases when the fire source is located far from the opening, flame detachment from the burner was observed under ventilation-controlled conditions, regardless the fuel type. When such conditions prevailed, the fire was detached the burner and propagated towards the opening seeking for oxygen.
6. Flame height of EVF, Z_f, normalised by the length scale, l_1, was correlated with dimensionless excess HRR calculated by Eq. 6.1, resulting a 2/3 power dependence for small flame heights.

7. A two-region correlation was found to exist between the heat flux distribution along the centreline of the façade and the dimensionless flame height according to Eqs. 6.4a and 6.4b. This correlation was found to reasonable agree with results using gaseous burner in corridors (Beji et. al., 2012) and in rectangular enclosures (Lee et. al., 2007). Unfortunately, it was not feasible to compare those results with other large-scale works, as no data regarding the excess HRR could be obtained (not feasible to measure HRR in large-scale tests).

CHAPTER 7
CONCLUSIONS AND RECOMMENDATIONS

7.1 Conclusions

The aim of this work was to investigate the fire dynamics and burning behaviours of liquid pool fires in a corridor-like enclosure and the burning characteristics of the resulting externally venting flames (EVF). Therefore, an experimental parametric study was performed to study the impact of the ventilation factor, the location and size of the pool fire on the burning rate, heat release rate, mass inflow rate, flame height of EVF and heat flux on the façade. More than 70 experiments were conducted using the experimental rig shown in Fig. 3.1, consisting of a three-metre long corridor-like enclosure having a cross section 0.5 m × 0.5 m and a façade extended above the front panel of the enclosure. Ethanol pool fires were used as fire source, having a constant fuel surface level to achieve steady-state conditions. In the present study eight opening dimensions, two pan sizes and two pan locations were examined. An extensive sensor network was used to monitor the temporal variation of several important physical parameters, such as mass loss and heat release rate, temperatures and heat fluxes inside the corridor and on the façade, gases and smoke production outside the enclosure. Videos were also recorded by a CCD camera facing the façade to determine the height of the external flame. Details of the experimental rig presented in Chapter 3. Repeatability of results was examined in detail and error analysis was presented. The discussions and experimental results were presented in in Chapters 4 and 5 for the cases when the fire was placed close to the opening and at the rear end of the enclosure, respectively. In Chapter 6, further detailed analyses were made for addressing the effects of (i) the pool location by comparing test data with the same fire size and opening dimensions presented in Chapter 4 and 5 and (ii) the fuel type by comparing the experimental data in this work with that in previous studies using the same experimental setup but with gaseous fuels. Based on the analyses made in previous chapters, the major contributions of this work are presented below.

1. The time to establishing steady-state conditions inside the enclosure is influenced mainly by the size of the pan, as using the larger pan the walls of the corridor and the gases inside the corridor are heated faster, therefore steady conditions are established in a shorter period. The ventilation factor

was also found to affect the time needed for steady conditions, but it needs to be further investigated.

2. For steady-state conditions of liquid pool fires inside corridors with an aspect ratio of 6:1, non-uniform gas temperature distribution inside the enclosure was found as shown in Fig. 6.7, opposed to nearly uniform one reported in cubic-like enclosures or in corridors using gaseous fuels. Therefore, it is suggested that the well-mixed fire environment (Kawagoe, 1958) does not properly describe the temperature formation inside the corridor and should be used cautiously.
3. Discussions in §4.4.2 and §5.4.2 revealed that the steady-state mass loss rate (MLR) for smaller openings increases almost linearly with the ventilation factor until reaching a critical point corresponding to the transition from ventilation- to fuel-controlled fires. Subsequently, the MLR decreases as the ventilation factor increases until it becomes constant for very large openings similar to free-burn burning rate. This behaviour is similar to the one proposed by many researchers in the past for cubic-like enclosures (Kawagoe, 1958; Drysdale, 2011; Delichatsios et. al., 2004). In addition, it was found that pan size also influences the burning rate, as higher burning rates were found using the larger pan. The location of the pan also affects the burning rate, as the burning rate (thus HRR) was enhanced when the pan is located close to the rear end of the corridor. This is due to the heat feedback from the closed end wall and the upper hot gas layer. The impact of all parameters to the burning rate is detailed in Table 24.
4. A linear relation between the $\dot{m}_T/A_f$ and $A_o H_o^{1/2}/A_f$ exists (Eq. 5.5 and Fig. 5.48), as reported in previous studies (Kawagoe, 1958; Delichatsios et. al., 2004; Drysdale, 2011; Delichatsios, 2014). However, the proportional constant in the present work for a 6:1 aspect ratio corridor was found about 2/3 of the one obtained for cubic-like enclosures. This finding is due to the non-uniform gas temperature distribution.
5. The combustion efficiency during steady-state period was found to increase as the ventilation factor increases, because there is more available oxygen for combustion entering through the opening. As expected, fuel-controlled cases were of higher combustion efficiency, approaching unity using the fully-open opening. However, the combustion efficiency for all ventilation-controlled

cases is less than 0.7. Using the same pan and same opening, the cases with the pan located closer to the opening were of higher combustion efficiency. In addition, a linear relationship between the combustion efficiency and the equivalence ratio exists for $1<\varphi<2.5$.

6. Regarding the parameters affecting the conditions leading to self-extinguishment, it was found that for the pool fires using very small openings -in the present study using 0.1 x 0.1 m^2 opening- the fire was self-extinguished regardless the pool location and pan size, while this was not the case for gaseous fuels for which a critical distance between the opening and the burner exists for self-extinguishment. Using liquid pool fires, the distance of the fuel surface and the floor was found to also affect self-extinguishment. Future experiments should be performed to address this effect in more detail.
7. For the ventilation-controlled fires, placing the pans at the rear box of the corridor, a simple approach was followed to calculate the heat released inside the enclosure (§5.4.3.2.1) based on the plateau observed before the flames ejected. It was found that the heat release inside the enclosure is less than the maximum value $1500A_oH_o^{1/2}$ which is verified for the cases using gaseous burners in similar and cubic-like enclosures. The experiments showed a proportional factor of 1110 instead of 1500 $kW/m^{5/2}$. This result is based on the finding that the ventilation coefficient, C, decreases for large openings, as in the present study was found to be approximately 0.39 for most of the cases. This suggests that inflow air entering the corridor is less than the proposed, $0.5A_oH_o^{1/2}$, due to non-uniform temperature distribution.
8. Experiments of equivalence ratio higher than unity, under ventilation-controlled conditions, characterised by flame detachment when the pan was located far from the opening. In those cases, the flame detached from the pool propagating towards the opening. This observation reveals that the flames seek available oxygen for combustion moving towards the opening. The same finding was observed in previous experiments conducted using gaseous burners. The main difference was that propagation using liquid pool fires observed between the Boxes F to C, opposed to cases using gaseous burners where flame propagation observed along the whole length of the corridor.
9. Excess HRR in ventilation-controlled cases using the pan inside the Box F, was calculated by extracting the heat released inside the enclosure from the

HRR measured in the hood. It was also validated that external burning resulted in a sudden decrease of carbon monoxide measured in the duct of the hood.

10. Flame height of EVF was calculated based on video recordings using an in-house image processing method as explained in Chapter 3. For both fire locations and using both pan sizes, the flame height increases as the HRR increases. Additionally, a correlation (Eq. 6.2) exists between the flame height of EVF, Z_f, normalised by the length scale, l_1, and the dimensionless excess HRR. The power dependence found in this work is 2/3, which agrees well with the proposed one using gaseous burners for small heat release rates.
11. Heat flux distribution along the centreline of the façade was found to increase with an increase of the ventilation factor. In addition, higher values of heat flux on the façade were observed on its centreline. Only exception was using the fully-open opening, 0.5 ×0.5 m^2; whereas the heat exposure of the façade was higher off the centreline. For larger widths, flames emerge through the opening as two separate fire plumes (as shown in Fig. 5.45). Correlations were developed between the heat flux distribution along the centreline of the façade and the dimensionless flame height, Z_f/Z ((Eqs. 6.4a and 6.4b). The correlations in this work generally agree with the ones obtained using gaseous burner in corridors (Beji et. al., 2012) and in rectangular enclosures (Lee et. al., 2007), although the present data is more scattering due to the difficulties in determining accurately the external heat release rate.
12. In practical, the correlations developed can be used in similar scenarios of fire development in corridor-like enclosures (such as long offices, trains, aeroplanes, tunnels etc.) and the heat exposure of facades in high-rise buildings. The extensive experimental data of the present study can also be used in CFD model validation which would contribute to fire safety design.

7.2 Recommendations for future work

Although the present study accomplished the objectives as outlined in the first chapter of the thesis, further research needs to be conducted to fully understand the fire dynamics in enclosures and fire spread to adjacent infrastructure. Therefore, some recommendations for future work are presented below, which would be highly

beneficial towards better understanding of the fundamentals of fire dynamics in order to develop fire safety design.

1. As a lot of work has been performed using a corridor of aspect ratio 6:1, it would be of great interest conducting experiments in different enclosure geometries. For example, investigation of wider enclosures or long enclosures of L-shape would add more insights of fire dynamics on types of infrastructure widely used in commercial spaces.
2. Due to time restrictions, only one liquid fuel was studied in the present research. However, the impact of different liquid fuels to the fire development and to the heat exposure of facades should be investigated. It would be interesting to use different type of liquid fuels (with different soot propensities) than the alcohol fuel used (ethanol) in this study, such as hydrocarbons (heptane) or kerosene.
3. In this research, the mass inflow rate through the opening was investigated using the actual HRR measured in the hood of the rig. To fully investigate the three-dimensional flow in the vicinity of the opening and thus inflow of fresh air and outflow of hot gases, it is suggested that PIV (Particle Image Velocimetry) systems would be the most appropriate technique to map the velocity field close to the opening.
4. Another aspect to be investigated in similar types of enclosures would be the combustion gases inside the enclosure. Due to resources restrictions, it was not feasible to perform such measurements within the corridor. However, gases concentration measured close to the pool fire would provide more information regarding combustion, flame detachment and propagation, and recirculation of hot gases.
5. Environmental conditions should also be investigated in future research, such as forced draught conditions outside the corridor or the effects of obstructions either facing or parallel to the façade.
6. Finally, CFD models could be used for validation and prediction regarding fire development inside the enclosure and fire spread on the façade. The CFD results would also provide more details on the smoke development, which is a major concern in enclosure fires.

APPENDIX A: LIST OF EXPERIMENTS INVESTIGATED IN THIS WORK

Date	Experiments' Names	Pan Size	Pan Location	Opening's Dimensions WxH (m)	Ventilation Factor ($AH^{1/2}$)
	FB20	20 cm	Free-burn	N.A.	N.A.
	FB30	30 cm	Free-burn	N.A.	N.A.
03/05/16	FR20W10xH10	20 cm	FRONT (Box A)	0.1 x 0.1	0.0032
06/05/16	FR20W15xH15			0.15 x 0.15	0.0087
26/04/16	FR20W10xH25			0.1 x 0.25	0.0125
21/04/16	FR20W20xH20			0.2 x 0.2	0.0179
10/05/16	FR20W25xH25			0.25 x 0.25	0.0313
20/04/16	FR20W30xH30			0.3 x 0.3	0.0493
03/05/16	FR20W50xH25			0.5 x 0.25	0.0625
22/03/16	FR20W50xH50			0.5 x 0.5	0.1767
19/05/16	FR30W10xH10	30 cm	FRONT (Box A)	0.1 x 0.1	0.0032
19/05/16	FR30W15xH15			0.15 x 0.15	0.0087
10/06/16	FR30W10xH25			0.1 x 0.25	0.0125
18/01/16	FR30W20xH20			0.2 x 0.2	0.0179
06/06/16	FR30W25xH25			0.25 x 0.25	0.0313
07/06/16	FR30W30xH30			0.3 x 0.3	0.0493
08/06/16	FR30W50xH25			0.5 x 0.25	0.0625
14/06/16	FR30W50xH50			0.5 x 0.5	0.1767
27/06/16	BC20W10xH10	20 cm	REAR (Box F)	0.1 x 0.1	0.0032
08/07/16	BC20W15xH15			0.15 x 0.15	0.0087
07/07/16	BC20W10xH25			0.1 x 0.25	0.0125
18/07/16	BC20W20xH20			0.2 x 0.2	0.0179
21/07/16	BC20W25xH25			0.25 x 0.25	0.0313
22/07/16	BC20W30xH30			0.3 x 0.3	0.0493
28/07/16	BC20W50xH25			0.5 x 0.25	0.0625
29/07/16	BC20W50xH50			0.5 x 0.5	0.1767
01/08/16	BC30W10xH10	30 cm	REAR (Box F)	0.1 x 0.1	0.0032
02/08/16	BC30W15xH15			0.15 x 0.15	0.0087
01/08/16	BC30W10xH25			0.1 x 0.25	0.0125
23/08/16	BC30W20xH20			0.2 x 0.2	0.0179
24/08/16	BC30W25xH25			0.25 x 0.25	0.0313
29/08/16	BC30W30xH30			0.3 x 0.3	0.0493
30/08/16	BC30W50xH25			0.5 x 0.25	0.0625
29/08/16	BC30W50xH50			0.5 x 0.5	0.1767

APPENDIX B: NOMENCLATURE AND LOCATION OF MEASUREMENT EQUIPMENT

*(x,y,z)=(0,0,0) at the floor level, in the vicinity of the opening

Thermocouples inside the enclosure				**Steel plate meters on the floor and on the façade**			
Thermocouple	**x (m)**	**y (m)**	**z (m)**	**Steel plate meter**	**x (m)**	**y (m)**	**z (m)**
AT1	0.2	0.05	0.02	ASP1	0	0.05	0
AT2	0.2	0.05	0.1	ASP2	0	0.45	0
AT3	0.2	0.05	0.2	BSP	0	0.75	0
AT4	0.2	0.05	0.3	CSP	0	1.25	0
AT5	0.2	0.05	0.4	DSP	0	1.75	0
AT6	0.2	0.05	0.48	ESP	0	2.25	0
BT1	0.2	0.95	0.02	FSP1	0	2.55	0
BT2	0.2	0.95	0.1	FSP2	0	2.95	0
BT3	0.2	0.95	0.2	P1	0	0	0.38
BT4	0.2	0.95	0.3	P2	0.1	0	0.38
BT5	0.2	0.95	0.4	P3	0	0	0.48
BT6	0.2	0.95	0.48	P4	0.1	0	0.48
CT1	0.2	1.45	0.02	P5	-0.1	0	0.63
CT2	0.2	1.45	0.1	P6	0	0	0.63
CT3	0.2	1.45	0.2	P7	0.1	0	0.63
CT4	0.2	1.45	0.3	P8	-0.02	0	0.705
CT5	0.2	1.45	0.4	P9-GG1 (gardon gauge)	0.02	0	0.705
CT6	0.2	1.45	0.48	P10	-0.1	0	0.78
DT1	0.2	1.95	0.02	P11	0	0	0.78
DT2	0.2	1.95	0.1	P12	0.1	0	0.78
DT3	0.2	1.95	0.2	P13-GG2 (gardon gauge)	-0.02	0	0.855
DT4	0.2	1.95	0.3	P14	0.02	0	0.855
DT5	0.2	1.95	0.4	P15	-0.1	0	0.93
DT6	0.2	1.95	0.48	P16	0	0	0.93
ET1	0.2	2.45	0.02	P17	0.1	0	0.93
ET2	0.2	2.45	0.1	P18	-0.1	0	1.08
ET3	0.2	2.45	0.2	P19	0	0	1.08
ET4	0.2	2.45	0.3	P20	0.1	0	1.08
ET5	0.2	2.45	0.4	P21	-0.1	0	1.23
ET6	0.2	2.45	0.48	P22	0	0	1.23
FT1	0.2	2.95	0.02	P23	0.1	0	1.23
FT2	0.2	2.95	0.1	P24	-0.1	0	1.38
FT3	0.2	2.95	0.2	P25	0	0	1.38
FT4	0.2	2.95	0.3	P26	0.1	0	1.38
FT5	0.2	2.95	0.4	P27	-0.1	0	1.53
FT6	0.2	2.95	0.48	P28	0	0	1.53
				P29	0.1	0	1.53

APPENDIX C: AUTHOR'S LIST OF PAPERS PUBLISHED AND SUBMITTED

Journals

Asimakopoulou, E.K., Chotzoglou, K., Kolaitis, D.I. and Founti, M.A., (2016) Characteristics of Externally Venting Flames and their effect on the façade: A detailed experimental study, Fire Technology, 52 (6), pp. 2043-2069.

Conferences

Chotzoglou, K., Zhang, J., Delichatsios, M.A. and Asimakopoulou, E.K., (2017) Experimental Study of Burning Behaviours of Liquid Pool Fires in a Corridor-like Enclosure, *10th Mediterranean Combustion Symposium*, Naples, Italy.

Chotzoglou, K., Asimakopoulou, E.K., Zhang, J. and Delichatsios, M.A. (2018) Experimental Investigation of Liquid Pool Fires and Externally Venting Flames in Corridor-like Enclosures, *10th International Conference in Structures in Fire*, 6-8 June, Belfast, UK.

Chotzoglou, K., Asimakopoulou, E.K., Zhang, J. and Delichatsios, M.A. (2018) Experimental investigation of externally venting flames geometric characteristics and impact on the façade of corridor-like enclosures, *3rd European Symposium on Fire Safety Science*, 12-14 September, Nancy, France.

Chotzoglou, K., Asimakopoulou, E.K., Zhang, J. and Delichatsios, M.A. (2018) An Experimental Investigation of Burning Behaviour of Liquid Pool Fire in Corridor-like Enclosures, *3rd European Symposium on Fire Safety Science*, 12-14 September, Nancy, France.

Asimakopoulou, E, Chotzoglou, K., Kolaitis, D., Zhang, J., Delichatsios, M. (2018) Numerical investigation of externally venting flame characteristics in a corridor-façade configuration, *Proceedings of the Ninth International Seminar on Fire and Explosion Hazards (ISFEH9)*, 21-26 April, St. Petersburg, Russia (submitted).

Posters

Chotzoglou, K., Zhang, J., Delichatsios, M.A. and Asimakopoulou, E.K., (2017) Burning Behaviour and External Flames in a Corridor-like Enclosure Using Liquid Pool Fires, *12th International Symposium in Fire Safety Science*, Lund, Sweden.

Chotzoglou, K., Asimakopoulou, E.K., Zhang, J. and Delichatsios, M.A. (2018) Burning Behaviour of a Liquid Pool Fire in a Corridor-like Enclosure and Thermal Characteristics of Resulting Externally Venting Flames, *37th International Symposium on Combustion*, 29 July-3 August, Dublin, Ireland (accepted)

REFERENCES

Akita, K., and Yumoto, Y., (1965) Heat Transfer in Small Pools and Rates of Burning of Liquid Methanol, *Proceedings of the Combustion Institute*, 10, pp. 943-948.

Asimakopoulou, E.K., (2016) Development and Assessment of Experimental and Numerical Tools for Characterization of Externally Venting Flames and Evaluation of their Effecton Building Facades, PhD Thesis, National Technical University of Athens.

Asimakopoulou, E.K., Chotzoglou, K., Kolaitis, D.I. and Founti, M.A., (2016) Characteristics of Externally Venting Flames and their effect on the façade: A detailed experimental study, Fire Technology, 52 (6), pp. 2043-2069. DOI: 10.1007/s10694-016-0575-5.

ASME PTC 19.1-1998, (1998) Test Uncertainty, Instruments and Apparatus, Supplement to the ASME Performance Test Codes.

Audouin, L., Kolb, G., Torero, J.L. and Most, J.M. (1995) Average centreline temperatures of a buoyant pool fire obtained by image processing of video recordings. *Fire Safety Journal,* 24(2), pp. 167-187.

Audouin, L., Such, J.M., Malet, J.C. and Casselman, C., (1997) A Real Scenario for A Ghosting Flame. *5th International Symposium on Fire Safety Science,* Interscience Communications Ltd, pp. 1261-1272

Babrauskas, V., (1983) Estimating large pool fire burning rates, *Fire Technology*, 19, pp. 251–261.

Babrauskas, V., (1986) Free Burning Fires, *Fire Safety Journal*, 11, pp. 33-51.

Babrauskas, V., and Grayson, S.J., (1992) Heat Release in Fires, Elsevier Applied Science, London and New York.

Babrauskas, V., and Peacock, R. D., (1992) Heat Release Rate: The Single Most Important Variable in Fire Hazard, *Fire Safety Journal*, 18, pp. 255-272.

Babrauskas, V., (2002) Heat release rates in: The SFPE Handbook of Fire Protection Engineering, third ed. The National Fire Protection Association, Quincy, Massachusetts, USA, Section 3, Chapter 1, pp. 3-1 to 3-37.

Beji, T., (2009) Theoretical and experimental investigation on soot and radiation in fires, PhD thesis, University of Ulster.

Beji, T., Ukleja, S., Zhang, J., Delichatsios, M.A. (2012) Fire behaviour and external flames in corridor and tunnel-like enclosures, *Fire and Materials*, 36, 636-647.

Blinov, V.I., and Khudiakov, G.N., (1957) Certain laws governing diffusive burning of liquid, Academiia Nauk, SSSR Doklady 113, pp. 1094–1098.

Blinov, V.I. and Khudyakov, G.N., (1961) Diffusion burning of liquids, U.S. Army Translation NTIS No. AD296762., Izdatel'stvo Akademii Nauk SSSR: Moscow. p. 208.

Boehmer H., Floyd J., Gottuk D.T., (2009) Fire dynamics and forensic analysis of limited ventilation compartment fires, Volume 2: modelling, Grant No. 2007-DN-BX-K240, Hughes Associates, Baltimore, USA.

Brohez, S., Delvosalle, C., and Marlair, G., (2004) A two-thermocouples probe for radiation corrections of measured temperatures in compartment fires. *Fire Safety Journal*, 39, pp. 399-411.

Bullen, M.L. and Thomas, P.H. (1979) Compartment Fires with Non-Cellulosic Fuels, *17th International Symposium on Combustion*, Combustion Institute, Leeds, England.

Byram, G.M., Clements, H.B., Bishop, M.E., and Nelson, Jr. R.M., (1966) Project Fire Model and Experimental Study of Model Fires, Final Report, U.S Forest Service, Southeastern Forest Experiment Station, Macon, GA.

Chatris, J.M., Quintela, J., Folch, J., Planas, E., Arnaldos, J. and Casal, J., (2001) Experimental study of burning rate in hydrocarbon pool fires, *Combustion and Flame*, 126, pp. 1373-1383.

Corlett, R.C., and Fu, T.M., (1966) *Pyrodynamics*, 1, pp. 253-269.

Delichatsios, M.A., (1990) The Outflow of Buoyant Releases Including Fire Gases From a Long Corridor Closed at One End. *Journal of Fluids Engineering*, 112 (1), pp. 28-32.

Delichatsios, M.A. and Silcock, G.W.H., (2002) Fully Involved Enclosure Fires: Effects of Fuel Type, Fuel Area and Geometry, *Proceedings of the 7th International Symposium of Fire Safety Science*, pp. 59-73.

Delichatsios, M.A., Silcock, G.W. H., Liu, X., Delichatsios, M., Lee, Y.P., (2004) Mass pyrolysis rates and excess pyrolysate in fully developed enclosure fires, Fire Safety Journal, 39, pp. 1– 21.

Delichatsios, M.A., (2014) Enclosure and Façade Fires: Physics and Applications, *Proceedings of the 11th International Symposium on Fire Safety Science*.

deRis, J., (1979) Fire Radiation - A Review, 17th International Symposium on Combustion, The Combustion Institute, Pittsburgh, pp. 1003-1016.

Dieck, R.H., (1997) Measurement Uncertainty Models, in *ISA Transactions*, 36(1), pp. 29-35.

Ditch, B.D., de Ris, J.L., Blanchat, T.K., Chaos, M. Bill, Jr.R.G., and Dorofeev, S.B. (2013) Pool Fires – An Empirical Correlation. *Combustion and Flame*, 160, pp. 2964-2974. http://dx.doi.org/10.1016/j.combustflame.2013.06.020

Drysdale, D., (2011) An introduction to fire dynamics, 3rd edition, J. Wiley and Sons Ltd, Sussex, England.

Empis, C.A., (2010) Analysis of the compartment fire parameters influencing the heat flux incident on the structural façade. Ph.D. Thesis, University of Edinburgh, U.K.

Fleischmann, C.M. and Parkes, A.R., (1997) Effects of Ventilation on the Compartment Enhanced Mass Loss Rate, *Proceedings of the 5th International Symposium on Fire Safety Science*, pp. 415-426.

Gottuk, D., T. and Lattimer, B., Y., (2002) Effect of Combustion Conditions on Species Production. In:*SFPE Handbook of Fire Protection Engineering.* eds. DiNenno,P.,J., D. Drysdale, C.L. Beyler, et. al, , Third edn, USA: National Fire Protection Association, pp.2-54-2-82.

Gross, D., and Robertson, A.F., (1965) Experimental fires in enclosures. *Proceedings of the Combustion Institute*, 10, pp. 931-942.

Hall, A.R., (1972) Pool Burning: A Review, Rocket Propulsion Establishment: Westcott.

Hamins, A., Fischer, S.J., Kashiwagi, T., Klassen, M.E, and Gore, J.P., (1994) Heat Feedback to the Fuel Surface in Pool Fires, *Combustion Science and Technology*, 97 (1-3), pp. 37-62.

Hamins, A., Yang, J.C., and Kashiwagi, T., (1999) A Global Model for Predicting the Burning Rates of Liquid Pool Fires, NISTIR 6381, National Institute of Standards and Technology, Gaithersburg, MD.

Hamins, A., Johnsson, E., Donnelly, M. and Maranghides, A., (2008) Energy balance in a large compartment fire, *Fire Safety Journal*, 43, pp. 180-188.

Hayasaka, H., (1997) Unsteady Burning Rates of Small Pool Fires, *Proceedings of the 5th International Symposium on Fire Safety Science*, pp. 499-510.

Heskestad, G., (1983) Luminous Heights of Turbulent Diffusion Flames, *Fire Safety Journal*, 5, pp. 103–108.

Himoto, K., Tsuchihashi, T., Tanaka, Y. and Tanaka, T. (2009) Modeling thermal behaviors of window flame ejected from a fire compartment. *Fire Safety Journal*, 44, pp. 230-240.

Hottel, H.C., (1959) Certain Laws Governing Diffusive Burning of Liquids, *Fire Res. Abstr. Rev*., 1, 41-44.

Hu, L.H., Liu, S., Peng, W. and Huo, R., (2009) Experimental study on burning rates of square/rectangular gasoline and methanol pool fires under longitudinal air flow in a wind tunnel, *Journal of Hazardous Materials*, 169, pp. 972-979.

Hu, L.H., Liu, S., and Wu, L., (2013) Flame radiation feedback to fuel surface in medium ethanol and heptane pool fires with cross air flow, *Combustion and Flame*, 160, pp. 295-306. http://dx.doi.org/10.1016/j.combustflame.2012.10.016

Huang, H., Ooka, R., Liu, N., Zhang, L., Deng, Z., and Kato, S., (2009) Experimental study of fire growth in a reduced-scale compartment under different approaching external wind conditions, *Fire Safety Journal*, 44, pp. 311–321.

Huggett, C., (1980) Estimation of rate of heat release by means of oxygen consumption measurements, *Fire and Materials*, 4 (2), pp. 61-65.

Hurley M.J., (2016) "SFPE Handbook of fire protection engineering", 5th Ed., SFPE, Quincy, Massachusetts, U.S.A.

Hwang C.H., Lock A., Bundy M., Johnsoon E., Ko G.H., (2011) Effects of fuel location and distribution on full-scale underventilated compartment fires, *Journal of Fire Science*, 29, 21-52.

Iqbal, N., and Salley, M.H., (2003) Fire Dynamics Tools (FDTS) Quantitative Fire Hazard Analysis Methods for the U.S. Nuclear Regulatory Commission Fire Protection Inspection Program, US. Nuclear Regulatory Commission, Draft Report, Washington.

ISO 9705, (1993) International Organization for Standardization, ISO 9705 Fire Tests: Full-Scale Room Test for Surface Products, 1st Edition, Geneva, Switzerland.

Jahn W., Rein G., Torero J. L., (2011) A posteriori modelling of the growth phase of Dalmarnock Fire Test One, *Building and Environment* 46, 1065-1073.

Jiang, P., and Lu, S., (2013) Effects of cross air flow on mass loss rates of circular aviation fuel pool fires in large open space, *Procedia Engineering*, 62, pp. 309-316.

Karlsson, B., and Quintiere, J.G., (2000) Enclosure Fire Dynamics, CRC Press LLC, New York.

Kawagoe, K., (1958) Fire Behaviour in Rooms, Report No 27, Building Research Institute, Tokyo, Japan.

Kawagoe, K. and Sekine, T. (1963) Estimation of Fire Temperature-Time Curves in Rooms, Building Research Institute of Japan.

Klassen, M., and Gore, P., (1992) Structure and radiation properties of pool fires, Final Report, Purdue University.

Klopovic, S. and Turan, Ö.F. (1998) Flames venting externally during full-scale flashover fires: Two sample ventilation cases, *Fire Safety Journal*, 31 (2), pp. 117-142.

Koseki, H. and Yumoto, T. (1988) Air entrainment and thermal radiation from heptane pool fires, *Fire Technology*, 24(1), pp. 33-47.

Lam, C.S., Randsalu, E.J., Weckman, E.J., Brown, A.L., Gill, W. and Gritzo, L.A., (2004) Fuel regression rates of hydrocarbon pool fires in cross winds, *Interflam '04: Proceedings of the 10th International Conference*, pp. 117-128, Interscience Communications, London.

Law, M. (1978) Fire safety of external building elements – The design approach, Engineering Journal, Second Quarter, pp.59-74, American Institute of Steel Construction (AISC), U.S.A.

Lee, Y.-P. (2006) Heat fluxes and flame heights in external facades from enclosure fires, Ph.D. Thesis, The University of Ulster, Belfast, U.K.

Lee, Y.-P., Delichatsios, M.A. and Silcock, G.W.H. (2007) Heat fluxes and flame heights in facades from fires in enclosures of varying geometry, Proceedings of the Combustion Institute, 31 (2), pp. 2521-2528.

Lee, Y.P., Delichatsios, M.A., Ohmiya, Y., Wakatsuki K., Yanagisawa, A. and Goto, D. (2009) Heat fluxes on opposite building wall by flames emerging from an enclosure, *Proceedings of the Combustion Institute*. 32, pp. 2551-2558.

Lee, Y.P., Delichatsios, M.A. and Ohmiya, Y. (2012) The physics of the outflow from the opening of an enclosure fire and re-examination of Yokoi's correlation. *Fire Safety Journal*, 49, pp. 82-88.

Li, Y.Z., Ingason, H. and Lonnermark, A., (2014) Fire Development in Different Scales of Train Carriages. *Proceedings of the 11th International Symposium on Fire Safety Science*, pp. 302-315.

Lu, K., Hu, L., Tang, F., Delichatsios, M.A., Zhang, X. and He, L., (2013) Facade flame heights from enclosure fires with side walls at the opening, *Procedia Engineering*, 62, pp. 202-210.

Lu, K., Hu, L., Delichatsios, M., Tang, F., Qiu, Z., and He, L. (2015) Merging behaviour of facade flames ejected from two windows of an under-ventilated compartment fire. *Proceedings of the Combustion Institute*, 35 (3), pp. 2615-2622.

Luketa, A., (2010) Assessment of Simulation Predictions of Hydrocarbon Pool Fire Tests, Report No. SAND2010-2511, Sandia National Laboratories.

Magnus, G., (1961) Tests on Combustion Velocity of Liquid Fuels and Temperature Distribution in Flames and Beneath Surface of the Burning Liquid,

Proceedings of 1st International on the Use of Models in Fire Research, Washington, D. C.: National Academy of Sciences – National Research Council.

Modak, A.T., and Croce, P.A. (1977) Plastic Pool Fires. *Combustion Flame*, 30, pp. 251–265.

Morton, B.R., Taylor, G., and Turner, J.S., (1956) Turbulent gravitational convection from maintained and instantaneous sources, *Proceedings of the Royal Society (London),* A234, pp. 1-23.

Most, J.M. and Saulnier, J.B., (2011) Under-ventilated Wall Fire Behaviour during the Post-Flashover Period. *Journal of Applied Fluid Mechanics,* 4, (3) pp.129-135.

Miyazaki, S., and Watanabe, Y., (1998) An Experimental Study on Fire Phenomena of Liquid Fuel in a Small-Sized Tunnel Burning Behaviour of N-Heptane (Part 1), paper B-14 and An Experimental Study on Fire Phenomena of Liquid Fuel in a Small-Sized Tunnel Relation Between Inside Temperature of the Tunnel and Burning Rate of N-Heptane (Part 2), paperA-15.

O'Connor, D., (2016) The Building Envelope: Fire Spread, Construction Features and Loss Examples, SFPE Handbook of Fire Protection Engineering (5th ed.) Hurley M.J., National Fire Protection Association, Quincy, MA 02269, pp. 3242-3512.

Ohmiya, Y., Satoh, M., Tanaka, T. and Wakamatsu, T. (1995) Burning Rate of Fuel in Enclosure and Generation Limit of the External Flame, *Journal of Structural and Construction Engineering*, AIJ, No. 469, pp. 149-158.

Ohmiya, Y., Tanaka, T. and Wakamatsu, T. (1998) A room fire model for predicting fire spread by external flames, *Fire Science and Technology,* 18 (1), pp. 11-21.

Ohmiya, Y., Hori, Y., Sagimori, K., and Wakamatsu, T., (2000) Predictive Method for Properties of Flame Ejected from an Opening Incorporating Excess Fuel, *Proceedings of 4th Asia-Oceania Symposium on Fire Science and Technology*, pp. 375-386.

Ohmiya, Y., Yusa, S., Matsuyama, K., and Harada, K., (2001) Prediction method of opening jet plume behavior in the presence of an opening soffit. *Proceedings of the 5th AOSFST*, pp. 171-185.

Ohmiya, Y., Yusa, S., Suzuki, J.I., Koshikawa, K. and Delichatsios, M.A., (2003) Aerodynamics of fully involved enclosure fires having external flames, Proceedings of the Fourth International Seminar on Fire and Explosion Hazards, University of Ulster, Belfast, U.K.

Oleszkiewicz, I., (1989) Heat transfer from a window fire plume to a building facade, HTD 123, ASME Collected papers on Heat Transfer, Book No. H00526, pp. 163-170.

Oleszkiewicz, I., (1990) Fire exposure to exterior walls and flame spread on combustible cladding, *Fire Technology*, 26, pp. 357-375.

Orloff, L. (1981) Simplified Radiation Modeling of Pool Fires. *18th International Symposium on Combustion*, The Combustion Institute, Waterloo, Ontario, Pittsburgh, PA.

Parkes, A.R. and Fleischmann, C.M., (2005) The Impact of Location and Ventilation on Pool Fire in a Compartment, *Proceedings of the 8th International Symposium on Fire Safety Science*, pp. 1289-1300.

Parkes, A.R., (2009) The Impact of Size and Location of Pool Fires on Compartment Fire Behaviour, PhD Thesis, University of Canterbury.

Pearson, A., Most, J. and Drysdale, D., (2007) Behaviour of a confined fire located in an unventilated zone. *Proceedings of the Combustion Institute*, 31(2), pp. 2529-2536.

Pitts, W.M., (1995) Global equivalence ratio concept and the formation mechanisms of carbon monoxide in enclosure fires. *Progress in Energy and Combustion Science*, 21, (3), pp.197-237.

Quintiere, J., (1989) Scaling applications in fire research, *Fire Safety Journal*, 15, pp. 3-29.

Quintiere, J., (2006) Fundamentals of Fire Phenomena, J. Wiley and Sons Ltd., Sussex.

Rasbach, D.J., Rogowski, Z.W., and Stark, G.W.V., (1956) Properties of fires of liquids, *Fuel*, 31, pp. 94-107.

Rockett, J.A., (1976) Fire Induced Gas Flow in an Enclosure, *Combustion Science and Technology*, 12, pp. 65–175.

Seigel, L.G. (1969) The projection of flames from burning buildings, *Fire Technology*, 5 (1), pp. 43-51.

Shinotake, A., Koda, S. and Akita, K., (1985) An experimental study of radiative properties of pool fires of an intermediate scale, *Combustion Science Technology*, 43, pp. 85.

Steckler, K.D., Quintiere J.G., and Rinkinen W.J., (1982) Flow Induced by Fire in a Compartment, *19th International Symposium on Combustion*, pp. 913-920.

Steinhaus, T., Welch, S., Carvel, R., and Torero, J.L., (2007) Large-Scale Pool Fires, *Thermal Science Journal*, 11 (3).

Sugawa, O., Kawagoe, K., Oka, Y. and Ogahara, I., (1989) Burning Behavior in a Poorly-Ventilated Compartment Fire-Ghosting Fire-. *Fire Science and Technology*, 9, (2), pp. 2_5-2_14.

Sun, J., Hu, L. and Zhang, Y. (2013) A review on research of fire dynamics in high-rise buildings. *Theoretical and Applied Mechanics Letters*, 3 (4).

Tao, C., He, Y., Li, Y. and Wang, X., (2013) Effects of oblique air flow on burning rates of square ethanol pool fires, *Journal of Hazardous Materials*, 260, pp. 552-562.

Tewarson, A., (1995) Generation of Heat and Chemical Compounds in Fires. In:*The SFPE Handbook of Fire Protection Engineering*, eds. J. Linville L. and et al, 2nd Edition edn,USA: National Fire Protection Association, pp.3-53-3-124.

Tewarson, A., (2008) Generation of Heat and Chemical Compounds in Fires. In:*The SFPE Handbook of Fire Protection Engineering* ., eds. DiNenno,P.,J., D. Drysdale, C.L. Beyler, et al, 4th Edition edn,USA: National Fire Protection Association

Tewarson, A., and Marlair G., (2004) Liquids and Chemicals. *Handbook of Building Materials for Fire Protection*, Harper C.A (Ed.), McGraw-Hill, pp. 8.1-8.43.

Thomas, I.R and Bennetts, I.D., (1999) Fires in Enclosures with Single Ventilation Openings - Comparison of Long and Wide Enclosures, *Proceedings of the 6th International Symposium on Fire Safety Science*, pp. 941-952.

Thomas, I.R, Moinuddin, K., and Bennetts, I.D., (2005) Fire Development in a Deep Enclosure, *Proceedings of the 8th International Symposium of Fire Safety Science*, p. 1277-1288.

Thomas, I.R, Moinuddin, K. and Bennetts, I.D., (2007) The Effect of Fuel Quantity and Location on Small Enclosure Fires, *Journal of fire Protection Engineering*, 17, pp. 85-102.

Thomas, P.H., (1962) The Size of Flames from Natural Fires, *9th International Symposium on Combustion*, The Combustion Institute, Pittsburgh, pp. 844-859.

Thomas, P. H., Heselden, A.J.M. and Law, M., (1967) Fully developed compartment fires: two kinds of behaviour, Fire Research Technical Paper No. 18, HMSO, London.

Thomas, P.H. and Law, M., (1974) The Projection of Flames from Burning Buildings on Fire, *Fire Prevention Science and Technology*, 10, pp. 19-26.

Thornton, W.M., (1917) The relation of oxygen to the heat of combustion of organic compounds, *Philosophical Magazine and Journal of Science*, 33, pp. 196-203.

Tofilo, P., Delichatsios, M.A., Silcock G.W.H. and Shields T.J., (2004) Wall Heat Fluxes in Enclosure Fires, *6th Asia-Oceania Symposium on Fire Science & Technology*, pp. 108-119.

Ukleja, S., (2012) Production of smoke and carbon monoxide in under-ventilated enclosure fires, PhD thesis, University of Ulster.

Utiskul, Y., Quintiere, J.G., Rangwala, A.S., Ringwelski, B.A., Wakatsuki, K. and Naruse, T., (2005) Compartment fire phenomena under limited ventilation, *Fire Safety Journal*, 40, pp. 367–390.

Vali, A., Nobes, D.S., and Kostiuk, L.W., (2013) Effects of Altering the Liquid Phase Boundary Conditions of Methanol Pool Fires, *Experimental Thermal and Fluid Science*, 44, pp.786-791.

Vali, A., (2014) Investigation of the Transport Phenomena within the Liquid Phase of a Methanol Pool Fire. PhD thesis, University of Alberta.

Webster, C.T., Raftery, M.M., and Smith, P.G. (1961) The burning of fires in rooms – Part III, FRN 474, Joint Fire Research Organization, Borehamwood, U.K.

White, N. and Delichatsios, M. (2014) Fire hazards of exterior wall assemblies containing combustible components, *1st Edition*, Springer Briefs in Fire, Springer, New York, U.S.A.

Yamaguchi, J.I. and Tanaka, T. (2005) Temperature of Window Jet Plume. *Fire Science Technology*, 24, pp. 17-38.

Yii, E.H., (2002) Modelling the Effects of Fuel Types and Ventilation Openings on Post-Flashover Compartment Fires, PhD Thesis, University of Canterbury.

Yii, E.H., Fleischmann, C.M. and Buchanan, A.H., (2007) Vent Flows in Fire Compartments with Large Openings. *Journal of Fire Protection Engineering*, 17 (3), pp. 211-237.

Yokoi, S., (1960) Study on the prevention of fire-spread caused by hot upward current, Report 34, Report of the Building Research Institute, Japanese Ministry of Construction.

Yuan, Z., Lei, B. and Kashef, A. (2015) Experimental and Theoretical Study for Tunnel Fires with Natural Ventilation, *Fire Technology*, 51, pp. 691–706.

Zabetakis, M.G., and Burgess, D.S., (1961) Research on the hazards associated with the production and handling of liquid hydrogen, US Bureau of Mines RI5707, Pittsburgh, PA.

Zhang, J. and Delichatsios, M.A., (2009) Determination of the convective heat transfer coefficient in three-dimensional inverse heat conduction problems, *Fire Safety Journal*, 44, pp. 681-690.

Zukoski, E.E., Kubota, T. and Cetegen, B. (1980) Entrainment in Fire Plumes, *Fire Safety Journal*, 3, pp. 107-121.

Zukoski, E.E., (1995) *Properties of fire plumes.* In: Combustion Fundamentals of Fire. Academic Press, pp. 101-219.